LEVEL

NAVAL POSTGRADUATE SCHOOL
Monterey, California

DTIC
SELECTE
SEP 28 1981

H

THESIS

SUBSONIC CASCADE WIND TUNNEL TESTS USING
A COMPRESSOR CONFIGURATION OF DCA BLADES.

by

Frank S. Cina

June 1981

Thesis Advisor: R. P. Shreeve

Approved for public release; distribution unlimited.

81 9 28 089

REPORT DOCUMENTATION PAGE	READ INSTRUCTIONS BEFORE COMPLETING FORM

1. REPORT NUMBER	2. GOVT ACCESSION NO.	3. RECIPIENT'S CATALOG NUMBER
	AD-A104 597	

4. TITLE (and Subtitle)	5. TYPE OF REPORT & PERIOD COVERED
Subsonic Cascade Wind Tunnel Tests Using a Compressor Configuration of DCA Blades	Master's thesis; June 1981
	6. PERFORMING ORG. REPORT NUMBER

7. AUTHOR(s)	8. CONTRACT OR GRANT NUMBER(s)
Frank S. Cina	

9. PERFORMING ORGANIZATION NAME AND ADDRESS	10. PROGRAM ELEMENT, PROJECT, TASK AREA & WORK UNIT NUMBERS
Naval Postgraduate School Monterey, California 93940	.

11. CONTROLLING OFFICE NAME AND ADDRESS	12. REPORT DATE
Naval Postgraduate School Monterey, California 93940	June 1981
	13. NUMBER OF PAGES 209

14. MONITORING AGENCY NAME & ADDRESS(if different from Controlling Office)	15. SECURITY CLASS. (of this report)
	Unclassified
	15a. DECLASSIFICATION/DOWNGRADING SCHEDULE

16. DISTRIBUTION STATEMENT (of this Report)

Approved for public release; distribution unlimited.

17. DISTRIBUTION STATEMENT (of the abstract entered in Block 20, if different from Report)

18. SUPPLEMENTARY NOTES

19. KEY WORDS (Continue on reverse side if necessary and identify by block number)

Subsonic Cascade Wind Tunnel Test
DCA Blading Cascade
Double Circular Arc Blading

20. ABSTRACT (Continue on reverse side if necessary and identify by block number)

Tests are reported in which air incidence angle was varied to a cascade of 20 blades, 5 inches in chord with aspect ratio of 2.0 and solidity of 1.67. Preliminary blade element performance data were obtained using pneumatic probe surveys and surface pressures were also measured. Results of preparatory tests of a similar cascade of 15 C-series blades at a solidity of 1.28 are also included. Whereas the flow in

(20. ABSTRACT Continued)

the C-series blading cascade was always acceptable, the flow in the DCA blading cascade was not acceptable at negative incidence angles. A modification of the cascade inlet guide vanes is recommended which will quarantee periodic conditions and serve to generate more nearly uniform inlet flow at all test conditions.

Accession For

NTIS CRA&I
DTIC TAB
Unannounced
Justification

By
Distribution

Availability Codes

Dist   Special

A

Subsonic Cascade Wind Tunnel Tests Using
a Compressor Configuration of DCA Blades

by

Frank S. Cina
Lieutenant, United States Navy
B.S., United States Naval Academy, 1974

Submitted in partial fulfillment of the
requirements for the degree of

MASTER OF SCIENCE IN AERONAUTICAL ENGINEERING

from the

NAVAL POSTGRADUATE SCHOOL

June   1981

Author _____

Approved by: _____
Thesis Advisor

_____
Chairman, Department of Aeronautics

_____
Dean of Science and Engineering

3

ABSTRACT

Tests are reported in which air incidence angle was varied to a cascade of 20 blades, 5 inches in chord with aspect ratio of 2.0 and solidity of 1.67. Preliminary blade element performance data were obtained using pneumatic probe surveys and surface pressures were also measureed. Results of preparatory tests of a similar cascade of 15 C-series blades at a solidity of 1.28 are also included. Whereas the flow in the C-series blading cascade was always acceptable, the flow in the DCA blading cascade was not acceptable at negative incidence angles. A modification of the cascade inlet guide vanes is recommended which will guarantee periodic conditions and serve to generate more nearly uniform inlet flow at all test conditions.

TABLE OF CONTENTS

LIST OF FIGURES

7

Figure

11

13

LIST OF TABLES

LIST OF SYMBOLS

AVDR	Axial Velocity--Density Ratio
C_{p1}	Coefficient of pressure at the inlet (III.D.4)
C_{p2}	Coefficient of pressure at the outlet (III.D.4)
$C_{p_{static}}$	Coefficient of static pressure rise (III.D.3)
C_{xB}	Coefficient of force in the x direction based on blade surface pressure integration
C_{yB}	Coefficient of force in the y direction based on blade surface pressure integration
C_{xM}	Coefficient of force in the x direction based on momentum conservation
C_{yM}	Coefficient of force in the y direction based on momentum conservation
c	Blade chord (inches)
D	Diffusion factor (III.D.2)
i	Incidence angle (degrees)
P	Pressure (in H_2O)
Q	Dyanamic Pressure (in H_2O)
s	Blade-to-blade spacing (inches)
T	Temperature (°R)
V	Velocity (ft/sec)
W	Relative velocity (ft/sec)
X	Velocity, non-dimensionalized by the "limiting" velocity, $V_T = \sqrt{2 C_p T_t}$
x	Coordinate in the blade-to-blade direction (inches)
y	Coordinate in the axial direction (inches)
z	Coordinate in the spanwise direction (inches)

β	Air angle, measured in the blade-to-blade plane (degrees)
γ	Stagger angle (degrees)
δ	Deviation angle (degrees)
σ	Solidity (C/S)
ϕ	Pitch angle (of air flow), measured in the spanwise, blade-to-blade plane
ϕ	Blade camber angle (degrees)
$\bar{\omega}$	Loss coefficient (III.D.1)

Subscripts

i	Refers to traversing plane; i = 1 for inlet, i = 2 for outlet
p	Pressure
plen	Plenum (supply)
s	Static
t	Total
u	In the blade-to-blade (x) direction
wℓ	North wall, lower plane
1	Inlet plane
2	Outlet plane

ACKNOWLEDGMENT

I. INTRODUCTION

Cascade tests provide two-dimensional blade-element performance data which are required in the design of compressors and turbines. Reference 1 describes how cascade measurements are obtained and then used in the design process. The importance of obtaining uniform inlet flow, periodic outlet flow and two-dimensional flow conditions in the cascade is emphasized, and reemphasized.

The present facility, as modified by Moebius [Ref. 2] from the original design described in detail by Rose and Guttormson [Ref. 3], permits a wider range of blading configurations to be tested (both compressor and turbine) than can normally be accommodated in a single cascade facility. The unusual arrangement of the facility however required that its suitability for testing compressor cascades be established very carefully. Preliminary studies were performed by Duval [Ref. 4] which indicated that excellent flow conditions could be achieved in the cascade, without suction, using 15 blades with an aspect ratio of approximately two. The absence of suction resulted necessarily in some degree of streamline contraction. Measured in terms of "Axial-Velocity-Density-Ratio (AVDR)," Duval's results were for AVDR ≈ 1.06.

In the study reported herein, a series of cascade wind tunnel tests were carried out using a specific compressor cascade of Double Circular Arc (DCA) blading. The testing

was undertaken to provide a baseline of experience and to document a reference set of performance data for the particular cascade. The data would later serve as a reference with which to compare the performance of a similar cascade of "controlled diffusion" (C.D.) blading to be tested in a subsequent phase of the program. The overall purpose of the program was to obtain data with which to verify design prediction and computational codes developed by NASA to compute two-dimensional flow through compressor cascades [Ref. 5].

Preliminary tests to vary air incidence angle were carried out using the C-series blading reported by Duval [Ref. 4]. The results are given in Appendix A. The results obtained for turning angle and losses agreed reasonably well with those calculated for C-series blading using Reference 1. The testing also showed that the cascade provided an acceptable area of spanwise uniform flow over a wide range of diffusion factors.

To meet the required cascade design solidity of 1.67 while maintaining an aspect ratio of approximately 2.0, the DCA blades were designed to have a 5.01 inch chord and were set at a spacing of 3 inches. This required 20 blades to be mounted in the test section. Tests were conducted at reference and at two positive and two negative incidence angles to obtain results at on- and off-design conditions.

The performance results obtained were found to follow qualitatively the data correlation given in Reference 1. Continuity and momentum balances showed the results to be

consistent with having two-dimensionality with a streamline contraction which was acceptable at all incidence angles. However, inlet conditions which were periodic in total pressure as a result of wakes from inlet guide vanes were found to be incompatible with the new 3 inch spacing of the test blades. The 2 inch separation of the guide vane wakes produced periodicity every two blade passages instead of every passage. The recommendation was made that the guide vane section be modified to provide guide vanes at 1 inch intervals, and the reported tests repeated.

The present report documents the tests and the experimental procedures followed in obtaining the data. Following a description of the facility and measurement techniques in Section II and a review of cascade concepts in Section III, Section IV reports the test program and procedures employed. Results, discussion and conclusions follow in the remaining sections. The form of the momentum balance and derivations of the loss coefficients used in analyzing the results are given in Appendices B and C respectively. Appendix D is reproduced without change from Duval [Ref. 4], and describes the calculation of the AVDR.

21

II. FACILITY AND MEASUREMENTS

A. CASCADE WIND TUNNEL

1. Wind Tunnel

Figure 1 is a schematic of the complete test facility. Figure 2(a) is a photograph of the subsonic cascade wind tunnel test section showing its relatively large size. A view of the test section with the DCA blading installed is shown in Figure 2(b). The dimensions of the cascade and the location of wall static pressure ports and upper and lower probe survey planes are shown in Figure 3.

2. Instrumentation

a) Wall Pressure Taps

Static pressure taps were located on the south wall, 16.25 inches axially ahead of mid-chord and 6.5 inches axially behind the mid-chord. Twenty taps were spaced at two inch intervals along the wall in the blade to blade direction at each axial location. The taps were connected to a water manometer board so that the static pressure distribution of the inlet and outlet could be monitored visually.

b) Survey Probes

A United Sensor Corporation DA-125 probe, Serial No. A847-1 (Fig. 4) was used in upper plane surveys. A United Sensor Corporation DC-125-24-F-22-CD probe, Serial No. A981-2 (Fig. 5) was used for lower plane measurements. A spanwise rake of static and total pressure sensors was also

used to rapidly obtain surveys of the inlet flow field. The probes are described in detail by Duval [Ref. 4].

c) Reference Measurements

Plenum chamber (supply) pressure and temperature were recorded for each probe data sample. The plenum pressure was also displayed on the manometer board. The total temperature in the test section was assumed to be that of the plenum.

B. TEST BLADING

1. Design and Construction

The test blading was representative, at larger scale, of the midspan section of the stator of the compressor stage reported in Reference 6. The blades were constructed using the coordinates listed in Table I. A detail of the blade tip is shown in Figure 6.

2. Instrumentation

Three blades were fitted with surface pressure taps along the midspan section (Figure 7). The centermost blade had 19 ports on each of the pressure and suction surfaces and one tap at the leading edge. A photograph of the centermost blade is shown in Figure 8 and the tap locations are given in Figure 9.

C. DATA ACQUISITION AND ANALYSIS

Data was logged, reduced, and plotted using the Hewlett-Packard HP-3052A Data Acquisition System shown in Fig. 10 [Ref. 7]. The system used an HP-9845A calculator as a

controller, with components connected on an HP-98034A HP-IB
Interface Bus. An HG-78K Scanivalve Controller was used with
two-scanivalves. This system allowed concurrent acquisition
of probe and blade surface pressure measurements.

The programs used in the present study were developed
from those described by Duval [Ref. 8]. The modifications
were documented in a revision of Reference 8 (Ref. 9).

The uncertainty in the measurements is given in Table
II.

III. REVIEW OF CASCADE AND TESTING CONCEPTS

A. NOMENCLATURE

The terminology used here follows Chapter 6 of Reference
1. Figure 11 shows a general cascade geometry and defines
inlet and outlet air angles, blade to blade and spanwise
coordinates.

B. REQUIREMENTS ON TEST CONDITIONS

For cascade wind tunnel data to be an accurate measure
of the two-dimensional performance of the test blading, the
flow field must be shown to meet conditions of inlet uni-
formity, two-dimensionality and periodicity between blade
rows. These fundamental conditions are discussed at length
in References 1, 4 and 10.

1. Uniform Inlet Flow

Uniform inlet flow is a requirement common to all wind
tunnels. Toward this aim, in the present facility, Moebius
[Ref. 2] incorporated a modified bellmouth contraction which
generated a uniform flow of air at the entrance to the test
section. There, a row of 30 adjustable inlet guide vanes
(Fig. 1) at 2 inch intervals provided the means by which the
flow to the test cascade could be turned uniformily to become
parallel to the lower end walls. A mechanism was incorporated
to allow the adjustment of the flow to be made with the cascade
in operation. The design of the lower section ensured that
all inlet air travelled the same distance between the turning

vanes and the test blading. This ensured a uniform boundary layer growth. The present inlet configuration was shown to provide flow to the test blading which was uniform but with an added periodic component in the total pressure which was the result of inlet guide vane wakes [Ref. 11].

   2. Two-Dimensional Flow

Two-dimensional flow conditions must also be approached in the test section. This implies that the flow in the central test plane is independent of spanwise displacement. Streamline contraction between the inlet and outlet test planes can however occur. As discussed by Erwin and Emery [Ref. 9] interaction of the tunnel side-wall boundary layers of the test airfoils is believed to be a primary cause for flow not remaining two-dimensional.

The problem is reduced in many facilities by using suction through porous walls in the area of the blade ends to remove the sidewall boundary layers. Because of the large scale, the inlet geometry and high Reynolds number of the present facility, the need for suction to obtain two dimensionality is reduced. Duval [Ref. 4] demonstrated that with an aspect ratio of approximately two the present facility provided nearly two-dimensional flow over greater than fifty percent of the span of a moderately loaded compressor cascade. However, without suction, because of the growth of the side wall boundary layers, the flow on the center plane through the blading must always correspond to a flow with some streamline contraction.

The degree to which truly two-dimensional flow (without streamline contraction) is achieved can be examined by checking continuity using the measured midspan inlet and outlet conditions. The "Axial-Velocity-Density-Ratio" (AVDR) described by Duval in Appendix D is a measure of the two dimensional continuity out-of-balance. Another check on the degree of two-dimensionality of the flow is made by performing a momentum balance over one blade passage. The change, in the momentum of the outlet compared to the inlet air is related vectorially to the pressure rise and the force on the blade. The components of force are obtained by integrating the pressures distributed over the blade surface area (Appendix B). A necessary condition for two-dimensionality with streamline contraction is that there exist at least some region of the flow in the center of the span which is independent of the spanwise displacement.

3. Periodic Flow

Since the cascade is simulating an infinite row of blades, the conditions in one blade passage should be identical to those in any other. Therefore in the blade-to-blade direction, all measurements should depend on position in a periodic fashion. This is the so-called periodicity requirement. Since the two end passages are bounded by walls rather than streamlines, they produce flows unlike those in the other passages through the cascade. For cascades having few blades (less than ten), the end passage flows are critical to the process of achieving truly periodic conditions over the more

central blade passages. By using 20 blades the importance
of the end passages was greatly reduced. In practice it has
been observed that the flows through the center blade passages
are not detectibly affected by the slight movement of the
exit end walls and hence the end passages themselves must
not be of critical importance. Periodicity can be examined
by comparing outlet conditions measured over two or more
blade passages. With pressure-instrumented blades, periodicity
is accurately checked by comparing surface pressure measure-
ments made on adjacent blades.

C. USE OF REFERENCE QUANTITIES

In practice small variations in the blower speed (and
therefore in the inlet dynamic pressure) during the time
required for a probe survey are unavoidable. This requires
that quantities derived from measurements be referenced in
some way to tunnel supply conditions before being integrated
in order to remove the effect of time dependent variations.
Duval [Ref. 4] demonstrated that the plenum conditions can
be used as a basis for obtaining suitable reference quanti-
ties. Similar procedures were followed throughout the present
work.

D. PERFORMANCE PARAMETERS

The performance of a cascade is specified in terms of the
deviation angle (δ) and the loss coefficient ($\bar{\omega}$) for given
inlet conditions. In Ref. 1 the loss coefficient is shown
to correlate in terms of the Diffusion Factor (D). In the

28

present wo..., the performance parameters were calculated using the following expressions:

1. <u>Loss Coefficient ($\bar{\omega}$)</u>

$$\bar{\omega} = \frac{\bar{C}_{p_{t_1}} - \bar{C}_{p_{t_2}}}{\bar{C}_{p_{t_1}} - \bar{C}_{p_1}} \tag{1}$$

where the mass averaged pressure coefficients in Eq. 1 are defined in Appendix C. It is shown in Appendix C that the effect of time dependent supply conditions are removed and the effect of AVDR is included in the use of Eq. (1).

2. <u>Diffusion Factor (D)</u>

$$D = 1 - \frac{W_2}{W_1} + \frac{\Delta W_u}{2\sigma W_1} \tag{2}$$

3. <u>Pressure Rise</u>

$$C_{p_{static}} = \frac{\bar{P}_2 - \bar{P}_1}{\bar{Q}_1} \tag{3}$$

4. <u>Blade Surface Pressure Coefficients</u>

$$C_{p1} = \frac{P_s - \bar{P}_1}{\bar{Q}_1} \tag{4}$$

$$C_{p2} = \frac{P_s - \bar{P}_2}{\bar{Q}_2} \tag{5}$$

Note: 1. Bars denote average quantities. Mass average is used except for 3 which is space averaged.

2. Time independence was obtained by referencing to local plenum conditions.

IV. TEST PROGRAM AND PROCEDURE

A. PROGRAM OF TESTS

Table III lists the cascade configurations tested. Five tests were conducted to provide data at design condition and at positive and negative incidence angles. Design incidence and probable deviation angles were computed using the procedures outlined in Ref. 1.

B. PROCEDURES TO ENSURE CONSISTENCY BETWEEN TESTS

Procedures were standardized from run to run in order to obtain measurements which were only a function of blade design and air inlet angle. The unique design of the cascade permitted data to be taken at a constant stagger angle, while varying only β_1. The same procedures were used to realign the cascade for each new configuration. The lower end walls were set to the desired inlet air angle and the inlet guide vanes were set so that their trailing edges were approximately aligned with the end walls. The upper end walls were set to the outlet air angle estimated using Ref. 1. The end wall spacings were set to precisely 1.5 inches. All tests were run at an average inlet velocity X_1 of .12. The same blade-to-blade distance was surveyed at each station in all tests.

C. TEST PROCEDURE AT EACH INCIDENCE ANGLE

The desired inlet dynamic pressure was set. Before
recording data, the manometer board was checked to ensure
that the distributions of static pressure at inlet and
outlet were acceptably uniform. If necessary the inlet
guide vanes and outlet end walls were adjusted in turn to
obtain an acceptably uniform distribution (± 0.5 inches H_2O).
The adjustments required were usually minor and easily
effected.

Probe surveys were carried out in the blade-to-blade
direction at midspan at the lower and upper planes in turn.
In each survey at the lower plane data were taken over two
blade passages at 1/2 inch intervals. In the upper plane
data were taken over four blade passages using 1/2 inch
intervals, except over one passage for which 0.2 inch
intervals were used. Surveys were also taken at the upper
plane in the spanwise direction 1 inch from both the pressure
and suction sides of the centermost blade. Periodically
throughout the run, measurements were taken of the pressure
distribution on the instrumented blades.

V. RESULTS

The results contained in Tables IV to XXIV and Figs. 12
to 85 are arranged in the following way.

The reduced data are given first in five sets of tables
which are of 4 types; namely, upper plane probe data, lower
plane probe data, center blade pressure tap data and adja-
cent blade pressure tap data. There is one table of each
type for each of five incidence angles. The final table
(Table XXIV) gives the blade performance parameters deduced
from measurements for each of the five configurations tested.

The results shown plotted in Figs. 12 to 85 are divided
into two separate groups. The first group (Figs. 12 to 72)
presents results which illustrate the quality of the wind
tunnel flow conditions. The second group (Figs. 73-85) gives
the blade element performance results deduced from the data.
In the first group, results are presented first to examine
the inlet flow uniformity (Figs. 12 to 18), second to examine
the outlet flow periodicity (Figs. 19 to 47) and finally to
examine outlet flow two-dimensionality (Figs. 48 to 72).

All points are shown connected with straight lines except
for Figs. 83 to 85 in which a curve was hand-faired between
points.

VI. DISCUSSION

A. INLET UNIFORMITY

The probe surveys at the lower plane in Figs. 13 to 17 showed that the inlet plane total pressure at midspan had a periodic variation in the blade to blade direction of approximately 1.5 inches of water peak-to-peak, with a spatial period of roughly 2 inches. This is the result of wakes from the inlet turning vanes and in agreement with the previous findings of Duval [Ref. 4] and McGuire [Ref. 11]. The wall pressure distributions (Figure 12) however showed that the static pressures at both upper and lower planes had minimal variations (.7 ins. water peak-to-peak at the lower plane, .4 ins. water peak-to-peak at the upper plane) in all runs except that for $\beta_1 = 46°$ (i = 8.8). In that one case the deviations were 1.1 ins. water peak-to-peak at both upper level and lower planes. This may have resulted from operating the turning vanes too far, or may have been the result of the high positive incidence in the test cascade itself. In all cases the static pressure variation over the four blade passages of interest in the center of the cascade did not exceed ± 0.1 inches of water.

B. TWO-DIMENSIONALITY

The data in Figures 48 to 67 showed that at all incidence angles a sizeable area of spanwise uniform conditions existed downstream of the test cascade. Most cases resulted in

uniform pressure and velocity over more than fifty percent
of the span. Reference 10 points out that at higher loadings
it is especially difficult to establish a substantial span-
wise area of uniform flow in the region near the suction side
of the blade. This begins to be evident in the data shown
in Fig. 56 and 64 in which only 30-40% of the spanwise dis-
tance is acceptably uniform. It is noted that the behavior
at reference incidence is not consistent with the general
trend toward a reduced extent of uniform flow as the loading
was increased.

However it is noted that the data are limited. A span-
wise survey was carried out at only one station close to the
suction surface. It is possible that the exact orientation
of the guide vane wakes (with peaks and valleys in total
pressure) with respect to the leading edges of the test blades,
may affect the suction-side wake region in a significant way.

Figures 68 to 72 show results for inlet and outlet angles,
the "reference" angle, β_∞ and blade force vectors derived in
two ways as shown in Appendix B, namely, from 1) the applica-
tion of momentum conservation using inlet and outlet probe
survey data, and 2) the integration of surface pressures over
the blade areas. As shown by Vavra [Ref. 12], in the two-
dimensional incompressible case without friction, the resul-
tant blade force should be perpendicular to the direction β_∞.
This is very nearly the case for all angles using the surface
pressure integration method and for positive incidence angles
using the momentum conservation method. At negative inci-
dence angles (Figs. 68 and 69) the momentum balance force

34

is markedly different from the surface pressure integration
vector. The force coefficients computed by the momentum
method tend to rotate downstream as incidence decreases. The
reason is not clear. According to Shultz [Ref. 13], the
magnitude of the blade force deduced from probe surveys de-
pends on the location of the outlet survey plane relative to
"fully mixed out" conditions. The present data were not re-
duced to calculate fully mixed out conditions, and the strictly
two-dimensional form of the momentum equation was used to
calculate the force components. A more detailed analysis
of the data is necessary in order to explain the differences
in magnitude and rotation of the force vector computed by the
momentum conservation method.

C. PERIODICITY

In order to examine periodicity, the probe survey data
obtained across 4 blade spaces at the upper plane were plotted
over a single blade space. As a result of an examination of
the data this was done in two ways. First data across three
blade spaces were plotted across a single blade space. Second
data from the four spaces were plotted across two spaces. As
can be seen in Figs. 20, 22, 27 and 29 at negative incidence
angles the total pressure and velocity did not repeat well
every blade passage, but repeated very closely indeed every
second blade passages (Figs. 21, 23, 28 and 30). Also, the
blade surface pressure data in Figs. 19 and 26 show a variation
in pressures between corresponding locations in the three

centermost passages. The disagreement is most pronounced at
the corresponding taps near the leading edges. The departure
from strict periodicity at the test cascade was attributed
to the inlet turning vanes which were spaced at two inch
intervals. Since the test blades were spaced at three inch
intervals, periodicity of the combined arrangement would occur
over a spatial period of 6 inches, or two blade spaces.

At the high blade loading (higher diffusion factors) the
lack of periodicity was still evident, but was less pronounced.
The data at positive incidence angles in Figs. 34-36, 39-41,
44-46 show more nearly periodic outlet conditions than is
seen in Figs. 20-24 and 27-31 for negative incidence angles.
However, in each of the former three sets of figures it is
evident that the data over the positive incidence angles in
one of the three passages departs detectibly from the data
over the remaining two passages. The surface pressure varia-
tion between adjacent blades is still apparent (Figs. 33, 38
and 43) with the largest variation again near the leading
edge.

If only the data at reference and positive incidence angles
were available, the flow might be thought to be periodic to
within reasonable tolerances. It is only in the data at
negative incidence angles that the lack of periodicity becomes
obvious. A reexamination of all the data then reveals that
the effect is progressive. As the cascade is increasingly
loaded, the preexisting inlet wake profiles tend to diminish,
possibly under the influence of the increasingly adverse
pressure gradient.

D. BLADE PERFORMANCE DATA

Figures 73 through 82 show detailed plots of the pressure
and velocity distributions over the centermost blade for
each incidence angle. The leading edge stagnation point was
noted to have traversed across the leading edge tap as the
incidence angle was varied. It was also noted that the
pressure at last pressure taps on the suction and pressure
sides of the blade were always nearly the same ($=$ .2" H_2O).

Figures 83 and 84 show the blade element performance
parameters and the AVDR variations with incidence and diffu-
sion factor. All trends qualitatively follow the results
given in Ref. 1. It is noted particularly that the AVDR is
a strong function of diffusion and/or incidence. Since the
AVDR is a measure of the departure from strictly two-dimensional
flow and its magnitude depends on the interaction between the
blade and sidewall boundary layers, the need for boundary
layer removal becomes more pronounced at higher diffusion
factors. The magnitude of the AVDR obtained entirely without
boundary layer removal is thought to be promising.

The data in Fig. 85 shows that due to the variation in
inlet total pressures between adjacent passages, different loss
coefficient values were calculated depending on which passage
or passages were used in the integration. Most points ob-
tained from the three methods were seen to agree; only in
the case of $i = 2.1$ are the results inconsistent. Since the
measurements of two-dimensionality were also inconsistent

(Section VI.B above), at this incidence angle, there is reason to repeat the test. The blade performance results shown in Figs. 83-85 are considered to be preliminary in nature. They show clearly however that consistent data can be obtained over a useful range of incidence angle, and that the AVDR remains in an acceptable range.

VII. CONCLUSIONS AND RECOMMENDATIONS

Two different cascades of blades were tested in the present work.

In preliminary measurements using a cascade of fifteen C series blades with four inch spacing, inlet uniformity (with a small but well-defined periodic velocity component imposed), outlet periodicity and outlet two-dimensionality were shown to be excellent and the axial-velocity-density ratio (AVDR) was shown to range from unity to 1.04. The loss coefficient obtained at reference incidence angle agreed well with published data. At incidence angles 10° greater and 10° less than reference incidence angle the loss coefficient increased substantially. The quality of the results obtained with the C Series cascade led to the selection of a similar aspect ratio (~2.0) for the second cascade.

The solidity required in the second cascade (1.67) of DCA blades resulted in a geometry of 20 blades with 3 inch spacing to maintain the aspect ratio close to 2.0. From a program of 5 tests of the DCA cascade at different air incidence angles, the following conclusions were drawn concerning the test conditions, the test procedures and the blade performance measurements obtained:

1. The inlet flow was uniform in direction and of uniform static pressure, but with an imposed variation in velocity and stagnation pressure resulting from the wakes of inlet guide vanes.

2.   Excellent periodicity was found over pairs of test
blades, whereas departures from strictly periodic conditions
were detected from one blade passage to another. This was
explained as being the result of the guide vane wakes being
separated at two inch intervals and entering the test cas-
cade with 3 inch blade spacing. The departure from period-
icity decreased significantly as the blade loading was
increased.

3.   An acceptable region of spanwise uniformity was found
downstream at midspan (over 30-50% of span), at all condi-
tions tested. The AVDR ranged from unity to 1.11 as the
loading was increased.

4.   Blade forces calculated from the integration of surface
pressure measurements agreed well in magnitude with blade
forces deduced from probe survey data, and were close in
direction to the theoretical direction for two-dimensional
incompressible flow without friction.

5.   The direction of the blade force deduced from probe
survey data departed significantly from the theoretical
direction for two-dimensional flow as the incidence became
negative. A more detailed review of the data and data reduc-
tion are required to explain this departure.

6.   The data obtained for pressure rise and deviation angle
(as well as AVDR) were well behaved with incidence angle.
However, the values obtained for the loss coefficient depended
to a degree on the interval used in the integration of the
outlet survey data. This was consistent with the observed

departure from strict periodicity. The uncertainty in the loss coefficient at different incidence angles ranged from ±5 to ±25%.

7. Complete pressure distributions were obtained over the centermost blade at each test condition.

8. The mechanical adjustments necessary to produce uniform static pressure at inlet and outlet at the start of a test were straightforward, and required only two or three minutes to complete. The hardware adjustments between tests associated with change of incidence angle required three hours to complete.

9. Probe traverse and data acquisition procedures were reduced to a straightforward routine, taking approximately two hours of test time for each incidence angle.

The following recommendations are made:

1. The inlet guide vane arrangement should be modified so that guide vanes are placed at 1 inch intervals. This can be accomplished using the right and left hand sets of guide vanes presently on-hand. A second set of vanes can be mounted on 2 inch spacings from the north side wall, so that they mesh, on assembly, with the present set mounted from the south side wall. A single hand crank can be arranged to adjust the vanes in unison. The advantage of this arrangement is that periodicity at the test section will result for any test blade spacing which is a multiple of 1 inch and, equally importantly, the wakes remaining at the inlet to the test cascade will be greatly reduced. The modification

should be carried out before further measurements are attempted.

2. Repeat the tests reported herein and compare results.

3. Incorporate five more pressure taps around the leading edge and at least one more tap on the trailing edge to better describe the distribution in those critical areas.

4. Describe the flow structure using flow visualization techniques in conjunction with pressure tap readings.

5. Install wall suction in the side walls, to control the AVDR and thereby examine its effect.

6. Replace the upper yaw mechanism with a manual system to improve the angular resolution.

7. Run tests at different inlet dynamic pressures to determine its effect.

8. Incorporate a disc memory in the data system to provide rapid access to programs and data and simplify continuity between investigators.
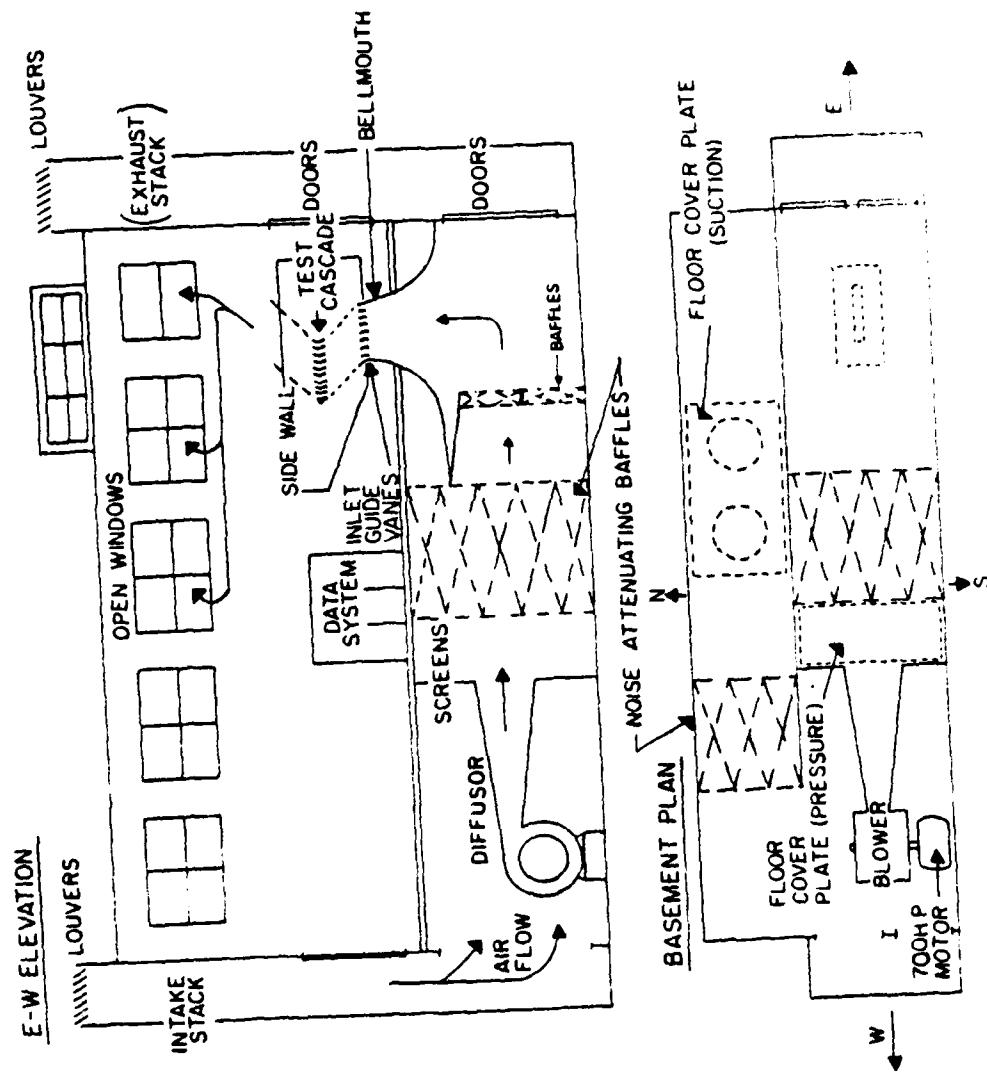
Fig. 1. Subsonic Cascade Facility

2a)
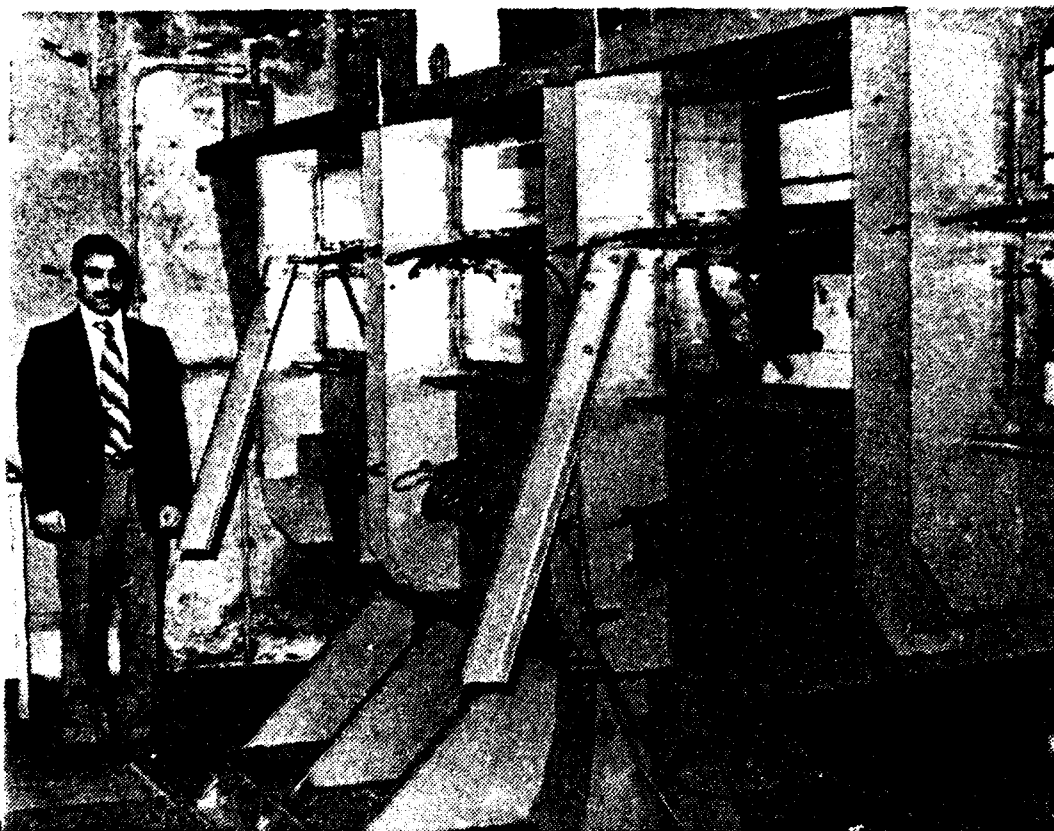
2b)
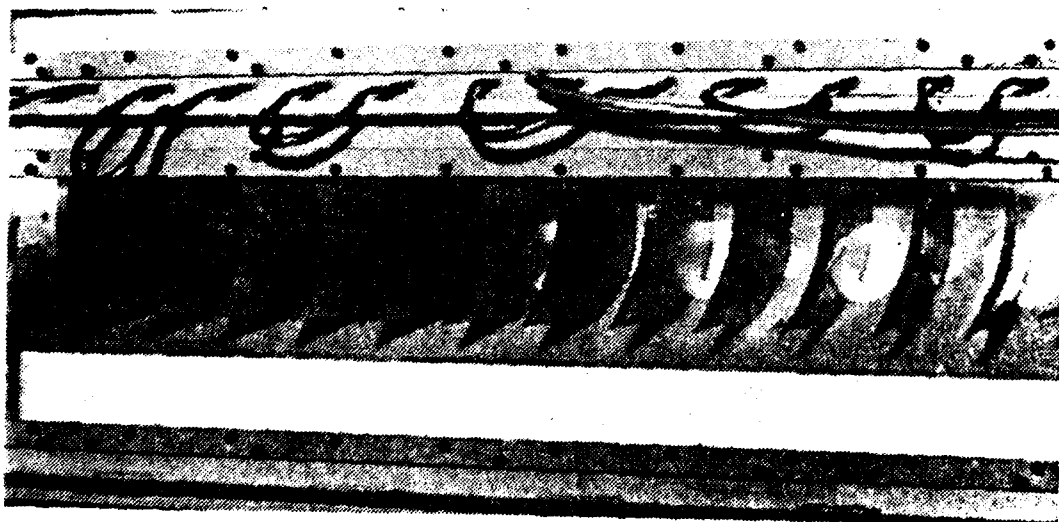
Fig. 2.   Photograph of Subsonic Cascade and Test Section
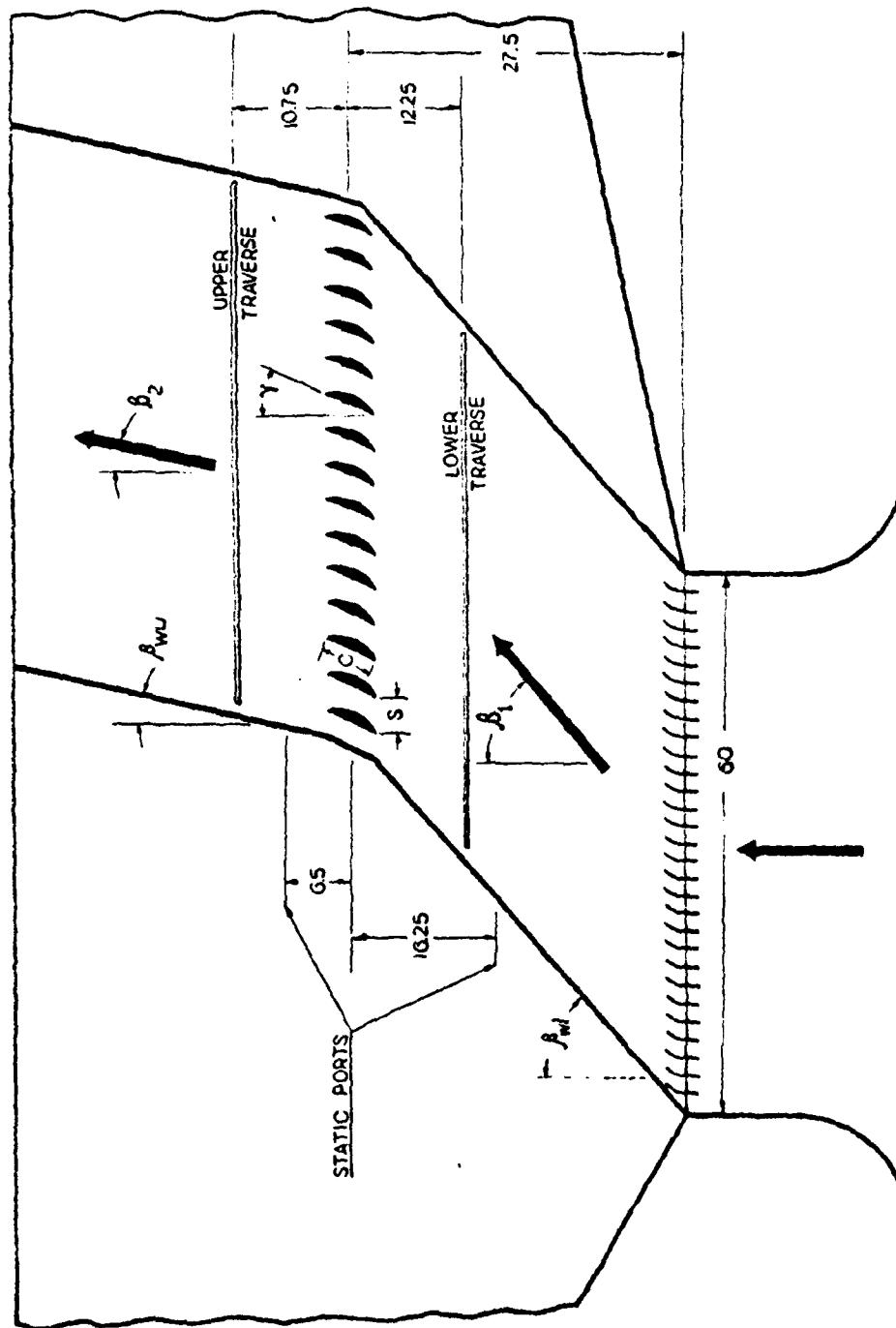
Fig. 3. Subsonic Cascade

45
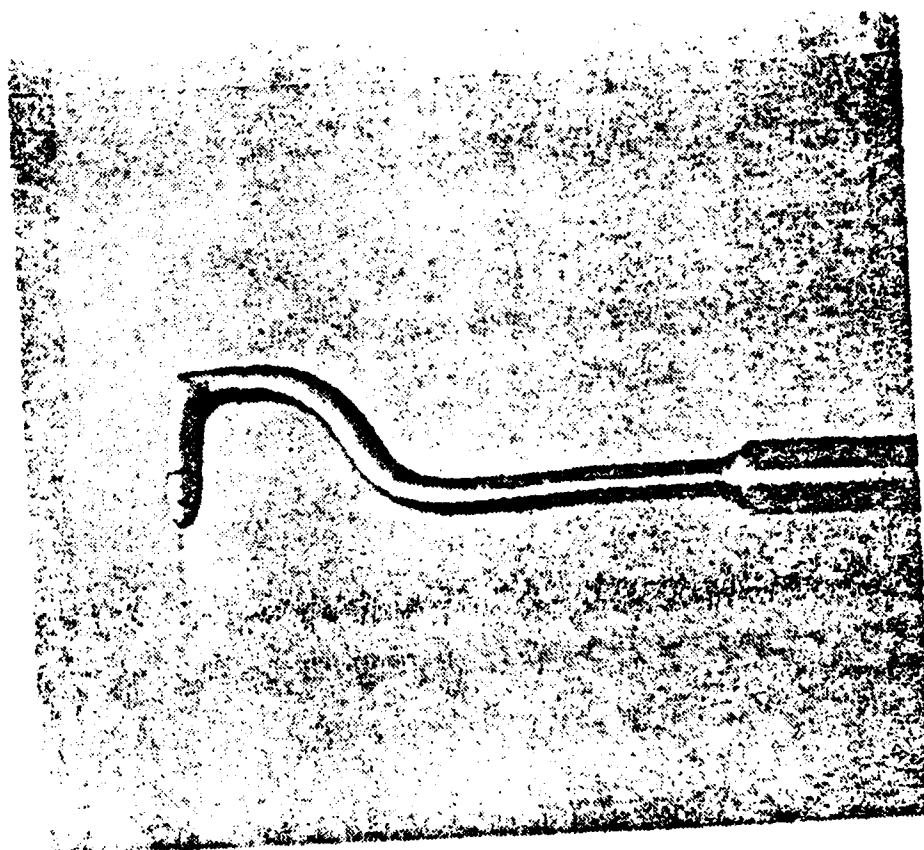
Fig. 4.   Upper Plane Survey Probe

46
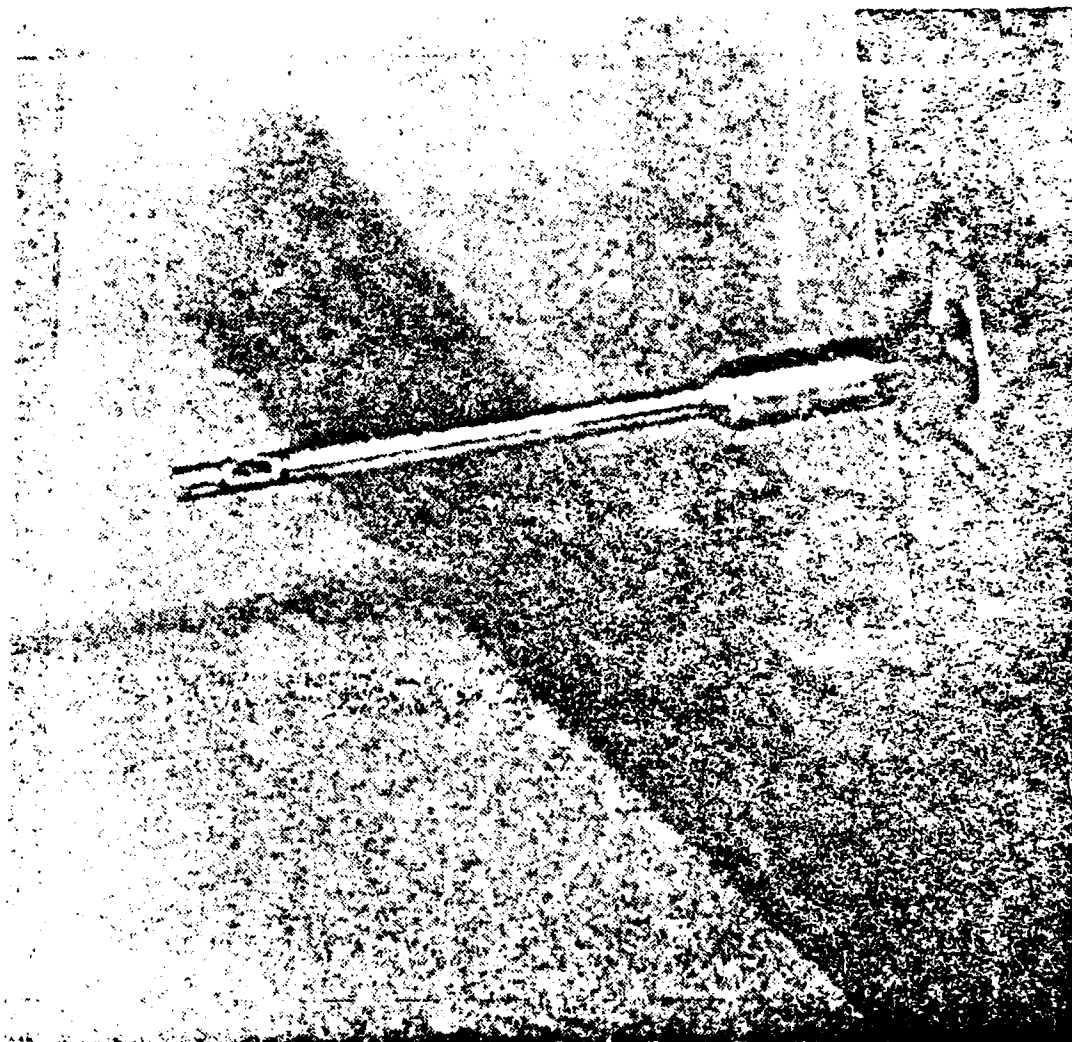
Fig. 5.   Lower Plane Survey Probe

47

EDGE DETAIL

.044 R

.021

.013

.044 R

.021

.013

4.92!

48
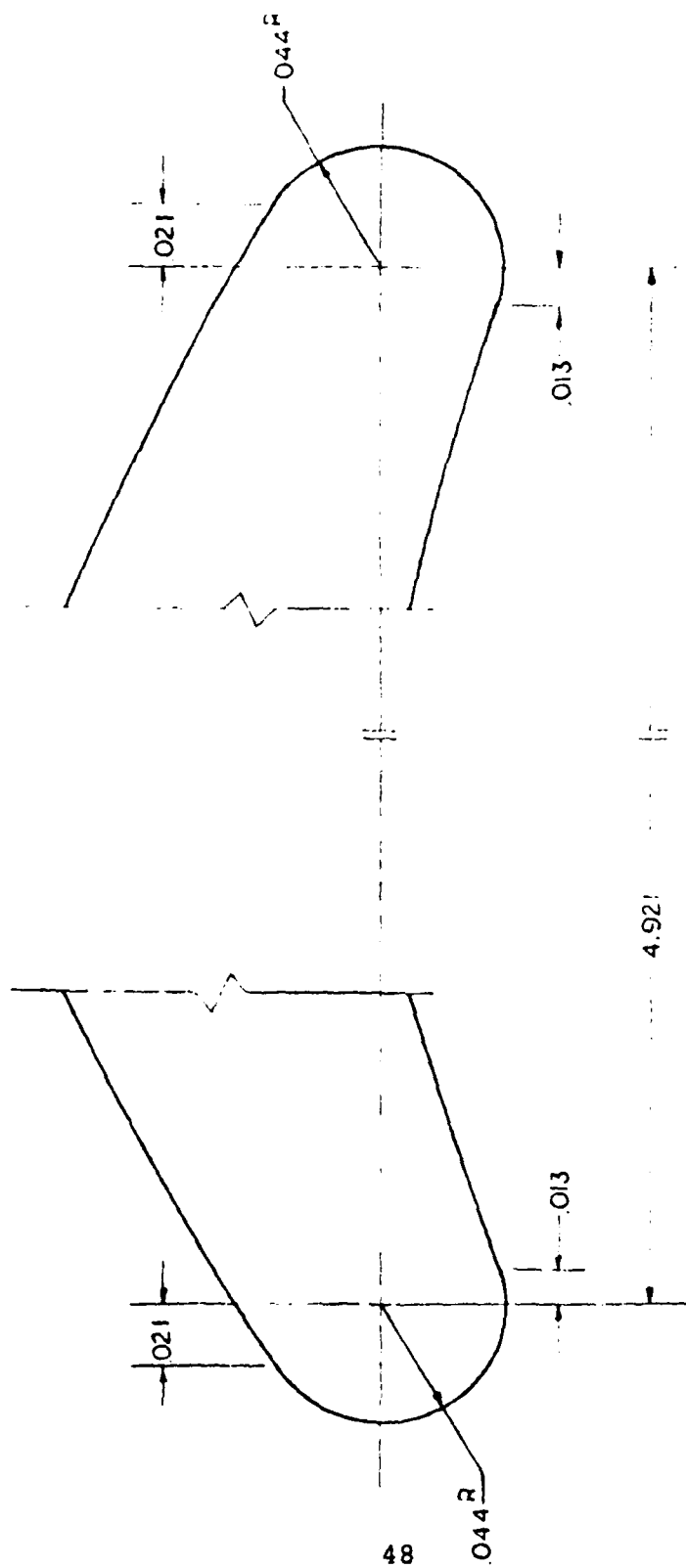
Fig. 6. Blade Edge Detail

PRESSURE TAP LOCATIONS

5.00

LEADING EDGE
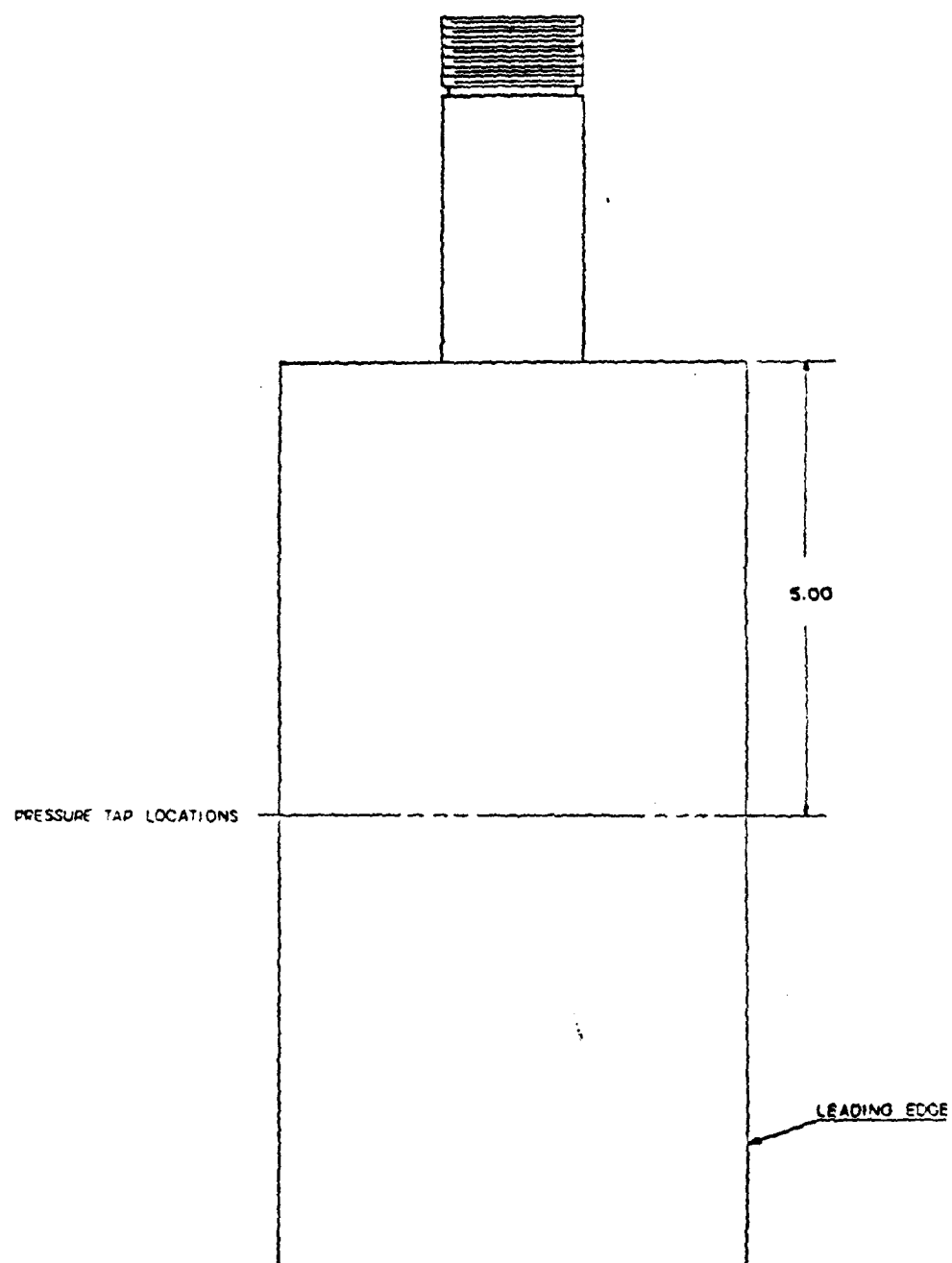
Fig. 7.   Instrumented Blade

49
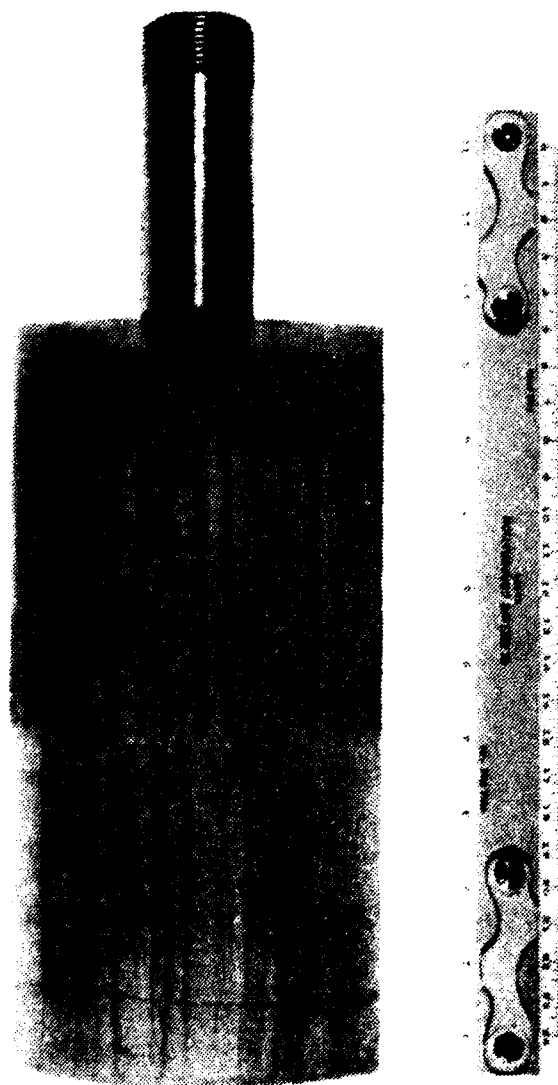
Fig. 8. Photograph of Instrumented Blade
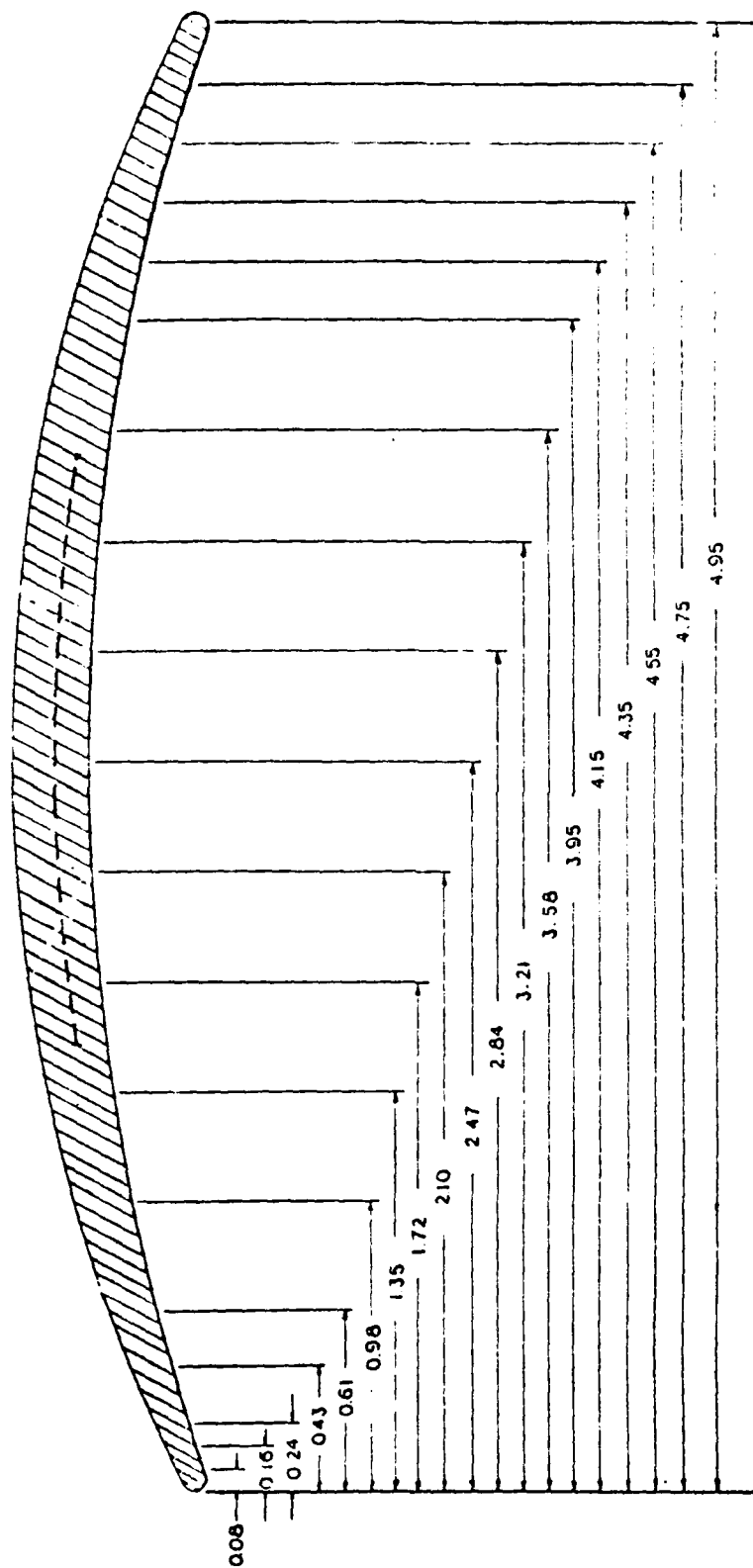
Fig. 9. Instrumented Blade Tap Locations
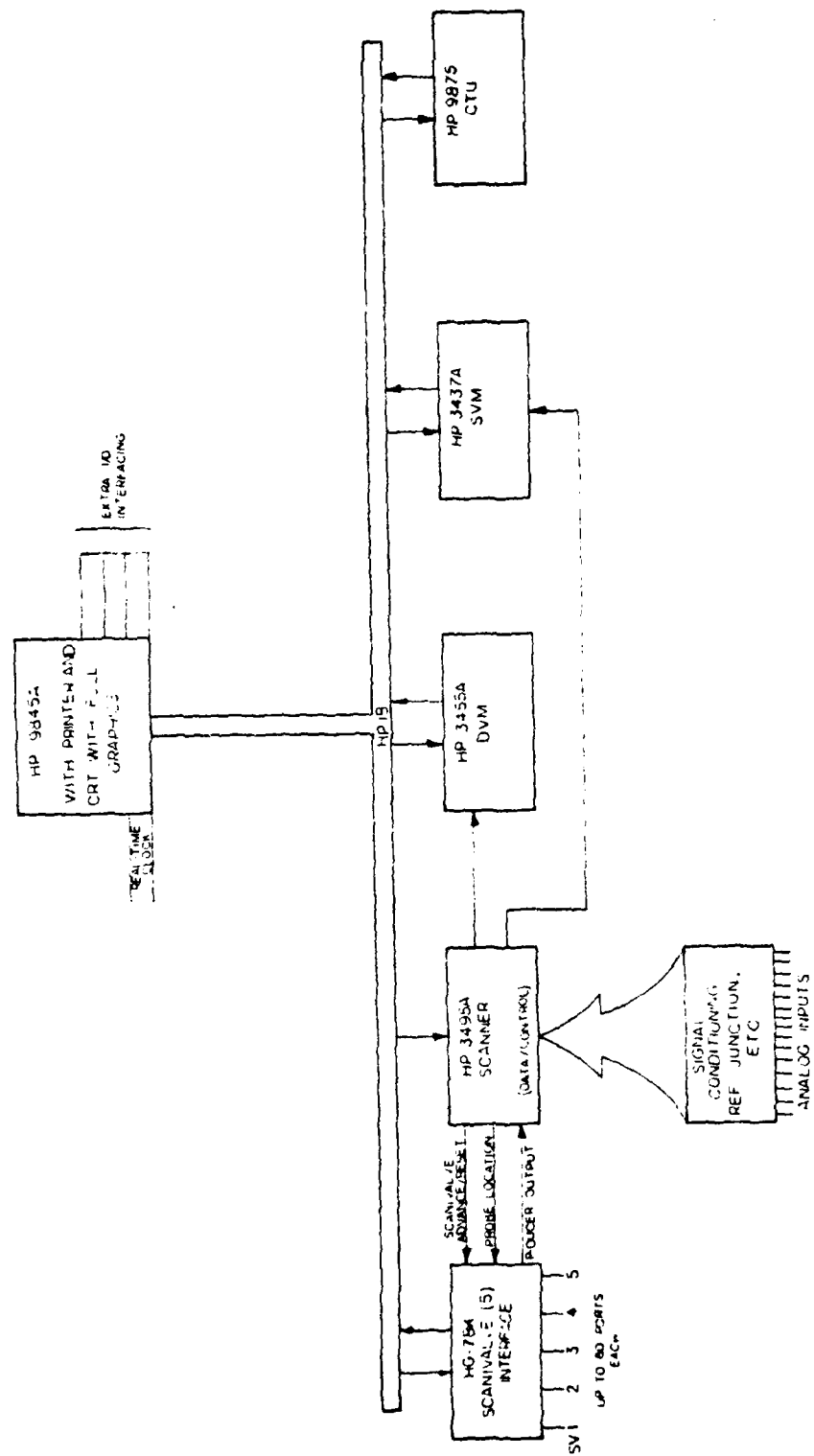
Fig. 10. Data Acquisition System
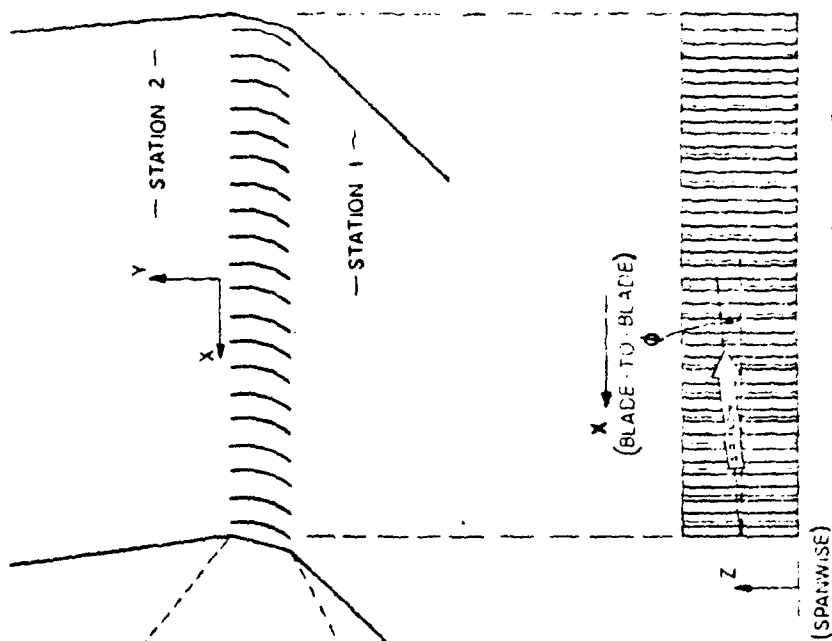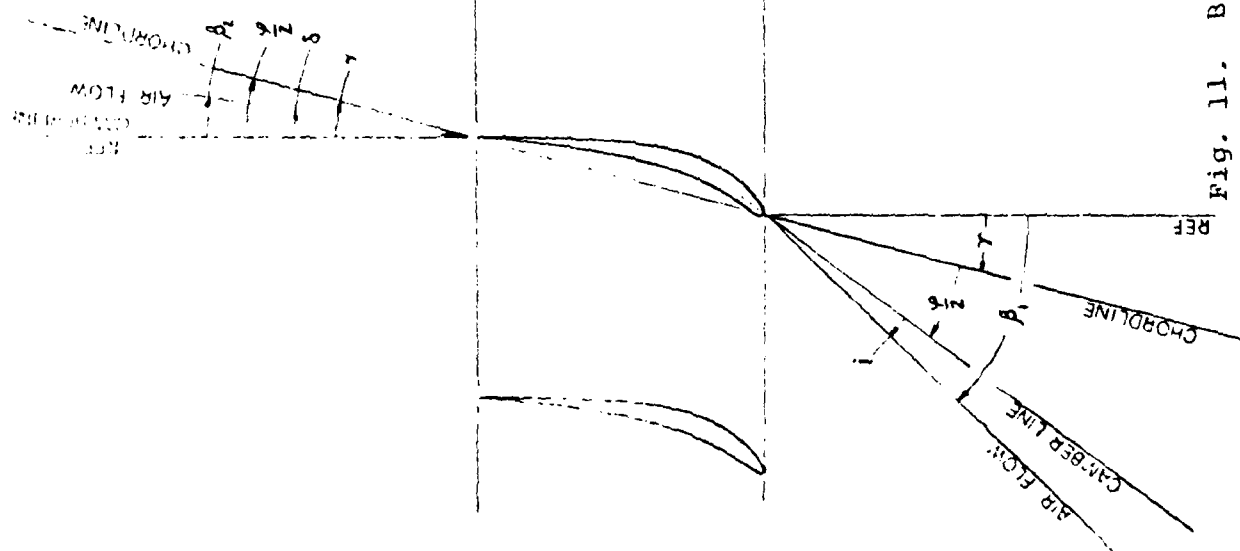
Fig. 11. Blade Angle Terminology and Cascade Coordinate System
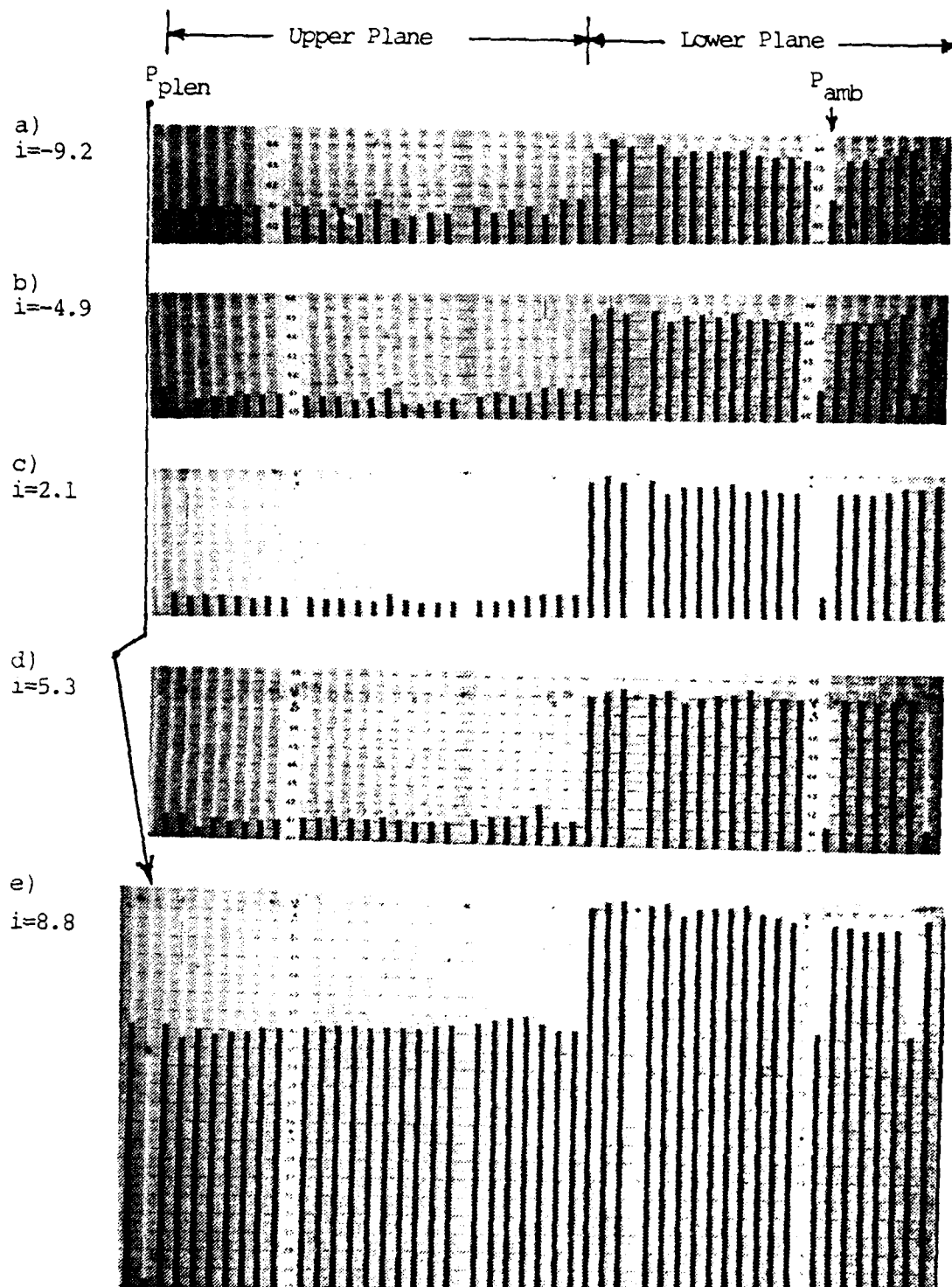
Fig. 12.   Wall Static Pressure Distributions (Lower and
           Upper Planes)
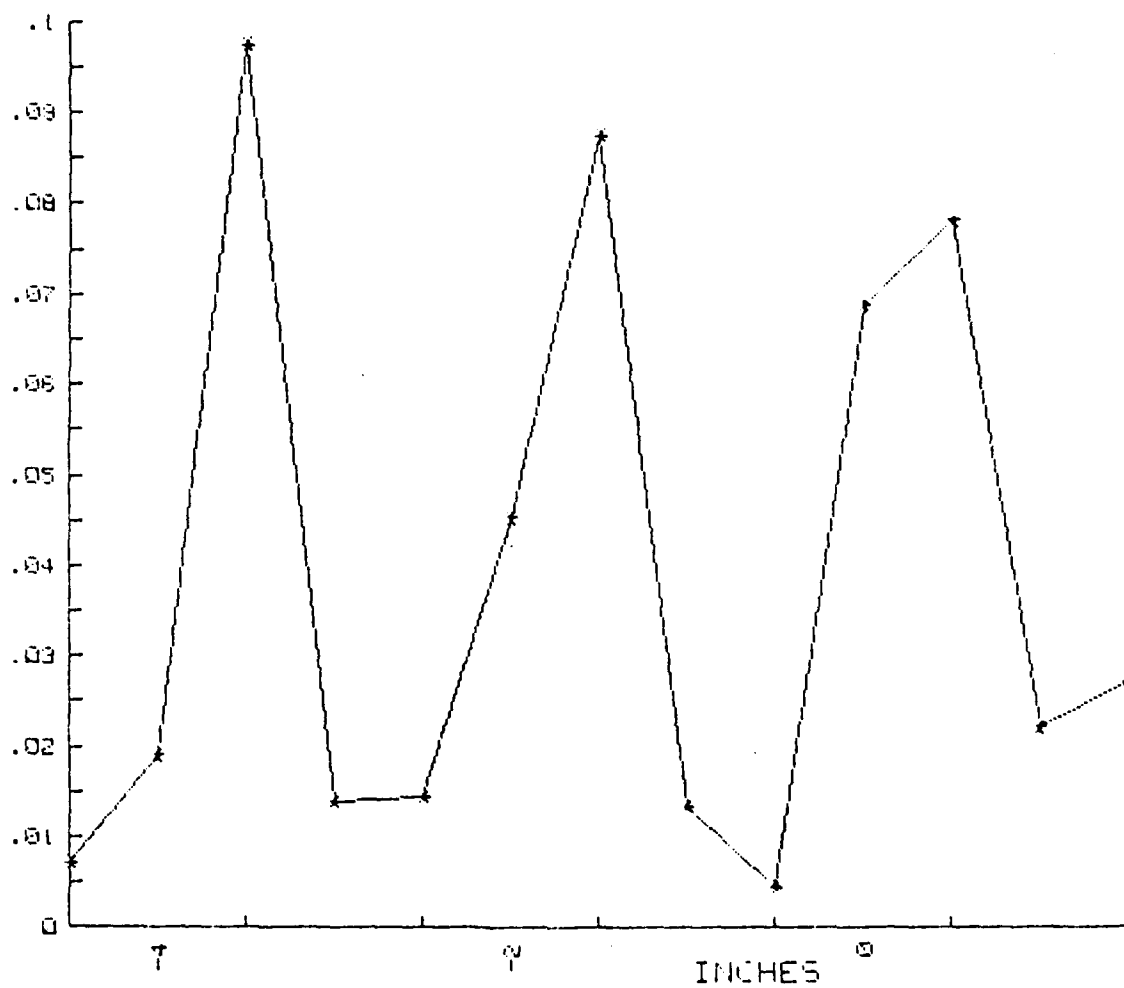
Fig. 13.   Probe Survey Data at Midspan
($i=-9.2$, $(P_{plen}-P_t/\bar{Q}_l)$, Lower Plane)

55

(Pplen-Pt)/Q1bar
LOWER PLANE MIDSPAN (i=-4.9)

Fig. 14.   Probe Survey Data at Midspan
(i=-4.9, $(P_{plen}-P_t)/\bar{Q}_1$, Lower Plane)

56

(Pplen-Pt)/Q1bar
LOWER PLANE MIDSPAN (i=2.1)

Fig. 15. Probe Survey Data at Midspan
($i=2.1$, $(P_{plen}-P_t)/\bar{Q}_1$, Lower Plane)

(Pplen-Pt)/Q1bar
LOWER PLANE MIDSPAN (i=5.3)

INCHES
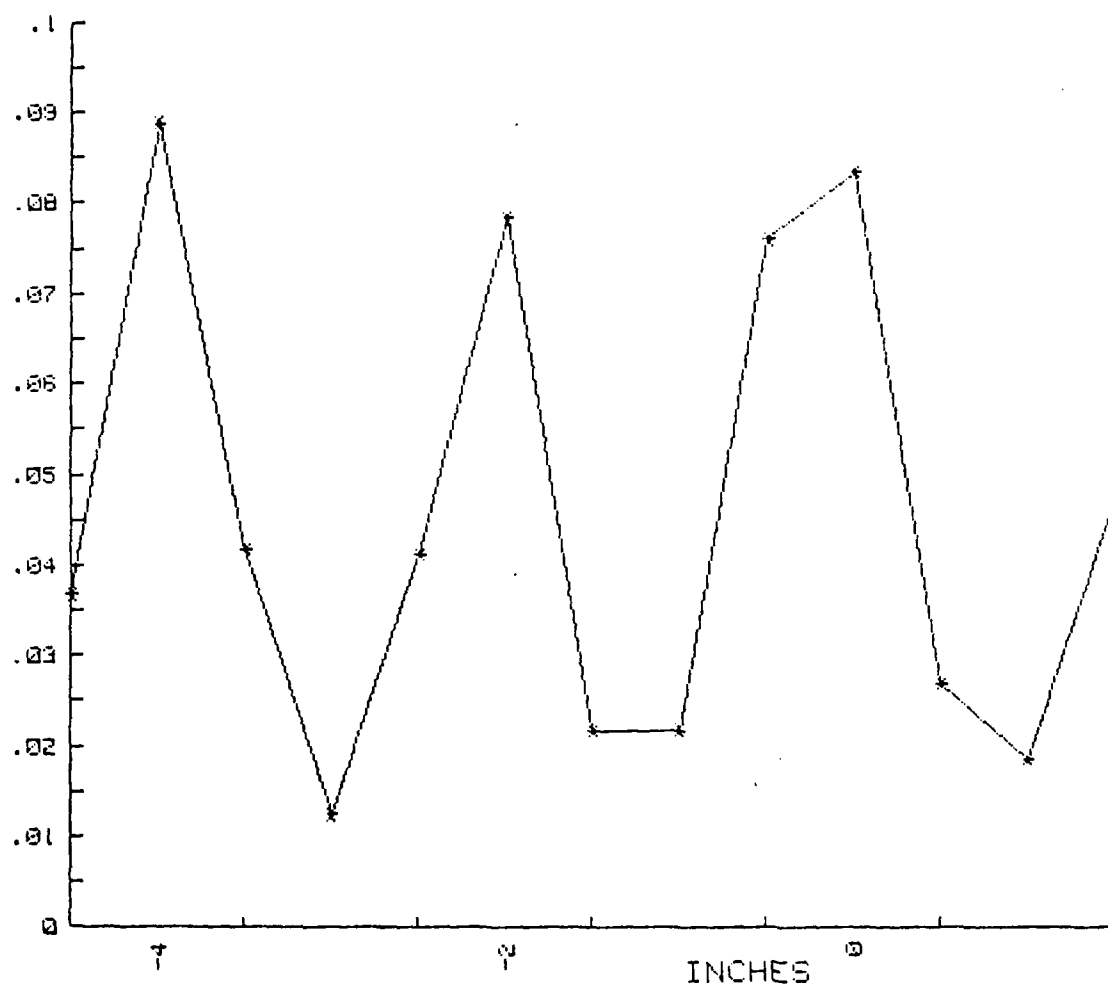
Fig. 16.   Probe Survey Data at Midspan
            (i=5.3, $(P_{plen}-P_t)/\bar{Q}_1$, Lower Plane)

58

(Pplen-Pt)/Q1bar
LOWER PLANE MIDSPAN (i=8.8)
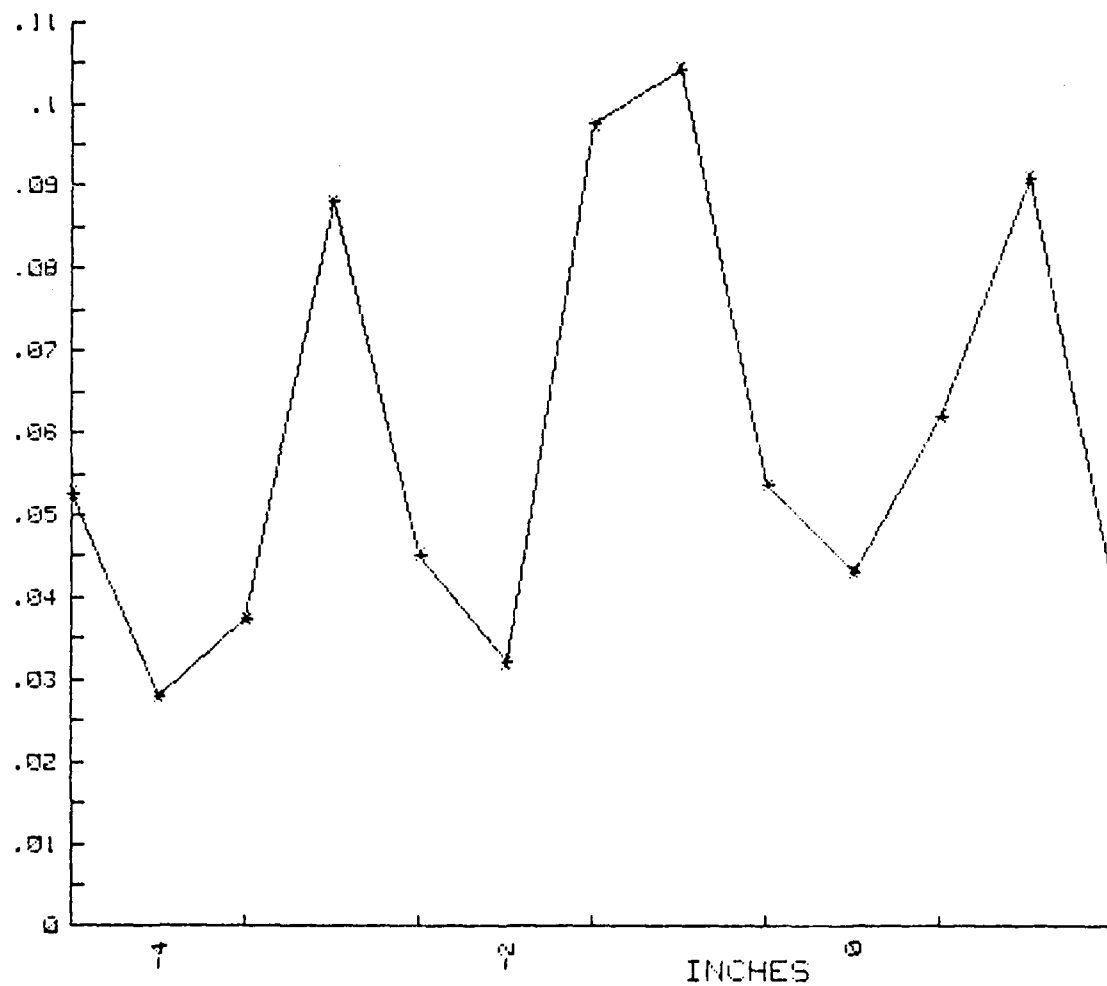
Fig. 17.   Probe Survey Data at Midspan
           (i=8.8, $(P_{plen}-P_t)/\bar{Q}_1$, Lower Plane)

59

Pt-Ps (in H2O)
LOWER PLANE

SPAN (INCHES)
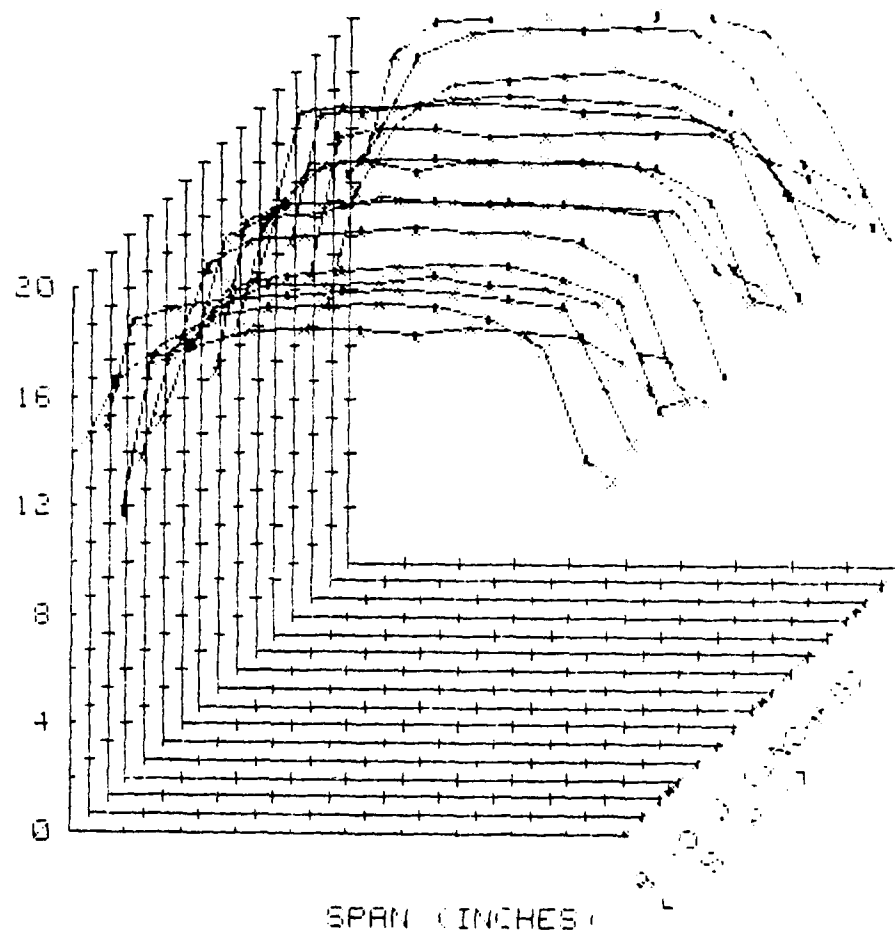
Fig. 18. Rake Impact Pressure at Lower Plane
(3-D Presentation)

60

SYMBOLS:

Blade	LEFT	CENTER	RIGHT
Pressure Surface	L	*	R
Suction Surface	l	+	r

Cp1 vs X/C
THREE CENTERMOST BLADES OVERLAYED
(i=-9.2)
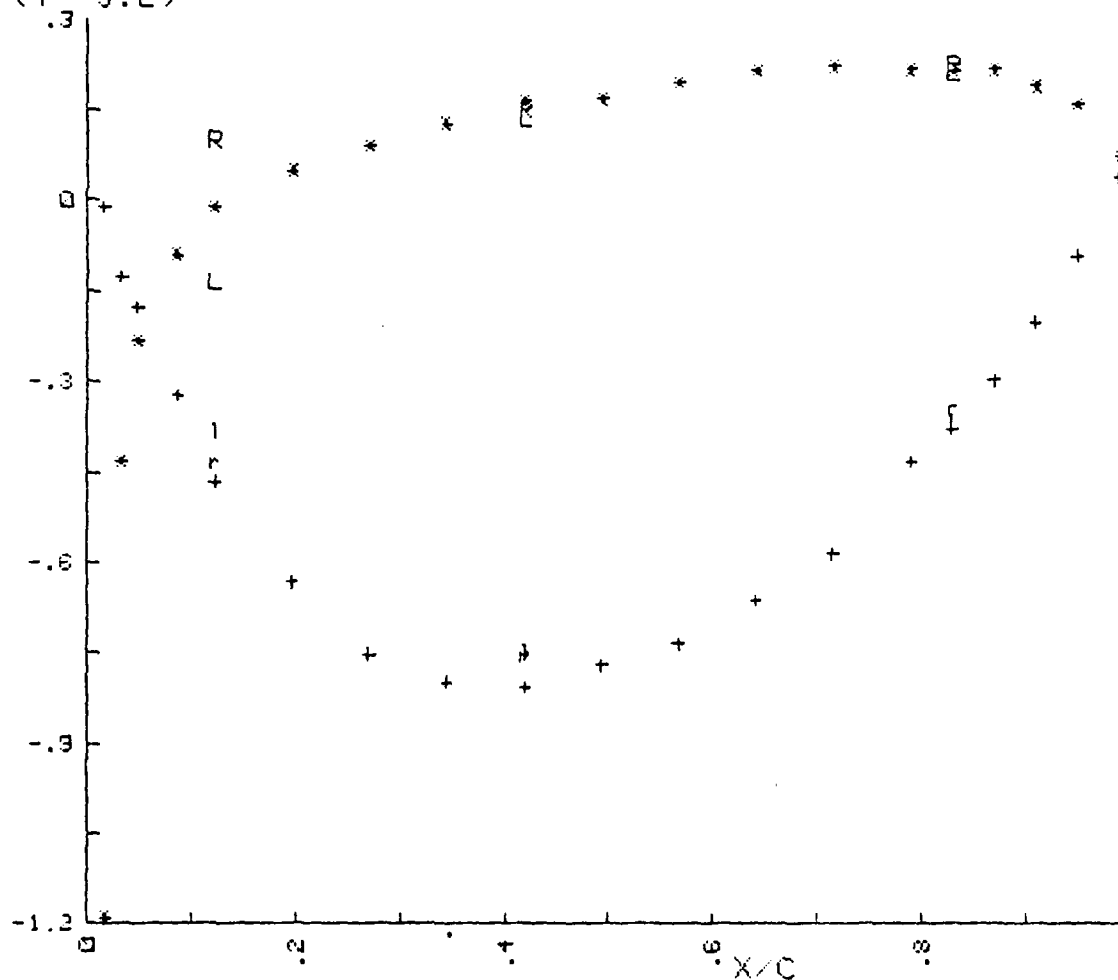
Fig. 19. Blade Surface Pressure Distribution
          (i=-9.2)

61

Fig. 20.   Probe Survey Data at Midspan
            (i=-9.2, $(P_{plen}-P_t)/\overline{Q}_1$, Upper Plane)

62

Fig. 21.   Probe Survey Data at Midspan
           (i=-9.2, $(P_{plen}-P_t)/\bar{Q}_1$, Upper Plane)

63

Fig. 22.   Probe Survey Data at Midspan
(i=-9.2, X/X, Upper Plane)

64

Fig. 23.   Probe Survey Data at Midspan
(i=-9.2, X/X̄, Upper Plane)

65

(P_s-P_w) .01bar
UPPER PLANE MIDSPAN (i=-9.2)
(THREE PASSAGES OVERLAYED)
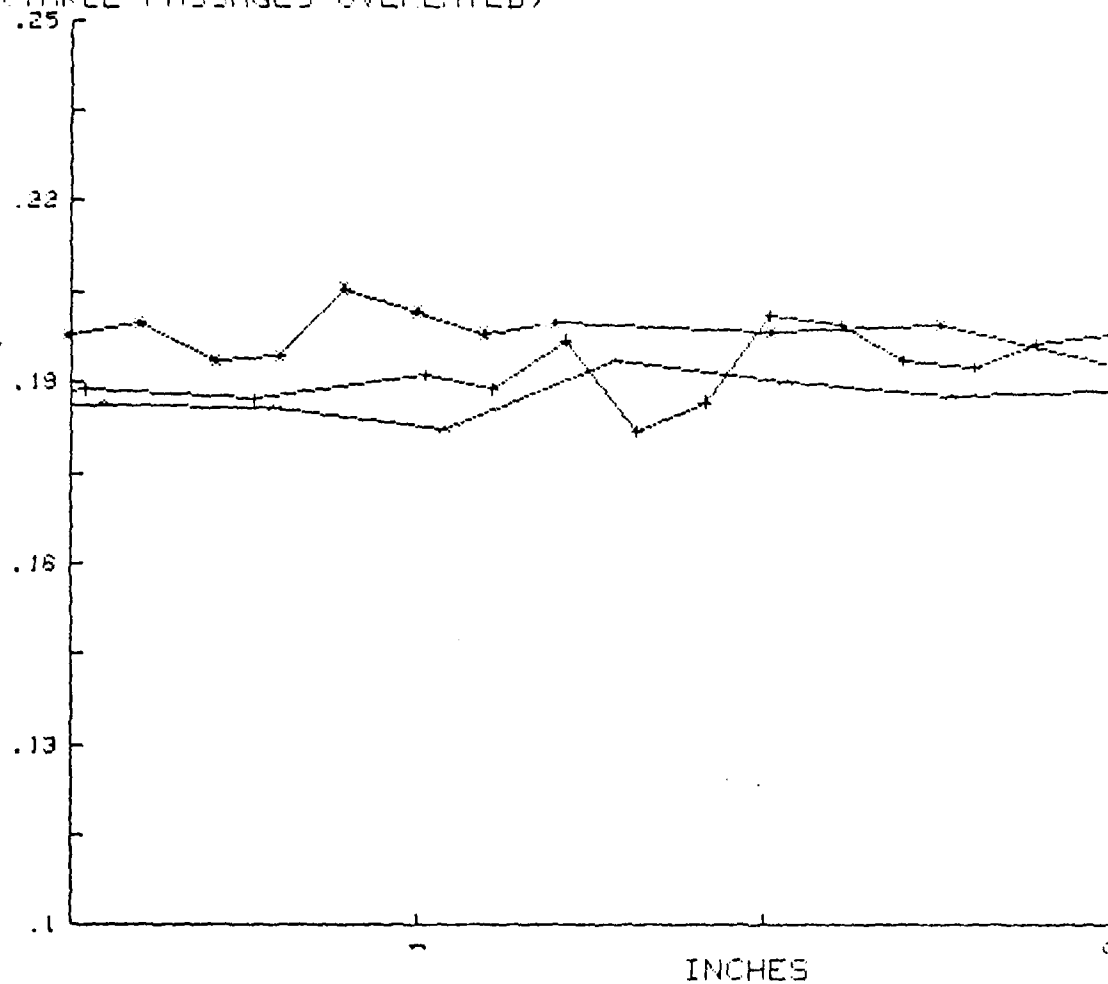
Fig. 24. Probe Survey Data at Midspan
(i=-9.2, $(P_s-P_{w\ell})/\overline{Q}_1$, Upper Plane)

66

OUTLET ANGLE
UPPER PLANE MIDSPAN (i=-9.2)
(FOUR PASSAGES OVERLAYED)
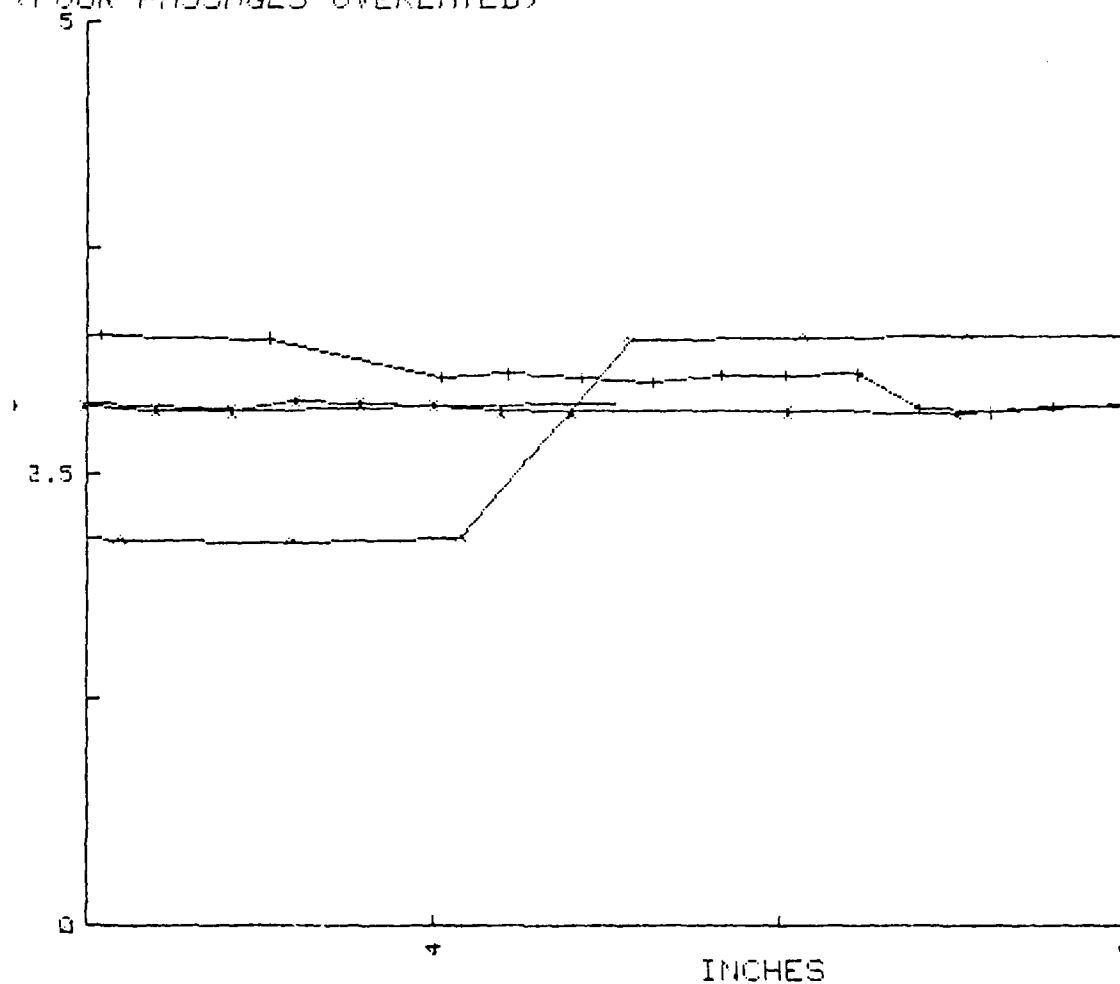
Fig. 25.   Probe Survey Data at Midspan
           (i=-9.2, Outlet Angle, Upper Plane)

67

SYMBOLS:

Blade	LEFT	CENTER	RIGHT
Pressure Surface	L	*	R
Suction Surface	l	+	r

Cp1 vs X/C
THREE CENTERMOST BLADES OVERLAYED
(i=-4.9)
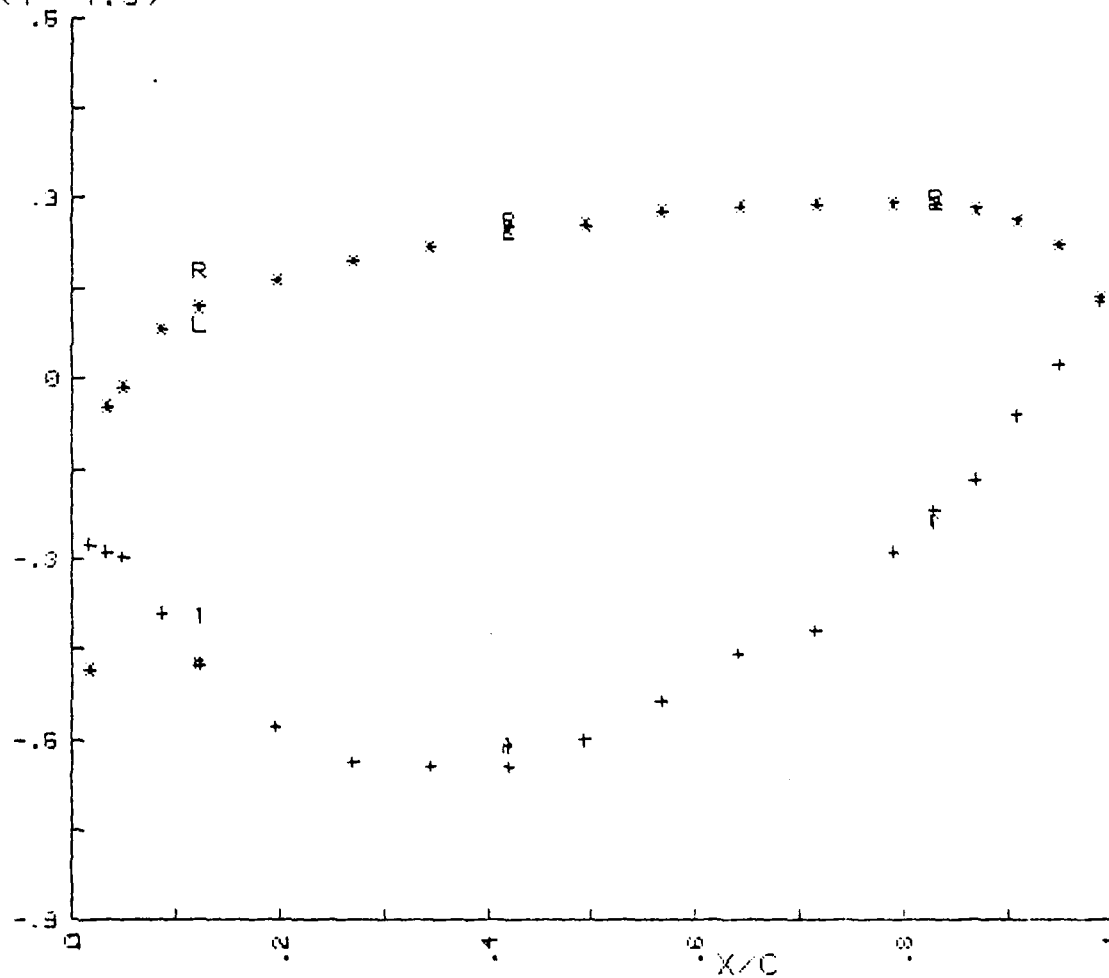
Fig. 26. Blade Surface Pressure Distribution
            (i=-4.9)

68

(Pplen-Pt)/Qlbar
UPPER PLANE MIDSPAN (i=-4.9)
(THREE PASSAGES OVERLAYED)
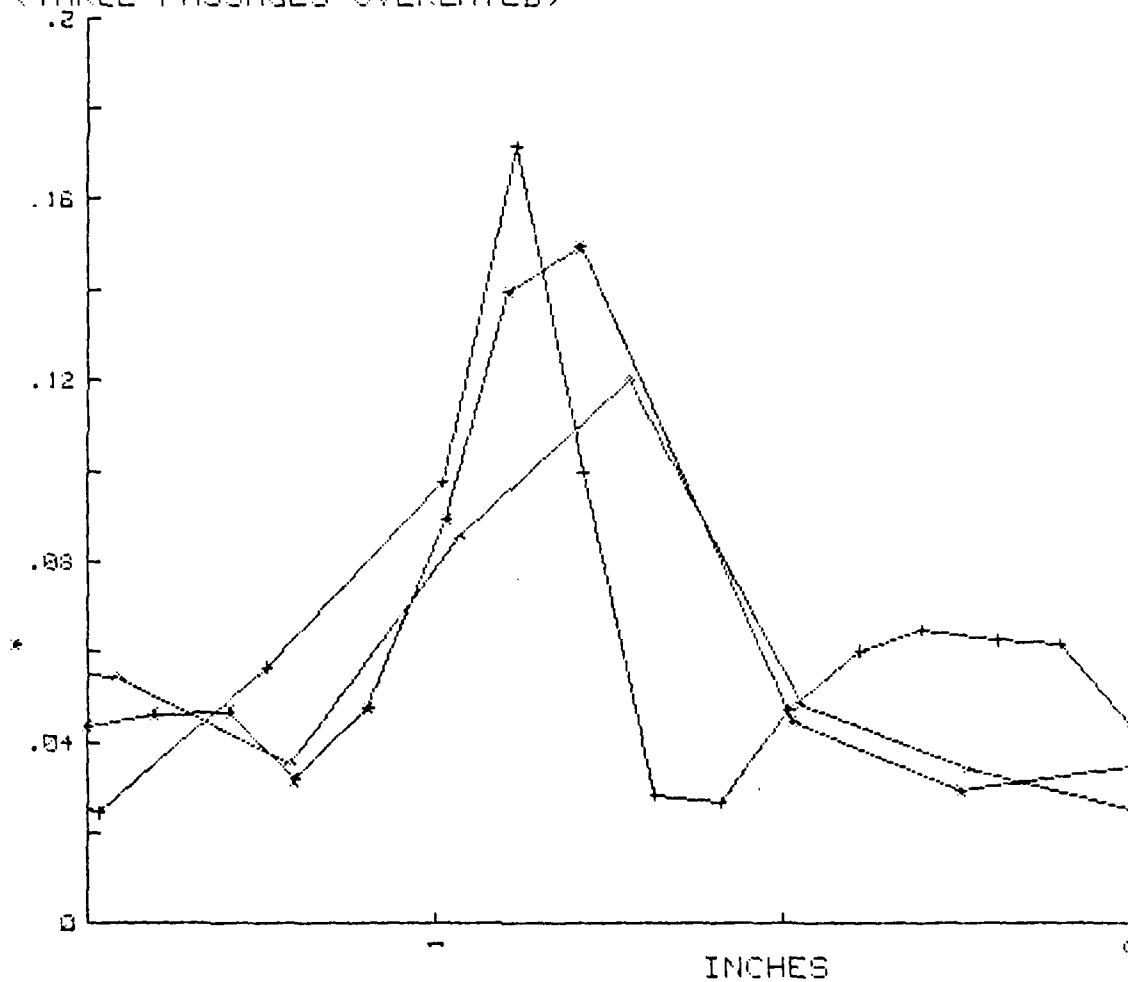
Fig. 27.   Probe Survey Data at Midspan
(i=-4.9, $(P_{plen}-P_t)/\bar{Q}_1$, Upper Plane)

69

Fig. 28.   Probe Survey Data at Midspan
($i=-4.9$, $(P_{plen}-P_t)/\bar{Q}_1$, Upper Plane)

70

Fig. 29. Probe Survey Data at Midspan
(i=-4.9, X/X̄, Upper Plane)

X/Xbar
UPPER PLANE MIDSPAN (i=-4.9)
TWO PASSAGES OVERLAYING TWO PASSAGES
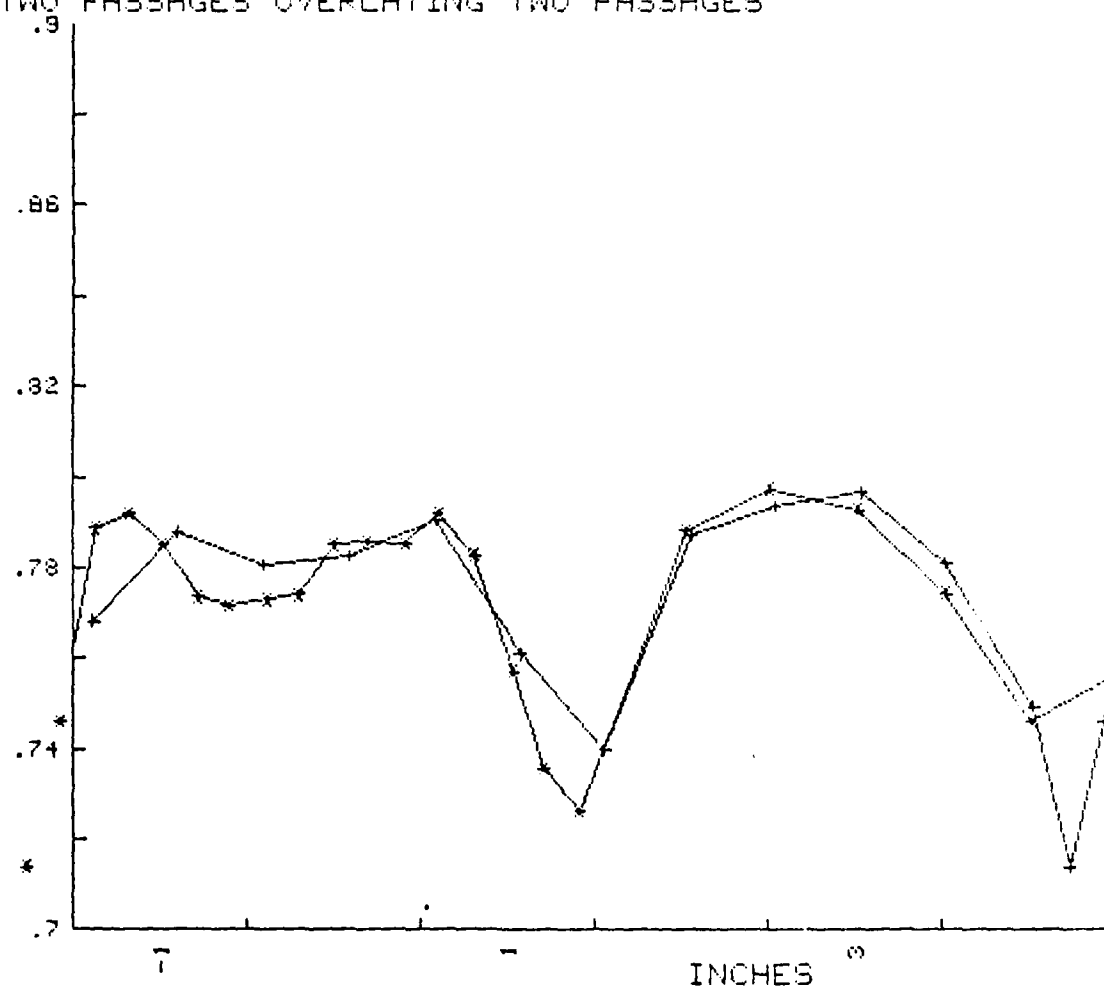
Fig. 30.   Probe Survey Data at Midspan
            (i=-4.9, X/X̄, Upper Plane)

(Ps-Pwl)/Q1bar
UPPER PLANE MIDSPAN (i=-4.9)
(THREE PASSAGES OVERLAYED)

INCHES
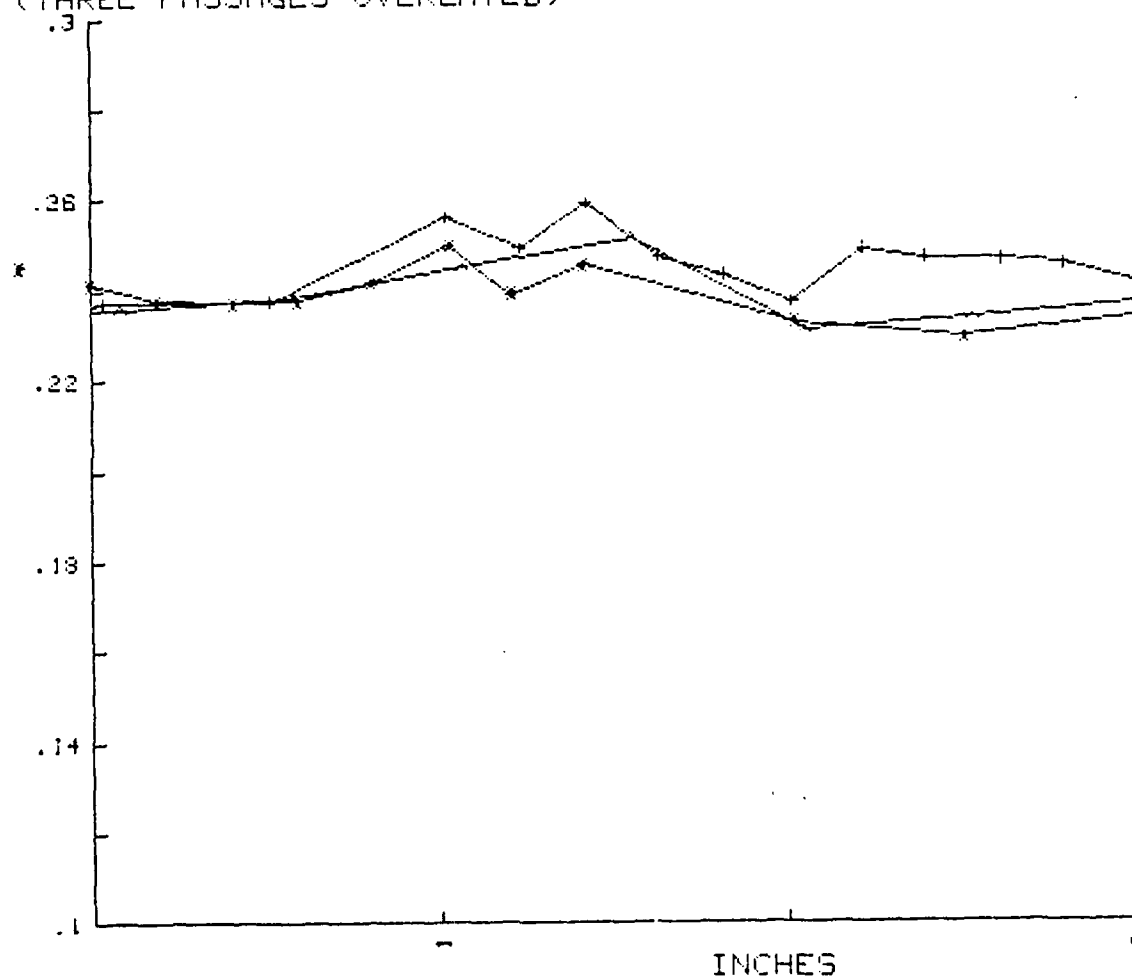
Fig. 31.   Probe Survey Data at Midspan
(i=-4.9, $(P_s-P_{w\ell})/\overline{Q}_1$, Upper Plane)

73

OUTLET ANGLE
UPPER PLANE MIDSPAN (i=-4.9)
(FOUR PASSAGES OVERLAYED)
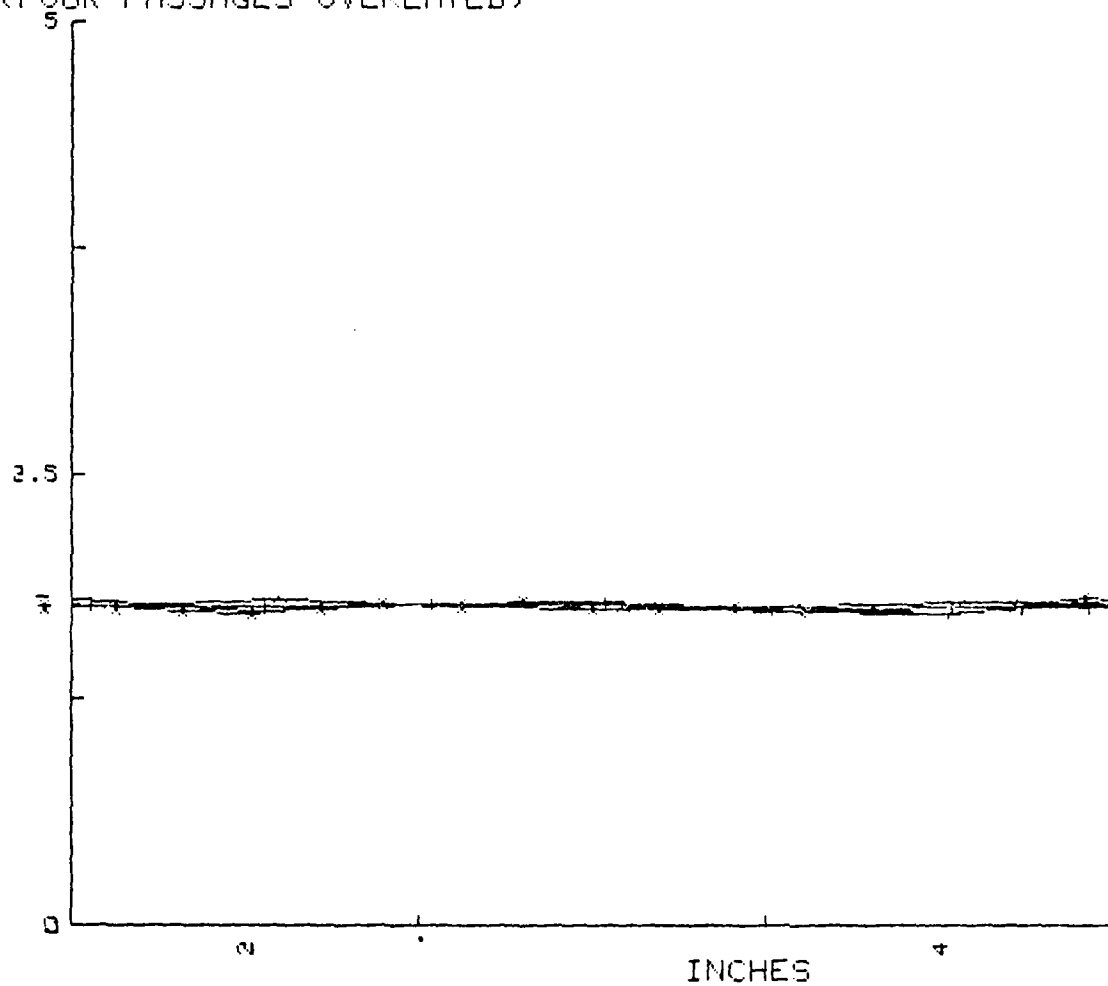
Fig. 32.   Probe Survey Data at Midspan
          (i=-4.9, Outlet Angle, Upper Plane)

SYMBOLS:

Blade	LEFT	CENTER	RIGHT
Pressure Surface	L	*	R
Suction Surface	l	+	r

Cp1 vs X/C
THREE CENTERMOST BLADES OVERLAYED
(i=2.1)
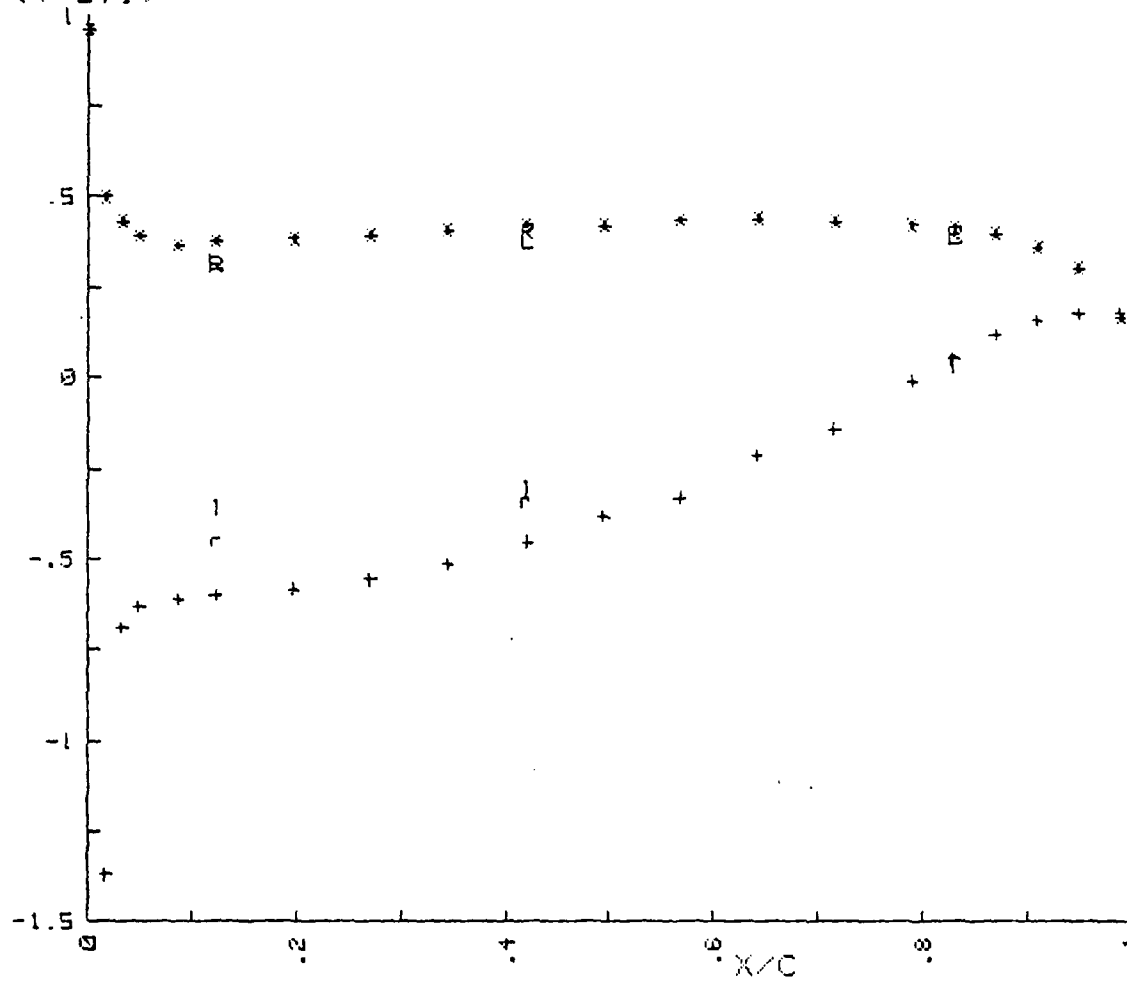
Fig. 33.   Blade Surface Pressure Distribution
(i=2.1)

75

(Pplen-Pt)/Q1bar
UPPER PLANE MIDSPAN (i=2.1)
(THREE PASSAGES OVERLAYED)

INCHES
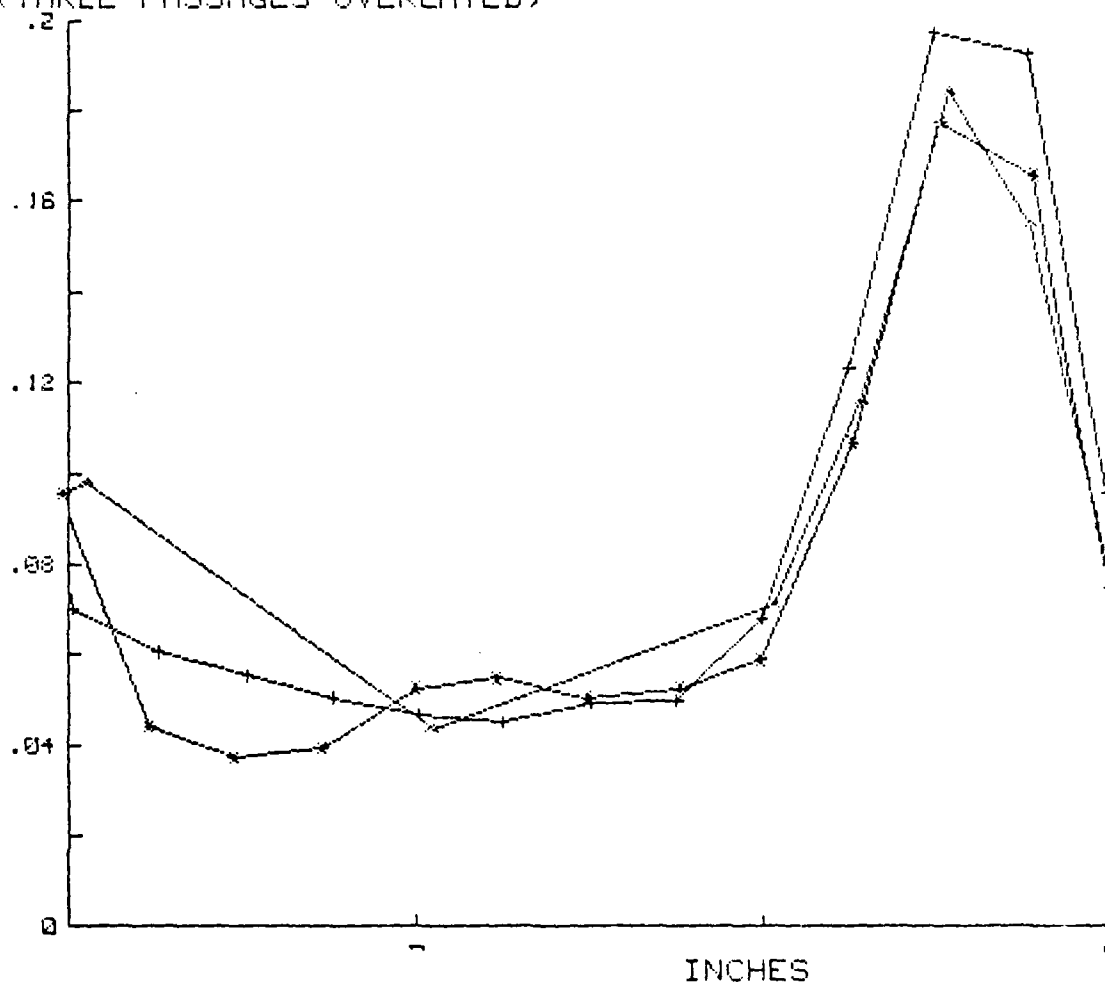
Fig. 34.   Probe Survey Data at Midspan
(i=2.1, $(P_{plen}-P_t)/\bar{Q}_1$, Upper Plane)

76

X/Xbar
UPPER PLANE MIDSPAN (i=2.1)
(THREE PASSAGES OVERLAYED)
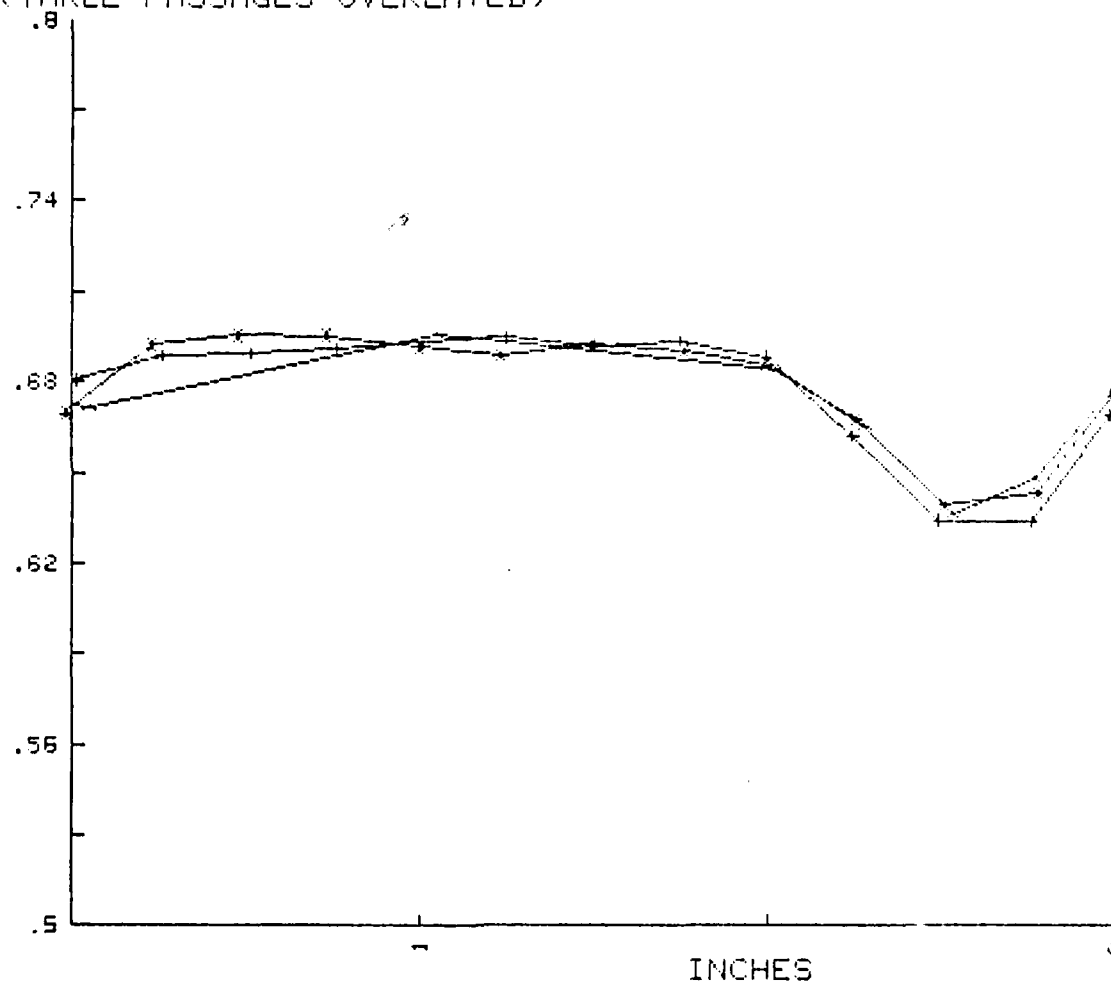
Fig. 35.   Probe Survey Data at Midspan
(i=2.1, X/$\overline{X}$, Upper Plane)

77

(Ps-Pwl)/Qlbar
UPPER PLANE MIDSPAN (i=2.1)
(THREE PASSAGES OVERLAYED)

Fig. 36.   Probe Survey Data at Midspan
           (i=2.1, $(P_s-P_{w\ell})/\overline{Q}_1$, Upper Plane)

78

OUTLET ANGLE
UPPER PLANE MIDSPAN
(THREE PASSAGES OVERLAYED) (i=2.1)
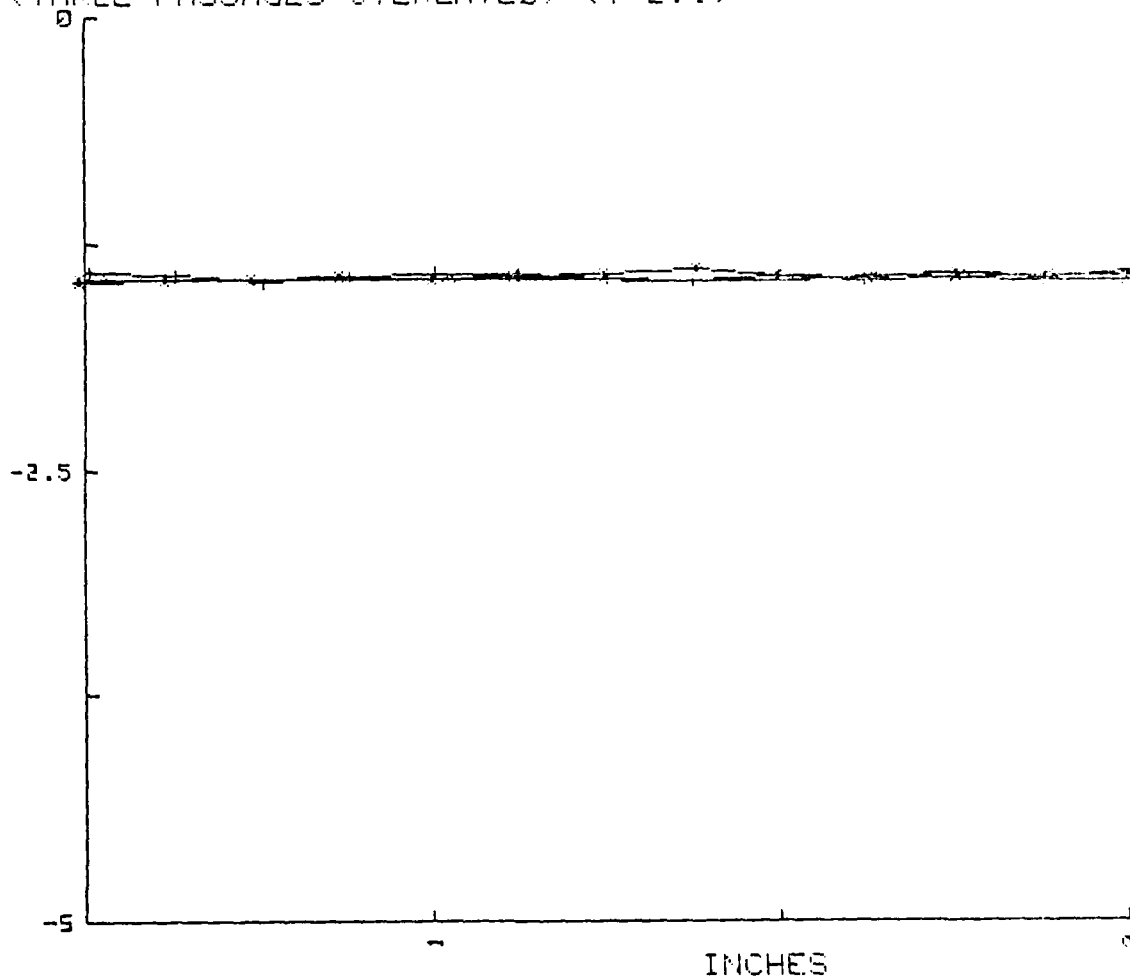
Fig. 37.   Probe Survey Data at Midspan
(i=2.1, Outlet Angle, Upper Plane)

79

SYMBOLS:

Blade	LEFT	CENTER	RIGHT
Pressure Surface	L	*	R
Suction Surface	l	+	r

Cpl vs X/C
THREE CENTERMOST BLADES OVERLAYED
(i=5.3)
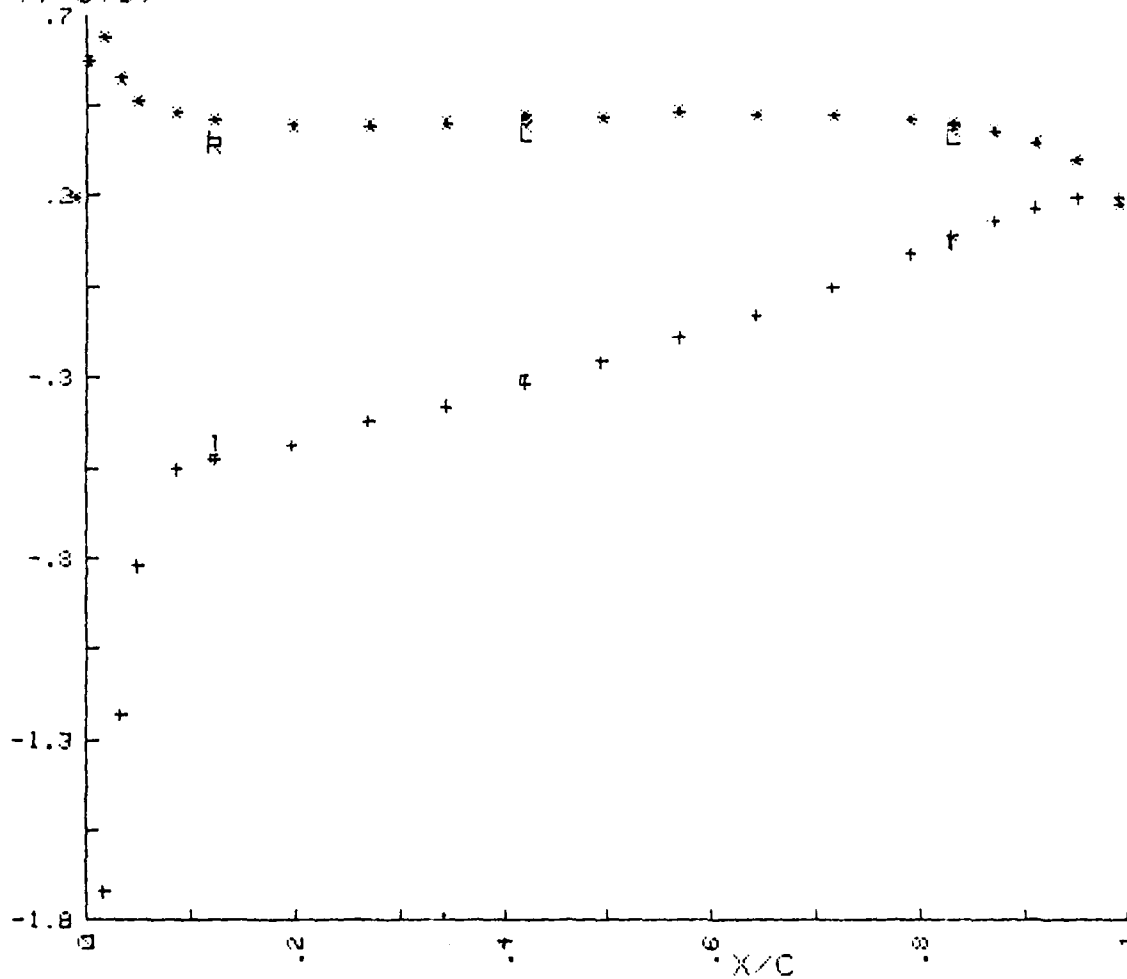
Fig. 38.   Blade Surface Pressure Distribution
(i=5.3)
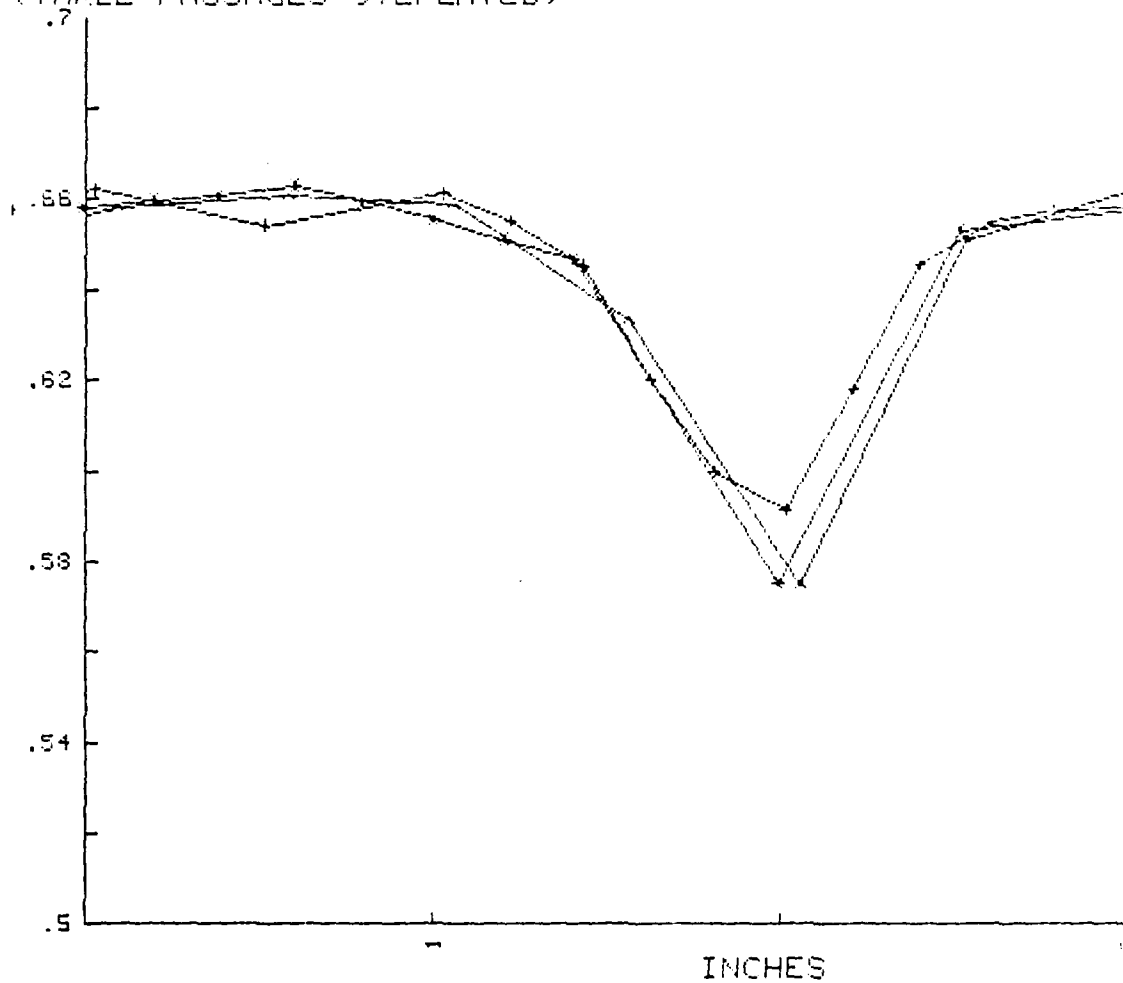
Fig. 39.   Probe Survey Data at Midspan
           (i=5.3, X/X̄, Upper Plane)

81

(Pplen-Pt)/Q1bar
UPPER PLANE MIDSPAN (i=5.3)
(THREE PASSAGES OVERLAYED)

INCHES
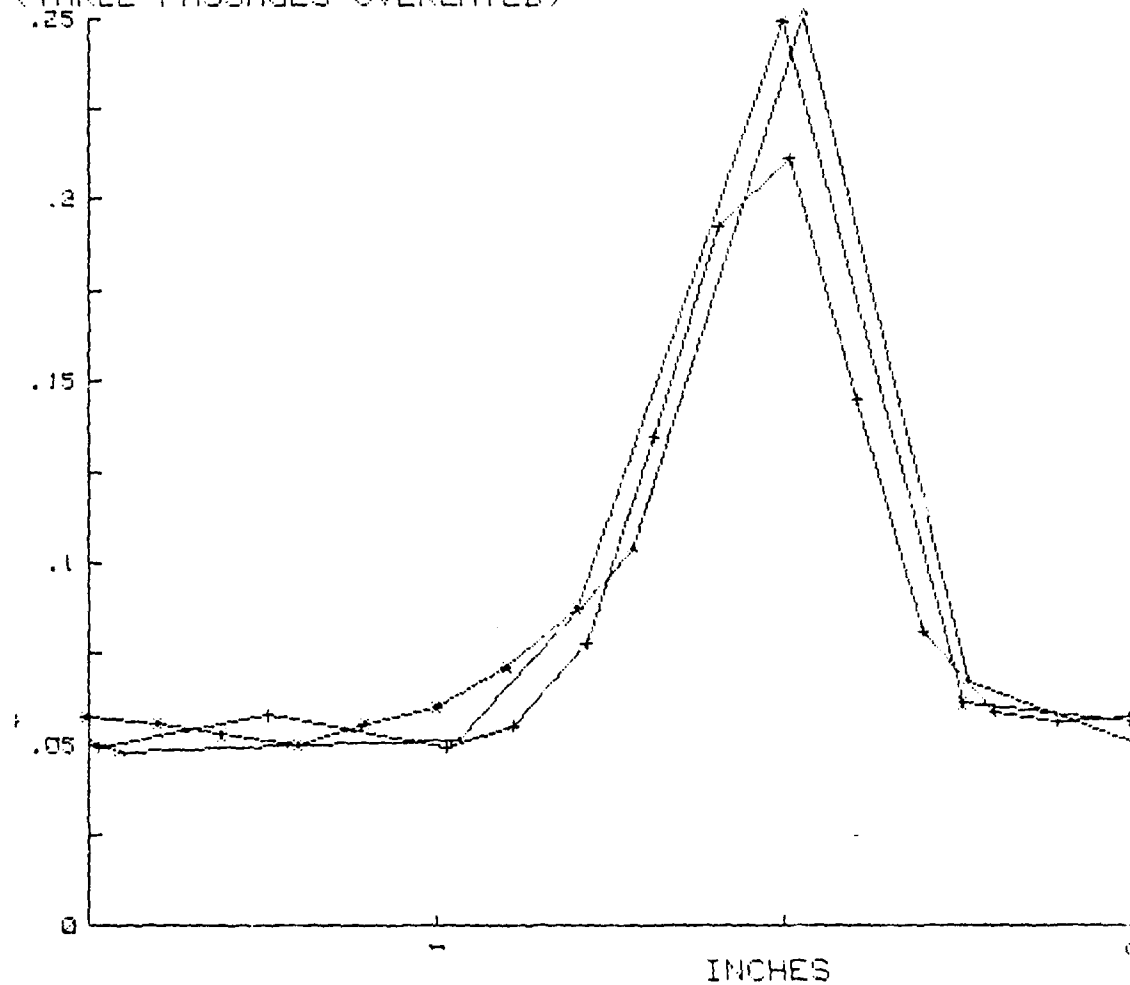
Fig. 40.   Probe Survey Data at Midspan
           (i=5.3, $(P_{plen}-P_t)/\bar{Q}_1$, Upper Plane)

82

(Ps-Pwl)/Q1bar
UPPER PLANE MIDSPAN (i=5.3)
(THREE PASSAGES OVERLAYED)
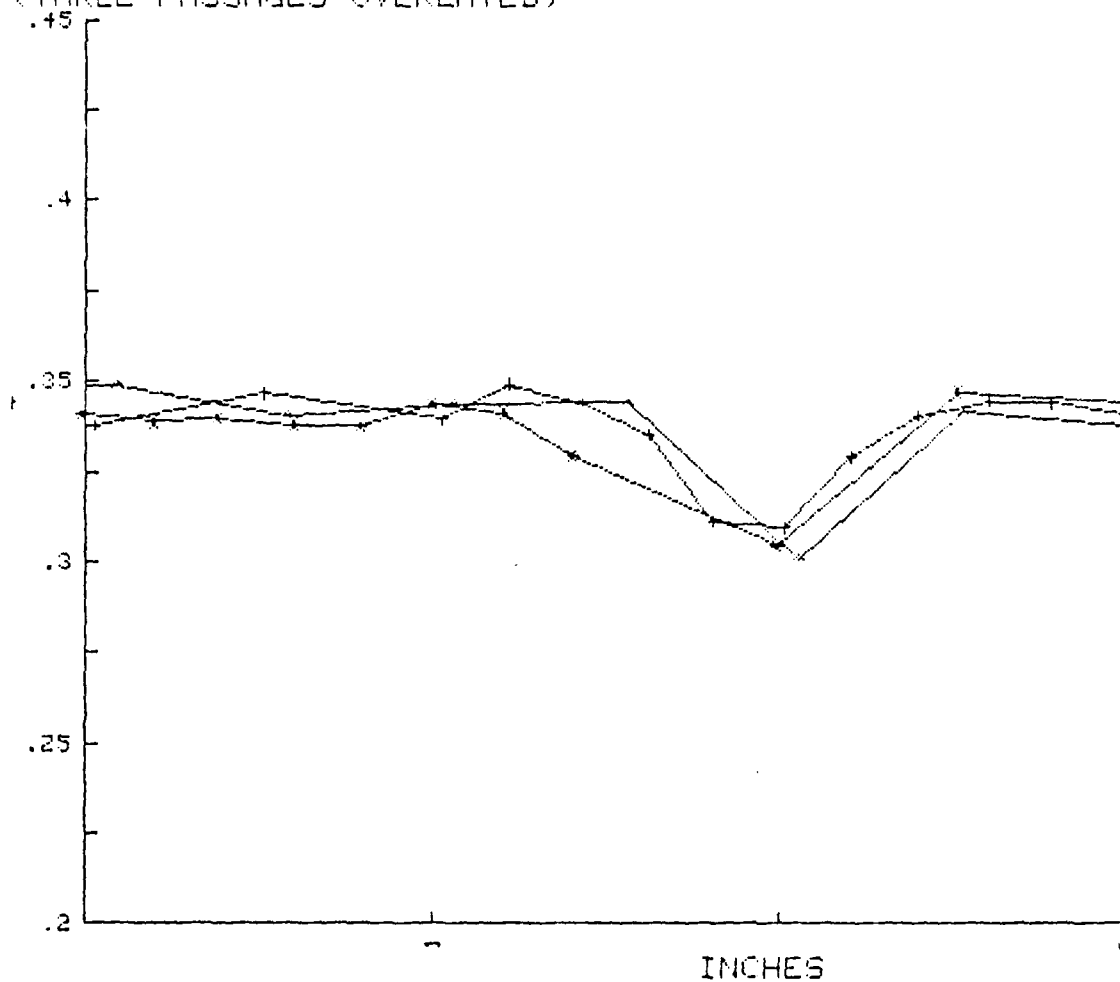
Fig. 41.   Probe Survey Data at Midspan
(i=5.3, $(P_s - P_{w\ell})/\bar{Q}_1$, Upper Plane)

83

OUTLET ANGLE
UPPER PLANE MIDSPAN (i=5.3)
(THREE PASSAGES OVERLAYED)
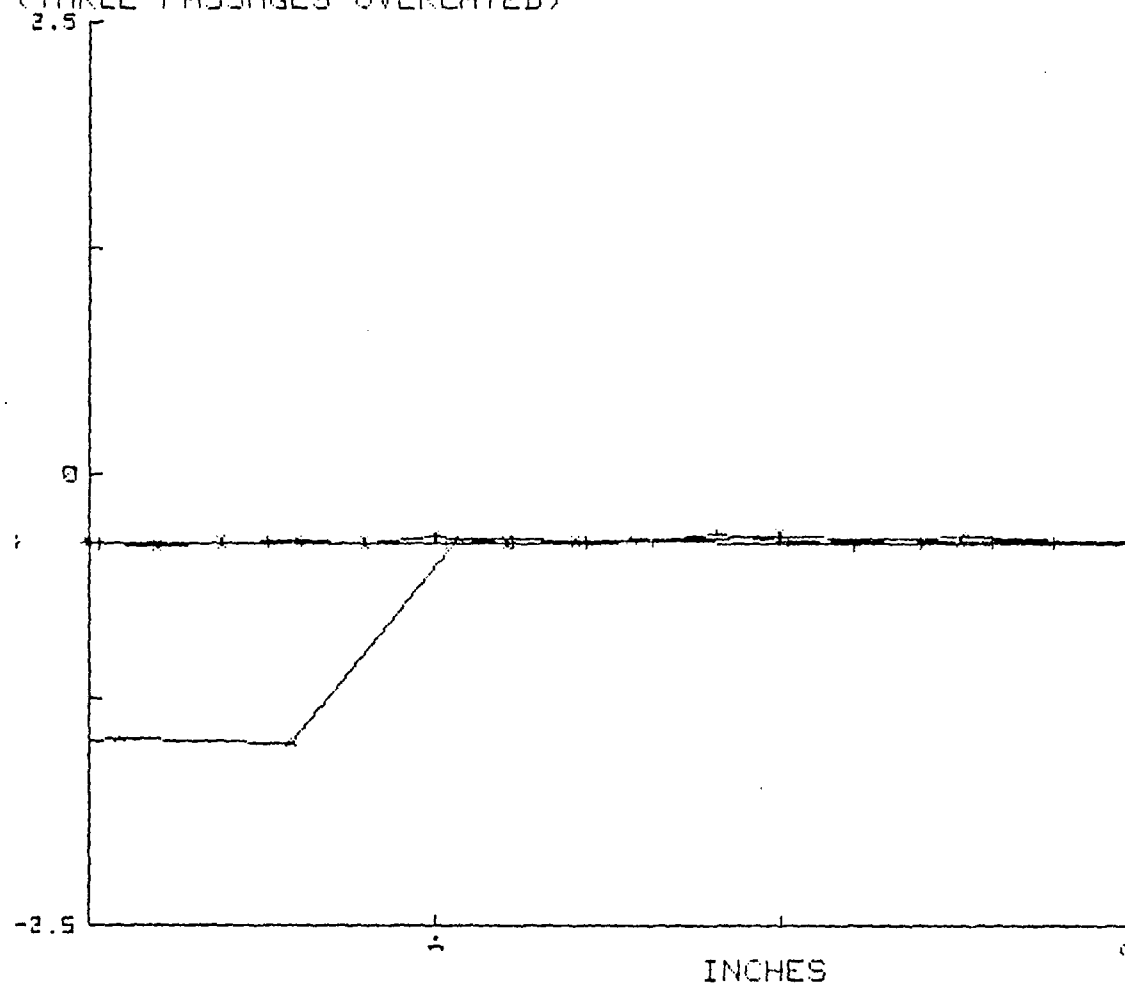
Fig. 42.   Probe Survey Data at Midspan
           (i=5.3, Outlet Angle, Upper Plane)

84

Blade	LEFT	CENTER	RIGHT
Pressure Surface	L	*	R
Suction Surface	l	+	r

Cp1 vs X/C
THREE CENTERMOST BLADES OVERLAYED
(i=8.8)
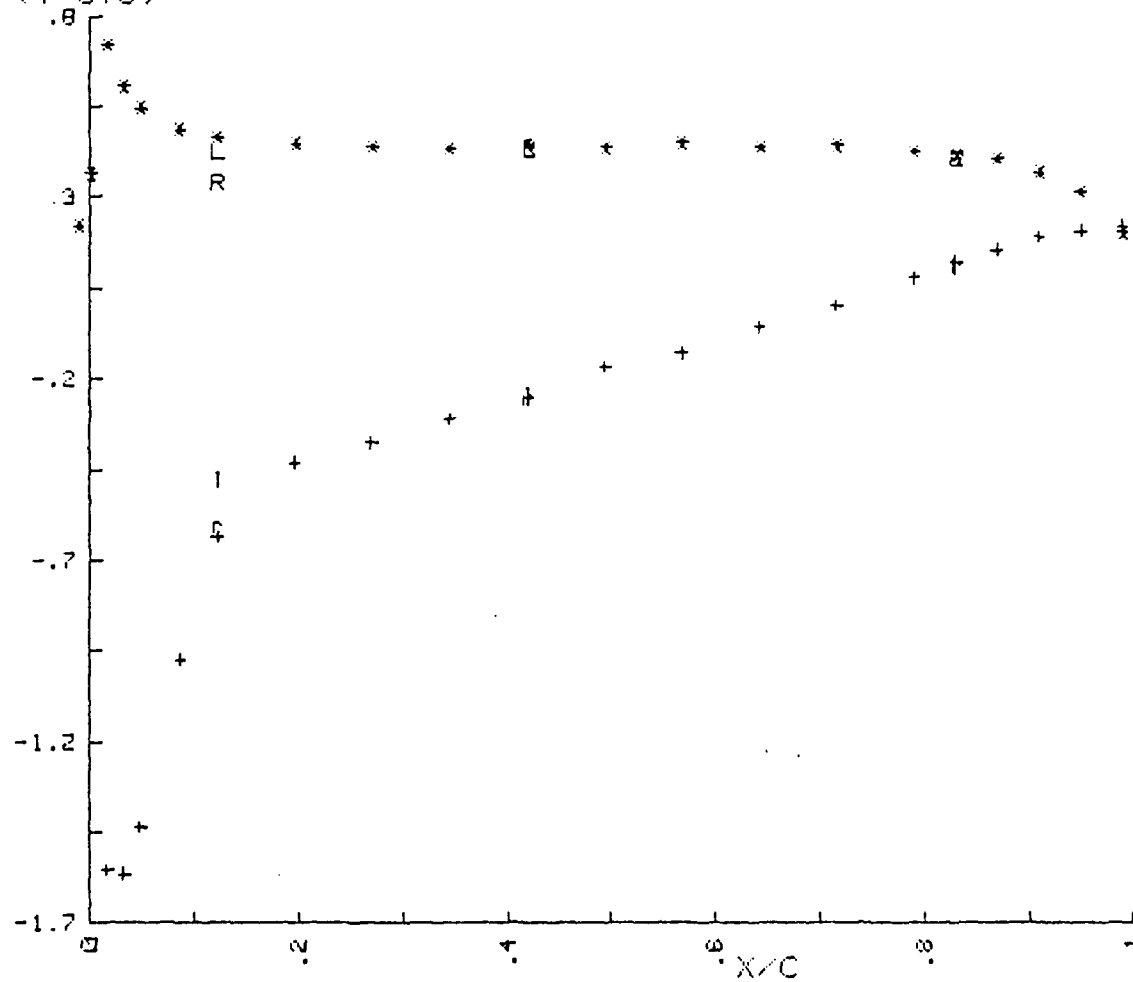
Fig. 43. Blade Surface Pressure Distribution
(i=8.8)

85
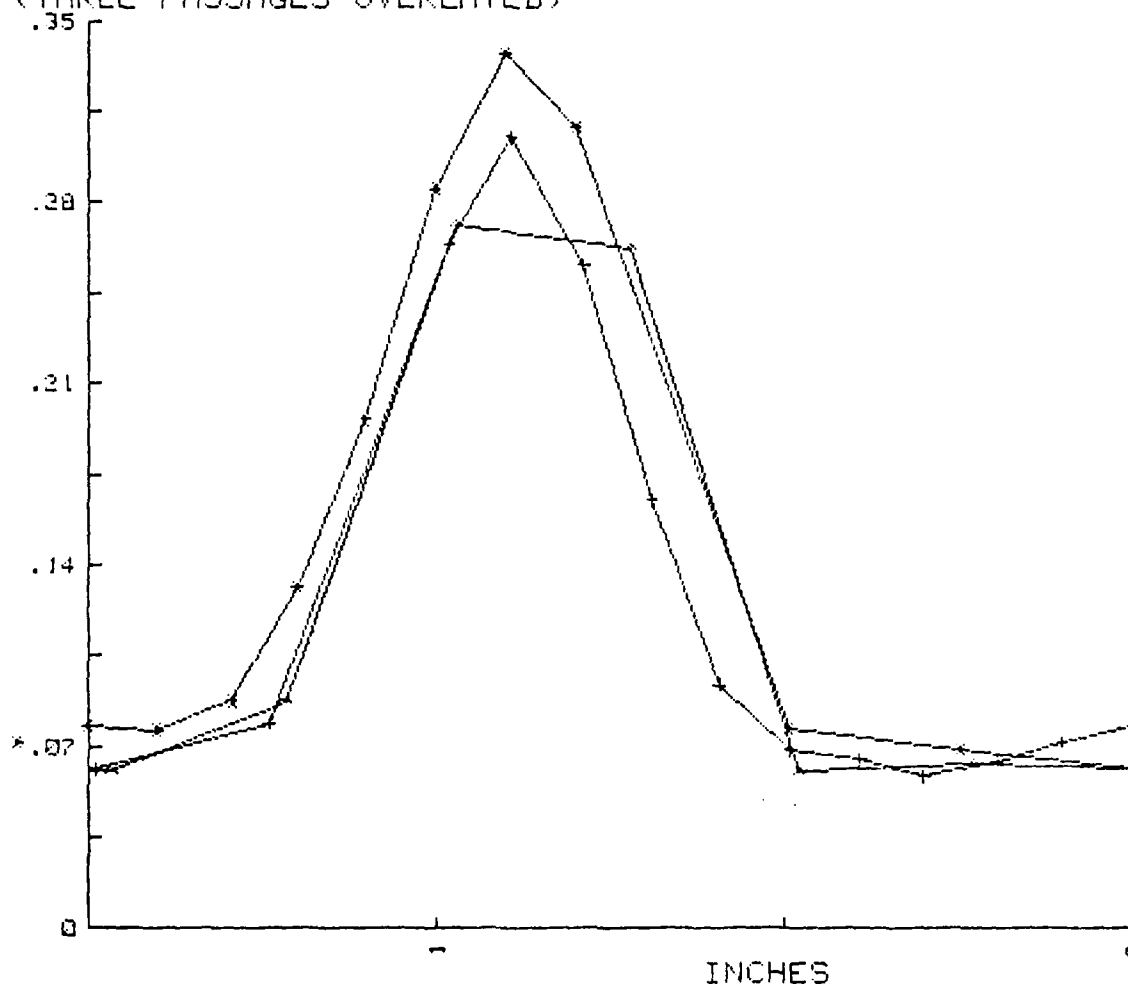
Fig. 44.   Probe Survey Data at Midspan
(i=8.8, $P_{plen}-P_t)/\overline{Q}_1$, Upper Plane)

86
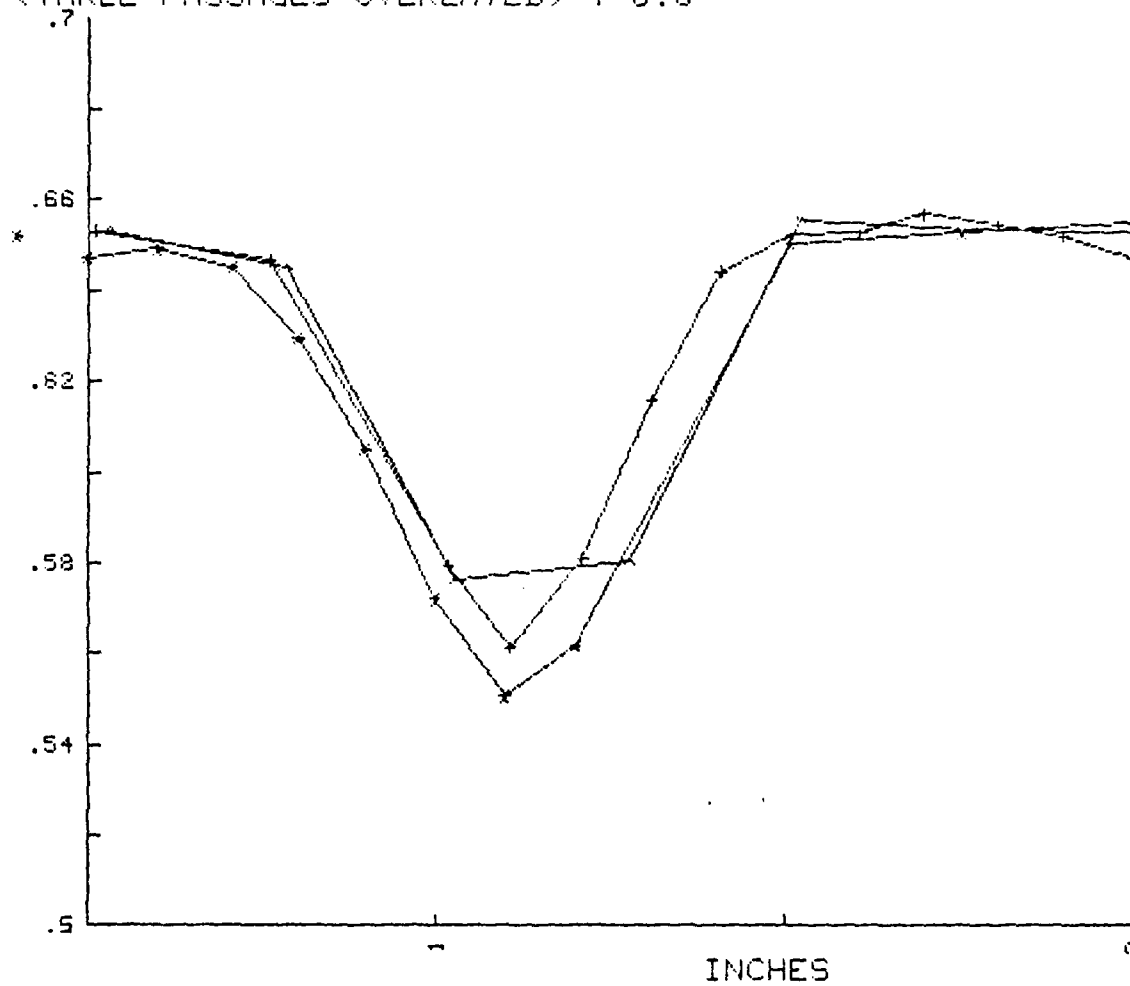
Fig. 45. Probe Survey Data at Midspan
(i=8.8, X/$\overline{X}$, Upper Plane)
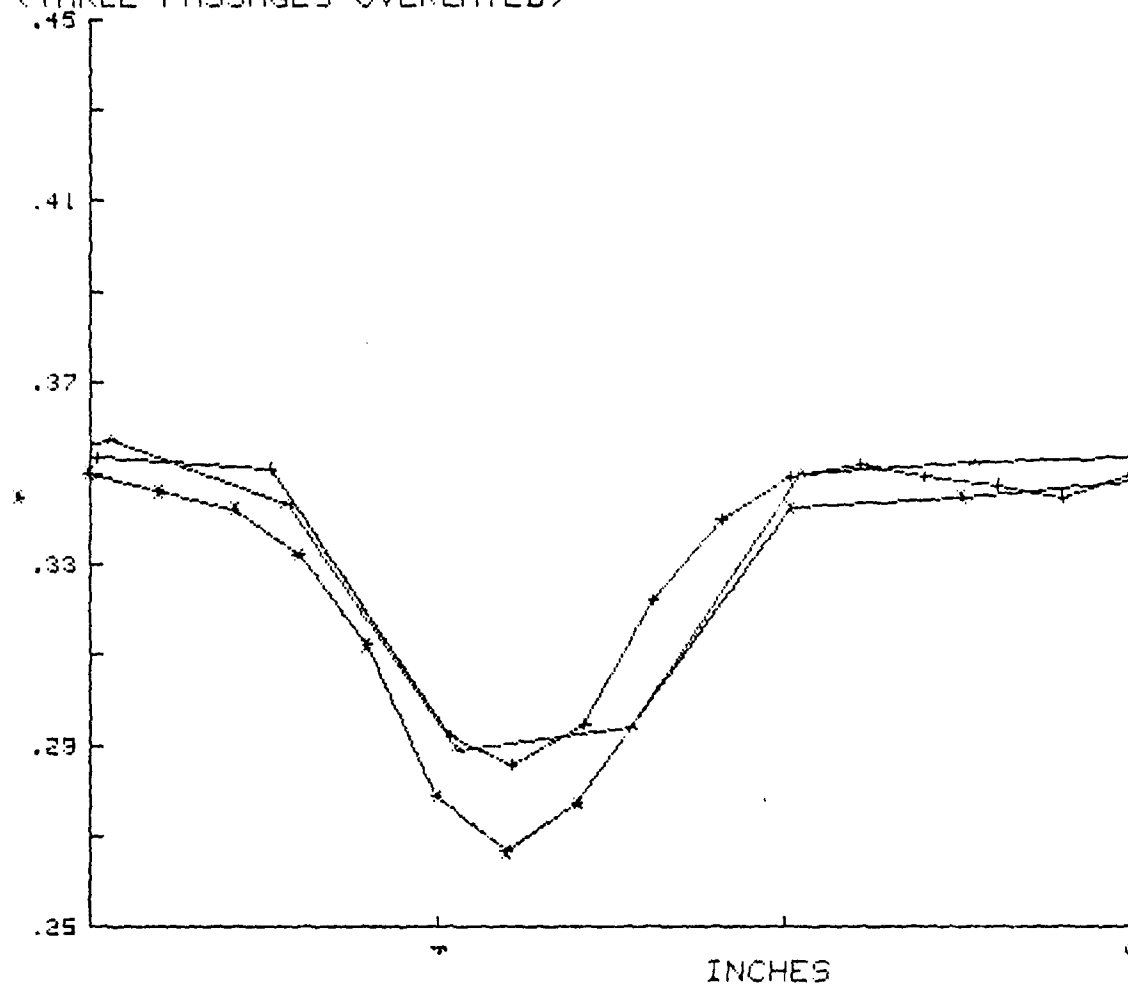
Fig. 46. Probe Survey Data at Midspan
$(i \approx 8.8, (P_s - P_{w\ell})/\bar{Q}_1,$ Upper Plane)

88

OUTLET ANGLE
UPPER PLANE MIDSPAN
(THREE PASSAGES OVERLAYED) i=8.8
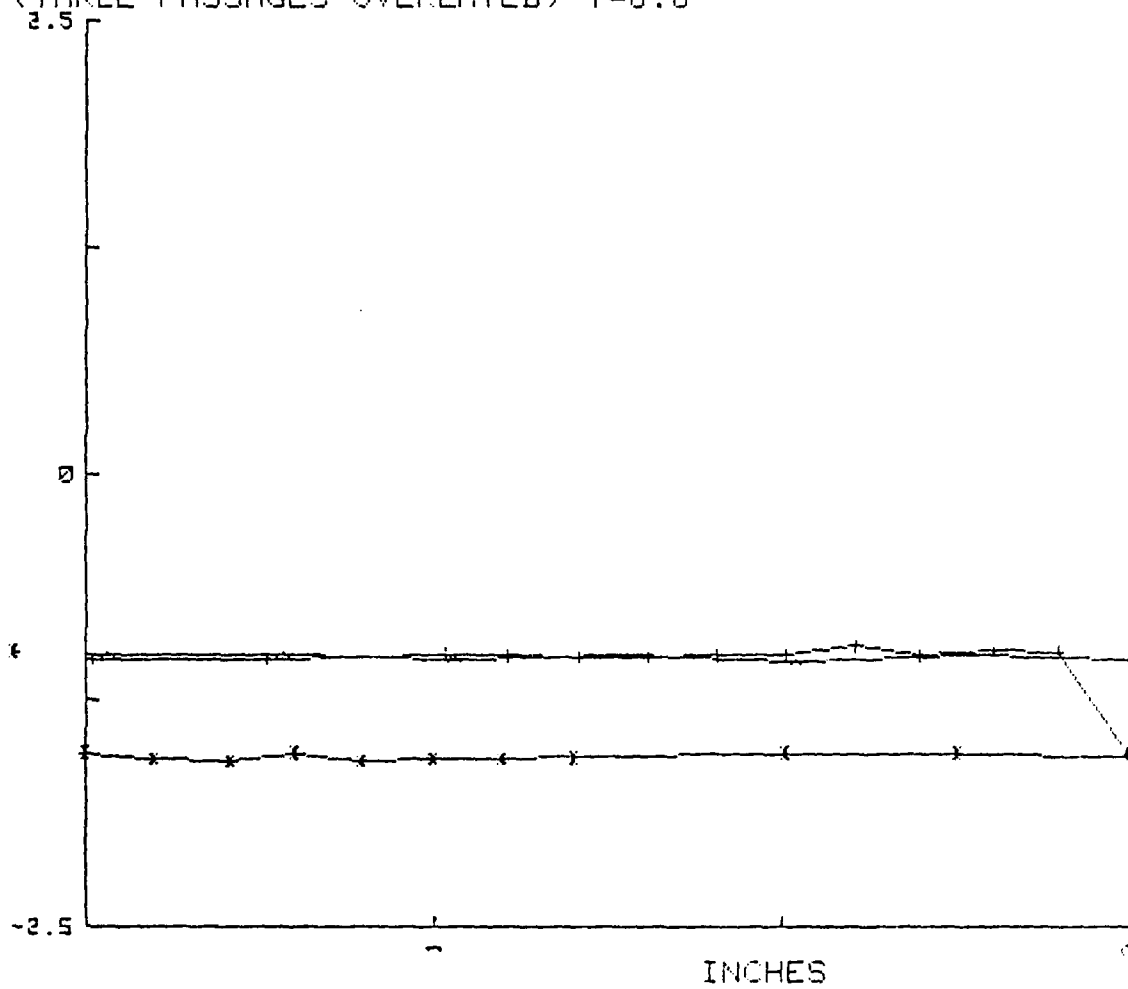
Fig. 47.   Probe Survey Data at Midspan
            (i=8.8, Outlet Angle, Upper Plane)
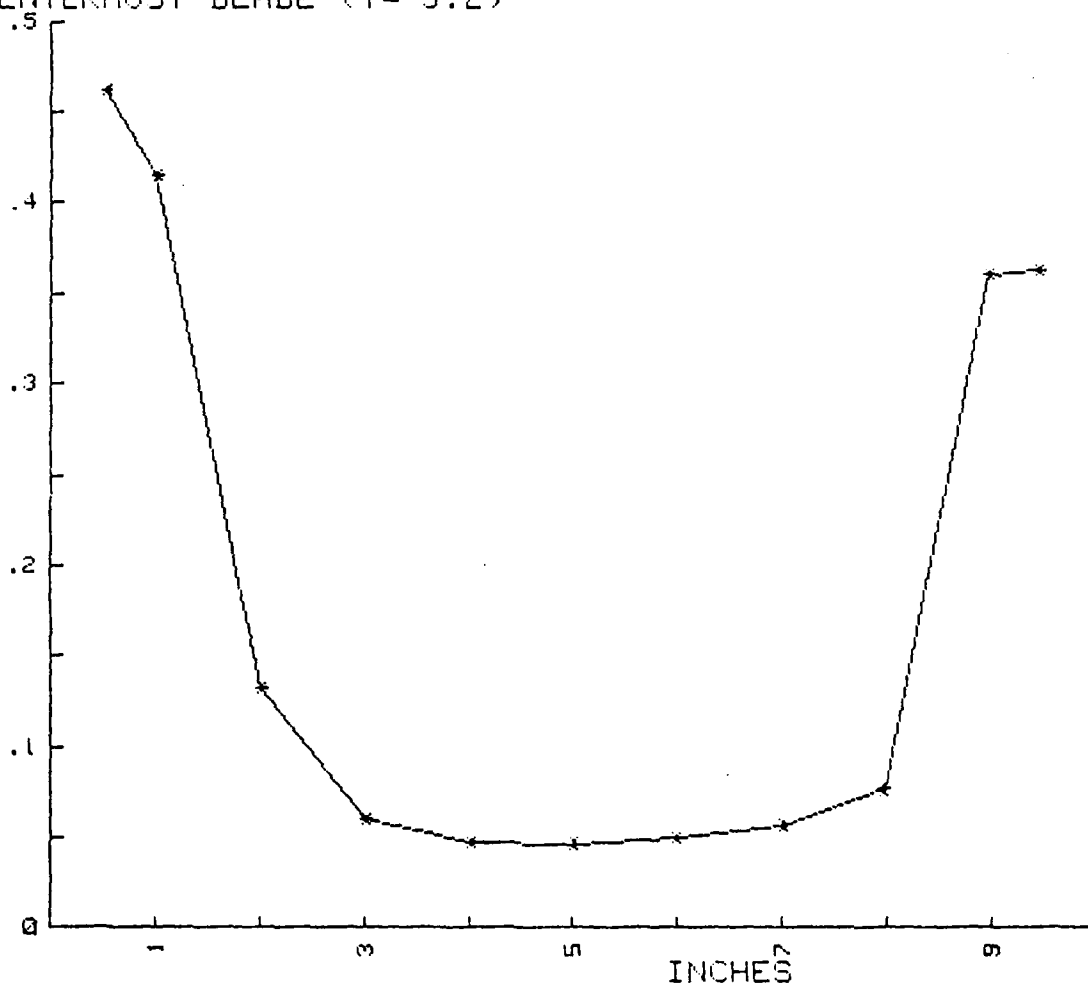
89

(Pplen-Pt)/Q1bar
1.0 in FROM SUCTION SIDE
CENTERMOST BLADE (i=-9.2)

Fig. 48. Spanwise Probe Data Surveyed 1 in. from
Suction Side of Centermost Blade
$(i=-9.2, (P_{plen}-P_t)/\bar{Q}_1$, Upper Plane)
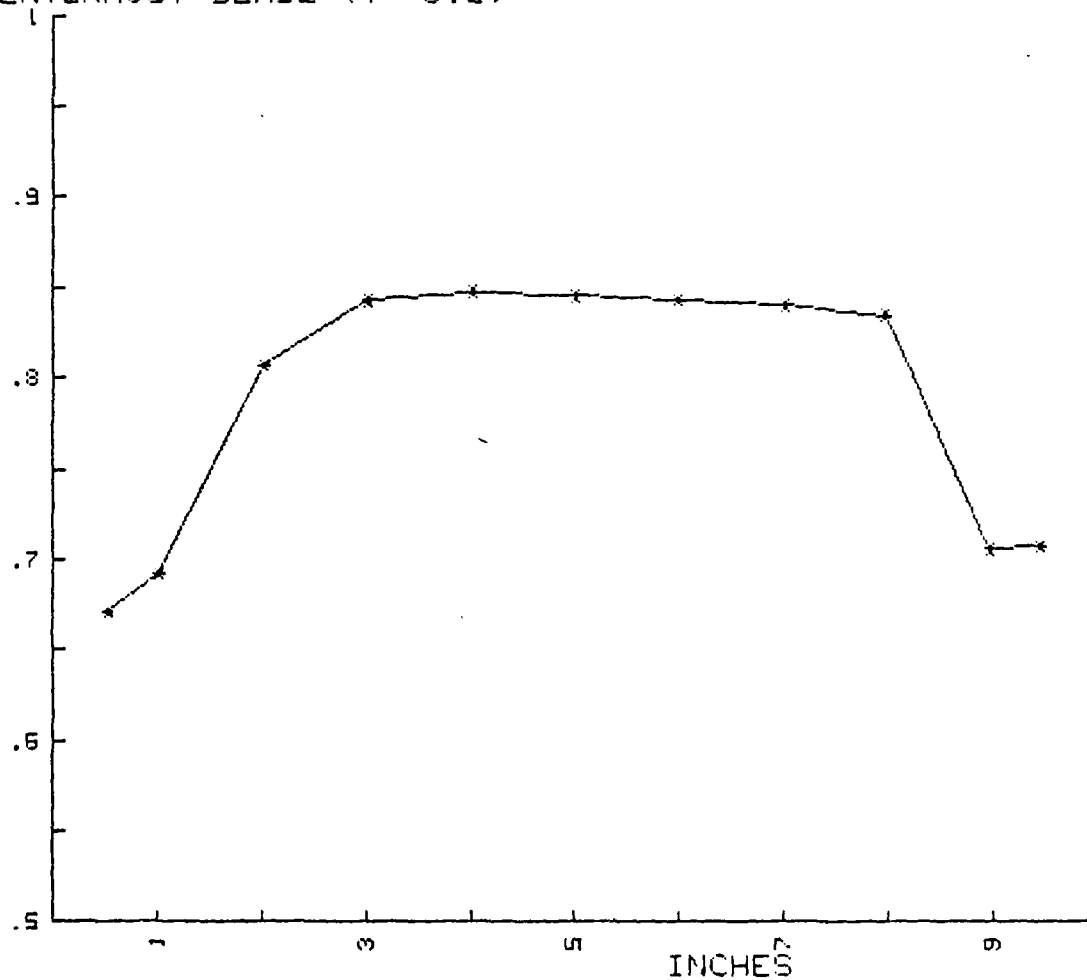
Fig. 49.   Spanwise Probe Data Surveyed 1 in. from
           Suction Side of Centermost Blade
           ($i=-9.2$, $X/\overline{X}$, Upper Plane)

(Pplen-Pt)/Q1bar
1.0 in FROM PRESSURE SIDE
CENTERMOST BLADE (i=-9.2)
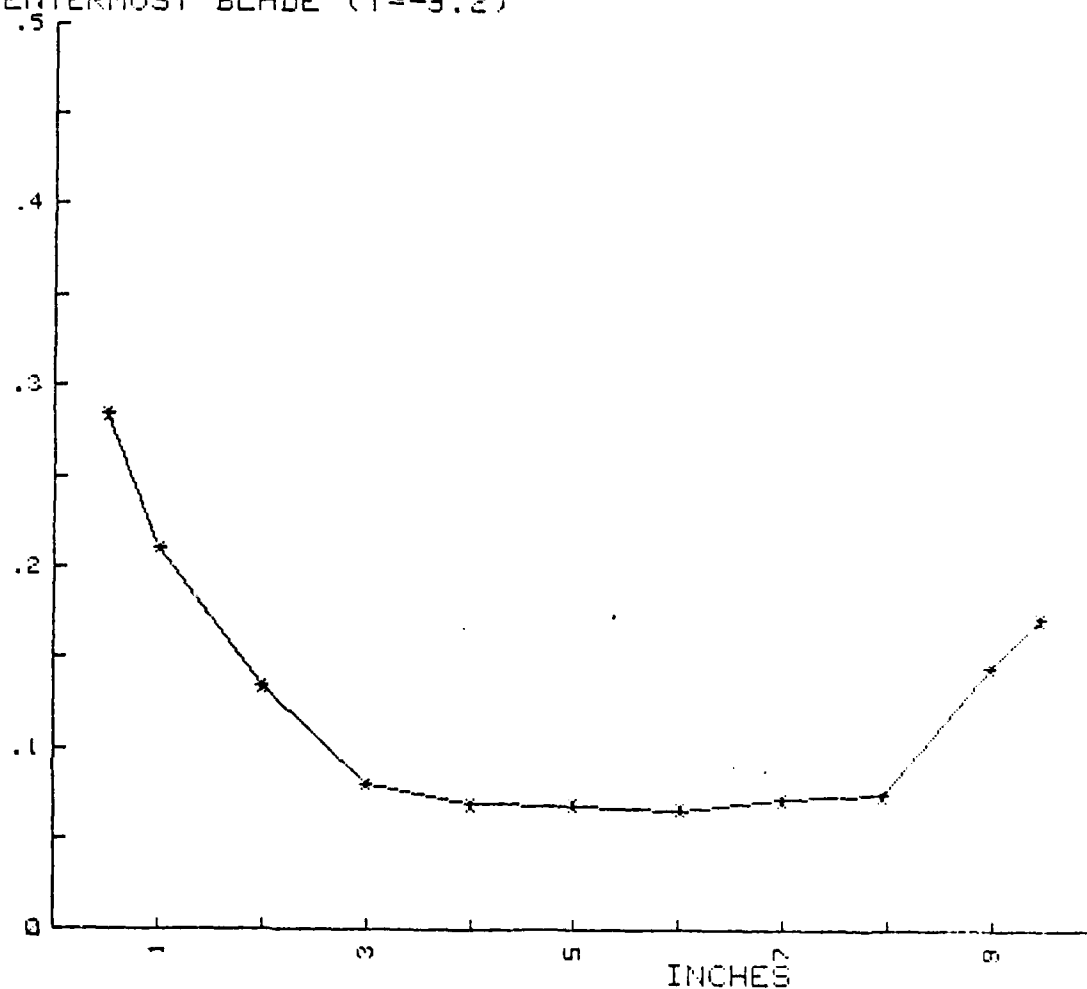
Fig. 50.   Spanwise Probe Data Surveyed 1 in. from
           Pressure Side of Centermost Blade
           (i=-9.2, $(P_{plen}-P_t)/\overline{Q}_1$, Upper Plane)

92

Fig. 51.   Spanwise Probe Data Surveyed 1 in. from
Pressure Side of Centermost Blade
(i=-9.2, X/$\overline{X}$, Upper Plane)

93
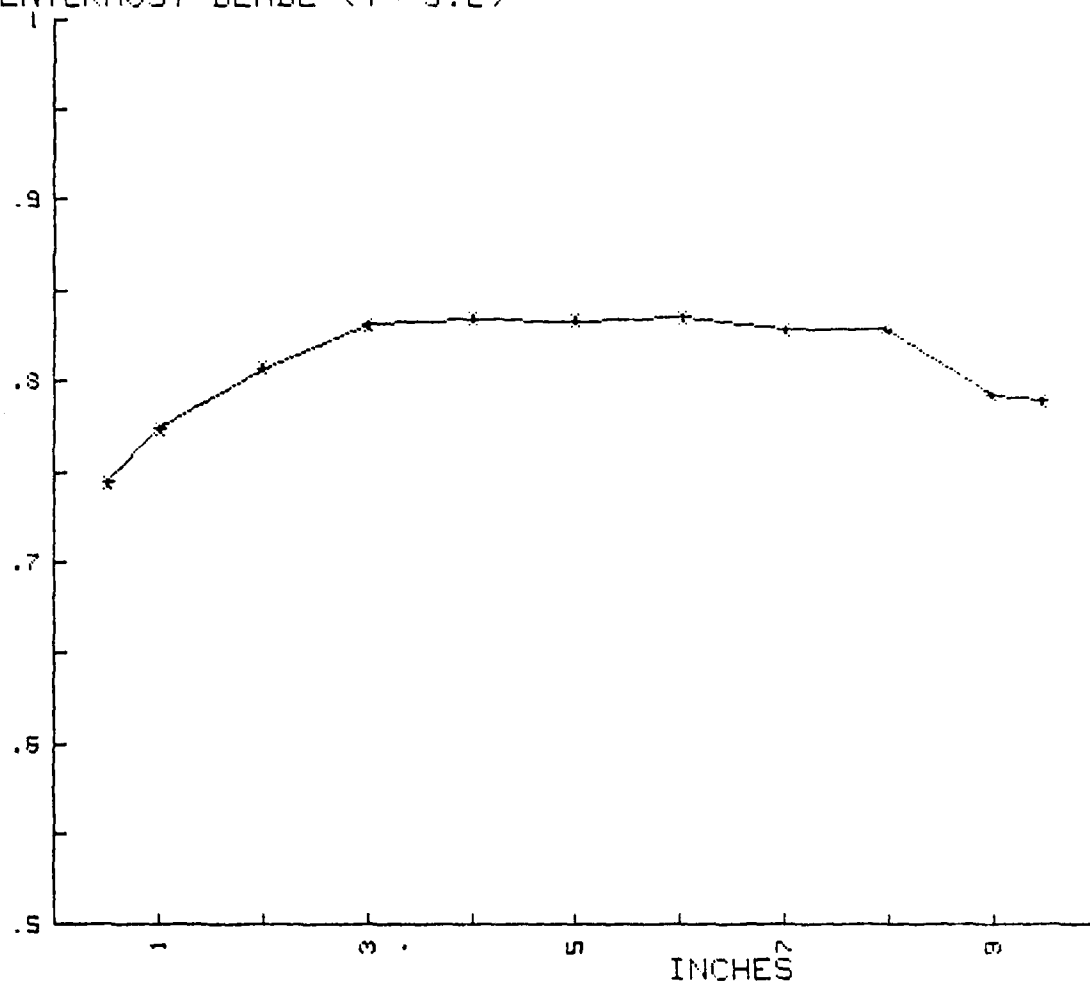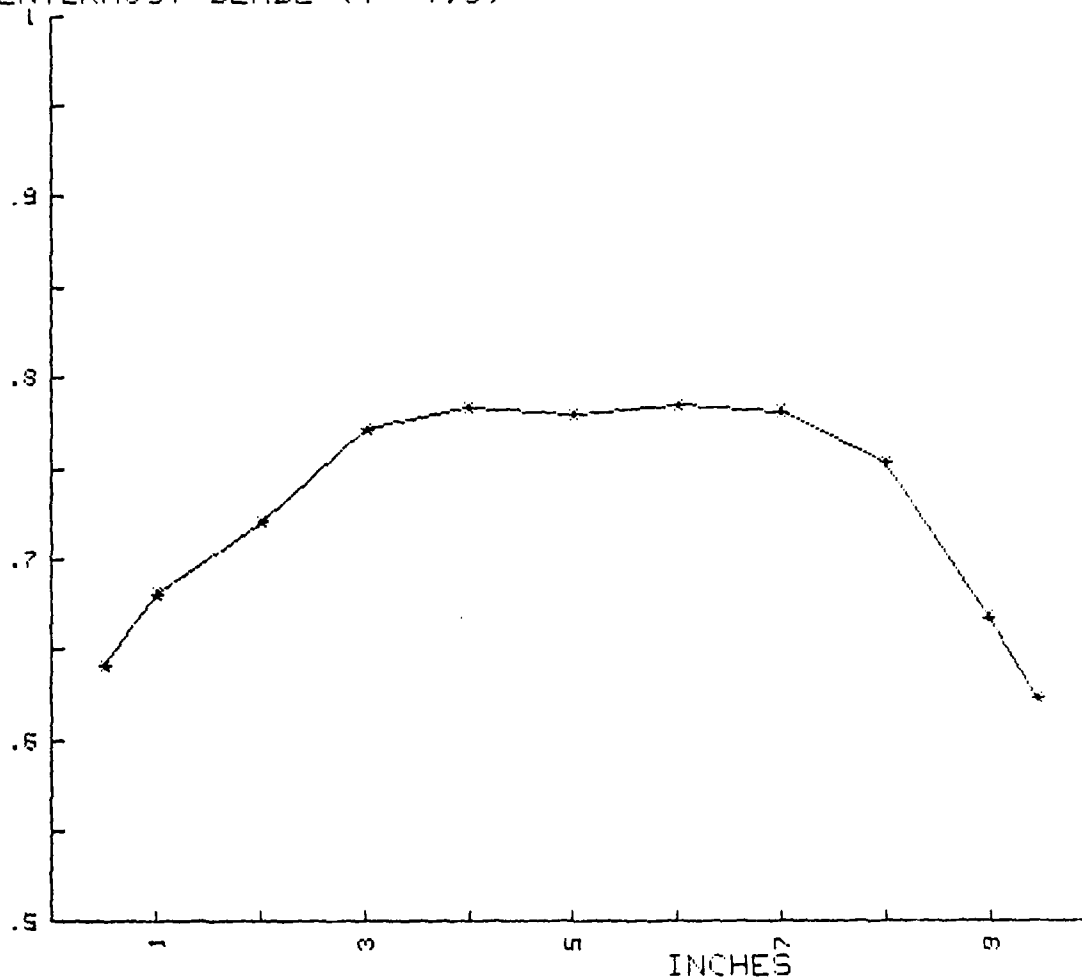
Fig. 52.   Spanwise Probe Data Surveyed 1 in. from
            Suction Side of Centermost Blade
            (i≈-4.9, X/X̄, Upper Plane)

94

(Pplen-Pt)/Q1bar
1.0 in FROM SUCTION SIDE
CENTERMOST BLADE (i=-4.9)

Fig. 53.   Spanwise Probe Data Surveyed 1 in. from
            Suction Side of Centermost Blade
            (i=-4.9, $(P_{plen}-P_t)/\bar{Q}_1$, Upper Plane)

95
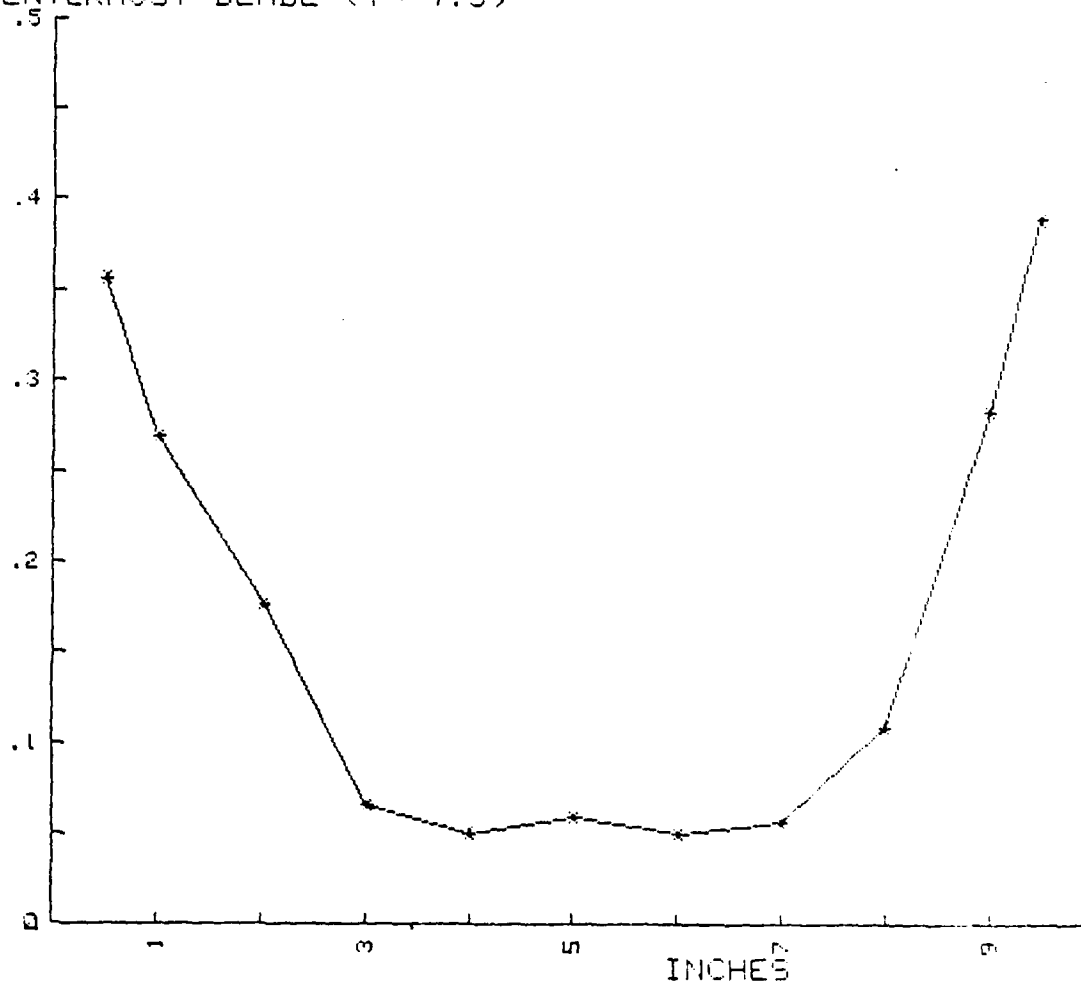
(Pplen-Pt)/Q1bar
1.0 in FROM PRESSURE SIDE
CENTERMOST BLADE (i=-4.9)
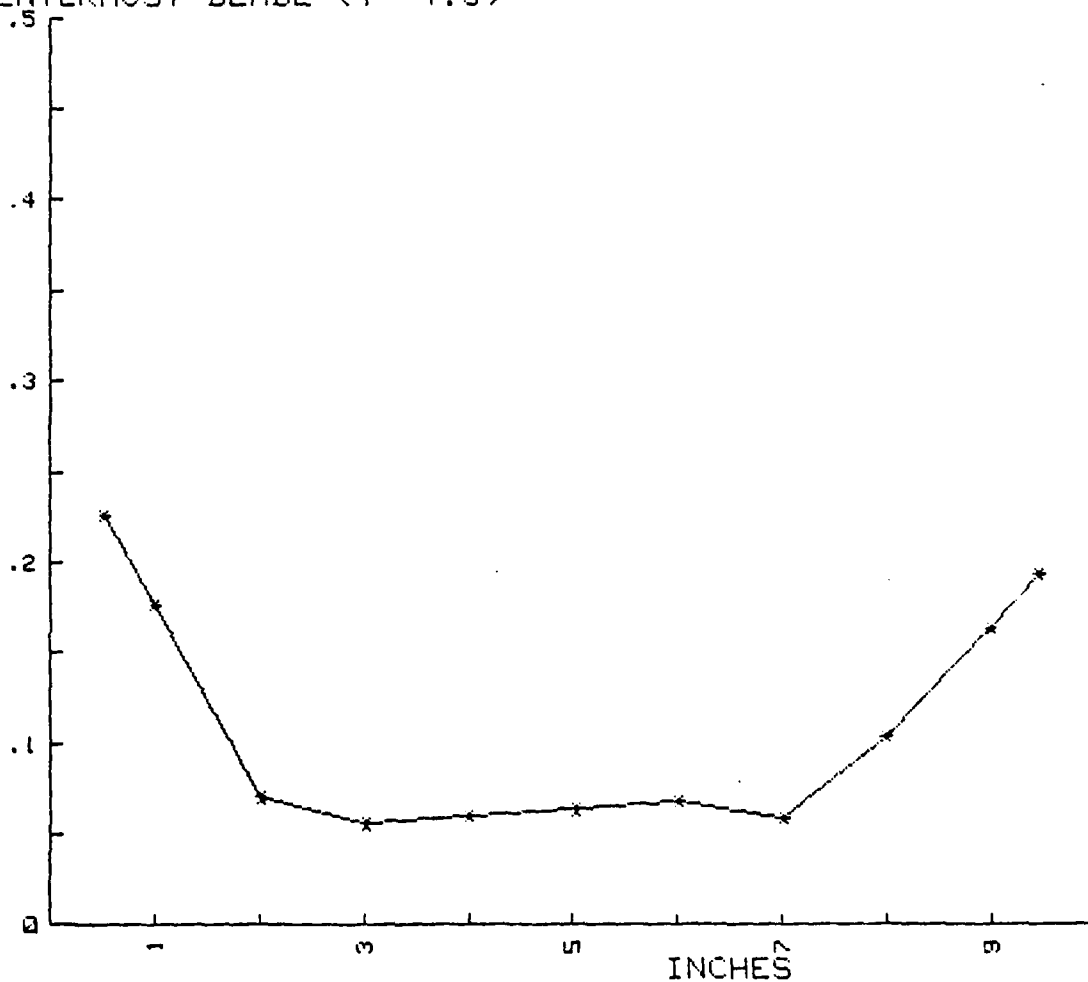
Fig. 54.   Spanwise Probe Data Surveyed 1 in. from
            Pressure Side of Centermost Blade
            (i=-4.9, $(P_{plen}-P_t)/\bar{Q}_1$, Upper Plane)

96

X/Xbar
1.0 in FROM PRESSURE SIDE
CENTERMOST BLADE (i=-4.9)

INCHES
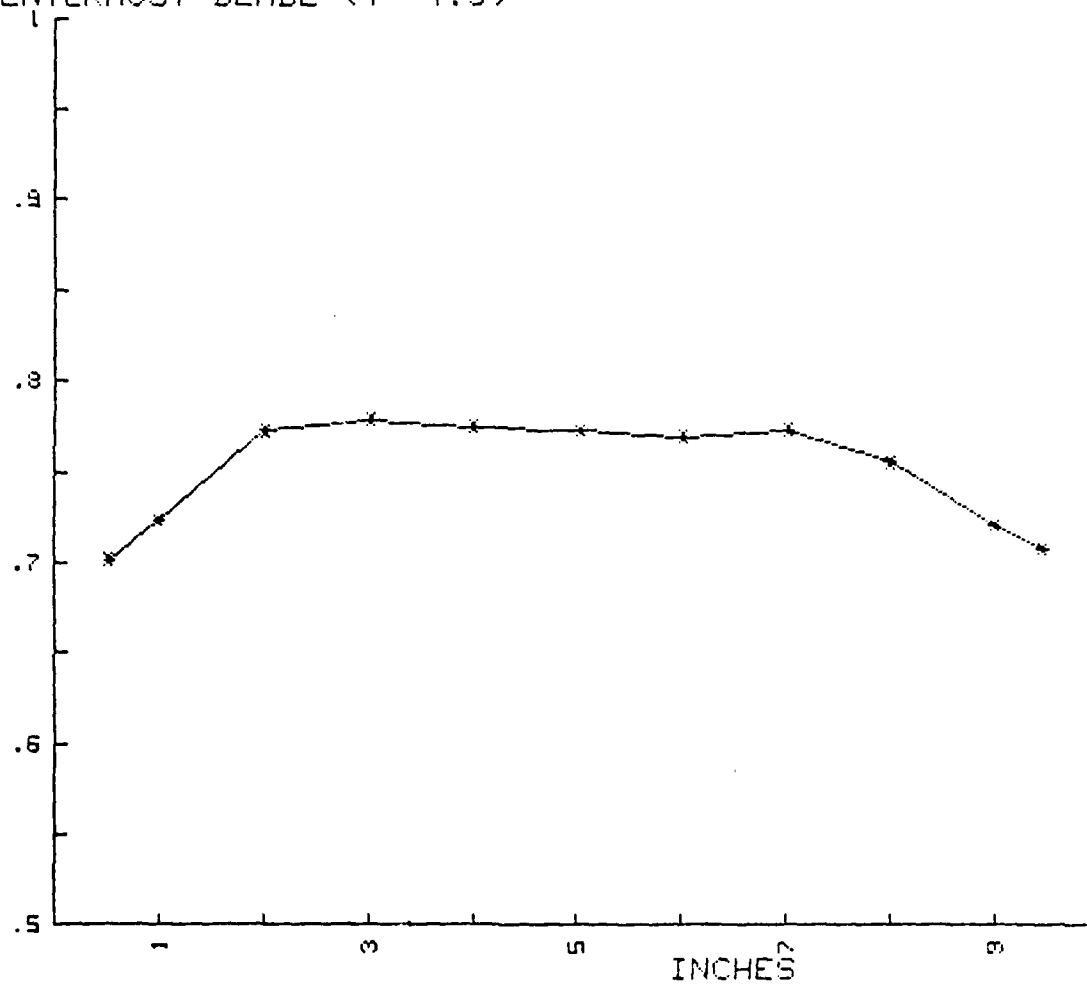
Fig. 55.   Spanwise Probe Data Surveyed 1 in. from
          Pressure Side of Centermost Blade
          (i=-4.9, X/$\bar{X}$, Upper Plane)

97

(Pplen-Pt)/Q1bar
1.0 in FROM SUCTION SIDE
CENTERMOST BLADE (i=2.1)
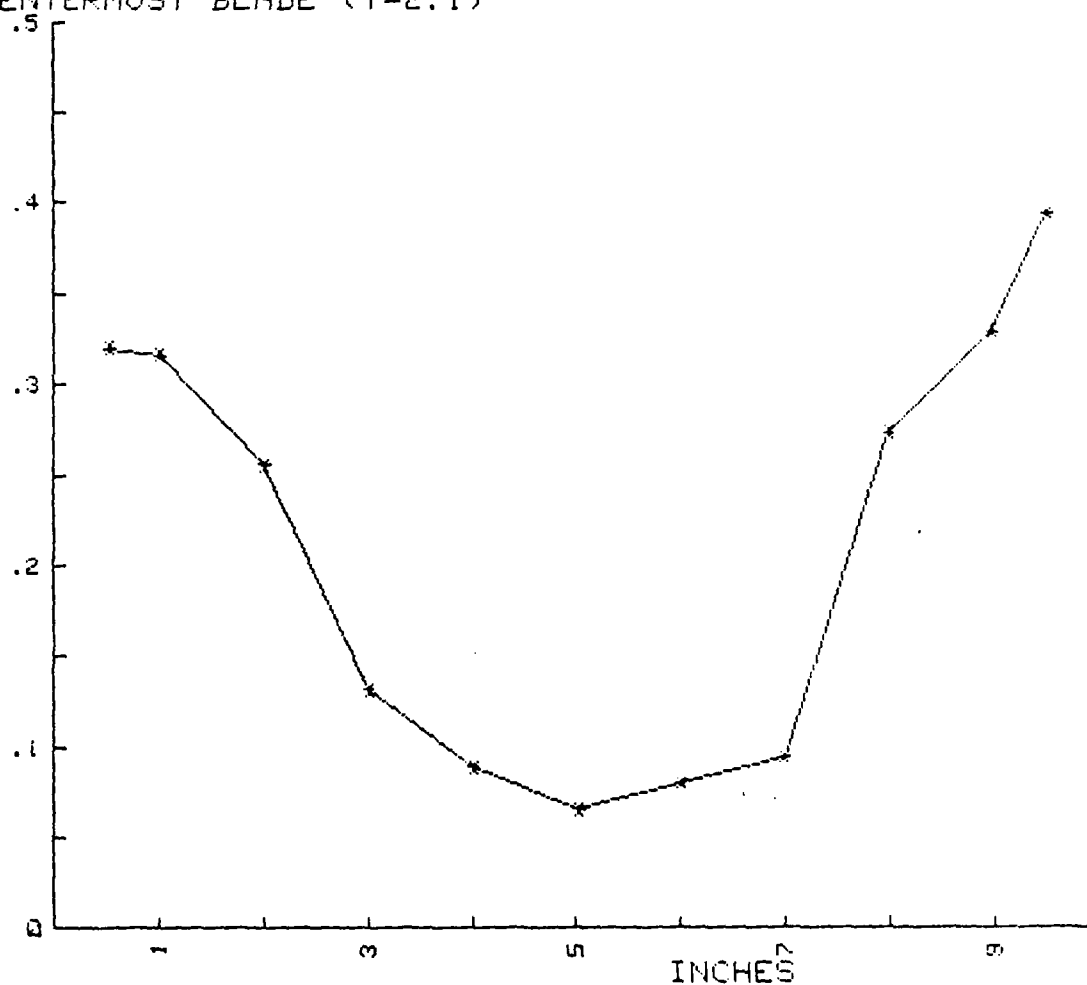
Fig. 56.   Spanwise Probe Data Surveyed 1 in. from
Suction Side of Centermost Blade
$(i=2.1, (P_{plen}-P_t)/\bar{Q}_1$, Upper Plane)

98

X/Xbar
1.0 in FROM SUCTION SIDE
CENTERMOST BLADE (i=2.1)

INCHES
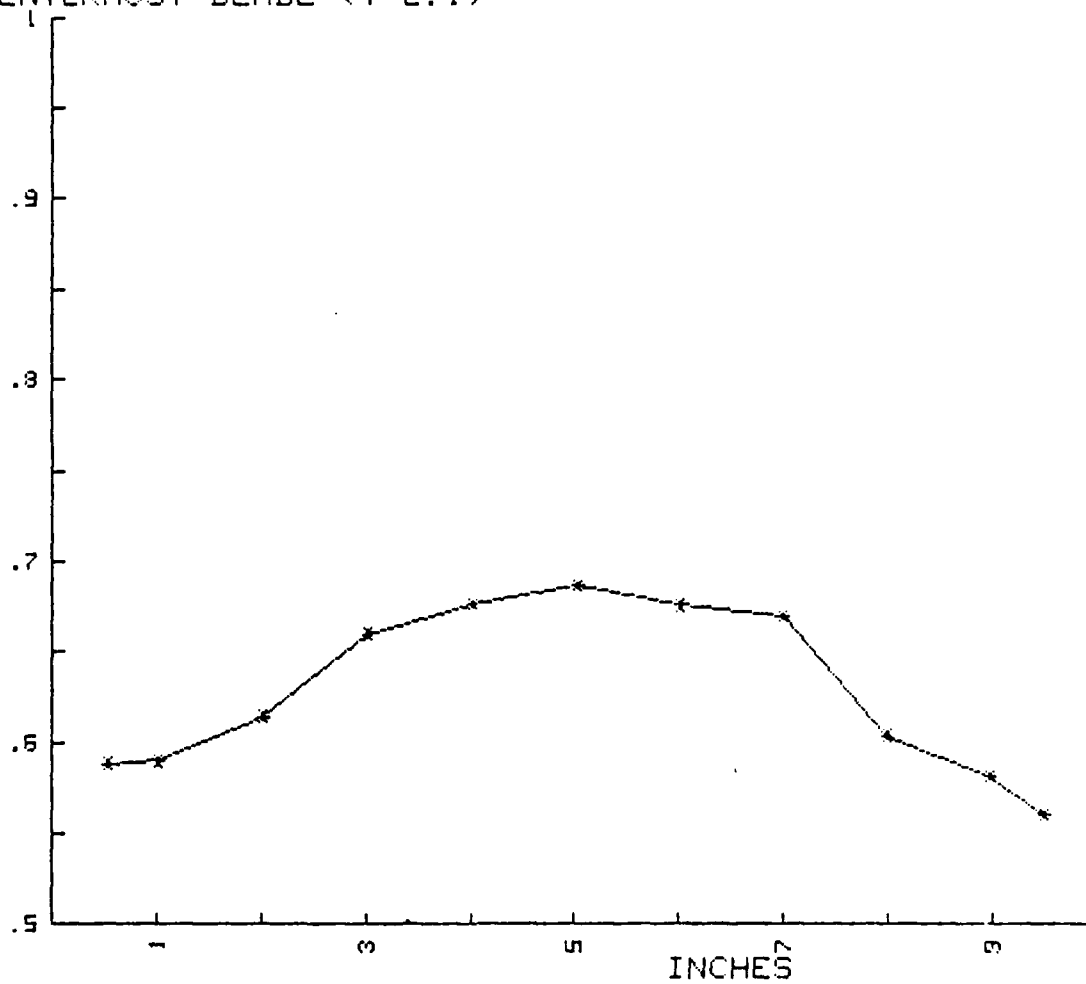
Fig. 57.   Spanwise Probe Data Surveyed 1 in. from
          Suction Side of Centermost Blade
          (i=2.1, X/X̄, Upper Plane)

(Pplen-Pt)/Q1bar
1.0 in FROM PRESSURE SIDE
CENTERMOST BLADE (i=2.1)
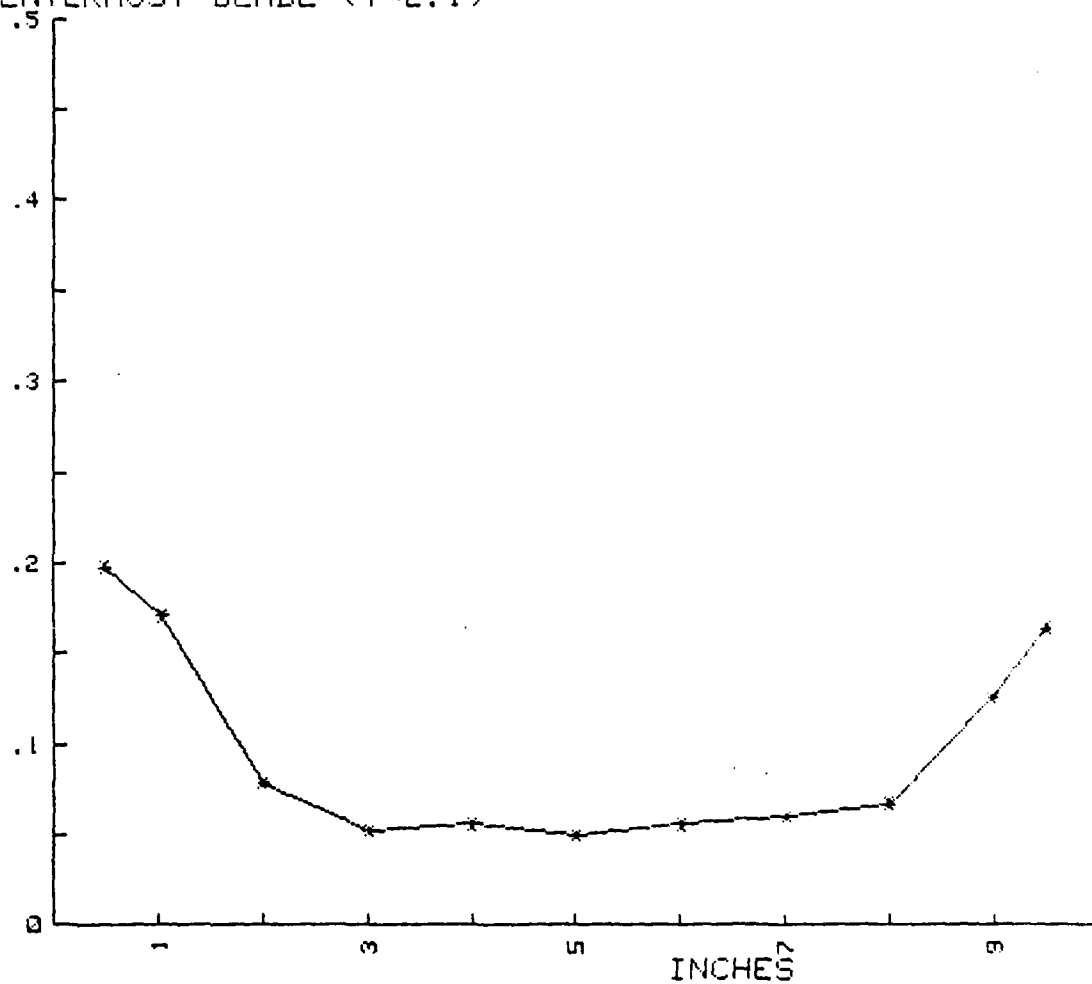
Fig. 58.   Spanwise Probe Data Surveyed 1 in. from
           Pressure Side of Centermost Blade
           (i=2.1, $(P_{plen}-P_t)/\bar{Q}_1$, Upper Plane)

100

X/Xbar
1.0 in FROM PRESSURE SIDE
CENTERMOST BLADE (i=2.1)
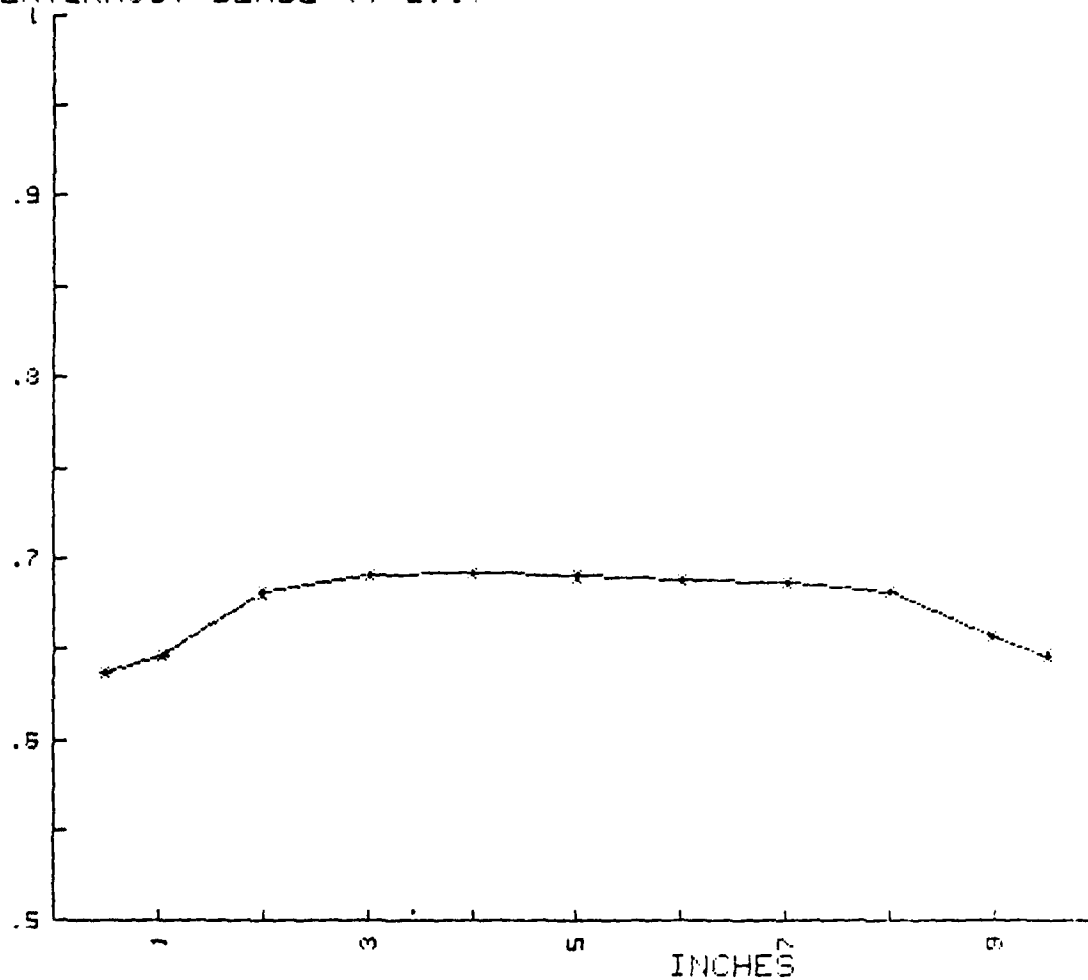
Fig. 59.   Spanwise Probe Data Surveyed 1 in. from
Pressure Side of Centermost Blade
(i=2.1, X/$\overline{X}$, Upper Plane)

101

(Pplen-Pt)/Qlbar
1.0 in FROM SUCTION SIDE
CENTERMOST BLADE (i=5.3)
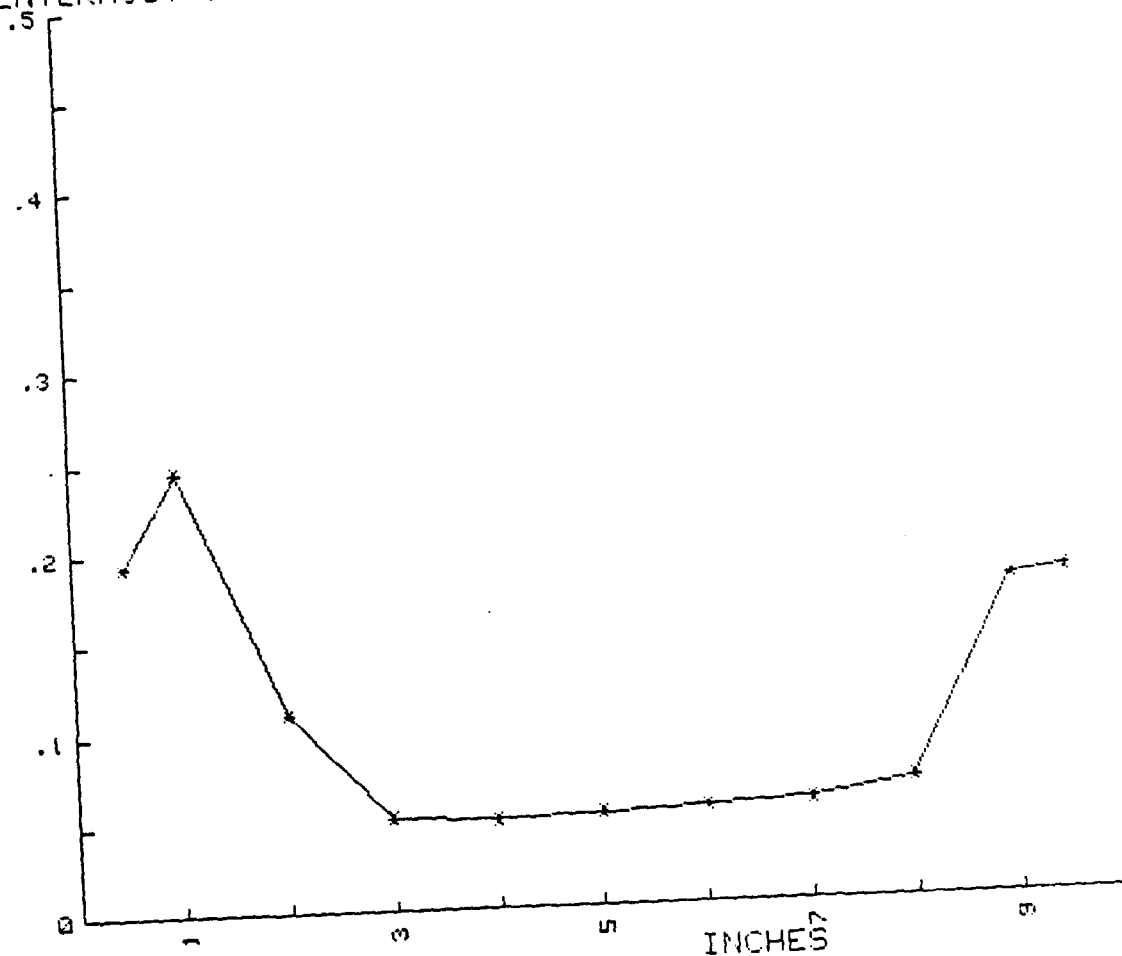
Fig. 60. Spanwise Probe Data Surveyed 1 in. from Suction Side of Centermost Blade $(i=5.3, (P_{plen}-P_t)/\overline{Q}_1$, Upper Plane)

102

X/Xbar
1.0 in FROM SUCTION SIDE
CENTERMOST BLADE (i=5.3)
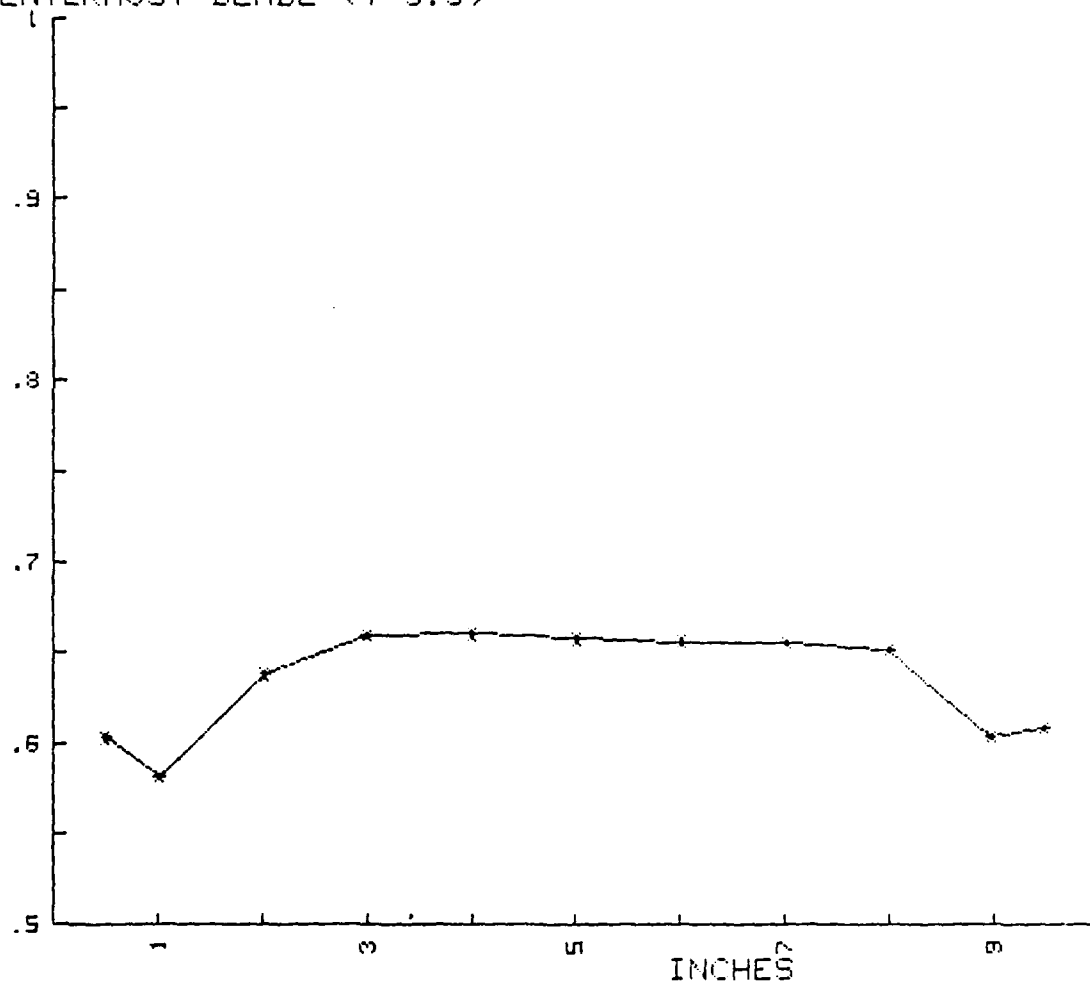
Fig. 61.   Spanwise Probe Data Surveyed 1 in. from
Suction Side of Centermost Blade
(i=5.3, X/$\overline{X}$, Upper Plane)

(Pplen-Pt)/Q1bar
1.0 in FROM PRESSURE SIDE
CENTERMOST BLADE (i=5.3)
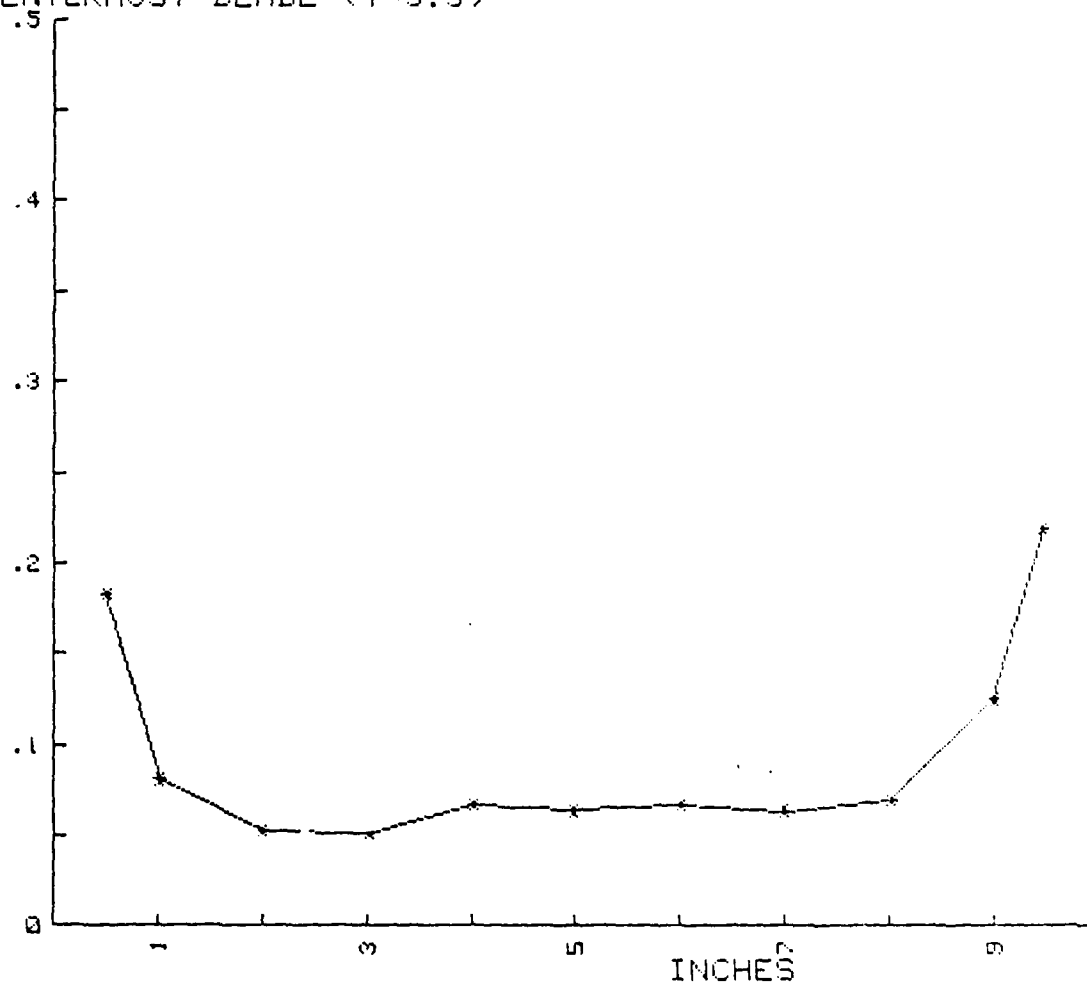
Fig. 62.   Spanwise Probe Data Surveyed 1 in. from
           Pressure Side of Centermost Blade
           (i=5.3, $(P_{plen}-P_t)/\bar{Q}_1$, Upper Plane)

X/Xbar
1.0 in FROM PRESSURE SIDE
CENTERMOST BLADE (i=5.3)
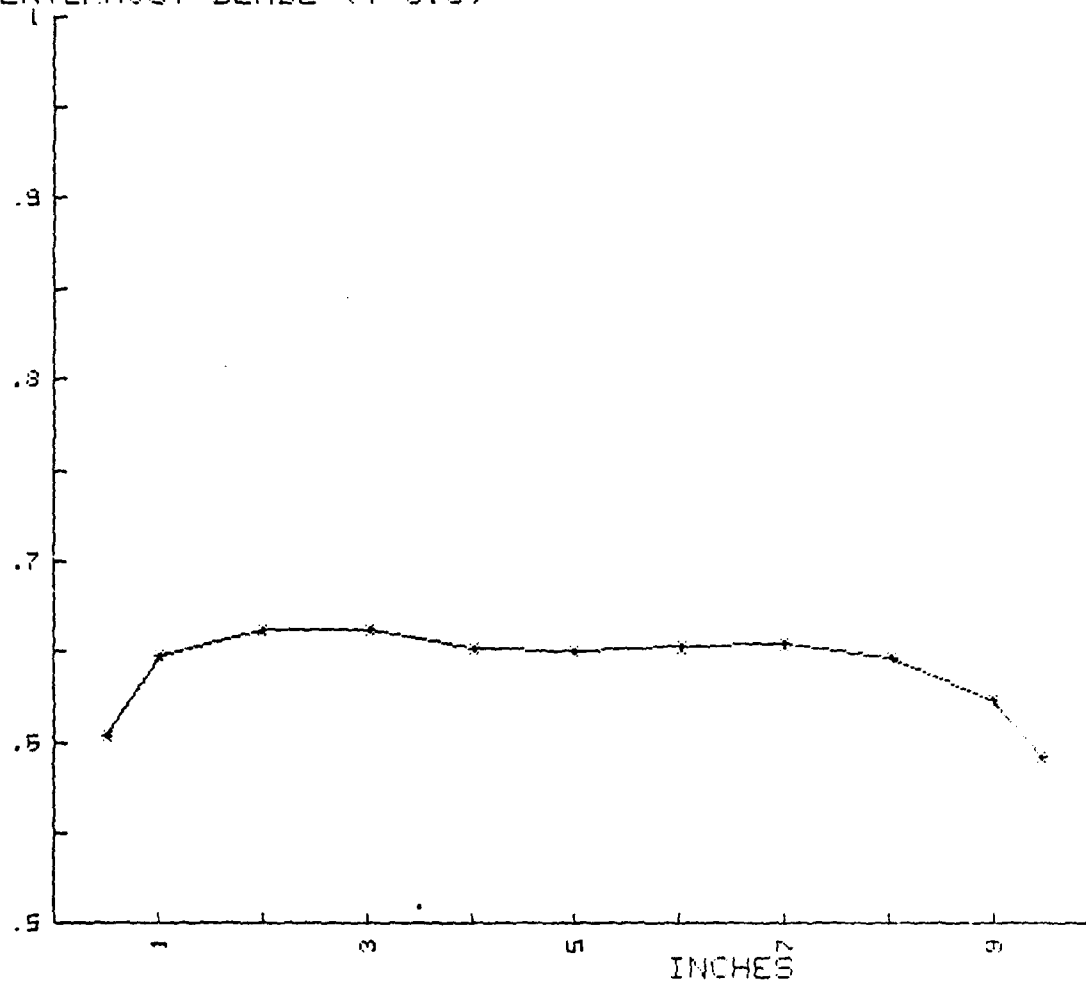
Fig. 63.   Spanwise Probe Data Surveyed 1 in. from
Pressure Side of Centermost Blade
(i=5.3, X/X̄, Upper Plane)

105

(Pplen-Pt)/Q1bar
1.0 in FROM SUCTION SIDE
CENTERMOST BLADE (i=8.8)
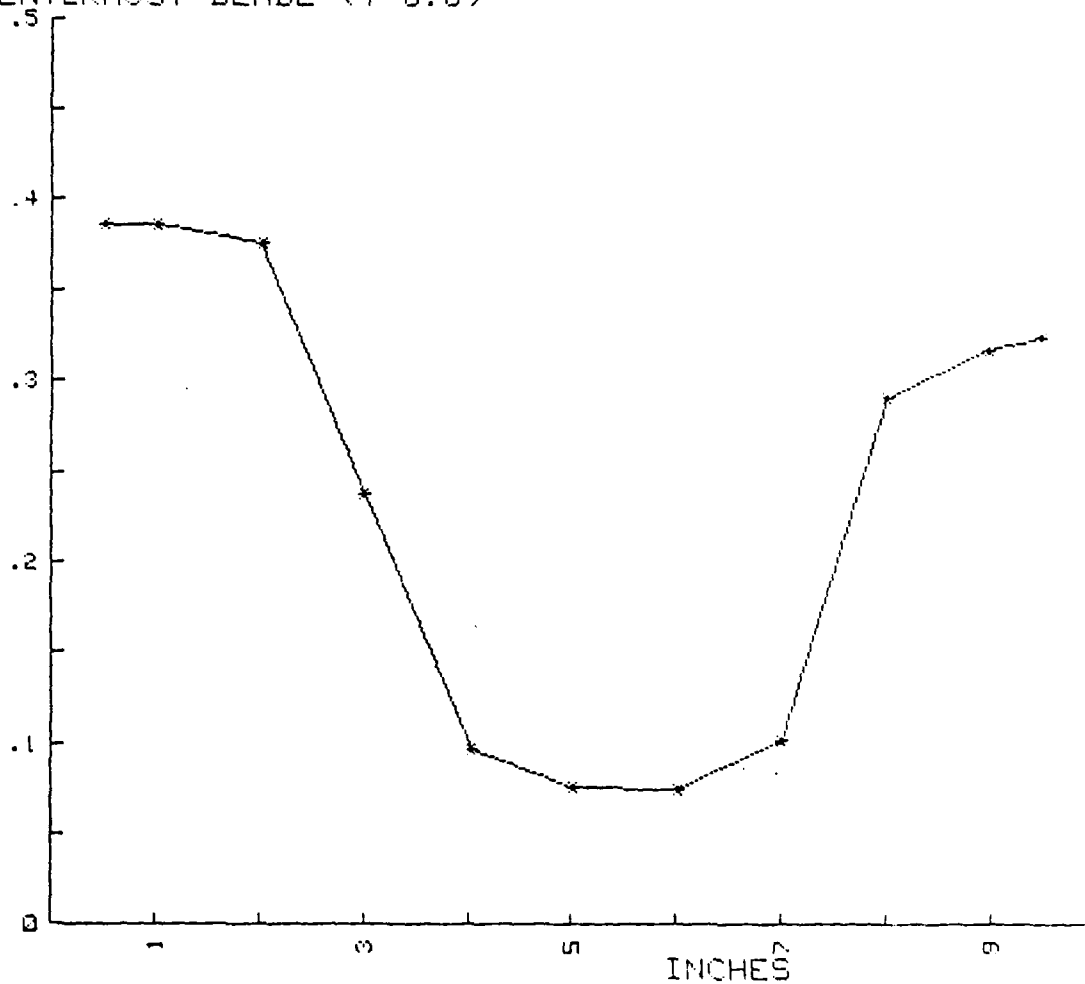
Fig. 64.   Spanwise Probe Data Surveyed 1 in. from
            Suction Side of Centermost Blade
            (i=8.8, $(P_{plen}-P_t)/\overline{Q}_1$, Upper Plane)

106

X/Xbar
1.0 in FROM SUCTION SIDE
CENTERMOST BLADE (i=8.8)

1

.9

.8

.7

.6

.5

INCHES
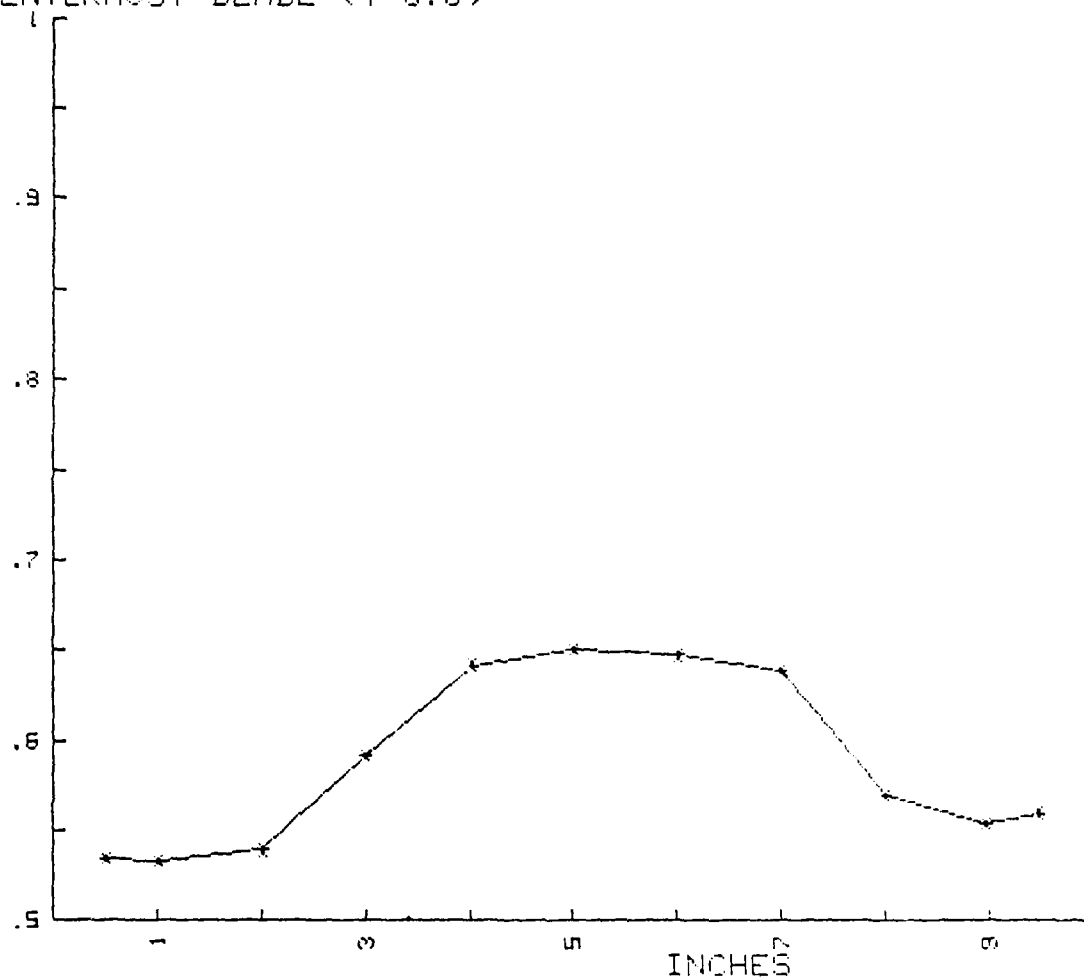
Fig. 65.   Spanwise Probe Data Surveyed 1 in. from
           Suction Side of Centermost Blade
           (i=8.8, X/$\bar{X}$, Upper Plane)

107

(Pplen-Pt)/Q1bar
1.0 in FROM PRESSURE SIDE
CENTERMOST BLADE (i=8.8)
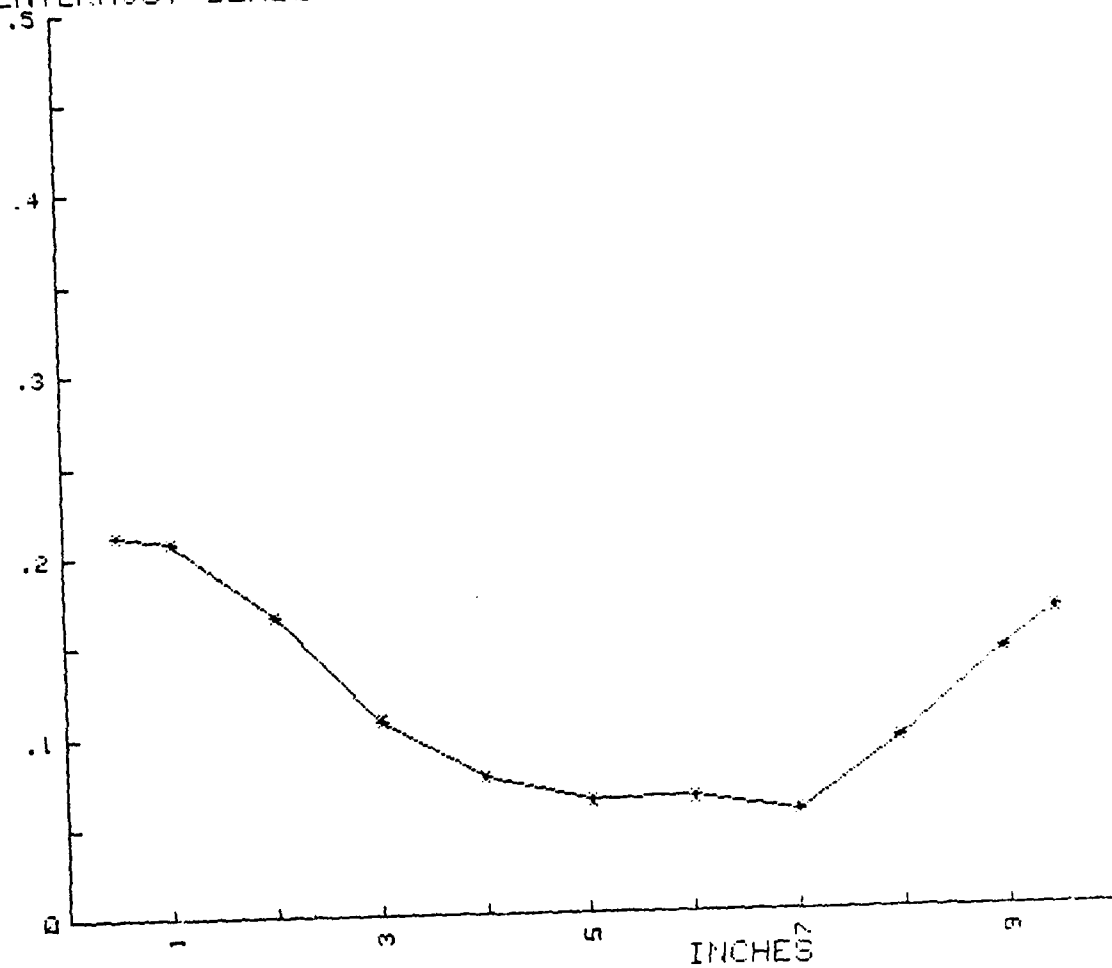
Fig. 66. Spanwise Probe Data Surveyed 1 in. from
Pressure Side of Centermost Blade
(i=8.8, $(P_{plen}-P_t)/\widetilde{Q}_1$, Upper Plane)

X/Xbar
1.0 in FROM PRESSURE SIDE
CENTERMOST BLADE (i=8.8)

INCHES
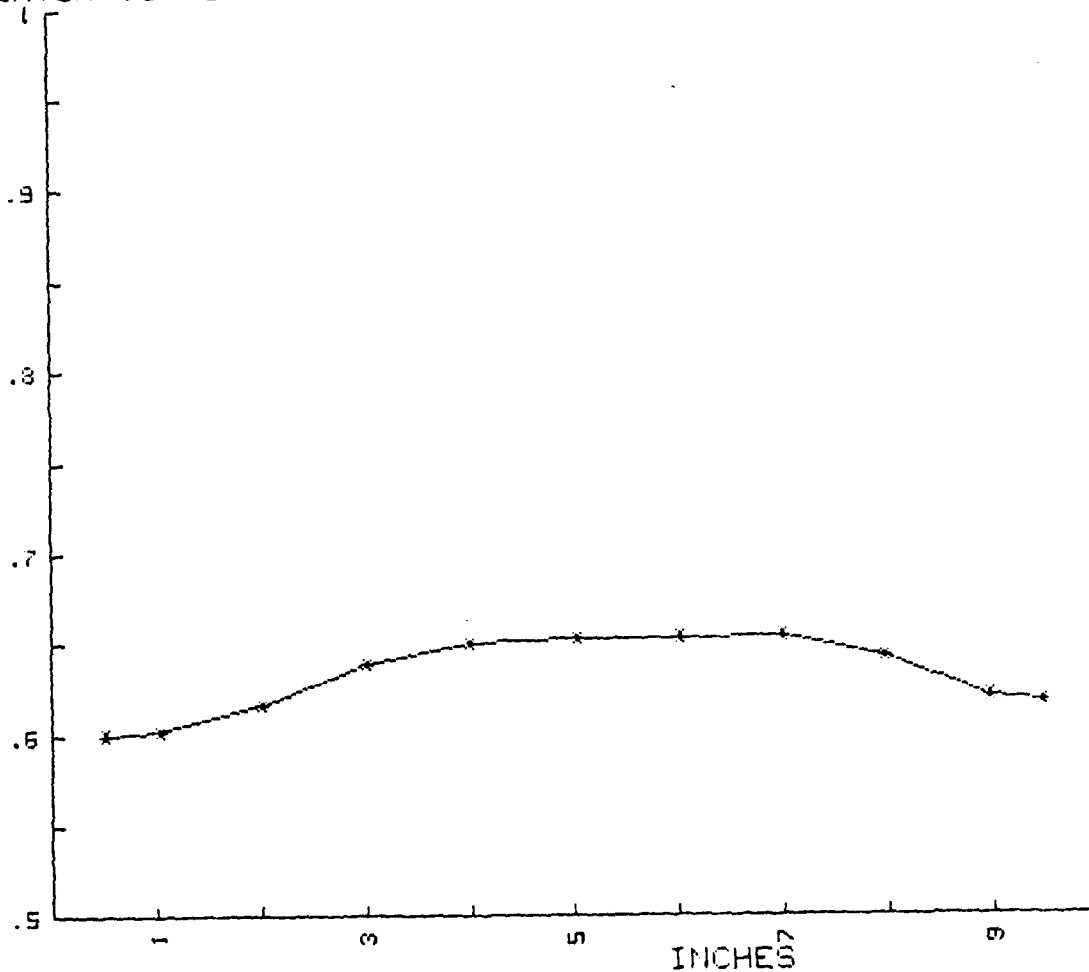
Fig. 67.   Spanwise Probe Data Surveyed 1 in. from
          Pressure Side of Centermost Blade
          i=8.8, X/$\overline{X}$, Upper Plane)

109
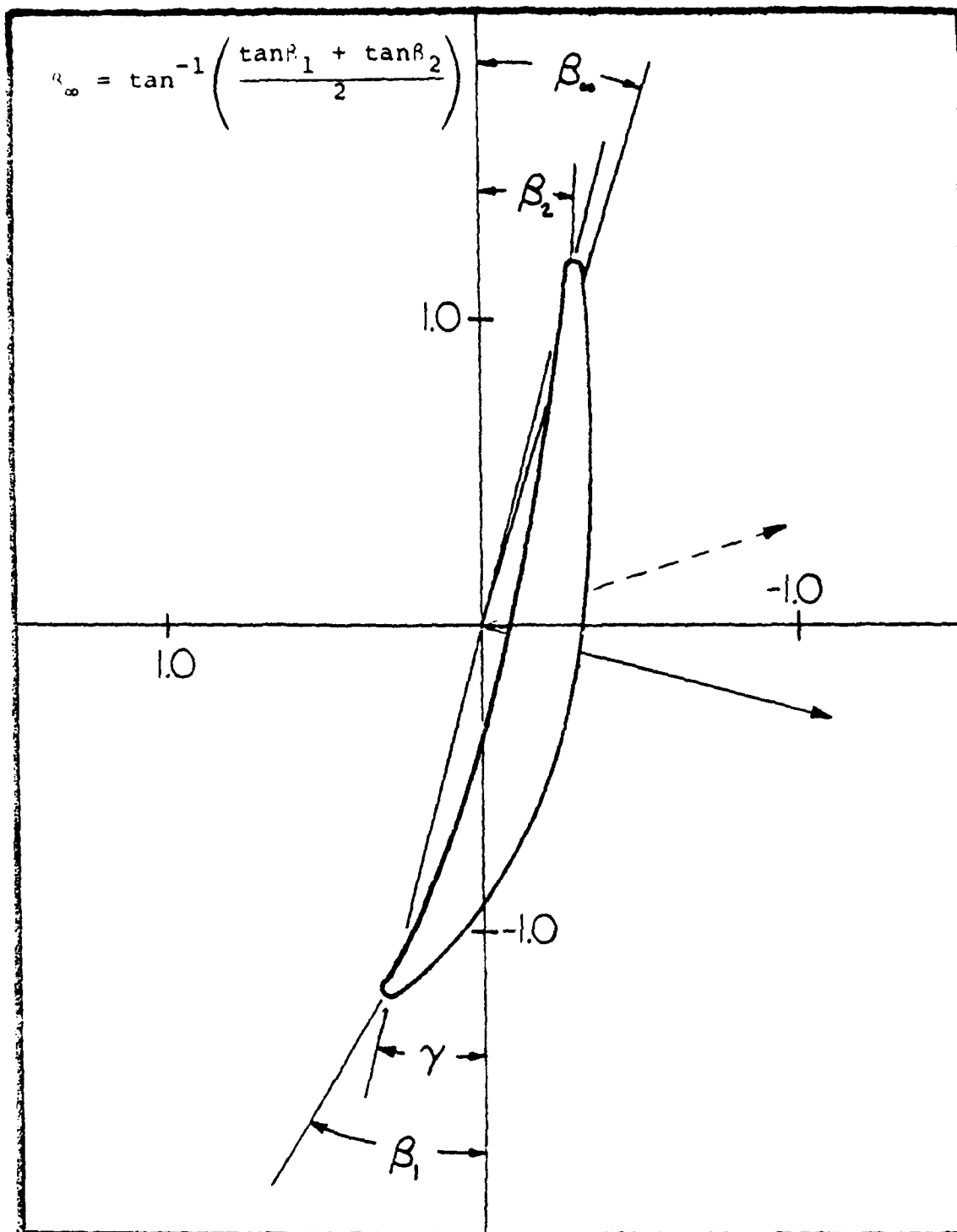
Fig. 68.   Resultant Blade Force Vectors by Momentum
           Balance (– – – –) and from Surface Pressure
           Integration (————)   i=–9.2

110
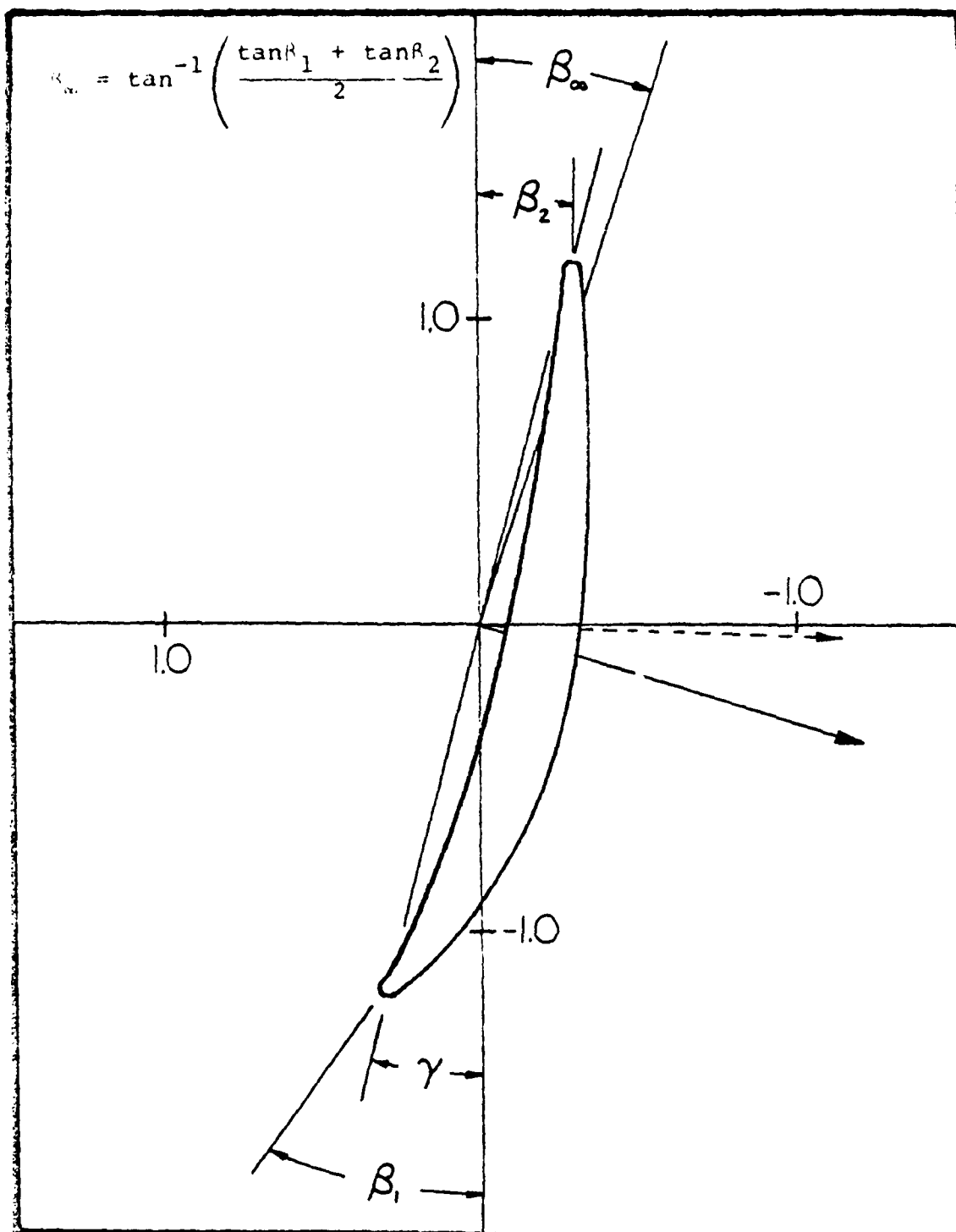
Fig. 69. Resultant Blade Force Vectors by Momentum
Balance (— — — —) and from Surface Pressure
Integration (————) i=-4.9

111

$$\beta_\infty = \tan^{-1}\left(\frac{\tan\beta_1 + \tan\beta_2}{2}\right)$$
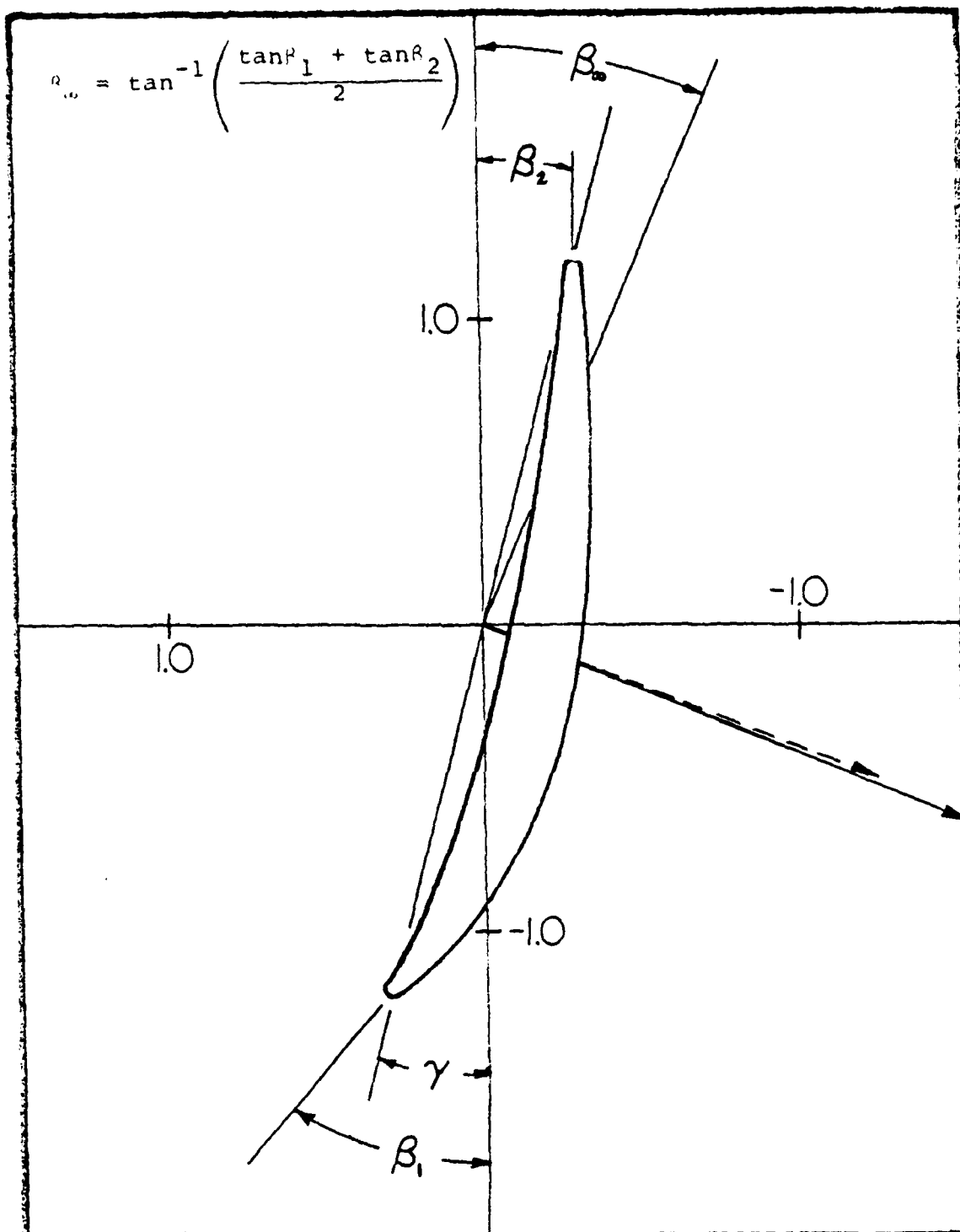
Fig. 70. Resultant Blade Force Vectors by Momentum Balance (− − − −) and from Surface Pressure Integration (————) i=2.1

112

$$\beta_\infty = \tan^{-1}\left(\frac{\tan\beta_1 + \tan\beta_2}{2}\right)$$
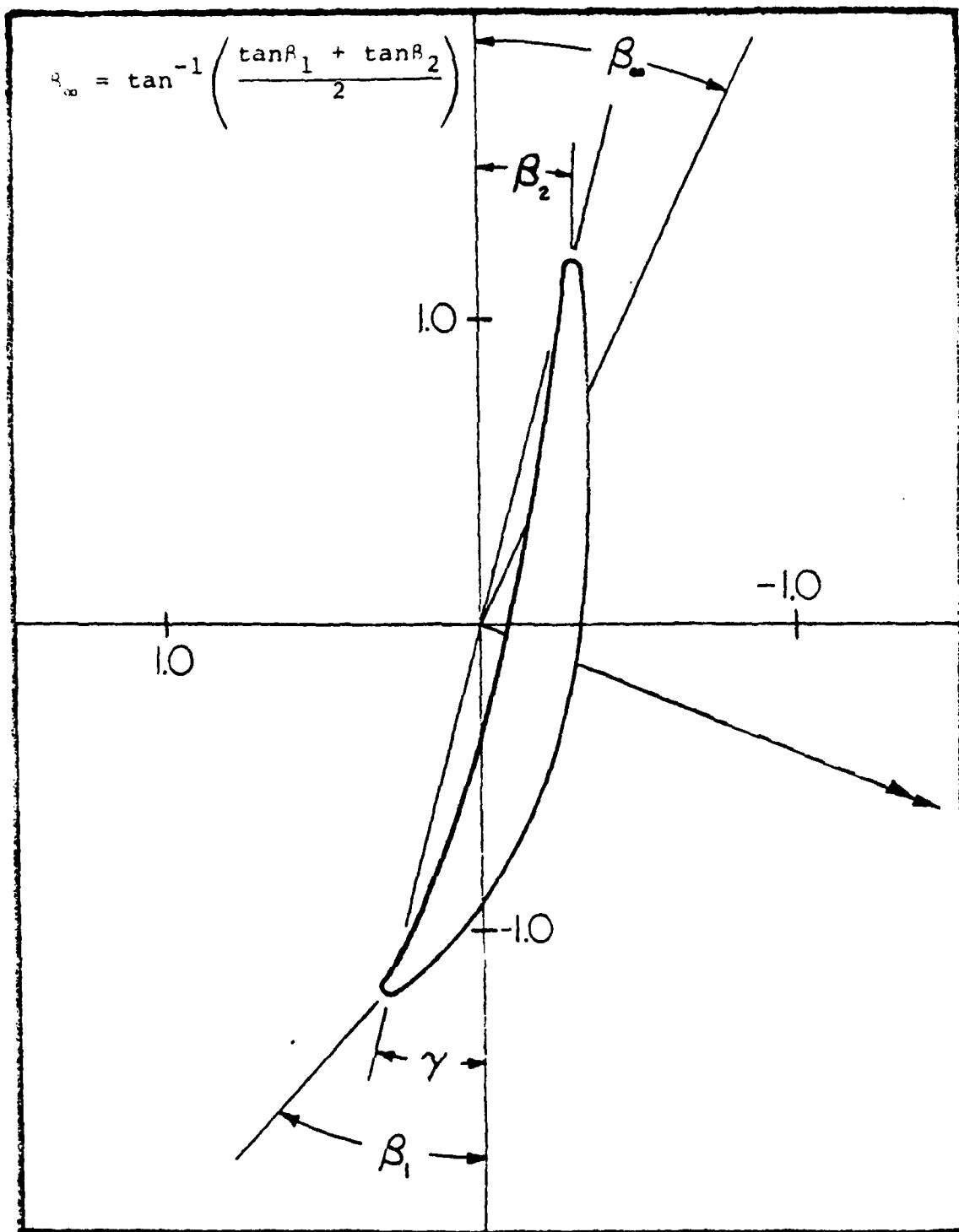
Fig. 71. Resultant Blade Force Vectors by Momentum
Balance (– – – –) and from Surface Pressure
Integration (————)   i=5.3

113
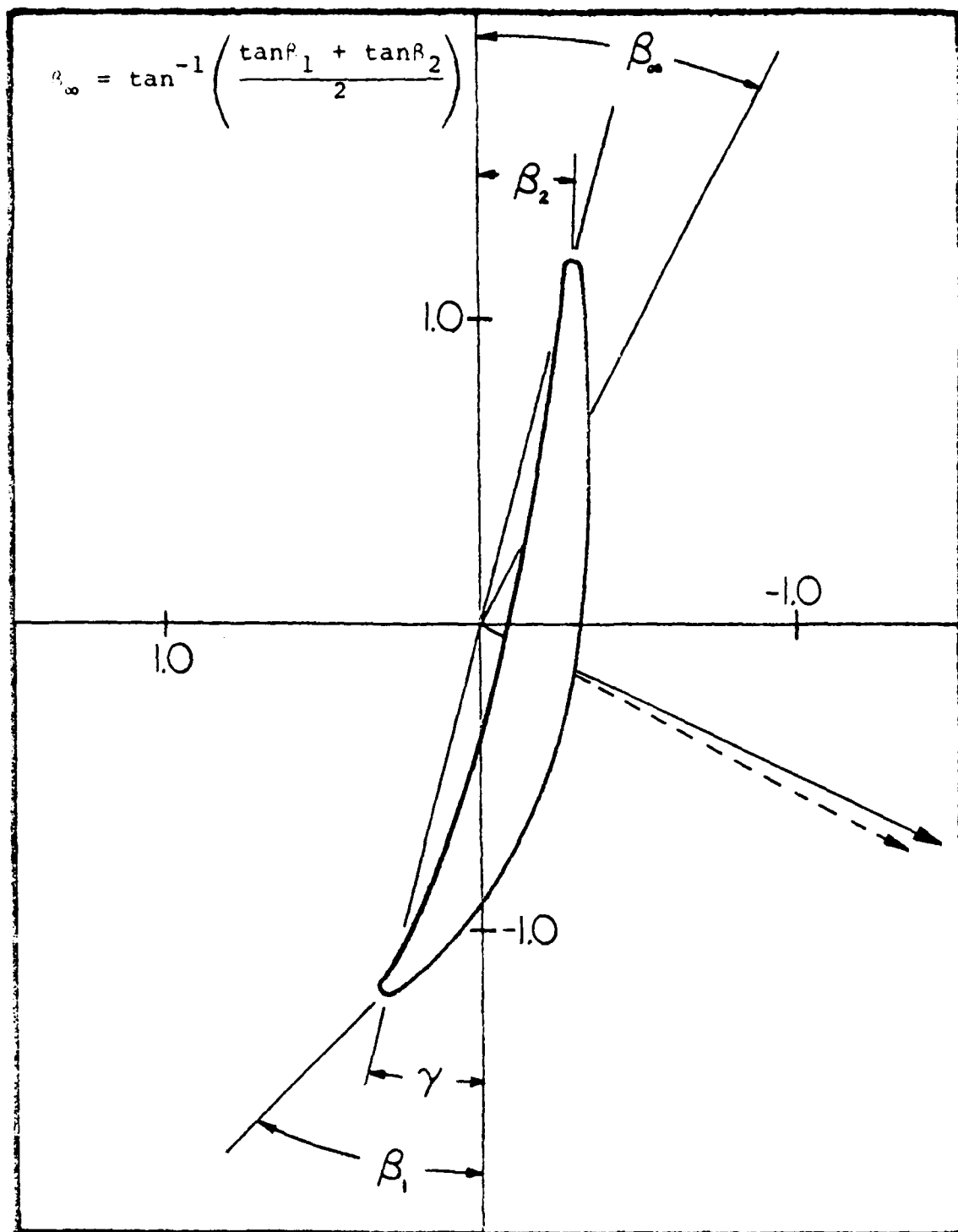
Fig. 72. Resultant Blade Force Vectors by Momentum
Balance (− − − −) and from Surface Pressure
Integration (——————) i=8.8

114

Cp1 vs X/C   (i=-9.2)
CENTERMOST BLADE
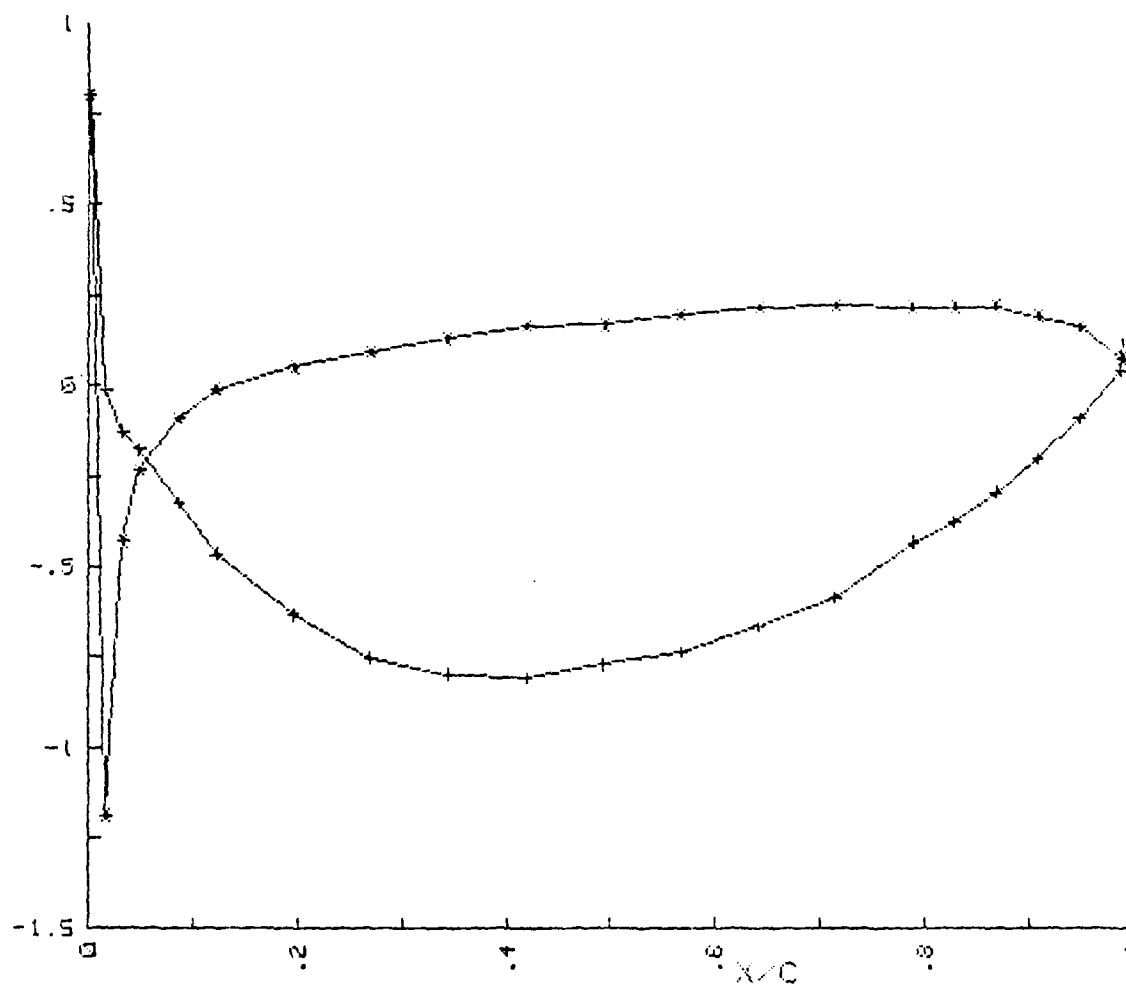
Fig. 73.   Blade Surface Pressure Distribution
(i=-9.2, * = Pressure Side, + = Suction Side)

Xvel vs X/C (i=-9.2)
CENTERMOST BLADE
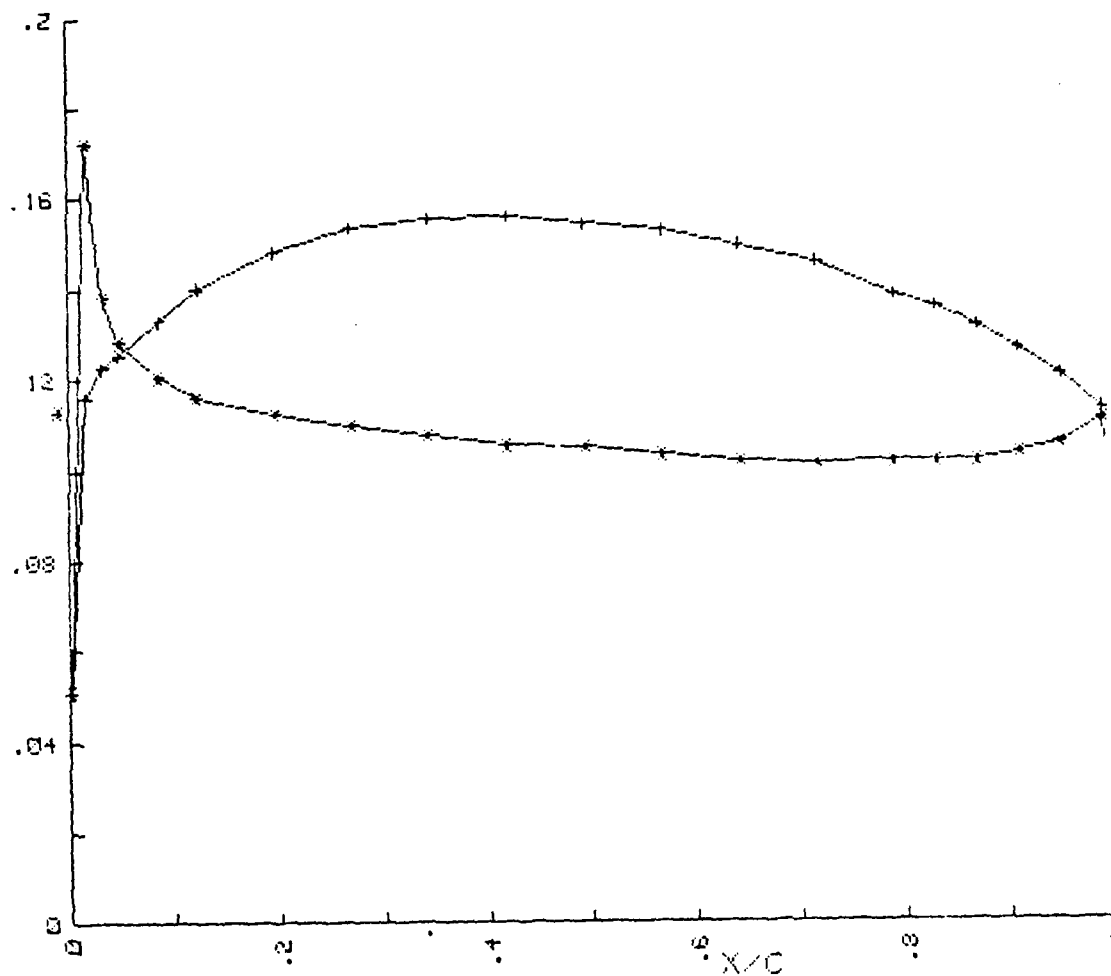
Fig. 74.   Blade Surface Velocity Distribution
(i=-9.2, * = Pressure Side,
+ = Suction Side)

116

Cpl vs X/C   (i=-4.9)
CENTERMOST BLADE
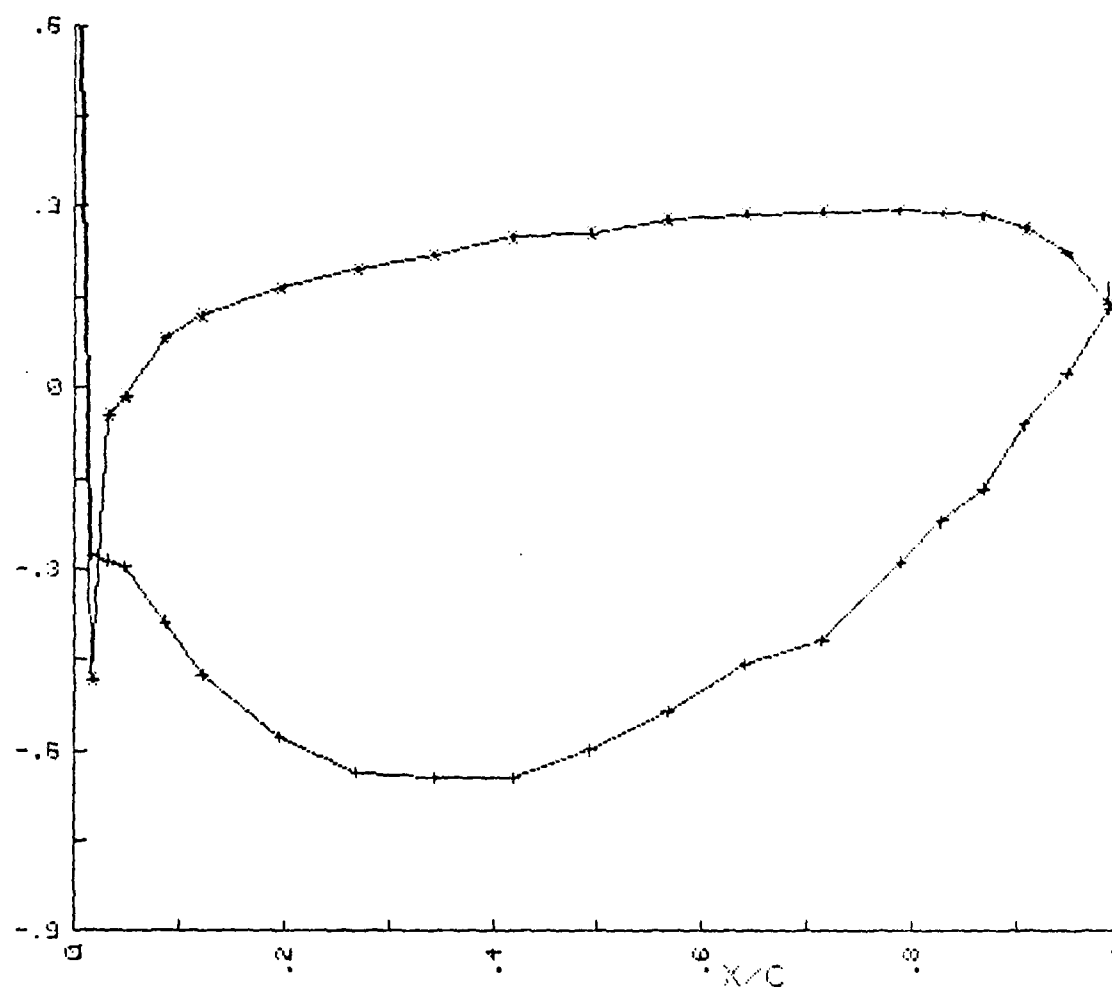
Fig. 75.   Blade Surface Pressure Distribution
(i=-4.9, * = Pressure Side,
+ = Suction Side)

117

Xvel vs X/C (i=-4.9)
CENTERMOST BLADE
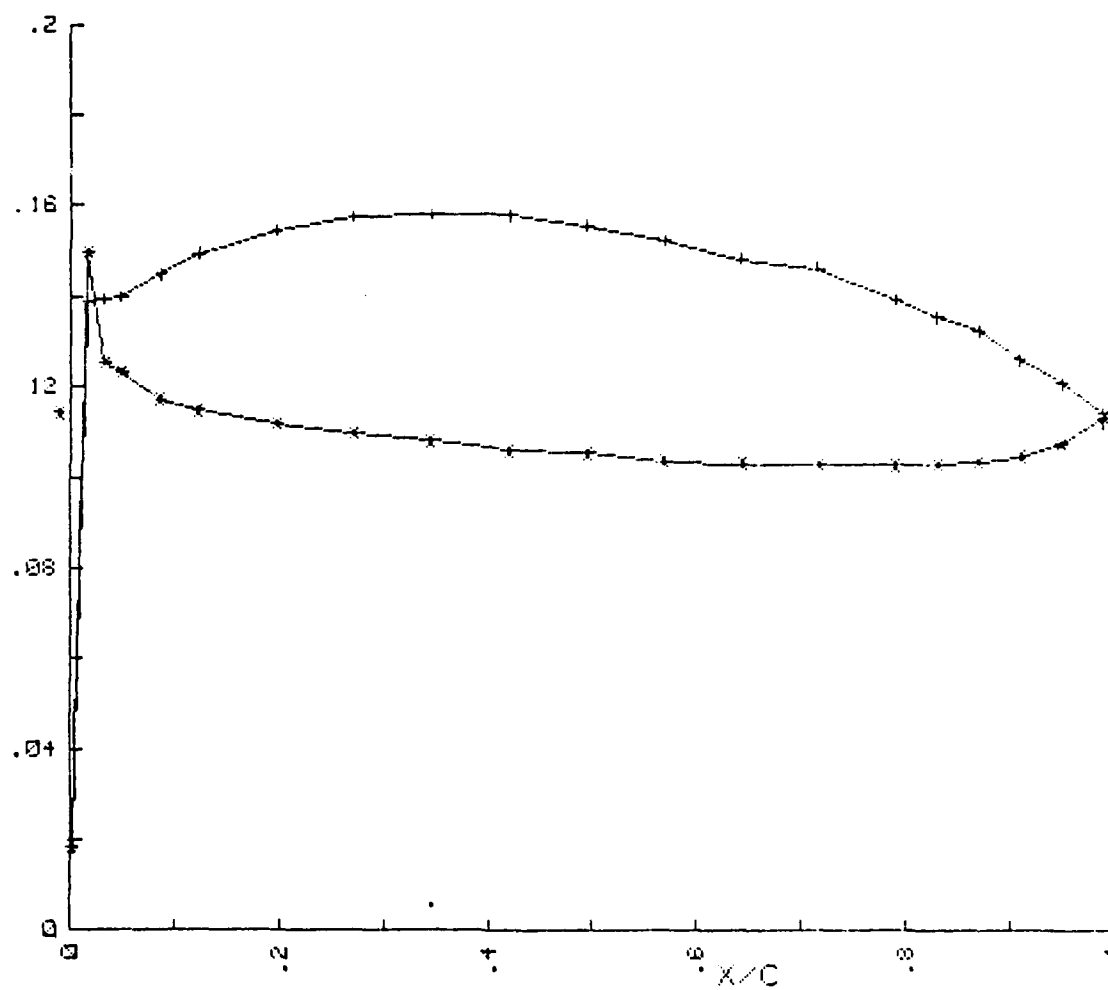
Fig. 76.   Blade Surface Velocity Distribution
(i=-4.9, * = Pressure Side,
+ = Suction Side)

118

Cp1 vs X/C (i=2.1)
CENTERMOST BLADE
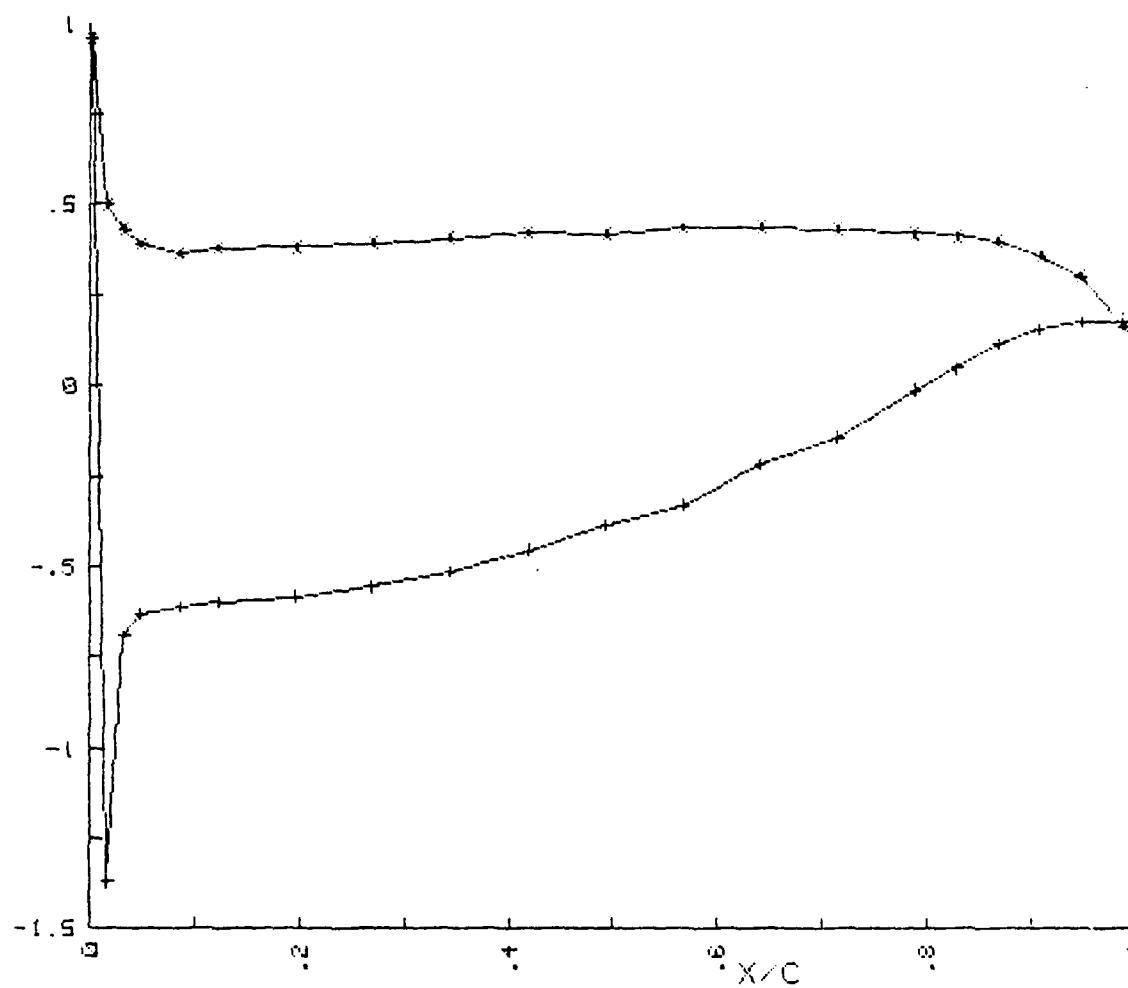
Fig. 77. Blade Surface Pressure Distribution
(i=2.1, * = Pressure Side,
+ = Suction Side)

119

Xvel vs X/C (i=2.1)
CENTERMOST BLADE
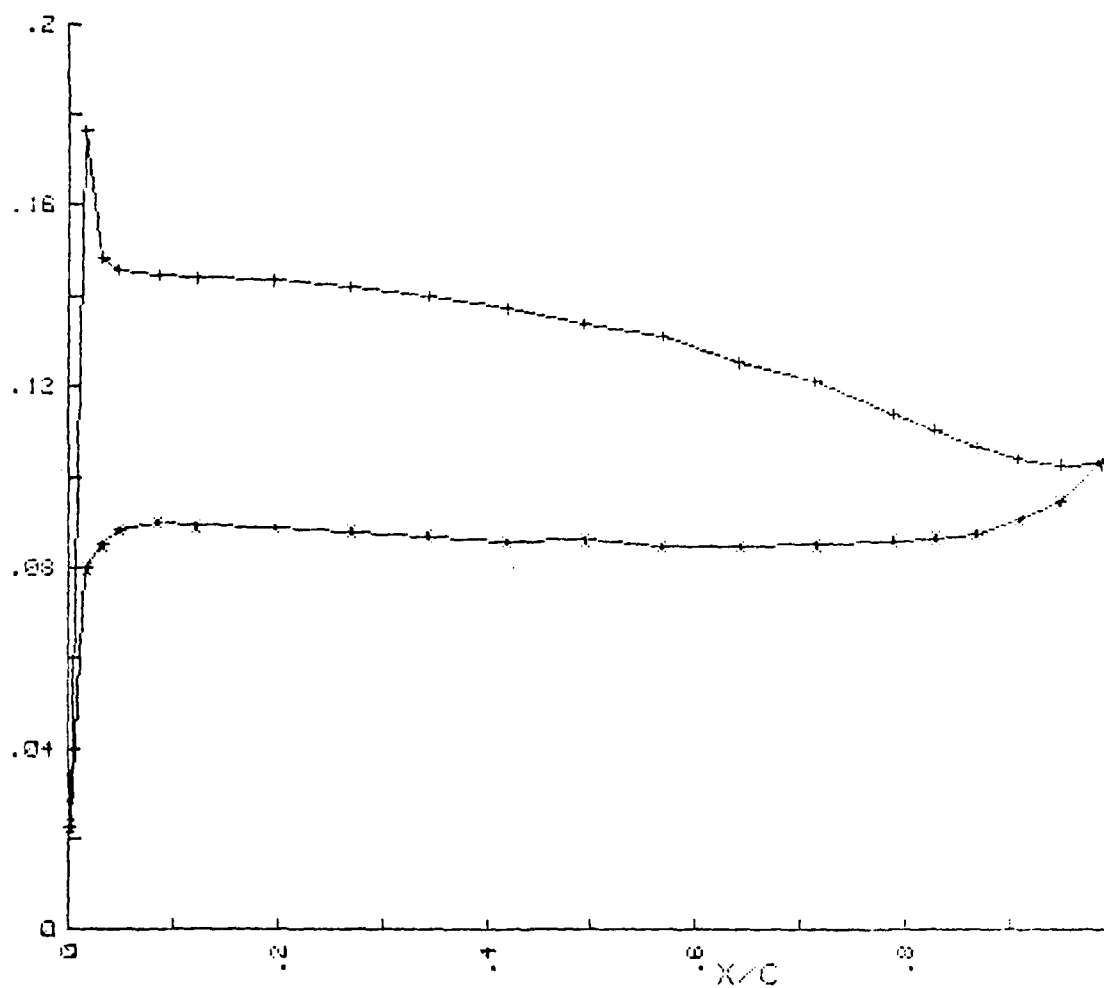
Fig. 78.   Blade Surface Velocity Distribution
(i=2.1, * = Pressure Side,
+ = Suction Side)

120

Cp1 vs X/C (i=5.3)
CENTERMOST BLADE
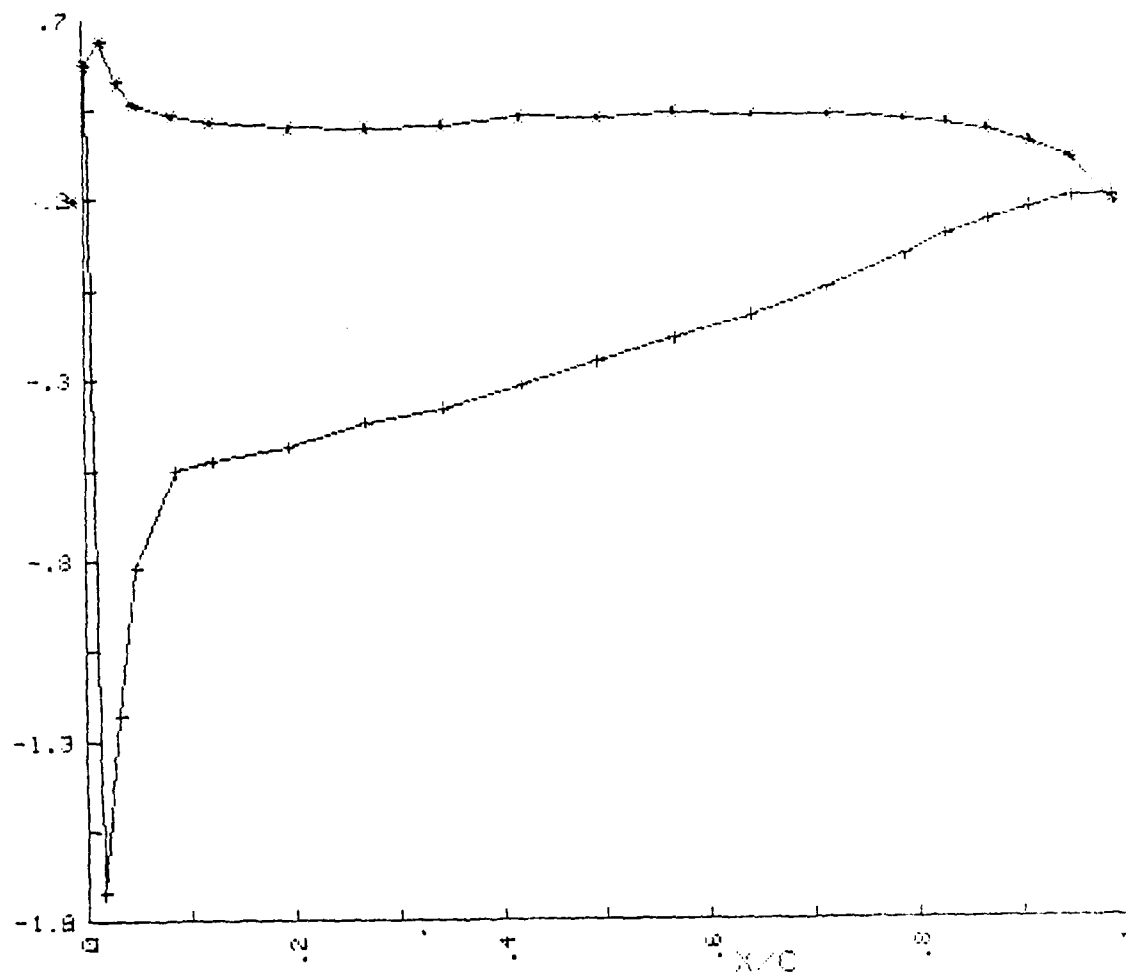
Fig. 79.   Blade Surface Pressure Distribution
(i=5.3, * = Pressure Side,
+ = Suction Side)

121

Xvel vs X/C (i=5.3)
CENTERMOST BLADE
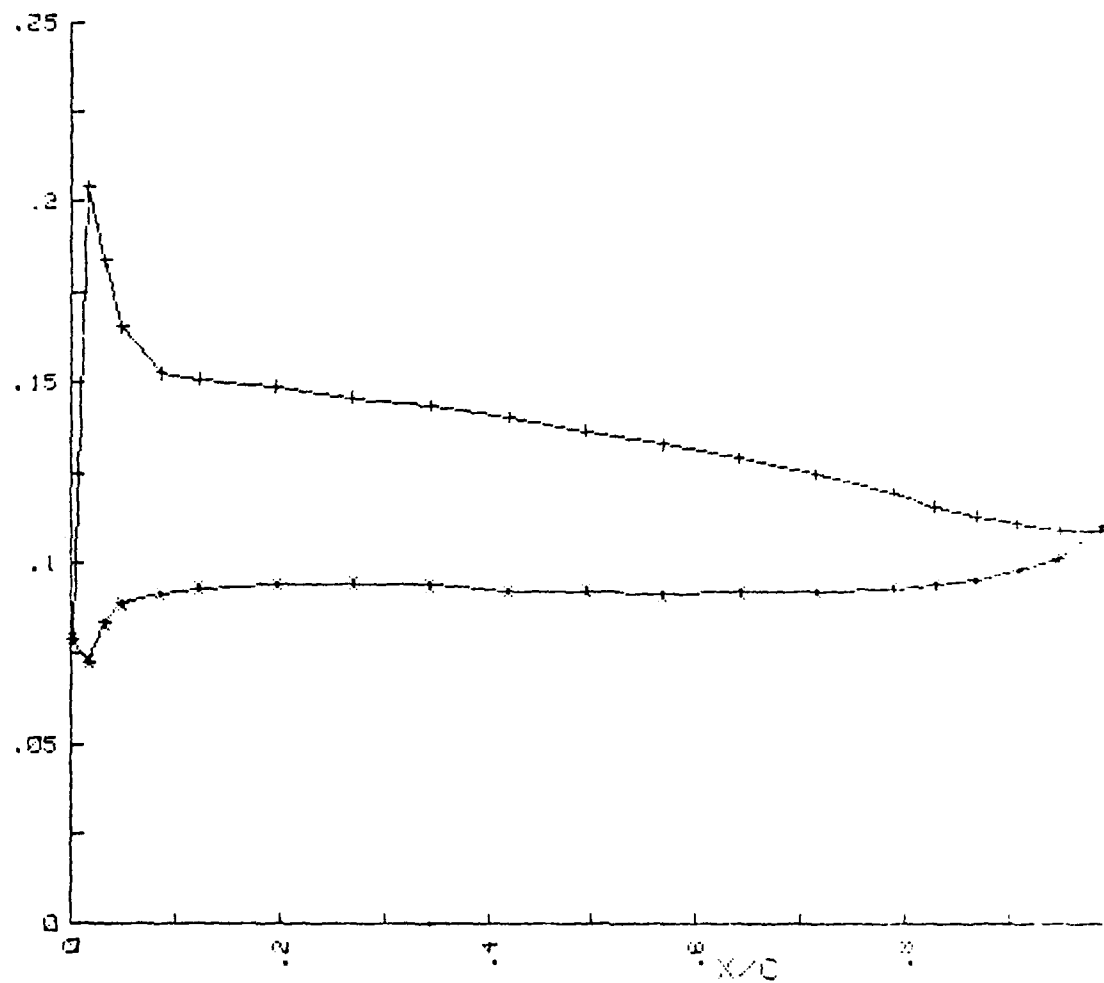
Fig. 80.   Blade Surface Velocity Distribution
(i=5.3, * = Pressure Side,
+ = Suction Side)

122

Cp1 vs X/C (i=8.8)
CENTERMOST BLADE
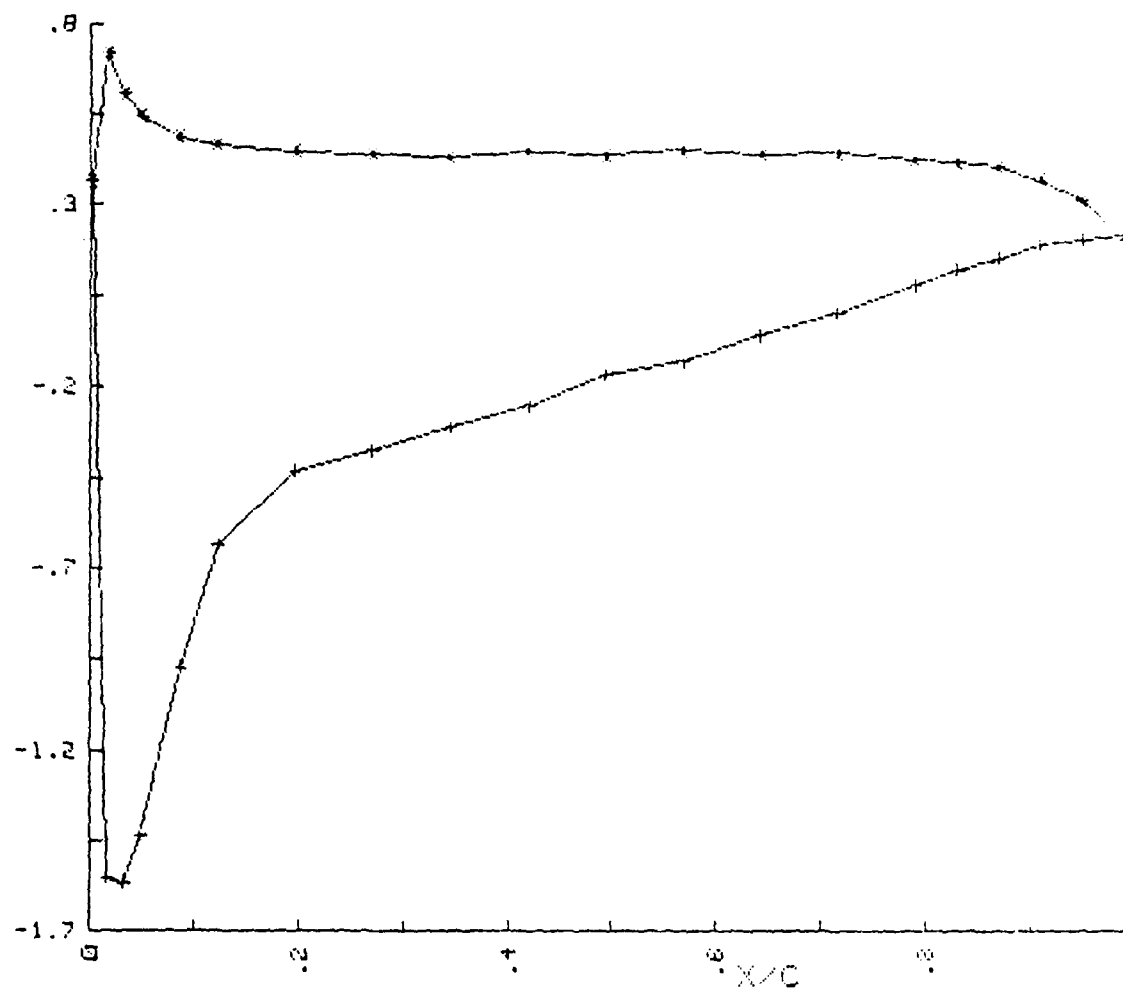
Fig. 81.   Blade Surface Pressure Distribution
           (i=8.8, * = Pressure Side,
                  + = Suction Side)

123

Xvel vs X/C   (i=8.8)
CENTERMOST BLADE
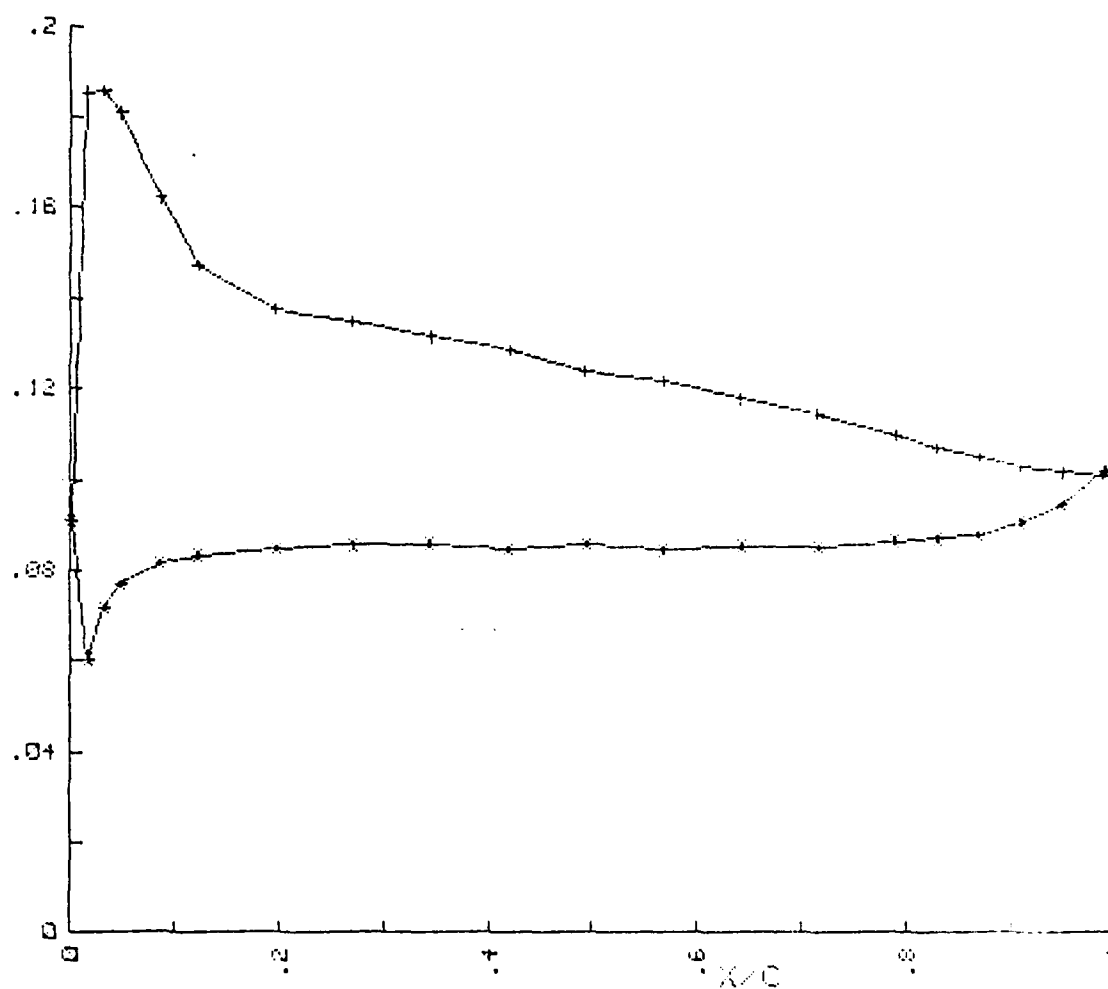
Fig. 82.   Blade Surface Velocity Distribution
(i=8.8, * = Pressure Side,
+ = Suction Side)

124
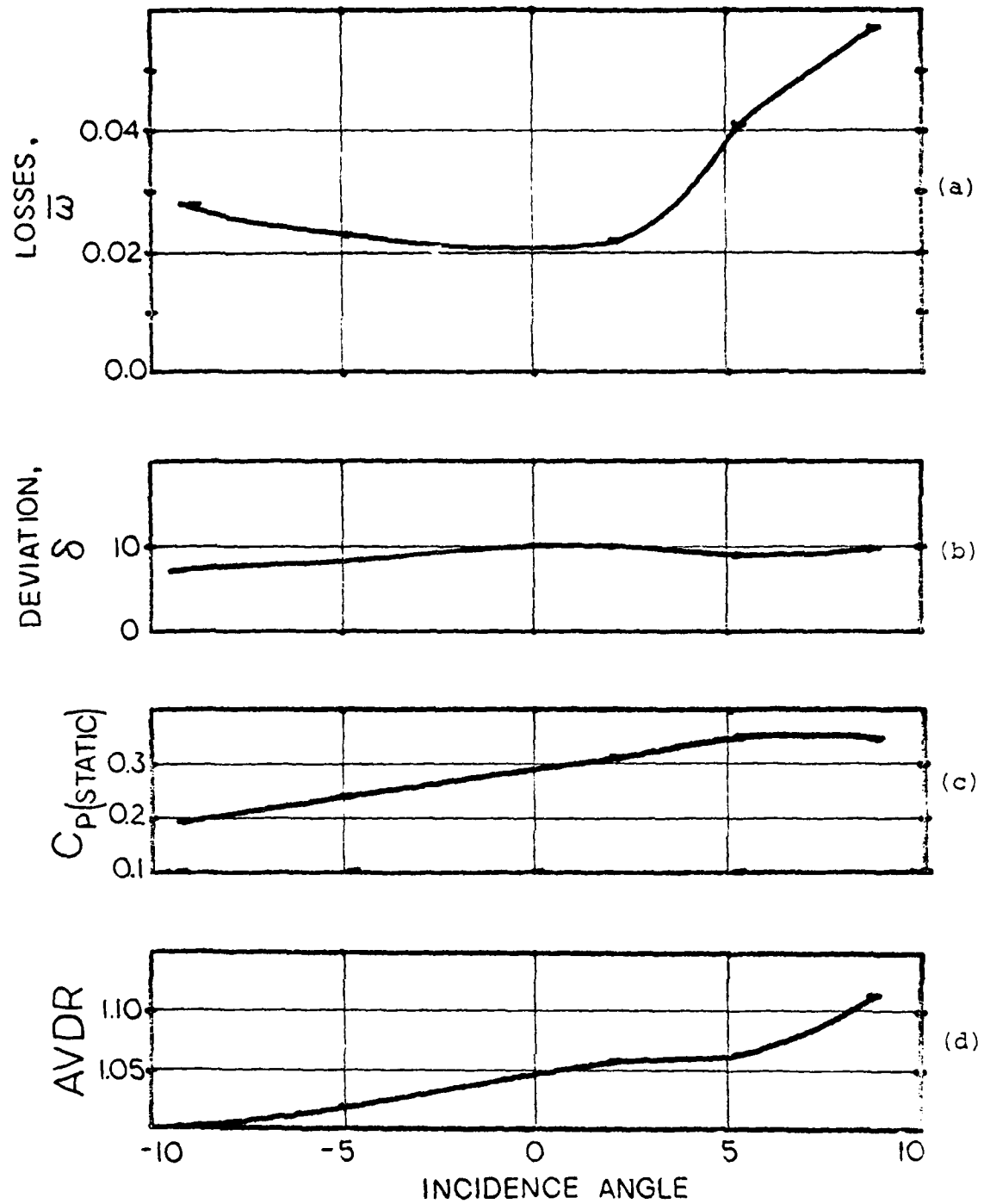
Fig. 83. Blade Element Performance Parameters and AVDR As a Function of Incidence Angle

(a)

$$\frac{\bar{\omega}\cos^3\beta_2}{2\sigma\cos^2\beta_1}$$

(b)

AVDR
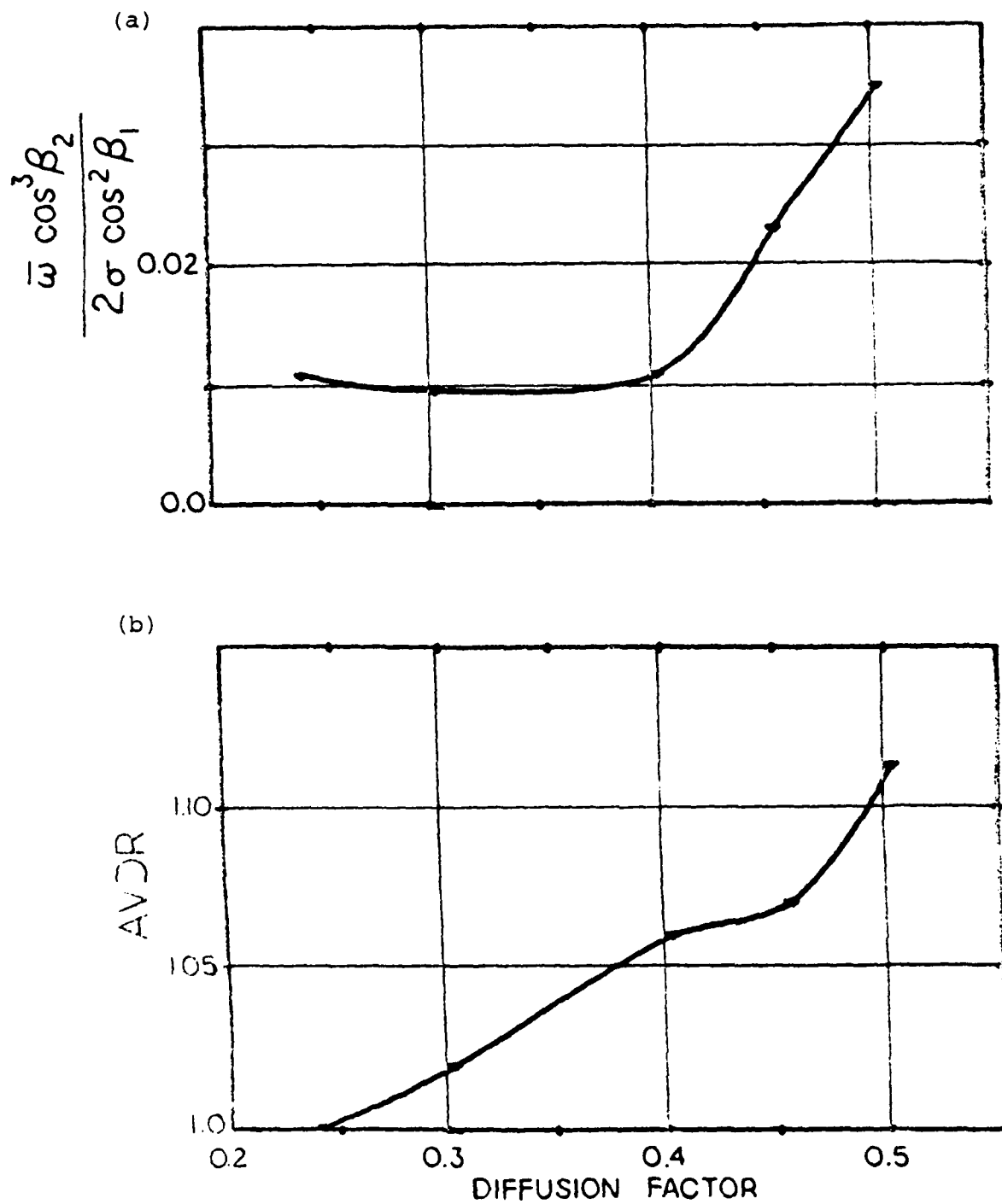
DIFFUSION FACTOR

Fig. 84.   Loss Parameter and AVDR as a Function
of Diffusion Factor

126
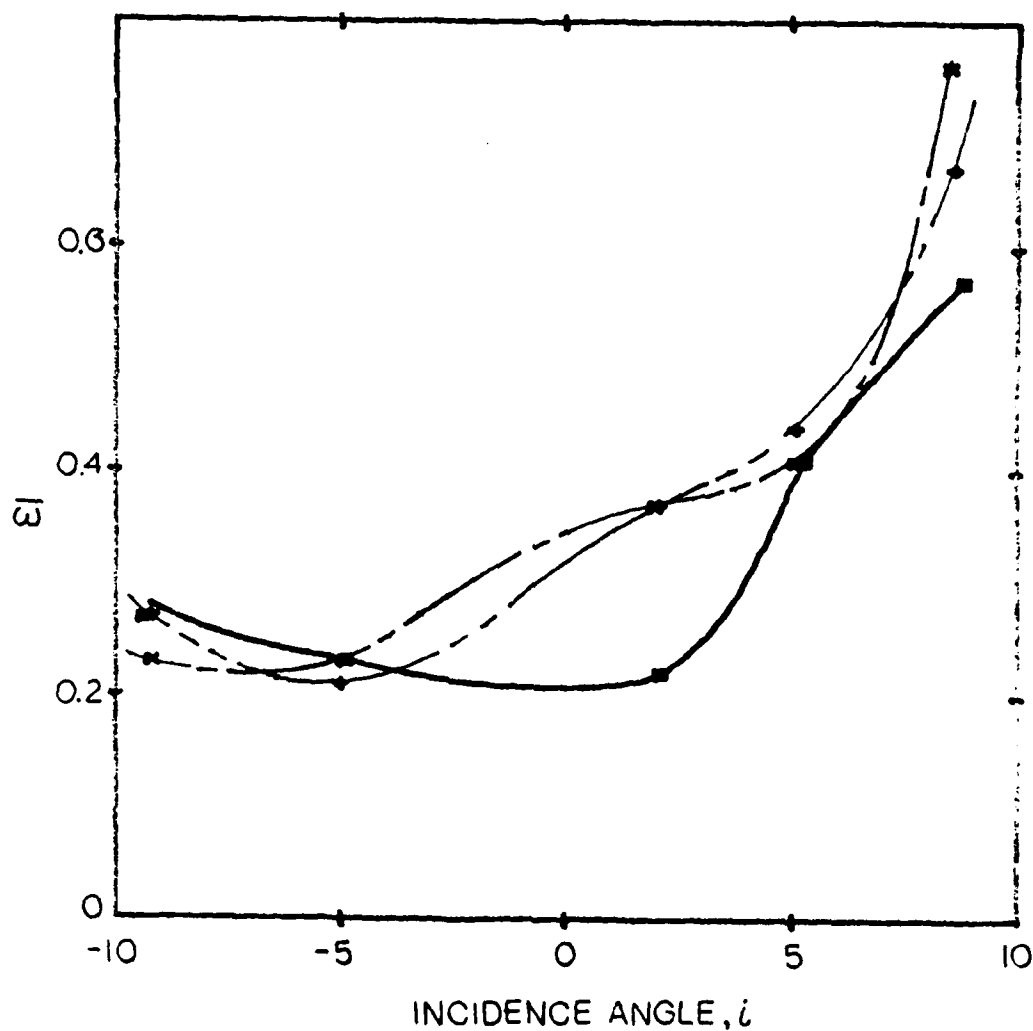
LOSS COEFFICIENTS

Fig. 85. Loss Coefficients Computed at 3 Blade-to-
Blade Locations

127

TABLE I. TEST BLADE COORDINATES

X-COORD.	Y-PRESS.	Y-SUCT.
-0.044	0.000	0.000
-0.021	-----	0.039
0.013	-0.042	-----
0.178	0.007	0.142
0.400	0.067	0.244
0.622	0.120	0.333
0.844	0.164	0.413
1.067	0.207	0.480
1.289	0.242	0.538
1.511	0.271	0.584
1.733	0.293	0.620
1.956	0.309	0.649
2.178	0.320	0.664
2.399	0.324	0.673
2.622	0.324	0.671
2.844	0.318	0.660
3.066	0.304	0.640
3.288	0.284	0.607
3.511	0.260	0.567
3.732	0.229	0.515
3.955	0.191	0.453
4.177	0.147	0.380
4.400	0.098	0.298
4.621	0.040	0.200
4.844	-0.022	0.091
4.908	-0.042	-----
4.943	-----	0.040
4.966	0.000	0.000

TABLE II.   MEASUREMENT UNCERTAINTY

Item	Description	Method	Uncertainty
x	Blade-to-Blade dimension $x = 0$ in. West end $x = 60$ in. East end	Position Potentiometer	$\pm$ .01 in.
z	Spanwise dimension $z = 0$ in. North wall $z = 10$ in. South wall	Position Potentiometer on probe mount	$\pm$ .01 in.
β_1	Inlet flow yaw angle	Angle Potentio- meter on probe mount (hand adjustment)	$\pm$ .1 deg.
β_2	Outlet flow yaw angle	Angle Potentio- meter on probe mount (motor driven adjustment)	$\pm$ .25 deg.
P_t	Total pressure at the test plane	Pneumatic probe	$\pm$ .1 in. H_2O
P_{plen}	Plenum total pressure	Static tap in plenum chamber $V \sim 0$	$\pm$ .1 in. H_2O
P_s	Static pressure at the test plane	Calibrated pneu- matic probe	$\pm$ .15 in. H_2O
$P_{w\ell}$	Static pressure at $x = 0$ in., $y = =16.25$ in., $z = 0$ in.	Static tap on North wall	$\pm$ .1 in H_2O
P_{ATM}	Atmospheric pressure	Absolute Strain Gauge Transducer	$\pm$ .6 in. H_2O
P_{TARE}	Transducer tare reading	Scanivalve	$\pm$ .01 in. H_2O

TABLE III. CASCADE CONFIGURATION DATA

Constant Parameters

Blade type	DCA
Number of blades	20
Spacing (inches)	3.0
Solidity	1.67
Thickness (% chord)	7.0
Camber angle	45.72
Stagger angle	14.27

Variable Parameters

	Test 1	Test 2	Test 3	Test 4	Test 5
β_1	39.2	45.9	42.4	32.2	27.9
i	2.1	8.8	5.3	-4.9	-9.2

TABLE IV. PROBE DATA, UPPER PLANE AT MIDSPAN
(i = -9.2)

BLADE TO BLADE TRAVERSE MIDSPAN

UPPER PLANE

Point	Loc(in)	Beta	Q/01bar	Ps/01bar	Pt/01bar	X/01bar
1	-7.34	2.17	.6971	.1325	.1671	.7845
2	-6.90	2.14	.7446	.1922	.1101	.8098
3	-6.39	2.16	.8008	.1850	.0535	.8420
4	-5.91	2.13	.7901	.1863	.0679	.8345
5	-5.42	2.12	.8055	.1857	.0525	.8427
6	-4.93	2.14	.8283	.1822	.0288	.8559
7	-4.44	3.24	.7572	.1935	.0963	.8162
8	-3.94	3.25	.7641	.1899	.0916	.8206
9	-3.47	3.26	.8142	.1876	.0484	.8445
10	-2.96	3.26	.8249	.1887	.0339	.8509
11	-2.48	3.24	.8157	.1872	.0370	.8492
12	-1.98	3.03	.8002	.1912	.0566	.8382
13	-1.79	3.05	.7908	.1888	.0673	.8339
14	-1.58	3.03	.7337	.1969	.1281	.7996
15	-1.37	3.00	.6792	.1819	.1941	.7716
16	-1.18	3.04	.7143	.1866	.1521	.7915
17	-.99	3.04	.7745	.2009	.0843	.8204
18	-.78	3.05	.7939	.1994	.0643	.8312
19	-.61	2.86	.8042	.1937	.0531	.8371
20	-.40	2.84	.8020	.1924	.0533	.8354
21	-.22	2.87	.7981	.1964	.0704	.8307
22	-.01	2.87	.8058	.1930	.0591	.8353
23	.19	2.85	.8008	.1998	.0698	.8299
24	.41	2.84	.8116	.1937	.0545	.8394
25	.60	2.90	.8184	.1943	.0482	.8424
26	.78	2.88	.8334	.2055	.0339	.8451
27	1.00	2.87	.8209	.2015	.0458	.8407
28	1.18	2.84	.8215	.1980	.0463	.8420
29	1.39	2.84	.7798	.1998	.0869	.8207
30	2.01	2.84	.7702	.1983	.1007	.8148
31	2.50	2.83	.8344	.1993	.0447	.8436
32	3.00	2.89	.8490	.1929	.0277	.8542
33	3.50	2.85	.8293	.2045	.0509	.8386
34	4.00	2.87	.8022	.2051	.0704	.8278
35	4.51	2.89	.7389	.1998	.1436	.7939

TABLE V. PROBE DATA, LOWER PLANE AT MIDSPAN
(i = -9.2)

BLADE TO BLADE TRAVERSE MIDSPAN

LOWER PLANE

Point	Loc(in)	Beta	Q/Q1bar	Ps/Q1bar	Pt/Q1bar	X/Xbar
1	-4.50	-28.06	1.0258	-.0156	.0072	.9626
2	-4.00	-28.04	1.0106	-.0190	.0191	.9589
3	-3.50	-28.07	.9459	-.0185	.0974	.9229
4	-3.00	-28.07	1.0175	-.0103	.0139	.9571
5	-2.50	-28.05	1.0186	-.0072	.0144	.9554
6	-2.00	-27.07	.9919	-.0097	.0453	.9427
7	-1.50	-28.56	.9480	-.0043	.0875	.9208
8	-1.00	-27.81	1.0183	-.0074	.0134	.9560
9	-.50	-27.81	1.0198	-.0103	.0046	.9613
10	0.00	-27.83	.9613	.0060	.0690	.9246
11	.50	-27.83	.9577	-.0069	.0782	.9263
12	1.00	-27.81	1.0122	-.0087	.0221	.9526
13	1.50	-27.80	1.0061	-.0103	.0273	.9511

132

TABLE VI. CENTER BLADE DATA (i = -9.2)

X/C	Y/C	Cp1	Cp2	Mach	Mrel
PRESSURE SIDE CENTER BLADE					
.0007	.0054	.8021	.7892	.1140	.0509
.0160	.0019	-1.1887	-1.7108	.3910	.1722
.0319	.0066	-.4314	-.7598	.3124	.1394
.0479	.0112	-.2339	-.5117	.2892	.1293
.0858	.0215	-.0907	-.3319	.2713	.1204
.1218	.0303	-.0096	-.2301	.2607	.1158
.1956	.0452	.0499	-.1554	.2527	.1123
.2695	.0576	.0919	-.1025	.2463	.1097
.3433	.0663	.1234	-.0568	.2417	.1079
.4192	.0716	.1638	-.0123	.2366	.1052
.4930	.0736	.1684	-.0065	.2359	.1049
.5669	.0727	.1961	.0283	.2319	.1031
.6407	.0678	.2161	.0534	.2289	.1018
.7146	.0601	.2233	.0624	.2278	.1014
.7884	.0487	.2192	.0572	.2285	.1016
.8283	.0411	.2132	.0560	.2286	.1017
.8683	.0327	.2192	.0572	.2285	.1016
.9082	.0230	.1920	.0231	.2325	.1034
.9481	.0123	.1617	-.0149	.2369	.1054
.9880	.0006	.0750	-.1238	.2492	.1108
SUCTION SIDE CENTER BLADE					
.0160	.0227	-.0102	-.2308	.2608	.1158
.0319	.0310	-.1266	-.3770	.2759	.1224
.0479	.0289	-.1774	-.4408	.2822	.1252
.0858	.0563	-.3237	-.6245	.2999	.1329
.1218	.0710	-.4658	-.8029	.3163	.1401
.1956	.0970	-.6331	-1.0130	.3348	.1481
.2695	.1170	-.7516	-1.1618	.3473	.1535
.3433	.1309	-.7933	-1.2205	.3522	.1556
.4192	.1399	-.8070	-1.2314	.3531	.1560
.4930	.1432	-.7701	-1.1850	.3493	.1543
.5669	.1412	-.7352	-1.1412	.3456	.1528
.6407	.1339	-.6623	-1.0497	.3379	.1494
.7146	.1209	-.5864	-.9543	.3297	.1459
.7884	.1021	-.4324	-.7610	.3125	.1384
.8283	.0895	-.3775	-.6921	.3062	.1357
.8683	.0755	-.2965	-.5903	.2967	.1315
.9082	.0593	-.2000	-.4692	.2850	.1264
.9481	.0407	-.0907	-.3319	.2713	.1204
.9880	.0206	.0391	-.1689	.2541	.1129

TABLE VII. ADJACENT BLADES DATA (i = -9.2)

X/C	Y/C	Cp1	Cp2	Mach	Mvel

PRESSURE SIDE LEFT BLADE

X/C	Y/C	Cp1	Cp2	Mach	Mvel
.1218	.0303	-.1369	-.3899	.2772	.1233
.4192	.0716	.1345	-.0491	.2408	.1071
.8283	.0411	.2120	.0482	.2295	.1021

SUCTION SIDE LEFT BLADE

X/C	Y/C	Cp1	Cp2	Mach	Mvel
.1218	.07.0	-.3827	-.6985	.3068	.1359
.4192	.1400	-.7490	-1.1586	.3471	.1534
.8283	.0895	-.3642	-.6754	.3047	.1350

PRESSURE SIDE RIGHT BLADE

X/C	Y/C	Cp1	Cp2	Mach	Mvel
.1218	.0303	.1012	-.0909	.2455	.1092
.4192	.0716	.1509	-.0284	.2385	.1060
.8283	.0411	.2264	.0663	.2274	.1012

SUCTION SIDE RIGHT BLADE

X/C	Y/C	Cp1	Cp2	Mach	Mvel
.1218	.0710	-.4324	-.7610	.3125	.1384
.4192	.1400	-.7521	-1.1625	.3474	.1535
.8283	.0895	-.3396	-.6444	.3018	.1338

TABLE VIII.   PROBE DATA, UPPER PLANE AT MIDSPAN
           (i = -4.9)

BLADE TO BLADE TRAVERSE MIDSPAN

UPPER PLANE

Point	Loc(in)	Beta	Q/Q1bar	Ps/Q1bar	Pt/Q1bar	M/Q1bar
1	-7.39	1.76	.7203	.2480	.0681	.7681
2	-6.90	1.80	.7594	.2382	.0399	.7879
3	-6.41	1.77	.7435	.2346	.0576	.7805
4	-5.92	1.75	.7516	.2358	.0544	.7824
5	-5.42	1.77	.7655	.2384	.0354	.7903
6	-4.94	1.79	.7082	.2451	.0857	.7610
7	-4.45	1.77	.6704	.2514	.1202	.7398
8	-3.95	1.76	.7577	.2308	.0481	.7875
9	-3.47	1.78	.7728	.2335	.0340	.7936
10	-2.97	1.79	.7778	.2371	.0245	.7964
11	-2.49	1.74	.7520	.2374	.0568	.7810
12	-1.98	1.73	.6891	.2561	.0976	.7494
13	-1.77	1.76	.6258	.2492	.1714	.7140
14	-1.58	1.76	.6808	.2592	.0998	.7450
15	-1.37	1.76	.7605	.2473	.0286	.7885
16	-1.18	1.74	.7684	.2433	.0268	.7919
17	-.99	1.73	.7562	.2374	.0472	.7851
18	-.79	1.76	.7390	.2489	.0603	.7735
19	-.61	1.78	.7322	.2469	.0649	.7715
20	-.39	1.77	.7345	.2464	.0626	.7730
21	-.21	1.79	.7367	.2454	.0617	.7740
22	-.00	1.75	.7565	.2413	.0435	.7850
23	.19	1.76	.7590	.2376	.0463	.7859
24	.40	1.76	.7540	.2371	.0467	.7851
25	.59	1.74	.7650	.2375	.0318	.7919
26	.80	1.75	.7515	.2415	.0477	.7827
27	1.03	1.76	.7036	.2497	.0894	.7572
28	1.20	1.77	.6596	.2391	.1394	.7356
29	1.41	1.81	.6423	.2454	.1496	.7262
30	2.02	1.74	.7576	.2327	.0445	.7881
31	2.51	1.78	.7761	.2292	.0295	.7974
32	3.01	1.78	.7691	.2338	.0349	.7927
33	3.51	1.77	.7332	.2413	.0631	.7745
34	4.00	1.73	.6803	.2473	.1118	.7461
35	4.52	1.80	.7022	.2598	.0793	.7571

.

TABLE IX. PROBE DATA, LOWER PLANE AT MIDSPAN
(i = -4.9)

BLADE TO BLADE TRAVERSE MIDSPAN

LOWER PLANE

Point	Loc(in)	Beta	Q/Q1bar	Ps/Q1bar	Pt/Q1bar	X/Xbar
1	-4.50	-31.35	.9060	-.0197	.0673	.8989
2	-4.00	-33.42	.9200	-.0100	.0628	.8967
3	-3.50	-31.13	.9830	-.0134	.0150	.9202
4	-3.00	-32.66	.9853	-.0081	.0086	.9206
5	-2.50	-31.37	.9421	-.0121	.0650	.8973
6	-2.00	-32.90	.9604	-.0083	.0509	.9020
7	-1.50	-31.89	1.0047	-.0093	.0082	.9213
8	-1.00	-31.90	.9965	.0008	.0177	.9126
9	-.50	-31.89	.9132	-.0012	.1108	.8723
10	0.00	-32.65	.9685	-.0004	.0522	.8981
11	.50	-32.67	1.0053	-.0029	.0150	.9155
12	1.00	-31.41	1.0143	-.0122	.0150	.9197
13	1.50	-31.38	.9607	-.0069	.0685	.8940

136

TABLE X.   CENTER BLADE DATA (i = -4.9)

X/C	Y/C	Cp1	Cp2	Mach	Mvel

PRESSURE SIDE CENTER BLADE

X/C	Y/C	Cp1	Cp2	Mach	Mvel
.0007	.0054	.9763	1.0002	.0418	.0187
.0160	.0019	-.4822	-.9555	.3386	.1497
.0319	.0066	-.0446	-.3687	.2821	.1252
.0479	.0112	-.0138	-.3273	.2778	.1233
.0858	.0215	.0828	-.1978	.2638	.1171
.1218	.0303	.1205	-.1473	.2581	.1147
.1956	.0452	.1645	-.0883	.2514	.1117
.2695	.0576	.1962	-.0457	.2464	.1095
.3433	.0663	.2193	-.0147	.2438	.1079
.4192	.0716	.2438	.0248	.2380	.1058
.4930	.0736	.2556	.0339	.2369	.1054
.5669	.0727	.2792	.0655	.2330	.1037
.6407	.0678	.2869	.0759	.2318	.1031
.7146	.0601	.2910	.0814	.2311	.1028
.7884	.0487	.2919	.0826	.2309	.1027
.8283	.0411	.2901	.0801	.2312	.1029
.8683	.0327	.2842	.0722	.2322	.1033
.9082	.0230	.2651	.0467	.2354	.1047
.9481	.0123	.2234	-.0093	.2421	.1076
.9880	.0006	.1377	-.1242	.2555	.1135

SUCTION SIDE CENTER BLADE

X/C	Y/C	Cp1	Cp2	Mach	Mvel
.0160	.0227	-.2750	-.6776	.3129	.1386
.0319	.0310	-.2868	-.6934	.3144	.1393
.0479	.0389	-.2968	-.7068	.3157	.1398
.0858	.0563	-.3893	-.8308	.3273	.1448
.1218	.0710	-.4763	-.9476	.3379	.1494
.1956	.0970	-.5770	-1.0826	.3499	.1546
.2695	.1170	-.6364	-1.1623	.3568	.1576
.3433	.1309	-.6451	-1.1738	.3578	.1580
.4192	.1399	-.6441	-1.1725	.3577	.1580
.4930	.1432	-.5988	-1.1118	.3524	.1557
.5669	.1412	-.5339	-1.0248	.3448	.1524
.6407	.1339	-.4564	-.9208	.3355	.1484
.7146	.1209	-.4169	-.8679	.3307	.1463
.7884	.1021	-.2872	-.6940	.3145	.1393
.8283	.0895	-.2197	-.6034	.3058	.1355
.8683	.0755	-.1661	-.5316	.2987	.1324
.9082	.0593	-.0596	-.3887	.2842	.1261
.9481	.0407	.0239	-.2768	.2724	.1209
.9880	.0206	.1291	-.1357	.2568	.1141

137

TABLE XI.   ADJACENT BLADES DATA (i = -4.9)

X/C	Y/C	Cp1	Cp2	Mach	Xvel
****

PRESSURE SIDE LEFT BLADE

X/C	Y/C	Cp1	Cp2	Mach	Xvel
.1218	.0303	.0915	-.1862	.2625	.1166
.4192	.0716	.2434	.0175	.2389	.1062
.8283	.0411	.2937	.0850	.2306	.1026

SUCTION SIDE LEFT BLADE

X/C	Y/C	Cp1	Cp2	Mach	Xvel
.1218	.0710	-.3938	-.8369	.3279	.1451
.4192	.1400	-.6083	-1.1246	.3535	.1562
.8283	.0895	-.2378	-.6277	.3081	.1365

PRESSURE SIDE RIGHT BLADE

X/C	Y/C	Cp1	Cp2	Mach	Xvel
.1218	.0303	.1799	-.0676	.2490	.1107
.4192	.0716	.2615	.0413	.2359	.1049
.8283	.0411	.3010	.0947	.2294	.1021

SUCTION SIDE RIGHT BLADE

X/C	Y/C	Cp1	Cp2	Mach	Xvel
.1218	.0710	-.4682	-.9367	.3369	.1490
.4192	.1400	-.6097	-1.1264	.3537	.1562
.8283	.0895	-.2305	-.6180	.3072	.1361

TABLE XII.   PROBE DATA, UPPER PLANE AT MIDSPAN
(i = 2.1)

BLADE TO BLADE TRAVERSE MIDSPAN

UPPER PLANE

Point	Loc(in)	Beta	Q/Q1bar	Ps/Q1bar	Pt/Q1bar	X/Xbar
1	-7.90	-1.45	.6732	.3135	.0563	.6916
2	-6.93	-1.44	.6632	.3146	.0649	.6866
3	-5.95	-1.45	.6333	.3115	.0978	.6713
4	-4.96	-1.45	.6819	.3182	.0436	.6957
5	-3.98	-1.46	.6585	.3135	.0712	.6841
6	-3.73	-1.44	.6225	.3061	.1159	.6652
7	-3.48	-1.43	.5733	.2968	.1842	.6361
8	-3.24	-1.45	.5913	.3016	.1546	.6478
9	-2.99	-1.41	.6533	.3223	.0700	.6806
10	-2.74	-1.43	.6708	.3169	.0605	.6887
11	-2.49	-1.47	.6720	.3198	.0553	.6896
12	-2.24	-1.44	.6777	.3235	.0505	.6909
13	-2.00	-1.42	.6778	.3209	.0467	.6930
14	-1.76	-1.43	.6822	.3196	.0451	.6947
15	-1.50	-1.45	.6792	.3218	.0494	.6921
16	-1.25	-1.46	.6785	.3174	.0500	.6933
17	-1.01	-1.44	.6702	.3110	.0680	.6882
18	-.76	-1.46	.6215	.3082	.1233	.6621
19	-.52	-1.45	.5686	.2867	.1970	.6343
20	-.25	-1.46	.5674	.2909	.1924	.6341
21	-.02	-1.46	.6342	.3198	.0956	.6695
22	.23	-1.45	.6819	.3276	.0441	.6923
23	.47	-1.45	.6873	.3279	.0372	.6954
24	.73	-1.44	.6839	.3242	.0393	.6954
25	1.00	-1.45	.6774	.3196	.0526	.6915
26	1.23	-1.44	.6713	.3232	.0547	.6886
27	1.49	-1.43	.6757	.3185	.0505	.6922
28	1.76	-1.40	.6770	.3229	.0525	.6903
29	1.99	-1.44	.6678	.3254	.0589	.6858
30	2.25	-1.45	.6308	.3133	.1067	.6675
31	2.50	-1.43	.5799	.2975	.1773	.6396
32	2.77	-1.44	.5844	.2999	.1656	.6434
33	2.99	-1.44	.6440	.3271	.0749	.6756
34	3.25	-1.44	.6747	.3245	.0483	.6907
35	3.49	-1.43	.6797	.3196	.0477	.6934
36	3.78	-1.44	.6831	.3240	.0446	.6936
37	4.00	-1.44	.6906	.3143	.0351	.7012
38	5.01	-1.45	.6596	.3222	.0632	.6839
39	6.02	-1.44	.6594	.3405	.0573	.6797
40	7.03	-1.45	.6665	.3310	.0536	.6854
41	8.04	-1.45	.6115	.3146	.1269	.6567
42	8.54	-1.43	.5576	.2932	.1963	.6297

139

TABLE XIII. PROBE DATA, LOWER PLANE AT MIDSPAN
(i = 2.1)

BLADE TO BLADE TRAVERSE MIDSPAN

LOWER PLANE

Point	Loc(in)	Beta	Q/Q1bar	Ps/Q1bar	Pt/Q1bar	X/Xbar
1	-4.00	-39.02	1.0049	-.0135	.0228	.8571
2	-3.00	-39.02	.9946	-.0195	.0361	.8542
3	-2.00	-39.89	.9985	-.0081	.0234	.8546
4	-1.50	-38.51	.9480	-.0199	.0382	.8328
5	-1.00	-39.02	.9938	-.0204	.0414	.8525
6	-.50	-39.27	1.0126	-.0184	.0131	.8612
7	0.00	-39.27	.9709	-.0170	.0658	.8410
8	.50	-39.30	.9388	-.0155	.0950	.8281
9	1.00	-40.27	.9939	-.0111	.0377	.8501
10	1.50	-38.76	1.0207	-.0173	.0207	.8596
11	2.00	-39.01	.9558	-.0050	.0170	.8556
12	3.00	-39.00	1.0113	-.0225	.0271	.8592
13	4.00	-39.03	.9872	-.0023	.0425	.8444

TABLE XIV. CENTER BLADE DATA (i = 2.1)

X/C	Y/C	Cp1	Cp2	Mach	Xuel

PRESSURE SIDE CENTER BLADE

X/C	Y/C	Cp1	Cp2	Mach	Xuel
.0007	.0054	.9590	.9840	.0509	.0229
.0160	.0019	.5000	.2889	.1790	.0798
.0319	.0066	.4335	.1882	.1907	.0850
.0479	.0112	.3904	.1229	.1980	.0882
.0858	.0215	.3665	.0867	.2019	.0899
.1218	.0303	.3782	.1044	.2000	.0891
.1956	.0452	.3824	.1108	.1993	.0888
.2695	.0576	.3936	.1278	.1975	.0880
.3433	.0663	.4074	.1487	.1952	.0869
.4192	.0716	.4239	.1737	.1924	.0857
.4930	.0736	.4196	.1672	.1931	.0860
.5669	.0727	.4367	.1930	.1902	.0848
.6407	.0678	.4393	.1970	.1897	.0846
.7146	.0601	.4335	.1882	.1907	.0850
.7884	.0487	.4212	.1696	.1928	.0859
.8283	.0411	.4154	.1608	.1938	.0864
.8683	.0327	.4000	.1374	.1964	.0875
.9082	.0230	.3617	.0794	.2027	.0903
.9481	.0123	.3037	-.0084	.2119	.0943
.9880	.0006	.1654	-.2178	.2324	.1034

SUCTION SIDE CENTER BLADE

X/C	Y/C	Cp1	Cp2	Mach	Xuel
.0160	.0227	-1.3686	-2.5409	.4008	.1764
.0319	.0310	-.6899	-1.5131	.3350	.1482
.0479	.0389	-.6314	-1.4245	.3289	.1455
.0858	.0563	-.6101	-1.3922	.3266	.1445
.1218	.0710	-.5968	-1.3721	.3252	.1439
.1956	.0970	-.5830	-1.3511	.3237	.1433
.2695	.1170	-.5553	-1.3093	.3207	.1420
.3433	.1309	-.5128	-1.2448	.3151	.1400
.4192	.1399	-.4521	-1.1530	.3094	.1371
.4930	.1432	-.3819	-1.0467	.3015	.1336
.5669	.1412	-.3287	-.9661	.2954	.1310
.6407	.1339	-.2154	-.7945	.2821	.1252
.7146	.1209	-.1399	-.6802	.2729	.1211
.7884	.1021	-.0091	-.4820	.2562	.1138
.8283	.0895	.0505	-.3918	.2483	.1104
.8683	.0755	.1181	-.2895	.2391	.1063
.9082	.0593	.1574	-.2299	.2336	.1039
.9481	.0407	.1776	-.1993	.2307	.1026
.9880	.0205	.1760	-.2017	.2309	.1027

TABLE XV.   ADJACENT BLADES DATA (i = 2.1)

X/C	Y/C	Cp1	Cp2	Mach	Xvel

PRESSURE SIDE LEFT BLADE

X/C	Y/C	Cp1	Cp2	Mach	Xvel
.1218	.0303	.3202	.0166	.2093	.0?..
.4192	.0716	.3792	.1060	.1998	.085?
.8283	.0411	.3920	.1253	.1977	.0881

SUCTION SIDE LEFT BLADE

X/C	Y/C	Cp1	Cp2	Mach	Xvel
.1218	.0710	-.3580	-1.0104	.2988	.1325
.4192	.1400	-.3059	-.9315	.2928	.1298
.8283	.0895	.0319	-.4200	.2508	.1115

PRESSURE SIDE RIGHT BLADE

X/C	Y/C	Cp1	Cp2	Mach	Xvel
.1218	.0303	.3138	.0069	.2103	.0936
.4192	.0716	.4069	.1479	.1952	.0870
.8283	.0411	.4005	.1382	.1963	.0875

SUCTION SIDE RIGHT BLADE

X/C	Y/C	Cp1	Cp2	Mach	Xvel
.1218	.0710	-.4436	-1.1401	.3085	.1367
.4192	.1400	-.3346	-.9750	.2961	.1313
.8283	.0895	.0526	-.3896	.2480	.1103

TABLE XVI. PROBE DATA, UPPER PLANE AT MIDSPAN
(i = 5.3)

BLADE TO BLADE TRAVERSE MIDSPAN

UPPER PLANE

Point	Loc(in)	Beta	Q/Q1bar	Ps/Q1bar	Pt/Q1bar	X/Xbar
1	-7.36	-.31	.5794	.3376	.1030	.6341
2	-6.90	-.25	.4983	.3102	.2182	.5874
3	-6.42	-1.50	.6140	.3468	.0660	.6501
4	-5.92	-1.47	.6284	.3489	.0478	.6580
5	-5.42	-1.49	.6301	.3406	.0497	.6605
6	-4.94	-.36	.6276	.3437	.0510	.6585
7	-4.44	-.37	.5846	.3442	.1035	.6331
8	-3.95	-.38	.4779	.3008	.2511	.5747
9	-3.48	-.34	.6122	.3415	.0672	.6510
10	-2.97	-.39	.6332	.3377	.0492	.6622
11	-2.49	-.38	.6214	.3456	.0580	.6541
12	-1.98	-.33	.6307	.3395	.0492	.6611
13	-1.78	-.38	.6250	.3491	.0552	.6550
14	-1.57	-.38	.6035	.3436	.0779	.6452
15	-1.38	-.37	.5567	.3351	.1345	.6200
16	-1.20	-.33	.5163	.3111	.1924	.5997
17	-.99	-.37	.5052	.3095	.2110	.5917
18	-.80	-.39	.5535	.3290	.1449	.6180
19	-.61	-.38	.6055	.3405	.0811	.6457
20	-.40	-.38	.6229	.3443	.0589	.6549
21	-.22	-.38	.6321	.3441	.0566	.6576
22	-.01	-.38	.6308	.3410	.0576	.6580
23	.19	-.40	.6334	.3388	.0557	.6593
24	.38	-.38	.6355	.3398	.0529	.6603
25	.60	-.37	.6383	.3380	.0496	.6629
26	.79	-.38	.6304	.3378	.0557	.6596
27	1.00	-.35	.6267	.3435	.0603	.6556
28	1.20	-.38	.6178	.3412	.0714	.6510
29	1.40	-.37	.6016	.3293	.0876	.6464
30	1.99	-.34	.4814	.3045	.2492	.5753
31	2.51	-.37	.6216	.3471	.0612	.6530
32	3.00	-.37	.6328	.3441	.0566	.6577
33	3.49	-.36	.6329	.3371	.0529	.6612
34	4.01	-.40	.6361	.3447	.0505	.6601
35	4.51	-.36	.5870	.3385	.1019	.6359

143

TABLE XVII.   PROBE DATA, LOWER PLANE AT MIDSPAN
(i = 5.3)

BLADE TO BLADE TRAVERSE MIDSPAN

LOWER PLANE

Point	Loc(in)	Beta	Q/Q1bar	Ps/Q1bar	Pt/Q1bar	X/Xbar
1	-4.50	-42.51	.9789	-.0204	.0367	.8344
2	-4.00	-41.52	.9396	-.0345	.0888	.8192
3	-3.50	-42.55	.9786	-.0228	.0418	.8334
4	-3.00	-42.56	1.0008	-.0153	.0125	.8420
5	-2.50	-41.48	.9842	-.0216	.0413	.8332
6	-2.00	-42.79	.9532	-.0304	.0784	.8218
7	-1.50	-42.38	1.0025	-.0253	.0218	.8425
8	-1.00	-42.39	1.0005	-.0208	.0218	.8406
9	-.50	-42.36	.9489	-.0209	.0761	.8187
10	0.00	-42.42	.9507	-.0295	.0836	.8194
11	.50	-42.41	.9981	-.0216	.0269	.8389
12	1.00	-42.39	1.0040	-.0188	.0186	.8411
13	1.50	-42.38	.9689	-.0088	.0474	.8253

TABLE XVIII.   CENTER BLADE DATA (i = 5.3)

X/C	Y/C	Cp1	Cp2	Mach	Mvel.

PRESSURE SIDE CENTER BLADE

X/C	Y/C	Cp1	Cp2	Mach	Mvel.
.0007	.0054	.5729	.3685	.1774	.0791
.0160	.0019	.6382	.4755	.1631	.0727
.0319	.0066	.5256	.2911	.1871	.0834
.0479	.0112	.4645	.1910	.1990	.0886
.0858	.0215	.4311	.1364	.2052	.0914
.1218	.0303	.4112	.1038	.2088	.0930
.1956	.0452	.3955	.0780	.2117	.0942
.2695	.0576	.3936	.0749	.2120	.0944
.3433	.0663	.4001	.0855	.2108	.0939
.4192	.0716	.4223	.1220	.2068	.0921
.4930	.0736	.4186	.1159	.2075	.0924
.5669	.0727	.4330	.1394	.2049	.0912
.6407	.0678	.4247	.1258	.2064	.0919
.7146	.0601	.4237	.1242	.2066	.0920
.7884	.0487	.4108	.1030	.2089	.0930
.8283	.0411	.4010	.0871	.2107	.0938
.8683	.0327	.3811	.0544	.2142	.0954
.9082	.0230	.3487	.0013	.2199	.0979
.9481	.0123	.3010	-.0768	.2282	.1014
.9880	.0006	.1760	-.2817	.2480	.1102

SUCTION SIDE CENTER BLADE

X/C	Y/C	Cp1	Cp2	Mach	Mvel.
.0160	.0227	-1.7220	-3.3908	.4662	.2041
.0319	.0310	-1.2292	-2.5835	.4181	.1838
.0479	.0389	-.8221	-1.9166	.3753	.1655
.0858	.0563	-.5558	-1.4804	.3451	.1525
.1218	.0710	-.5266	-1.4326	.3417	.1511
.1956	.0970	-.4882	-1.3696	.3372	.1491
.2695	.1170	-.4238	-1.2642	.3294	.1457
.3433	.1309	-.3807	-1.1936	.3241	.1435
.4192	.1399	-.3201	-1.0942	.3166	.1402
.4930	.1432	-.2557	-.9888	.3034	.1366
.5669	.1412	-.1909	-.8825	.3000	.1330
.6407	.1339	-.1274	-.7786	.2916	.1293
.7146	.1209	-.0519	-.6549	.2813	.1248
.7884	.1021	.0370	-.5093	.2688	.1193
.8283	.0895	.0912	-.4205	.2609	.1159
.8683	.0755	.1324	-.3530	.2547	.1132
.9082	.0593	.1658	-.2984	.2498	.1109
.9481	.0407	.1936	-.2528	.2453	.1090
.9880	.0206	.1959	-.2490	.2449	.1089

TABLE XIX.   ADJACENT BLADES DATA (i = 5.3)

X/C	Y/C	Cp1	Cp2	Mach	Mvel
*****	*****	*****	*****	*****	*****
PRESSURE SIDE LEFT BLADE					
.1218	.0303	.3598	.0195	.2179	.0970
.4192	.0716	.3733	.0415	.2156	.0960
.8283	.0411	.3658	.0294	.2169	.0965
SUCTION SIDE LEFT BLADE					
.1218	.0710	-.4799	-1.3560	.3362	.1437
.4192	.1400	-.3117	-1.0806	.3156	.1397
.8283	.0895	.0713	-.4531	.2638	.1172
PRESSURE SIDE RIGHT BLADE					
.1218	.0303	.3422	-.0093	.2210	.0983
.4192	.0716	.3973	.0810	.2113	.0941
.8283	.0411	.3881	.0658	.2130	.0948
SUCTION SIDE RIGHT BLADE					
.1218	.0710	-.5164	-1.4159	.3405	.1505
.4192	.1400	-.2955	-1.0540	.3135	.1389
.8283	.0895	.0810	-.4372	.2624	.1165

TABLE XX.   PROBE DATA, UPPER PLANE AT MIDSPAN
(i = 8.8)

BLADE TO BLADE TRAVERSE MIDSPAN

UPPER PLANE.

Point	Loc(in)	Beta	Q/Q1bar	Ps/Q1bar	Pt/Q1bar	X/Xbar
1	-7.39	-1.03	.5344	.3131	.2045	.6000
2	-6.92	-.95	.6361	.3515	.0621	.6537
3	-6.42	-.97	.6377	.3529	.0600	.6543
4	-5.94	-1.00	.6387	.3571	.0606	.6530
5	-5.44	-1.00	.6181	.3431	.0874	.6451
6	-4.95	-1.02	.4914	.2890	.2717	.5761
7	-4.45	-1.00	.5014	.2939	.2624	.5802
8	-3.96	-1.04	.6404	.3498	.0607	.6556
9	-3.46	-.99	.6385	.3522	.0637	.6535
10	-2.98	-1.02	.6347	.3534	.0612	.6531
11	-2.48	-1.02	.6246	.3510	.0791	.6465
12	-1.97	-.99	.4985	.2919	.2640	.5795
13	-1.79	-1.00	.4690	.2858	.3046	.5611
14	-1.58	-1.01	.4989	.2944	.2558	.5811
15	-1.39	-1.01	.5631	.3223	.1650	.6160
16	-1.19	-1.00	.6182	.3398	.0937	.6442
17	-.99	-1.00	.6348	.3491	.0685	.6523
18	-.79	-.95	.6357	.3519	.0647	.6527
19	-.60	-1.00	.6427	.3493	.0585	.6569
20	-.40	-.97	.6368	.3474	.0642	.6545
21	-.21	-.98	.6299	.3448	.0716	.6517
22	-.01	-1.54	.6245	.3499	.0779	.6471
23	.19	-1.57	.6260	.3459	.0765	.6491
24	.41	-1.58	.6166	.3421	.0875	.6450
25	.60	-1.54	.5911	.3321	.1316	.6294
26	.79	-1.58	.5431	.3120	.1961	.6051
27	.99	-1.57	.4809	.2789	.2851	.5720
28	1.19	-1.57	.4473	.2667	.3368	.5505
29	1.40	-1.56	.4667	.2773	.3085	.5616
30	2.01	-1.54	.6276	.3425	.0769	.6504
31	2.50	-1.54	.6309	.3448	.0689	.6527
32	3.01	-1.56	.6375	.3483	.0616	.6552
33	3.50	-1.59	.6211	.3436	.0923	.6441
34	4.01	-1.59	.4793	.2831	.2908	.5688
35	4.52	-1.58	.5113	.2937	.2455	.5878

.

147

TABLE XXI.   PROBE DATA, LOWER PLANE AT MIDSPAN
(i = 8.8)

BLADE TO BLADE TRAVERSE MIDSPAN

LOWER PLANE

Point	Loc(in)	Beta	Q/Q1bar	Ps/Q1bar	Pt/Q1bar	M/Mbar
1	-4.50	-45.60	1.0023	-.0256	.0527	.8296
2	-4.00	-45.59	1.0240	-.0238	.0279	.8386
3	-3.50	-45.59	1.0137	-.0234	.0374	.8347
4	-3.00	-45.60	.9690	-.0345	.0880	.8191
5	-2.50	-45.58	1.0128	-.0261	.0453	.8328
6	-2.00	-45.60	1.0174	-.0247	.0321	.8373
7	-1.50	-45.62	.9618	-.0329	.0975	.8147
8	-1.00	-45.59	.9574	-.0388	.1043	.8143
9	-.50	-46.22	.9985	-.0203	.0537	.8270
10	0.00	-46.21	1.0066	-.0181	.0432	.8303
11	.50	-46.23	.9906	-.0233	.0622	.8249
12	1.00	-45.72	.9708	-.0274	.0911	.8152
13	1.50	-45.71	1.0215	-.0274	.0406	.8352

148

TABLE XXII.   CENTER BLADE DATA (i = 8.8)

X/C	Y/C	Cp1	Cp2	Mach	Qvel

PRESSURE SIDE CENTER BLADE

X/C	Y/C	Cp1	Cp2	Mach	Qvel
.0007	.0054	.3652	.0320	.2041	.0909
.0160	.0019	.7188	.6249	.1352	.0603
.0319	.0066	.6055	.4349	.1603	.0715
.0479	.0112	.5465	.3360	.1721	.0767
.0858	.0215	.4875	.2370	.1831	.0816
.1218	.0303	.4659	.2007	.1870	.0833
.1956	.0452	.4490	.1725	.1893	.0846
.2695	.0576	.4379	.1539	.1919	.0855
.3433	.0663	.4322	.1442	.1929	.0859
.4192	.0716	.4474	.1698	.1902	.0848
.4930	.0736	.4364	.1513	.1921	.0855
.5669	.0727	.4506	.1751	.1897	.0845
.6407	.0678	.4401	.1574	.1915	.0853
.7146	.0601	.4427	.1619	.1910	.0851
.7884	.0487	.4258	.1336	.1940	.0864
.8283	.0411	.4174	.1194	.1954	.0871
.8683	.0327	.4058	.1000	.1974	.0879
.9082	.0230	.3700	.0399	.2033	.0906
.9481	.0123	.3152	-.0520	.2122	.0945
.9880	.0006	.2019	-.2420	.2294	.1021

SUCTION SIDE CENTER BLADE

X/C	Y/C	Cp1	Cp2	Mach	Qvel
.0160	.0227	-1.5540	-3.1876	.4218	.1854
.0319	.0310	-1.5651	-3.2061	.4228	.1858
.0479	.0389	-1.4360	-2.9896	.4111	.1808
.0858	.0563	-.9724	-2.2119	.3672	.1621
.1218	.0710	-.6347	-1.6454	.3326	.1471
.1956	.0970	-.4303	-1.3025	.3101	.1374
.2695	.1170	-.3771	-1.2133	.3040	.1347
.3433	.1309	-.3091	-1.0993	.2961	.1313
.4192	.1399	-.2527	-1.0047	.2894	.1284
.4930	.1432	-.1658	-.8589	.2788	.1237
.5669	.1412	-.1295	-.7979	.2743	.1218
.6407	.1339	-.0583	-.6786	.2652	.1179
.7146	.1209	.0033	-.5752	.2572	.1143
.7884	.1021	.0786	-.4488	.2470	.1099
.8283	.0895	.1229	-.3746	.2408	.1071
.8683	.0755	.1550	-.3207	.2362	.1051
.9082	.0593	.1903	-.2615	.2311	.1029
.9481	.0407	.2077	-.2323	.2286	.1017
.9880	.0206	.2198	-.2120	.2268	.1009

TABLE XXIII.   ADJACENT BLADES DATA (i = 8.8)

X/C	Y/C	Cp1	Cp2	Mach	Mvel

PRESSURE SIDE LEFT BLADE

X/C	Y/C	Cp1	Cp2	Mach	Mvel
.1218	.0303	.4258	.1336	.1940	.0864
.4192	.0716	.4316	.1433	.1930	.0860
.8283	.0411	.4090	.1053	.1968	.0877

SUCTION SIDE LEFT BLADE

X/C	Y/C	Cp1	Cp2	Mach	Mvel
.1218	.0710	-.4798	-1.3856	.3157	.1398
.4192	.1400	-.2469	-.9950	.2887	.1281
.8283	.0895	.1097	-.3967	.2427	.1079

PRESSURE SIDE RIGHT BLADE

X/C	Y/C	Cp1	Cp2	Mach	Mvel
.1218	.0303	.3415	-.0078	.2080	.0926
.4192	.0716	.4364	.1513	.1921	.0856
.8283	.0411	.4084	.1044	.1969	.0877

SUCTION SIDE RIGHT BLADE

X/C	Y/C	Cp1	Cp2	Mach	Mvel
.1218	.0710	-.6005	-1.5880	.3289	.1455
.4192	.1400	-.2522	-1.0038	.2894	.1283
.8283	.0895	.1145	-.3887	.2420	.1076

TABLE XXIV. BLADE PERFORMANCE DATA

β_1	27.9	32.2	39.2	42.4	45.9
i	-9.2	-4.9	2.1	5.3	8.8
β_2	-2.9	-1.8	1.4	0.4	1.2
δ	5.7	6.8	10.0	9.0	9.8
D	.269	.319	.403	.456	.503
$\bar{\omega}$	.028	.023	.022	.041	.057
$\dfrac{\bar{\omega}\cos^3\beta_2}{2\sigma\cos^2\beta_1}$	.011	.009	.011	.023	.035
$\dfrac{\bar{\omega}\cos\beta_2}{2\sigma}\ (\times 10^2)$	0.849	0.690	0.658	1.242	1.719
AVDR	1.001	1.019	1.059	1.065	1.114
$C_{p_{static}}$	.194	.241	.313	.351	.348
C_{xM}	-.982	-1.108	-1.254	-1.380	-1.364
C_{yM}	.33	-.022	-.498	-.566	-.734
C_{xB}	-1.106	-1.218	-1.596	-1.476	-1.503
C_{yB}	-.304	-.380	-.643	-.645	-.711
$\bar{Q}_1$ (in H_2O)	20	22	19	22	19
$\bar{x}$	.12	.12	.12	.12	.12

APPENDIX A

PRELIMINARY TESTS WITH FIFTEEN C-SERIES BLADES

A cascade performance evaluation was conducted using fif-
teen C-series blades in preparation for a similar evaluation
at comparable diffusion factors but higher solidity using
DCA blading. The cascade configurations tested are given in
Table A-I.

Measurements were made using the apparatus and instrumen-
tation described in Section II.A. Acquisition and reduction
techniques were, with noted variations, those described in
Section II.C. Q_{ref} (inlet dynamic pressure) and X_{ref} (inlet
velocity) were used as reference parameters and were deter-
mined by correlating plenum pressure to inlet conditions as
outlined in Ref. 8, p. 45. Pressure instrumentation was not
installed in the test blades so that a momentum balance could
not be made.

As reported by Duval [Ref. 4] and McGuire [Ref. 11], the
conditions at the lower plane were not uniform in the blade
to blade direction because of wakes from the turning vanes
located at the test section inlet. Rather, on the spanwise
centerline at the lower measurement plane, the impact pressure
had a well defined periodic variation. However, about the
spanwise centerline, the impact pressure was uniform over
more than fifty percent of the span. Since the inlet flow
conditions were not uniform, mass averages were used to
calculate properties at the inlet plane from the probe survey

measurements. An additional check for inlet and outlet uniformity was made by recording the wall static pressures at the upper and lower planes on both the north and south walls. Figures A-1 (a)-(c) are photographs of the manometer board recording static pressure along the upper and lower south wall. As can be seen there is little variation on each wall, (about ±.02 inches water at the upper station and ±0.35 inches at the lower station).

To obtain performance characteristics over a range of incidence angles three test runs were conducted nominally at i_{ref}, (i_{ref} + 10°) and (i_{ref} - 10°), respectively. The actual incidence angles achieved deviated from the nominal values by up to a degree but a desired twenty degree range of incidence was covered.

The procedure for setting wall angles was identical to that used for the DCA blading.

Run I was conducted with the same geometry at the same conditions as the tests reported by Duval; that is, with $i \approx i_{ref}$ + 10°. The results are given in Tables A-II and A-III and results are shown plotted in Figs. A-2 to A-5. Tables A-II and A-III contain the lower and upper plane probe data respectively. Figures A-2 to A-4 show the distribution of the total pressure, static pressure and velocity on the spanwise centerline in the blade to blade direction, across two adjacent passages. The results illustrate the near periodicity of the two centermost blade passages. Figure A-5 shows the measured air outlet angle variation at comparable

153

locations between the two blades. It is noted that the measurement uncertainty resulting from the course resolution of the electrical probe actuator (Table II) is responsible for the apparent lack of agreement here. The degree of two-dimensionality available at this angle was earlier demonstrated by Duval [Ref. 4]. The value of the AVDR was 1.039, considered to be acceptable.

Runs 2 and 3 were conducted at inlet air angles corresponding to approximately i_{ref} and i_{ref} - 10°. In both cases two-dimensionality was checked using spanwise measurements. The results shown plotted in Figures A-6 to A-9 and A-10 to A-13 show that in each case the total and static pressures were acceptably uniform over nearly fifty percent of the span about midspan.

In each case the AVDR was also found to be acceptable (Table A-I).

In runs 2 and 3 the periodicity of the centermost blades was examined as before. The results in Figures A-14-A-15 and A-17-A-19 show that the magnitudes of the total pressure, static pressure and velocity at corresponding positions in two different blade passages were very similar for each of the two incidence conditions. The data in Figures A-20 and A-21 show that the outlet angle measured over four passages varied insignificantly.

After noting the two-dimensionality and periodicity available in each run, blade-element performance calculations were made using the probe data. All calculations

154

followed the procedure described in Appendix C. The results are given in Table A-I.

The magnitude of the loss coefficients and the variation with incidence were as expected. The losses were the least at a nominal incidence of i_{ref} and increased substantially in the other two cases. The deviation angle and diffusion factor decreased with decreasing incidence angle as expected. The AVDR was also calculated to be least for an incidence angle close to i_{ref}, at which the magnitude was close to unity.
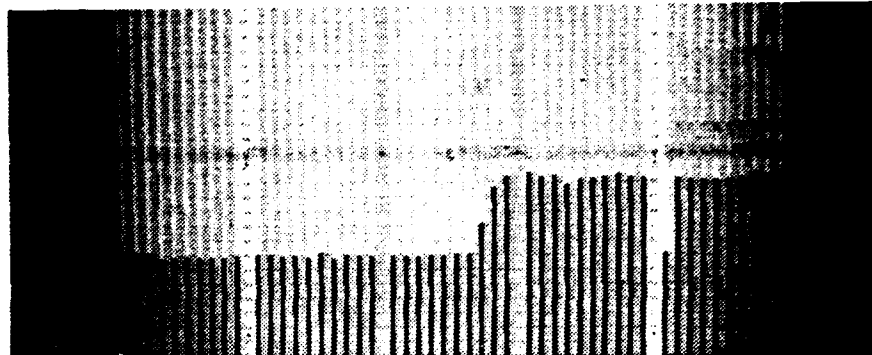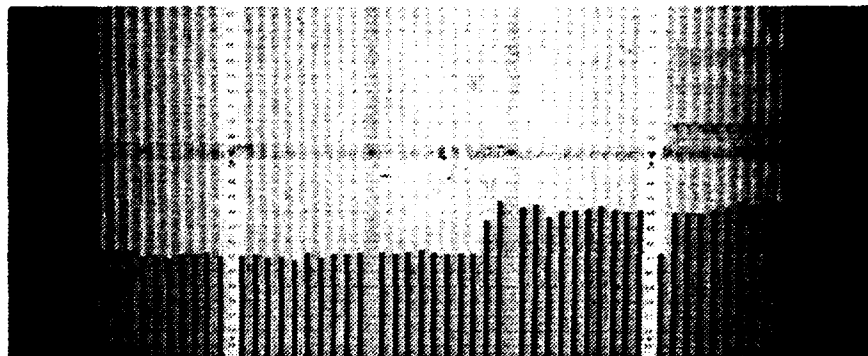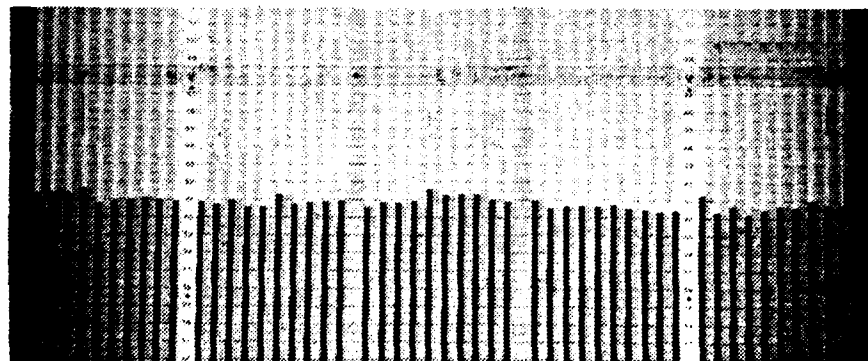
Fig. A-1.   Wall Static Pressure
Distributions (Lower
and Upper Planes)

Fig. A-2.   Probe Survey Data at Midspan
$(i \gg i_{ref}, (P_{plen}-P_t)/Q_{ref},$
Upper Plane)

Fig. A-3. Probe Survey Data at Midspan
($i >> i_{ref}$, $(P_s-P_{w\ell})/Q_{ref}$,
Upper Plane)

158
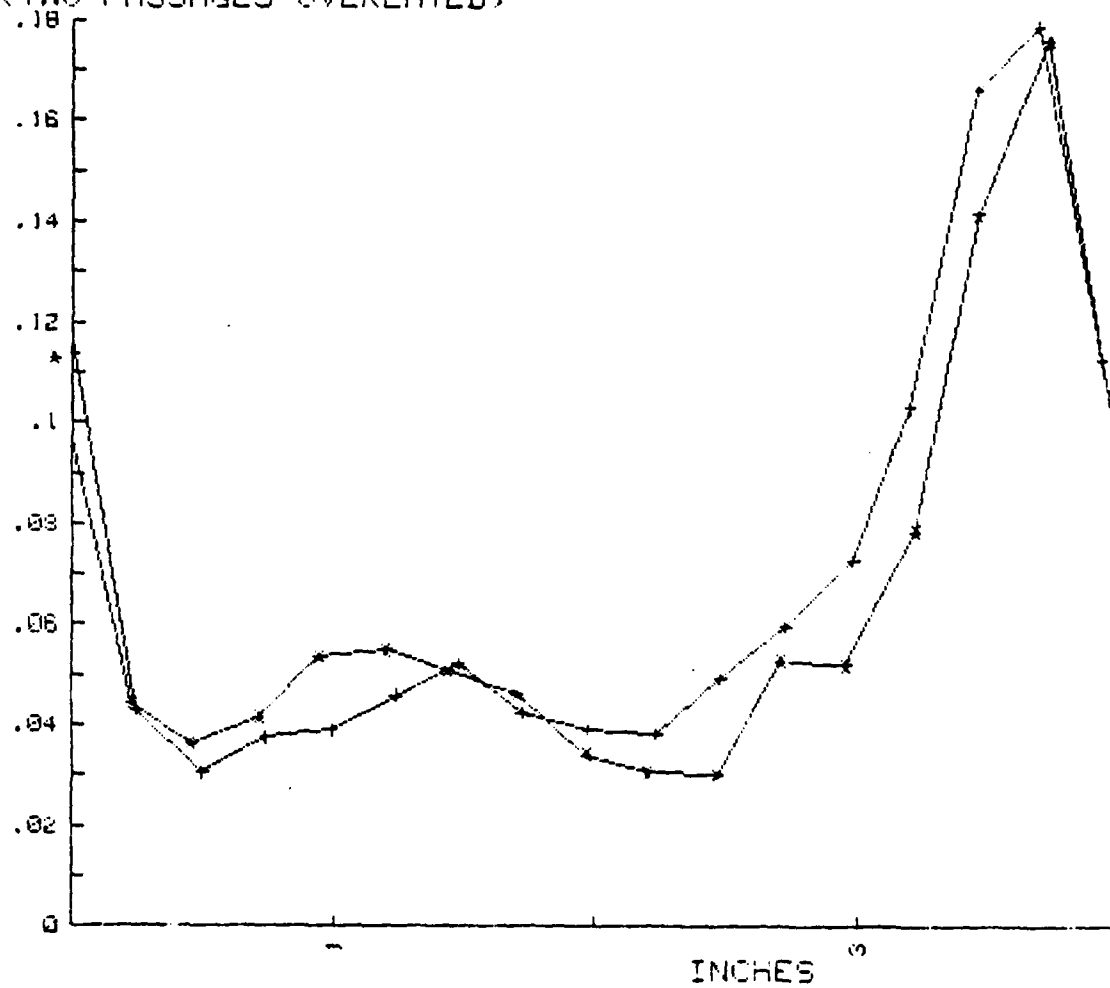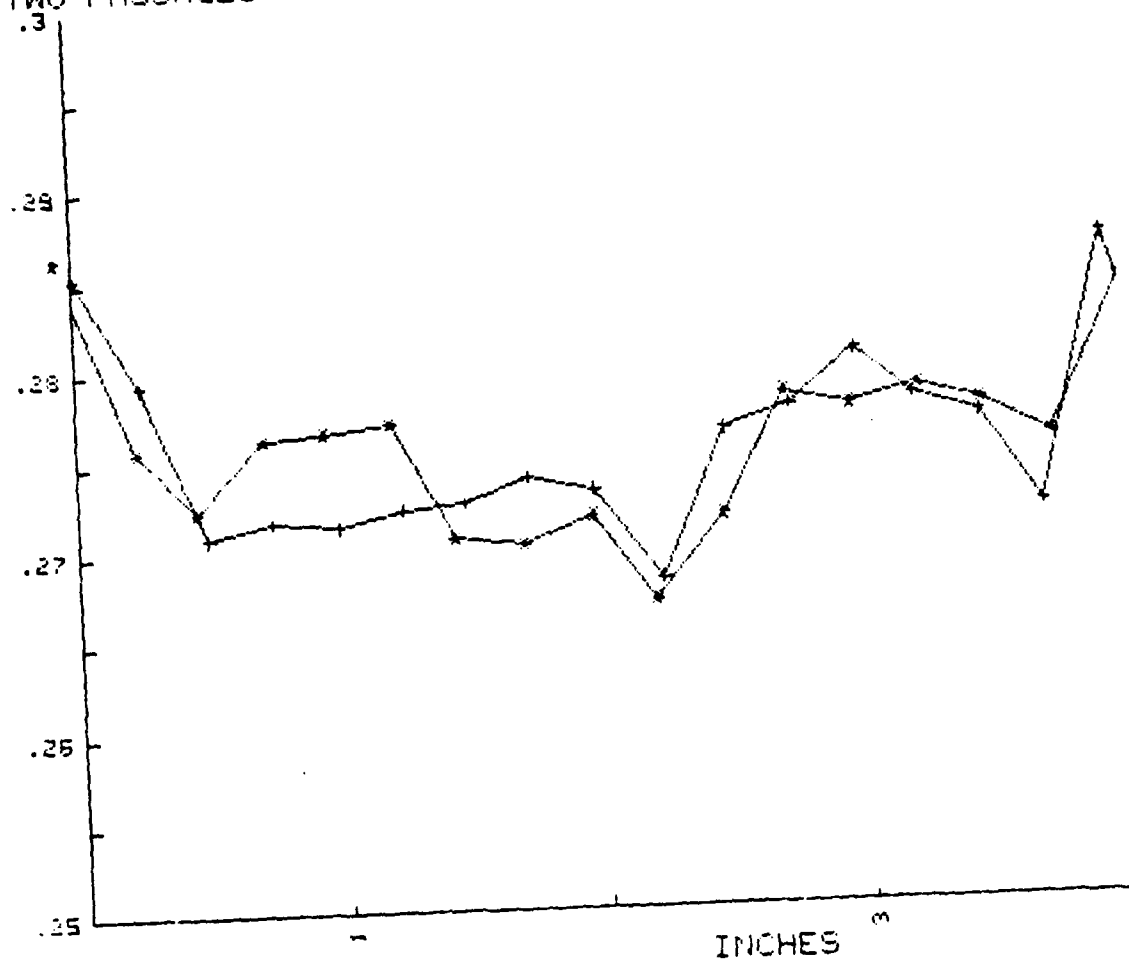
Fig. A-4.   Probe Survey Data at Midspan
(i $\gg$ i$_{ref}$, X/X$_{ref}$, Upper Plane)

OUTLET ANGLE (TWO PASSAGES)
PLOTS OVERLAYED
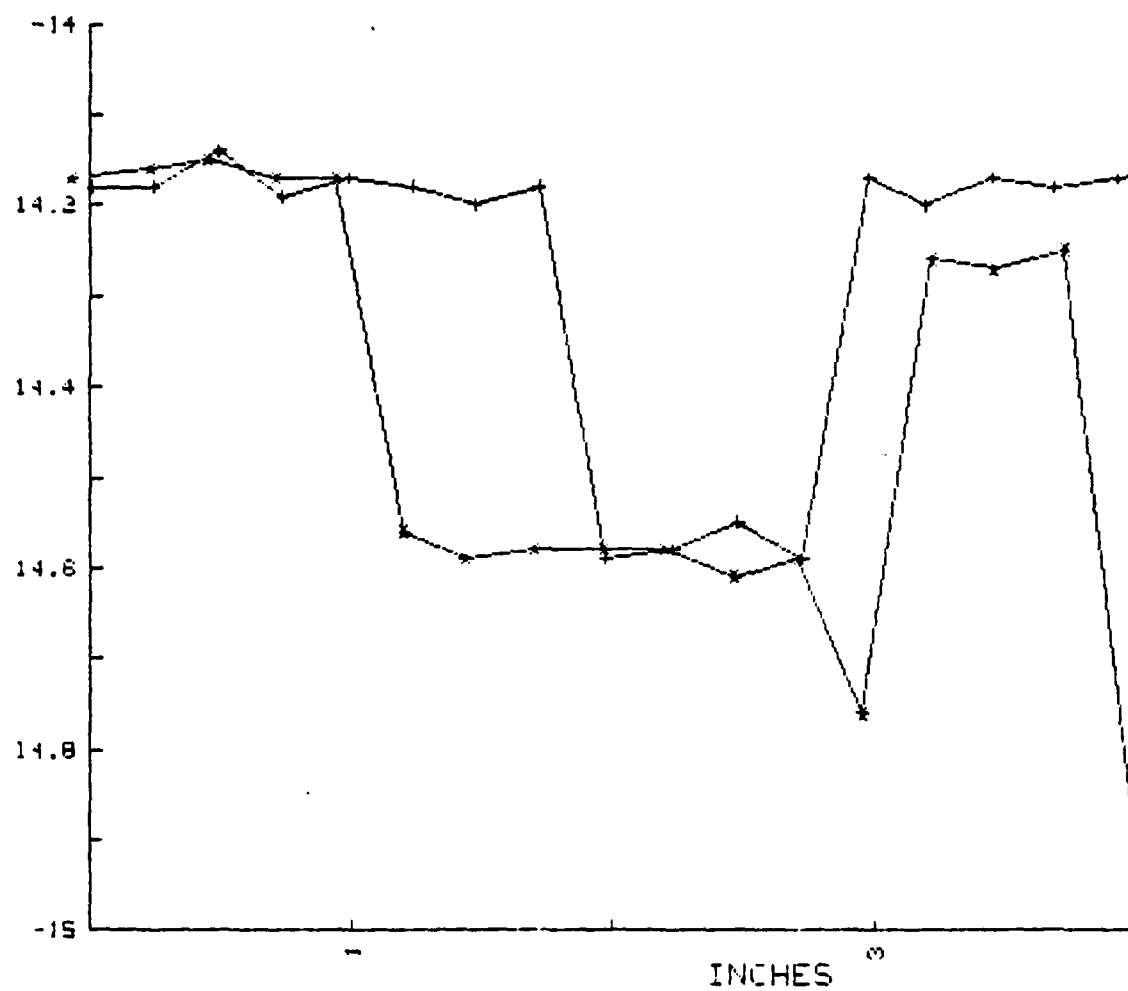
Fig. A-5.   Probe Survey Data at Midspan
             (i >> i_{ref}, Outlet Angle, Upper Plane)

160

(Pplen-Pt)/Qref
1.0 in. FROM PRESSURE SIDE OF CENTERLINE BLADE

Fig. A-6.   Spanwise Probe Data Surveyed 1 in. from
Pressure Side of Center Blade (i ≃ i_{ref},
$(P_{plen}-P_t)/Q_{ref}$, Upper Plan)

161

(Ps-Pwl)/Qref
1.0 in. FROM PRESSURE SIDE OF CENTERLINE BLADE
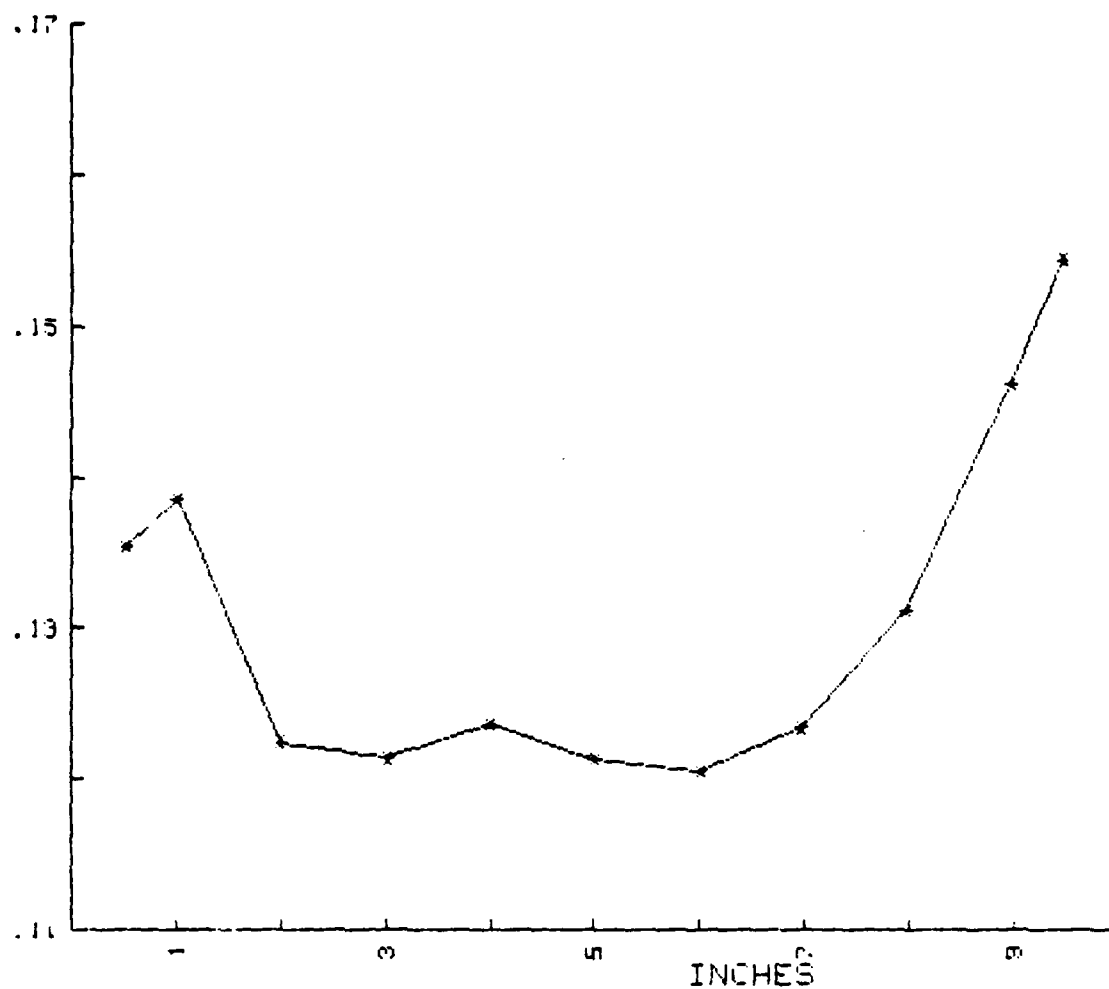
Fig. A-7. Spanwise Probe Data Surveyed 1 in. from
Pressure Side of Center Blade ($i \simeq i_{ref}$,
$(P_s - P_{w\ell})/Q_{ref}$, Upper Plane)

162

(Pplen-Pt)/Qref
1.0 in. FROM SUCTION SIDE OF CENTERLINE BLADE

Fig. A-8.   Spanwise Probe Data Surveyed 1 in. from
            Suction Side of Center Blade (i ≈ i_{ref},
            $(P_{plen}-P_t)/Q_{ref}$, Upper Plane)

163

(Ps-Pwl)/Qref
1.0 in. FROM SUCTION SIDE OF CENTERLINE BLADE
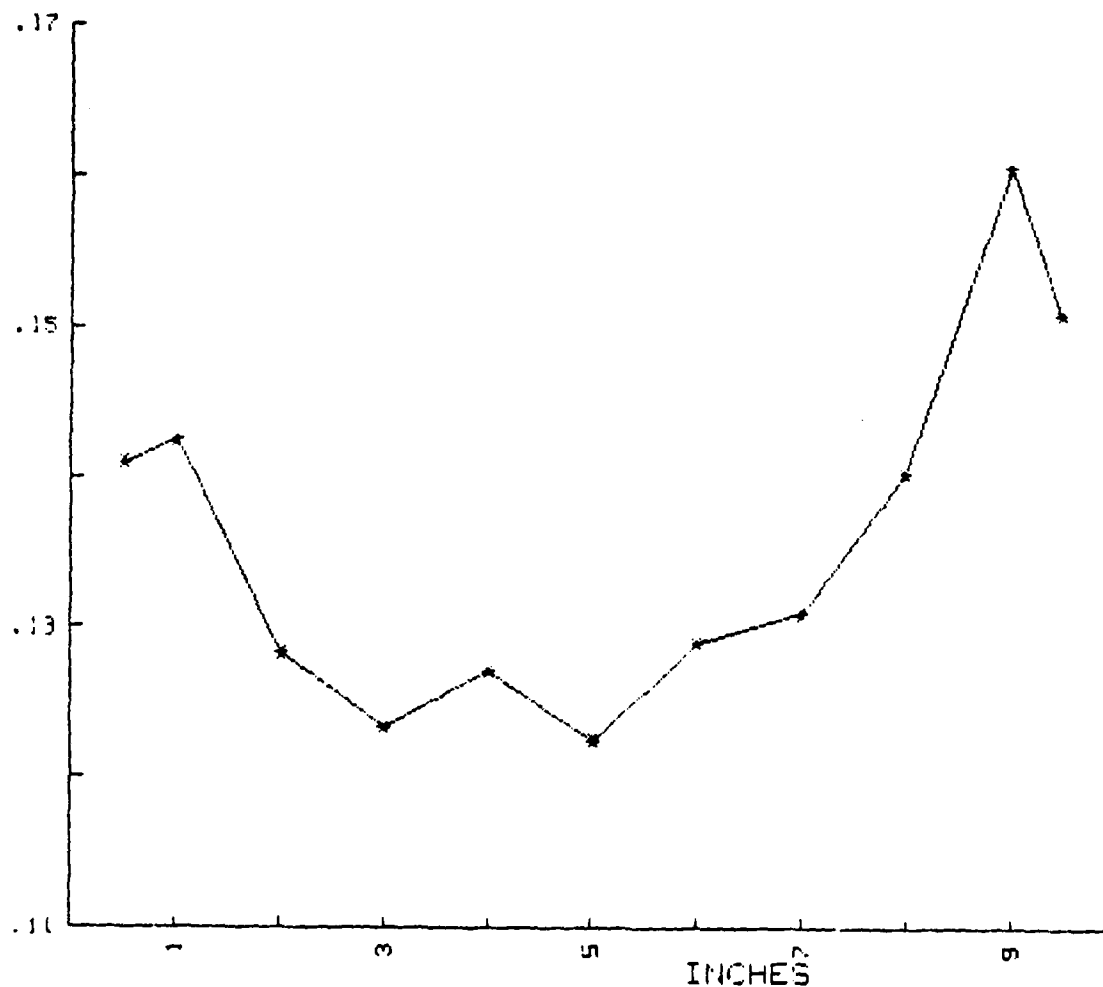
Fig. A-9.   Spanwise Probe Data Surveyed 1 in. from
Suction side of Center Blade ($i \simeq i_{ref}$,
$(P_s-P_{w\ell})/Q_{ref}$, Upper Plane)

164

(Pplen-Pt)/Qref
1.0 in. FROM PRESSURE SIDE OF CENTERLINE BLADE

Fig. A-10. Spanwise Probe Data Surveyed 1 in. from
Pressure Side of Center Blade ($i \ll i_{ref}$,
$(P_{plen}-P_t)/Q_{ref}$, Upper Plane)

165

(Ps-Pwl)/Qref
1.0 in. FROM PRESSURE SIDE OF CENTERLINE BLADE
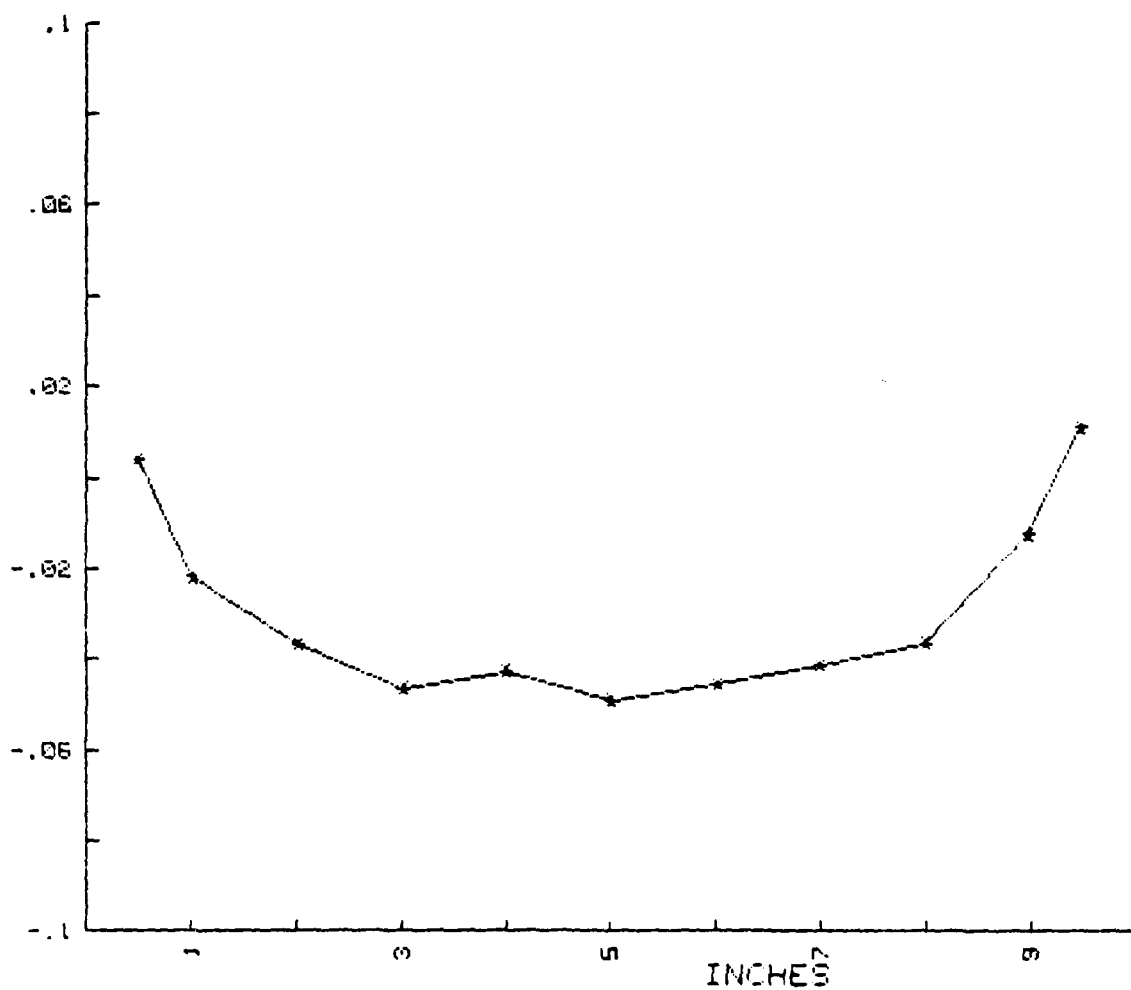
Fig. A-11. Spanwise Probe Data Surveyed 1 in. from
Pressure Side of Center Blade ($i \ll i_{ref}$,
$(P_s-P_{w\ell})/Q_{ref}$, Upper Plane)

(Pplen-Pt)/Qref
1.0 in. FROM SUCTION SIDE OF CENTERLINE BLADE
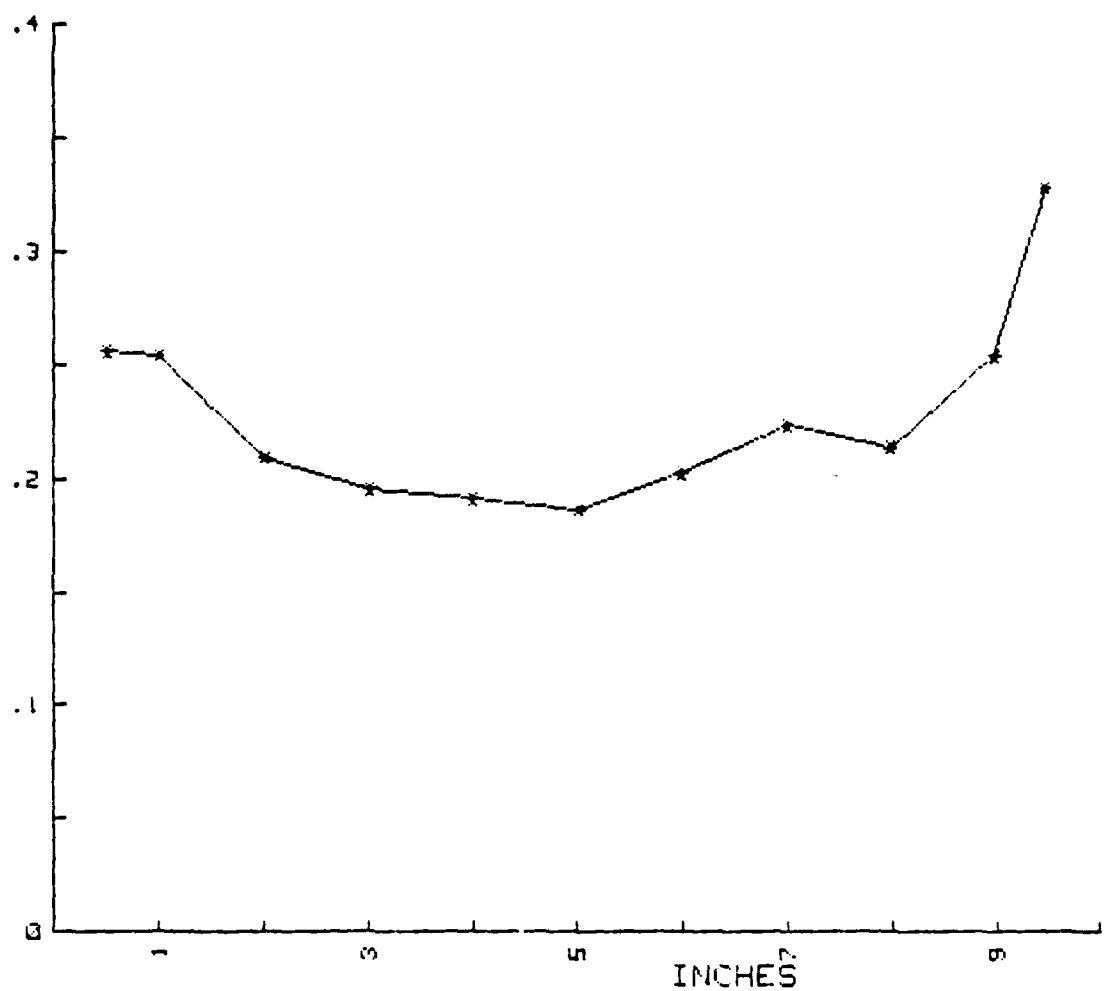
Fig. A-12. Spanwise Probe Data Surveyed 1 in. from Suction Side of Center Blade ($i \ll i_{ref}$, $(P_{plen}-P_t)/Q_{ref}$, Upper Plane)

Fig. A-13.   Spanwise Probe Data Surveyed 1 in. from
              Suction Side of Center Blade ($i \ll i_{ref}$,
              $(P_s - P_{w\ell})/Q_{ref}$, Upper Plane)

Fig. A-14.   Probe Survey Data at Midspan ($i \simeq i_{ref}$, $(P_{plen} - P_t)/Q_{ref}$, Upper Plane)

169

Fig. A-15.   Probe Survey Data at Midspan ($i \approx i_{ref}$, $(P_s - P_{w\ell})/Q_{ref}$, Upper Plane)

Fig. A-16. Probe Survey Data at Midspan (i $\simeq$ i$_{ref}$, X/X$_{ref}$, Upper Plane)

171

Fig. A-17. Probe Survey Data at Midspan ($i \ll i_{ref}$, $(P_{plen}-P_t)/Q_{ref}$, Upper Plane)

Fig. A-18.   Probe Survey Data at Midspan ($i \ll i_{ref}$, $(P_s - P_{w\ell})/Q_{ref}$, Upper Plane)

173

X/Xref
UPPER PLANE MIDSPAN
(TWO PASSAGES OVERLAYED)

Fig. A-19.   Probe Survey Data at Midspan ($i \ll i_{ref}$, X/X_{ref}, Upper Plane)

174

Fig. A-20. Probe Survey Data at Midspan ($i \simeq i_{ref}$, Outlet Angle, Upper Plane)

175

OUTLET ANGLE (FOUR PASSAGES)
PLOTS OVERLAYED
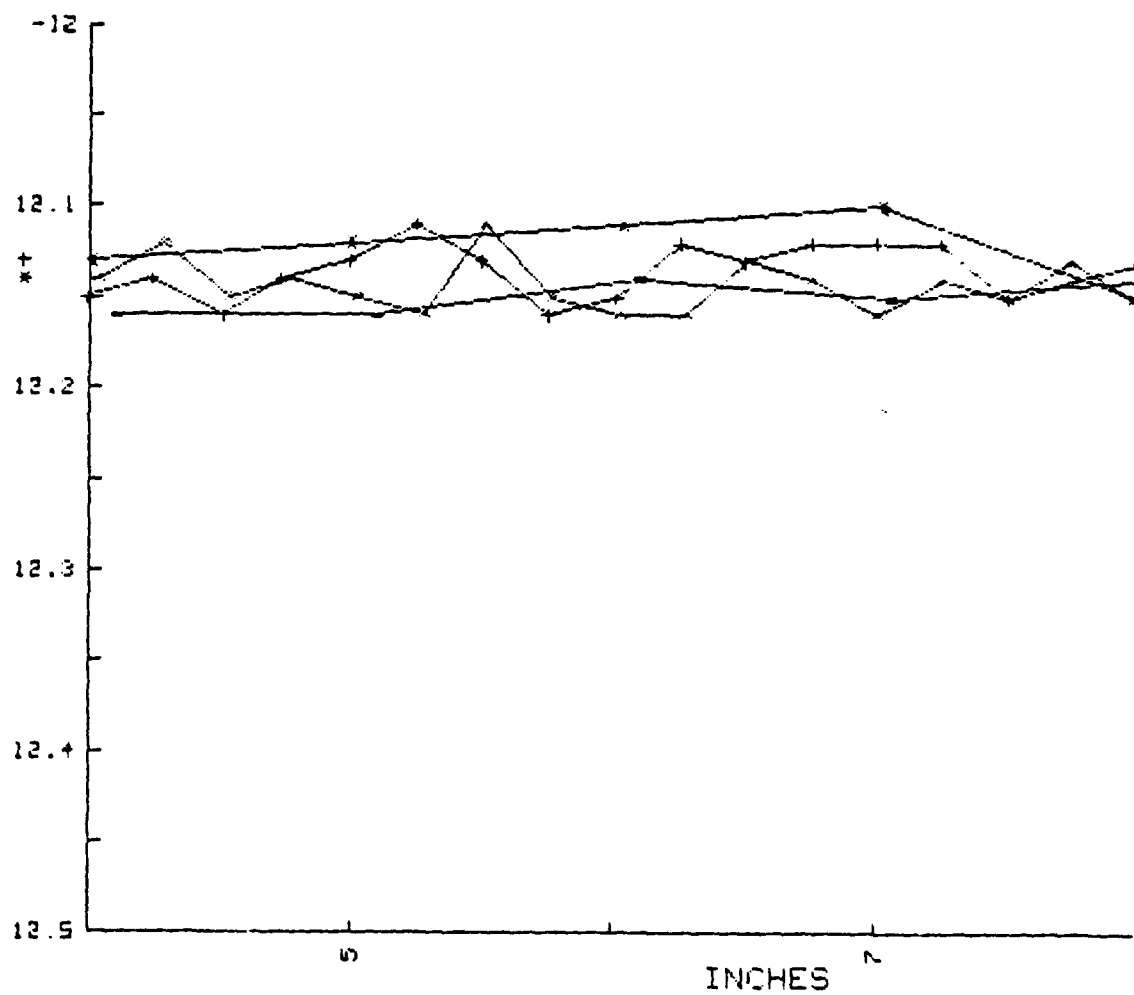
Fig. A-21. Probe Survey Data at Midspan ($i << i_{ref}$, Outlet Angle, Upper Plane)

176

TABLE A-I. CONFIGURATION AND PERFORMANCE DATA OF PRELIMINARY TESTS

	Run 1	Run 2	Run 3
Blade type	C series	C series	C series
Number of blades	15	15	15
Spacing (S) (inches)	4	4	4
Chord (c) (inches)	5.12	5.12	5.12
Solidity (σ)	1.28	1.28	1.28
Thickness (% chord)	13.5	13.5	13.5
Camber angle (ϕ)	20	20	20
Stagger angle (γ)	16.2	16.2	16.2
Air inlet angle (β_1)	39.26	27.57	16.50
Incidence angle (i)	13.06	1.37	-9.69
Deviation angle (δ)	8.15	6.61	5.94
Air outlet angle (β_2)	14.35	12.81	12.14
Diffusion factor (D)	.3613	.1900	.0413
AVDR	1.039	1.008	1.017
LOSS COEFFICIENT ($\bar{\omega}$)	2.936×10^{-2}	2.016×10^{-2}	4.125×10^{-2}

BLADE TO BLADE TRAVERSE MIDSPAN

LOWER PLANE

Point	Loc(in)	Beta	Q/Q1ref	Ps/Q1ref	Pt/Q1ref	X/Xref
1	-4.00	-39.04	.9574	-.0143	.0550	.9800
2	-3.00	-39.54	1.0035	-.0203	.0128	1.0031
3	-2.00	-38.79	.9611	-.0204	.0572	.9821
4	-1.00	-39.27	1.0068	-.0182	.0076	1.0047
5	0.00	-39.29	.9215	-.0182	.0964	.9620
6	1.00	-39.53	1.0048	-.0146	.0053	1.0037
7	2.00	-39.04	.9519	-.0264	.0732	.9777
8	3.00	-39.79	1.0093	-.0202	.0072	1.0051
9	4.00	-39.63	.9264	-.0156	.0889	.9644

TABLE A-III.   PROBE DATA, UPPER PLANE AT MIDSPAN

$$(i \gg i_{ref}, \ Q_{1ref} = 23° \ H_2O, \ X_{ref} = .13)$$

BLADE TO BLADE TRAVERSE MIDSPAN

UPPER PLANE

Point	Loc(in)	Beta	Q/Q1ref	Ps/Q1ref	Pt/Q1ref	X/Q1ref
1	-4.00	-14.18	.6110	.2854	.1139	.7785
2	-3.76	-14.18	.6862	.2793	.0429	.8246
3	-3.51	-14.14	.7061	.2709	.0305	.8365
4	-3.26	-14.19	.6985	.2717	.0376	.8321
5	-3.01	-14.17	.6974	.2714	.0389	.8314
6	-2.76	-14.18	.6901	.2723	.0459	.8271
7	-2.53	-14.20	.6834	.2726	.0523	.8231
8	-2.28	-14.18	.6920	.2739	.0424	.8282
9	-2.03	-14.59	.6959	.2732	.0391	.8306
10	-1.77	-14.58	.7011	.2682	.0382	.8337
11	-1.53	-14.55	.6824	.2763	.0495	.8224
12	-1.28	-14.59	.6716	.2775	.0597	.8159
13	-1.02	-14.17	.6557	.2805	.0728	.8062
14	-.81	-14.20	.6283	.2779	.1033	.7894
15	-.55	-14.17	.5683	.2769	.1662	.7512
16	-.32	-14.18	.5605	.2718	.1791	.7462
17	-.07	-14.17	.6109	.2865	.1130	.7784
18	.23	-14.16	.6882	.2757	.0443	.8259
19	.45	-14.15	.6991	.2723	.0363	.8324
20	.71	-14.17	.6904	.2762	.0417	.8272
21	.94	-14.17	.6781	.2766	.0537	.8199
22	1.20	-14.56	.6765	.2770	.0549	.8189
23	1.44	-14.59	.6868	.2706	.0510	.8252
24	1.70	-14.58	.6917	.2702	.0461	.8281
25	1.96	-14.58	.7020	.2717	.0341	.8341
26	2.20	-14.58	.7099	.2670	.0305	.8389
27	2.46	-14.61	.7053	.2716	.0303	.8361
28	2.70	-14.59	.6775	.2782	.0530	.8195
29	2.95	-14.76	.6786	.2775	.0521	.8201
30	3.21	-14.26	.6519	.2785	.0787	.8040
31	3.45	-14.27	.5912	.2776	.1417	.7661
32	3.72	-14.25	.5593	.2756	.1763	.7453
33	4.01	-14.90	.6331	.2841	.0925	.7923

179

TABLE A-IV. PROBE DATA, LOWER PLANE AT MIDSPAN
$(i \approx i_{ref}, Q_{1ref} = 26" H_2O, X_{ref} = .13)$

BLADE TO BLADE TRAVERSE MIDSPAN

LOWER PLANE

Point	Loc(in)	Beta	Q/Q1ref	Ps/Q1ref	Pt/Q1ref	X/Xref
1	-4.00	-27.09	.9541	-.0165	.0621	.9751
2	-3.00	-27.57	.9866	-.0073	.0189	.9908
3	-2.00	-27.59	.9356	-.0049	.0696	.9651
4	-1.00	-27.58	.9957	-.0102	.0121	.9952
5	0.00	-27.57	.9039	-.0094	.1070	.9490
6	1.00	-27.53	.9923	-.0100	.0154	.9935
7	1.50	-27.56	.9809	-.0081	.0255	.9878
8	2.00	-27.58	.9187	.0048	.0774	.9560
9	3.00	-27.57	1.0111	-.0193	.0050	1.0029
10	4.00	-27.52	.9244	-.0119	.0882	.9595

TABLE A-V. PROBE DATA, UPPER PLANE AT MIDSPAN
$(i \simeq i_{ref}, \; Q_{1ref} = 26" \; H_2O, \; X_{ref} = .13)$

BLADE TO BLADE TRAVERSE MIDSPAN

UPPER PLANE

Point	Loc(in)	Beta	Q/Q1ref	Ps/Q1ref	Pt/Q1ref	X/X1ref
1	-7.92	-12.79	.8177	.1377	.0498	.8989
2	-6.91	-12.81	.8149	.1288	.0614	.8976
3	-5.92	-12.78	.8340	.1329	.0376	.9077
4	-4.94	-12.83	.8053	.1369	.0634	.8921
5	-3.97	-12.84	.8148	.1394	.0510	.8972
6	-3.72	-12.82	.8350	.1311	.0384	.9083
7	-3.47	-12.81	.8335	.1337	.0374	.9074
8	-3.23	-12.80	.8362	.1298	.0384	.9089
9	-2.98	-12.81	.8260	.1294	.0494	.9035
10	-2.73	-12.80	.8273	.1320	.0455	.9041
11	-2.48	-12.78	.8287	.1304	.0456	.9049
12	-2.23	-12.82	.8367	.1319	.0358	.9092
13	-1.99	-12.80	.8471	.1282	.0289	.9148
14	-1.74	-12.81	.8313	.1361	.0373	.9061
15	-1.49	-12.81	.8312	.1350	.0385	.9061
16	-1.24	-12.81	.8213	.1333	.0504	.9008
17	-1.00	-12.81	.7800	.1411	.0955	.8780
18	-.76	-12.83	.7050	.1561	.1482	.8348
19	-.50	-12.82	.6493	.1607	.2010	.8015
20	-.26	-12.82	.7348	.1586	.1149	.8520
21	-.01	-12.82	.8296	.1349	.0402	.9052
22	.24	-12.77	.8368	.1308	.0368	.9091
23	.49	-12.82	.8381	.1256	.0406	.9100
24	.74	-12.81	.8250	.1288	.0510	.9029
25	.99	-12.82	.8163	.1286	.0583	.8992
26	1.23	-12.78	.8201	.1284	.0565	.9002
27	1.49	-12.80	.8270	.1278	.0501	.9039
28	1.74	-12.83	.8380	.1292	.0371	.9099
29	1.99	-12.83	.8397	.1273	.0373	.9108
30	2.24	-12.82	.8406	.1287	.0350	.9112
31	2.49	-12.82	.8273	.1297	.0478	.9040
32	2.77	-12.80	.8222	.1300	.0528	.9012
33	2.99	-12.81	.8028	.1343	.0687	.8906
34	3.24	-12.81	.7146	.1583	.1362	.8402
35	3.51	-12.80	.6560	.1625	.1926	.8053
36	3.74	-12.81	.7491	.1555	.1033	.8601
37	4.01	-12.84	.8407	.1309	.0327	.9111
38	5.02	-12.83	.8364	.1234	.0446	.9090
39	6.03	-12.83	.8556	.1248	.0233	.9192
40	7.00	-12.82	.8071	.1338	.0647	.8829
41	8.01	-12.80	.8364	.1343	.0337	.9086

TABLE A-VI. PROBE DATA, LOWER PLANE AT MIDSPAN
$(i << i_{ref}, Q_{1ref} = 27'' H_2O, X_{ref} = .13)$

BLADE TO BLADE TRAVERSE MIDSPAN

LOWER PLANE

Point	Loc(in)	Beta	Q/Q1ref	Ps/Q1ref	Pt/Q1ref	X/Xref
1	-4.00	-16.43	.9359	.0056	.1156	.9666
2	-3.00	-16.40	.9840	-.0058	.0766	.9910
3	-2.00	-16.45	.9582	-.0026	.1004	.9781
4	-1.50	-16.43	.9935	.0058	.0550	.9953
5	-1.00	-16.46	1.0077	.0022	.0439	1.0024
6	-.50	-16.45	.9772	.0041	.0739	.9873
7	0.00	-16.66	.9245	.0033	.1296	.9608
8	.50	-16.69	.9783	.0014	.0753	.9879
9	1.00	-16.46	.9786	.0057	.0707	.9879
10	1.50	-16.46	.9302	.0030	.1239	.9637
11	2.00	-16.44	.9388	.0045	.1134	.9680
12	3.00	-16.65	.9870	.0026	.0648	.9921
13	4.00	-16.70	.9307	.0072	.1192	.9638

182

TABLE A-VII.   PROBE DATA, UPPER PLANE AT MIDSPAN
$$(i << i_{ref}, \; Q_{1ref} = 27" \; H_2O, \; X_{ref} = .13)$$

BLADE TO BLADE TRAVERSE MIDSPAN

UPPER PLANE

Point	Loc(in)	Beta	Q/Q1ref	Ps/Q1ref	Pt/Q1ref	X/Xref
1	-7.91	-12.16	.9896	-.0413	.1060	.9947
2	-6.91	-12.16	.9744	-.0424	.1227	.9872
3	-5.90	-12.14	1.0109	-.0473	.0895	1.0054
4	-4.95	-12.15	.8944	-.0060	.1700	.9454
5	-3.97	-12.14	1.0014	-.0435	.0955	1.0006
6	-3.72	-12.12	1.0043	-.0504	.0995	1.0022
7	-3.46	-12.15	.9987	-.0457	.1005	.9993
8	-3.23	-12.14	1.0032	-.0502	.1003	1.0017
9	-2.97	-12.15	1.0068	-.0468	.0930	1.0033
10	-2.73	-12.16	1.0177	-.0511	.0860	1.0088
11	-2.49	-12.11	1.0098	-.0494	.0925	1.0049
12	-2.23	-12.15	1.0175	-.0510	.0860	1.0087
13	-1.98	-12.16	1.0197	-.0489	.0816	1.0097
14	-1.73	-12.16	.9865	-.0368	.1043	.9930
15	-1.49	-12.13	.8621	-.0050	.2026	.9294
16	-1.25	-12.14	.8036	.0122	.2463	.8963
17	-1.00	-12.16	.8843	-.0058	.1802	.9401
18	-.75	-12.14	.9462	-.0331	.1427	.9727
19	-.50	-12.15	.9707	-.0364	.1204	.9851
20	-.26	-12.13	.9695	-.0388	.1240	.9846
21	-.02	-12.15	.9700	-.0413	.1261	.9849
22	.23	-12.14	.9806	-.0421	.1156	.9902
23	.51	-12.16	.9876	-.0475	.1137	.9938
24	.73	-12.14	.9976	-.0446	.1002	.9987
25	.99	-12.13	1.0144	-.0504	.0885	1.0071
26	1.25	-12.11	1.0009	-.0454	.0976	1.0003
27	1.49	-12.13	1.0081	-.0497	.0943	1.0040
28	1.75	-12.16	1.0162	-.0506	.0868	1.0079
29	2.01	-12.15	1.0131	-.0464	.0858	1.0063
30	2.25	-12.12	.9813	-.0375	.1103	.9903
31	2.50	-12.13	.8713	-.0052	.1926	.9334
32	2.75	-12.12	.8137	.0096	.2384	.9019
33	3.00	-12.12	.8849	-.0091	.1829	.9404
34	3.25	-12.12	.9734	-.0409	.1219	.9865
35	3.50	-12.15	.9968	-.0465	.1029	.9983
36	3.75	-12.14	.9894	-.0459	.1100	.9946
37	4.01	-12.13	.9871	-.0412	.1073	.9933
38	5.00	-12.12	.9851	-.0455	.1141	.9925
39	6.03	-12.11	1.0039	-.0438	.0926	1.0017
40	7.02	-12.10	.9159	-.0180	.1592	.9567
41	8.02	-12.15	.9999	-.0477	.1007	.9998

183

APPENDIX B

BLADE FORCE EVALUATION

B.1 Using Probe Survey Data and Momentum Conservation

The application of the principle of momentum conservation to a control volume enclosing a single blade results in the following expressions for the components of force acting on the blade [Ref. 12, Eq. 5 (33) and Eq. 5 (34)]:

$$R_{tM} = m_s V_{t_1} - \int_0^s \rho_2 \, \Delta h \, V_{a_2} V_{t_2} \, dx + E \qquad \text{B-(1)}$$

$$R_{aM} = m_s V_{a_1} - \int_0^s \rho_2 \, \Delta h \, V_{a_2} \, dx + p_1 \, \Delta h \, s \qquad \text{B-(2)}$$

$$- \int_0^s \rho_2 \, \Delta h \, dx$$

It was assumed in the analysis that the flow was steady, that the body forces were negligible, that the flow was uniform at the inlet station (subscript 1) and not necessarily uniform at the outlet station (subscript 2), and that the flow was two-dimensional over the constant depth Δh. In Eq. B-(1) and Eq. B-(2);

R_{tM} = component of force in the blade-to-blade ("tangential" direction, x)

R_{aM} = component of force, normal to the cascade face ("axial" direction, y)

p = static pressure

ρ = density

m_s = mass flow rate through one blade space

V_t = component of velocity in the blade-to-blade direction (x)

V_a = component of velocity in the axial direction (y)

dx = an element of length in the blade-to-blade direction

s = the blade spacing

E = component of shear force in the blade-to-blade direction acting on the control surface at the downstream plane

It is argued by Vavra [Ref. 12] that for a symmetrical wake, E will vanish and that in general E will be small and may properly be neglected. In the present case the inlet conditions are not strictly uniform and therefore an integration is also required over the inlet control surface. Using $\Delta h = 1$, so that the equations are written for unit span, Eq. B-(1) and Eq. B-(2) become, respectively;

$$R_{tM} = \int_0^s \rho_1 V_{a_1} V_{t_1} \, dx - \int_0^s \rho_2 V_{a_2} V_{t_2} \, dx \qquad \text{B-(3)}$$

$$R_{aM} = \int_0^s \rho_1 V_{a_1}^2 \, dx - \int_0^s \rho_2 V_{a_2}^2 \, dx + \int_0^s p_1 \, dx \qquad \text{B-(4)}$$
$$- \int_0^s p_2 \, dx$$

Each of the terms on the RHS of Eq. B-(3) and Eq. B-(4) can be evaluated from the probe survey data obtained at the midspan at lower and upper planes.

185

B.2 Using Blade Surface Pressure Measurements

The force on the blade, excluding the component due to
shear stresses at the surface, can be obtained by integrating
the pressure distribution measured over the blade surface.

The resultant force per unit span, $\vec{F}_B$, can be written
as

$$\vec{F}_B = \int_{surface} d\vec{F}_B = - \int_{surface} p_s \, \hat{s} \, d\xi \qquad\qquad B-(5)$$

where

$$d\vec{F}_B = \text{resultant force on an element of area of the blade surface}$$

$$p_s = \text{static pressure on the blade surface}$$

$$d\xi = \text{element of distance along the surface}$$

$$\hat{s} = \text{outward normal unit vector at the surface}$$

In order to evaluate F_B from measurements, it is con-
venient to first evaluate the components of F_B in a blade
coordinate system, and from these deduce the components in
the "axial" and "tangential" directions.
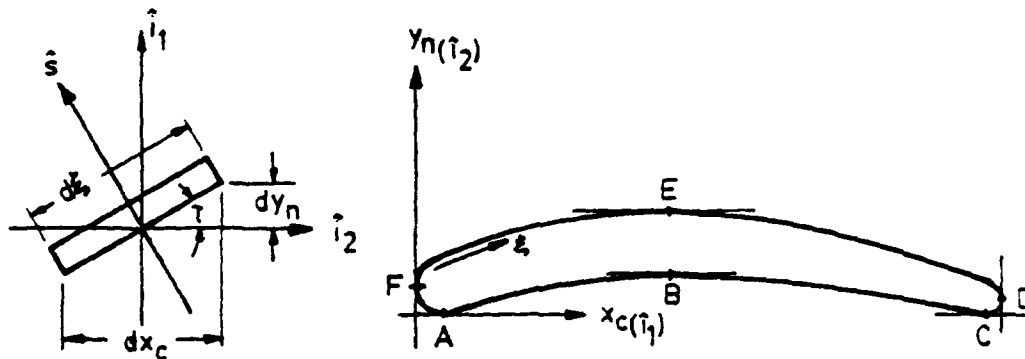
The blade coordinate system which was used and an elemental surface distance are shown in the preceding sketch.

The components of the elemental blade force in the coordinate directions x_c and y_n are obtained by taking the dot produce of $d\vec{F}_B$ with the unit vectors $(\hat{i}_1)$ and $(\hat{i}_2)$ respectively:

$$\hat{i}_1 \cdot d\vec{F}_B = -p_s (\hat{i}_1 \cdot \hat{s}) d\xi = p_s \sin \tau \, d\xi = p_s \, dy_n$$

$$\hat{i}_2 \cdot d\vec{F}_B = -p_s (\hat{i}_2 \cdot \hat{s}) d\xi = -p_s \cos \tau \, d\xi = -p_s \, dx_c$$

Then, the components of the blade force F_{x_c} and F_{y_n} are obtained by integration:

$$F_{x_c} = \int_{\text{surface}} p_s \, dy_n \qquad \text{B-(6)}$$

$$F_{y_n} = -\int_{\text{surface}} p_s \, dx_c \qquad \text{B-(7)}$$

In practice the integration was performed in sections so that dx_c and dy_c were always positive. Referring to the preceding sketch.

$$F_{x_c} = \int_{AFE} p_s \, dy_n - \int_{CDE} p_s \, dy_n - \int_{AB} p_s \, dy_n$$
$$+ \int_{CB} p_s \, dy_n \qquad \text{B-(6a)}$$

$$F_{y_n} = -\int_{FED} p_s \, dx_c + \int_{FABCD} p_s \, dx_c \qquad \text{B-(7a)}$$
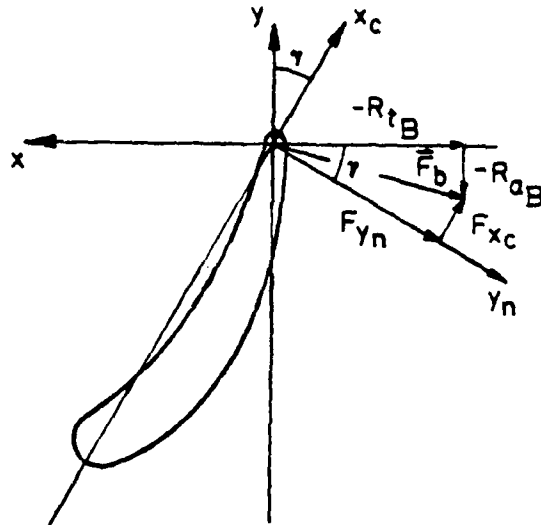
The relationship of the force components (F_{x_c}, F_{y_n}) in the blade coordinate frame (x_c, y_n) to the force components (R_{t_B}, R_{a_B}) in the cascade coordinate system (x,y) is shown in the sketch. From the geometry

$$R_{t_B} = -(F_{y_n} \cos \gamma + F_{x_c} \sin \gamma) \qquad \text{B-(8)}$$

$$R_{a_B} = -(F_{y_n} \sin \gamma - F_{x_c} \cos \gamma) \qquad \text{B-(9)}$$

where γ is the stagger angle.

B.3 Reduction to Force Coefficients

As reported by Duval [Ref. 4] all measurements are subject to some time dependence as a result of fluctuations in supply conditions. To greatly reduce the effect of non-constant supply conditions on data which must be integrated, all terms are referenced to the plenum conditions recorded at

188

the time of the individual measurement. This has the effect of reducing all quantities to non-dimensional coefficients which may then be compared.

The quantity $\frac{1}{2}\rho_{ref}\,V^2_{ref}$ was used as a reference quantity for measurements of pressure where ρ_{ref} and V_{ref} were determined from plenum conditions as described in Appendix D. Since the stagnation temperature is taken to be constant throughout,

$$\frac{1}{2}\,\rho_{ref}\,V^2_{ref} \;=\; P_{tref}\,X^2_{ref}[1 - X^2_{ref}]^{\frac{1}{\gamma-1}}\,\frac{C_p}{R} \qquad\qquad \text{B-(10)}$$

where

$$P_{tref} \;=\; \text{plenum total pressure}$$

$$X_{ref} \;=\; \sqrt{1 - (\frac{P_{ref}}{P_{tref}})^{\gamma-1/\gamma}} \qquad\qquad \text{B-(11)}$$

$$P_{ref} \;=\; \begin{array}{l}\text{wall static pressure at the lower}\\ \text{(inlet) plane}\end{array}$$

It is noted that X is a dimensionless velocity defined by

$$X \;=\; \frac{V}{V_t} \;=\; \frac{V}{\sqrt{2\,C_p\,T_t}} \qquad\qquad \text{B-(12)}$$

where V is the local velocity, $V_t = \sqrt{2\,C_p\,T_t}$ is the "limiting" velocity and T_t is the stagnation temperature.

Using the perfect gas equation of state, the stagnation density is given by

$$\rho_t \;=\; \frac{P_t}{R\,T_t} \qquad\qquad \text{B-(13)}$$

so that the local density, ρ, can be written as

$$\rho \approx \rho_t (1 - X^2)^{1/(\gamma-1)} \qquad \text{B-(14)}$$

The "axial" and "tangential" components of the velocity can be written respectively as

$$V_a = V \cos \beta_i \qquad \text{B-(15)}$$

and

$$V_t = - V \sin \beta_i \qquad \text{B-(16)}$$

where β_i is the air angle at inlet (i = 1) or outlet (i = 2) defined in Fig. 11. Using the relations given in Eq. B-(10)-Eq. B-(16), the blade force components R_{t_M} and R_{a_M} given by the equations B-(3) and B-(4) can be written as force coefficients C_{x_m} and C_{y_M} given by

$$C_{x_m} = \frac{R_{t_m}}{\frac{1}{2} \rho_{ref} V_{ref}^2 s} \qquad \text{B-(17)}$$

$$C_{y_m} = \frac{R_{a_m}}{\frac{1}{2} \rho_{ref} V_{ref}^2 s} \qquad \text{B-(18)}$$

so that

$$C_{x_M} = -\frac{2}{s} \int_0^s \frac{P_{t_1}(\eta,t)}{P_{tref}(t)} \left[\frac{X_1(\eta,t)}{X_{ref}(t)}\right]^2 \left[\frac{1 - X_1^2(\eta,t)}{1 - X_{ref}^2(t)}\right]^{1/(\gamma-1)}$$

$$\cdot \cos \beta_1(\eta) \sin \beta_1(\eta) dX$$

$$+ \frac{2}{s} \int_0^s \frac{P_{t_2}(\eta,t)}{P_{tref}} \left[\frac{X_2(\eta,t)}{X_{ref}(t)}\right]^2 \left[\frac{1 - X_1^2(\eta,t)}{1 - X_{ref}^2(t)}\right]^{1/(\gamma-1)}$$

$$\cdot \cos \beta_1(\eta) \sin \beta_2(\eta) dX \qquad\qquad B\text{-}(19)$$

$$C_{y_M} = \frac{2}{s} \int_0^s \frac{P_{t_1}(\eta,t)}{P_{tref}(t)} \left[\frac{X_1(\eta,t)}{X_{ref}(t)}\right]^2 \left[\frac{1 - X_1^2(\eta,t)}{1 - X_{ref}^2(t)}\right]^{1/(\gamma-1)}$$

$$\cdot \cos^2 \beta_1(\eta) dX$$

$$- \frac{2}{s} \int_0^s \frac{P_{t_2}(\eta,t)}{P_{tref}(t)} \left[\frac{X_2(\eta,t)}{X_{ref}(t)}\right]^2 \left[\frac{1 - X_2^2(\eta,t)}{1 - X_{ref}^2(t)}\right]^{1/(\gamma-1)}$$

$$\cdot \cos^2 \beta_1(\eta) dX$$

$$+ \frac{1}{s} \int_0^s \frac{P_1(\eta,t)}{P_{tref}(t) \ X_{ref}^2(t) [1 - X_{ref}^2(t)]^{1/(\gamma-1) \frac{C_p}{R}}} dX$$

$$- \frac{1}{s} \int_0^s \frac{P_2(\eta,t)}{P_{tref}(t) \ X_{ref}^2(t) [1 - X_{ref}^2(t)]^{1/(\gamma-1) \frac{C_p}{R}}} dX$$

$$B\text{-}(20)$$

where (η) denotes spatial and (t) denotes possible time dependence as described in Appendix D.

Similarly, blade force coefficients can be obtained from the surface pressure measurements using the relations

$$C_{x_c} = \frac{F_{x_c}}{\frac{1}{2}\rho_{ref} V_{ref}^2 s} \qquad \text{B-(21)}$$

$$C_{y_n} = \frac{F_{y_n}}{\frac{1}{2}\rho_{ref} V_{ref}^2 s} \qquad \text{B-(22)}$$

If the surface pressure coefficient, C_s, is defined as

$$C_s = \frac{p_s}{\frac{1}{2}\rho_{ref} V_{ref}^2}$$

then, using Eq. B-(10),

$$C_s = \frac{p_s}{p_{tref}} \frac{1}{x_{ref}^2 [1 - x_{ref}^2]^{1/(\gamma-1)(\frac{R}{C_p})}} \qquad \text{B-(23)}$$

Using Eq. B-(23) with Eq. B-(21), Eq. B-(22), Eq. B-(6a) and Eq. B-(6b), these results follow:

$$C_{x_c} = \frac{1}{s}[\int_{AFE} C_s \, dy_c - \int_{CDE} C_s \, dy_c - \int_{AB} C_s \, dy_c$$

$$+ \int_{CB} C_s \, dy_c] \qquad \text{B-(24)}$$

$$C_{y_n} = \frac{1}{s}[\int_{FABCD} C_s \, dx_c - \int_{FED} C_s \, dx_c] \qquad \text{B-(25)}$$

Finally, defining

$$C_{x_B} = \frac{R_{t_B}}{\frac{1}{2}\rho_{ref} V_{ref}^2 s} \qquad \text{B-(26)}$$

and

$$C_{Y_B} = \frac{R_{a_B}}{\frac{1}{2} \rho_{ref} V_{ref}^2 s} \qquad \text{B-(27)}$$

using Eq. B-(8) and Eq. B-(9),

$$C_{x_B} = -(C_{y_n} \cos \gamma + C_{x_c} \sin \gamma) \qquad \text{B-(28)}$$

$$C_{y_B} = -(C_{y_n} \sin \gamma - C_{x_c} \cos \gamma) \qquad \text{B-(29)}$$

B.4 Data Reduction

All integrals were evaluated using a general integration subroutine. The subroutine FNInteg on the Hewlett-Packard System 45 [Ref. 7] carries out the integration using a succession of overlapping quadratic curves through the individual data points.

The values of C_{x_M} and C_{y_M} (components of the blade force coefficient based on momentum balance) were obtained from the prove survey data using Eq. B-(19) and Eq. B-(20).

The procedure to evaluate C_{x_B} and C_{y_B} (components of the blade force coefficient based on blade surface pressure measurements) was as follows:

i)   The value of C_s at each pressure tap was calculated using Eq. B-(23).

ii) C_{x_c} and C_{y_n} were calculated using Eq. B-(24) and Eq. B-(25) respectively.

193

iii) C_{x_B} and C_{y_B} were calculated using Eq. B-(28) and Eq. B-(29) respectively.

APPENDIX C

LOSS COEFFICIENT EVALUATION

C.1 Analysis

The total pressure loss coefficient $\bar{\omega}$ is defined in Ref. 1 as the ratio of the "mass averaged loss in total pressure," $\overline{\Delta P}$, across the blade row from inlet to outlet to some reference inlet dynamic pressure, $(P_{t_1} - P_1)_{ref}$ which is expected to be uniform. When the inlet conditions are not strictly uniform it is necessary to mass average the inlet and exit measurements separately, and to define the loss coefficient as

$$\bar{\omega} = \frac{\bar{P}_{t_1} - \bar{P}_{t_2}}{\bar{P}_{t_1} - P_1} \qquad\qquad C-(1)$$

where the bars denote mass-averaged quantities, P_t, and P_1, are inlet total and static pressures respectively, and P_{t_2} is the total pressure at the outlet plane.

Since the individual pressure measurements can depend somewhat on time (t) as well as position(η) as a result of small variations in supply conditions, i.e., $P_t(\eta,t)$ and $P(\eta,t)$, they are referred to plenum pressure at the time of measurement, $P_{plen}(t)$.

Hence the pressure coefficients

$$C_{P_t}(\eta) = \frac{P_t(\eta,t)}{P_{plen}(t)} \qquad\qquad C-(2)$$

and

$$C_p(\eta) = \frac{P(\eta,t)}{P_{plen}(t)} \qquad \text{C-(3)}$$

are expected to depend only on position in the survey.

In calculating the mass averaged conditions at the inlet and outlet planes, it must be remembered that the mass flux on the midspan centerline at the inlet plane is different from the mass flux on the midspan centerline at the outlet plane. The ratio of the two mass fluxes is the value of the AVDR which is a measure of the centerline stream surface contraction.

If $m(\eta,t)$ is the local mass flux and $m_{ref}(t)$ is a reference mass flux based on plenum supply conditions, the ratio

$$k(\eta) = \frac{m(\eta,t)}{m_{ref}(t)} \qquad \text{C-(4)}$$

is expected to depend on position only. We can then express the mass averaged total pressure coefficient as

$$\bar{C}_{p_t} = \frac{\int_0^s C_{p_t}(\eta)\ k(\eta)\ d\eta}{\int_0^s k(\eta)\ d\eta} \qquad \text{C-(5)}$$

and the mass averaged static pressure coefficient as

196

$$\overline{C}_p = \frac{\int_0^s C_p(\eta) \ k(\eta) \ d\eta}{\int_0^s k(\eta) \ d\eta} \qquad \text{C-(6)}$$

The loss coefficient expressed by Eq. C-(1) is equivalent to the loss coefficient expressed by

$$\overline{\omega} = \frac{\overline{C}_{p_{t_1}} - \overline{C}_{p_{t_2}}}{\overline{C}_{p_{t_1}} - \overline{C}_{p_1}} \qquad \text{C-(7)}$$

when conditions do not depend on time. In practice, the effect of fluctuations in the supply conditions are reduced or removed if the loss coefficient is evaluated using the definition in Eq. C-(7).

Expanding Eq. C-(7) using Eq. C-(5) and Eq. C-(6), the loss coefficient becomes

$$\overline{\omega} = \frac{\dfrac{\int_0^s C_{p_{t_1}} \ k_1 \ d\eta}{\int_0^s k_1 \ d\eta} - \dfrac{\int_0^s C_{p_{t_2}} \ k_2 \ d\eta}{\int_0^s k_2 \ d\eta}}{\dfrac{\int_0^s C_{p_{t_1}} \ k_1 \ d\eta}{\int_0^s k_1 \ d\eta} - \dfrac{\int_0^s C_{p_1} \ k_1 \ d\eta}{\int_0^s k_1 \ d\eta}} \qquad \text{C-(8)}$$

Re-arranging,

$$\overline{\omega} = \frac{\int_0^s C_{p_{t_1}} k_1 \, d\eta - \int_0^s C_{p_{t_2}} k_2 \, d\eta \left[\frac{\int_0^s k_1 \, d\eta}{\int_0^s k_2 \, d\eta}\right]}{\int_0^s C_{p_{t_1}} k_1 \, d\eta - \int_0^s C_{p_1} k_1 \, d\eta} \qquad \text{C-(9)}$$

and following Appendix D, Eq. D-(8),

$$\text{AVDR} = \frac{\int_0^s k_2 \, d\eta}{\int_0^s k_1 \, d\eta} \quad ,$$

so that

$$\overline{\omega} \equiv \frac{\int_0^s C_{p_{t_1}} k_1 \, d\eta - \frac{1}{\text{AVDR}} \int_0^s C_{p_{t_2}} k_2 \, d\eta}{\int_0^s C_{p_{t_1}} k_1 \, d\eta - \int_0^s C_{p_1} k_1 \, d\eta} \qquad \text{C-(10)}$$

C.2 Data Reduction

From recorded data, at each point in each survey $k(\eta)$ was calculated using Eq. D-(15) (and Eq. D-(5)), C_{p_t} and C_p were calculated using Eq. C-(2) and Eq. C-(3) respectively, the AVDR was obtained according to Appendix D and the loss coefficient was calculated using Eq. C-(10).

198

APPENDIX D

CALCULATION OF THE AXIAL VELOCITY-DENSITY RATIO (AVDR)

(By D.A. Duval; Reproduced without change from Ref. 4.)

Continuity requires that:

$$\int_0^s \bar{h}_1 \, \rho_1 \, V_1 \, \cos \beta_1 \, d\eta \; = \; \int_0^s \bar{h}_2 \, \rho_2 \, V_2 \, \cos \beta_2 \, d\eta \qquad D\text{-}(1)$$

where

ρ_i = density

V_i = velocity

β_1 = air inlet angle

β_2 = air outlet angle

$\bar{h}_i$ = spanwise streamtube depth

s = blade spacing

η = blade-to-blade dimension, normal to axial direction,

and subscripts 1 and 2 refer to the test cascade inlet and outlet respectively.

As air passes through the cascade, boundary layers build up along the side walls, contracting the streamtube in the spanwise direction. As a measure of the two-dimensionality of the flow, the AVDR is the ratio of the equivalent depths

of the streamtube at inlet and outlet. The equivalent streamtube depth, h_i, replaces $\bar{h}_i$ and is taken to be constant over the η dimension:

$$\text{AVDR} = \frac{h_1}{h_2} = \frac{\int_0^s \rho_2 \, V_2 \, \cos \beta_2 \, d\eta}{\int_0^s \rho_1 \, V_1 \, \cos \beta_1 \, d\eta} \qquad \text{D-(2)}$$

In practice, uncommanded variations in blower speed may be experienced during the time required to survey the flow. As a result, the total mass flow rate in the wind tunnel is not exactly constant. Measurements, therefore, actually have a weak (and undesirable) time dependence. Equation D-(2) assumes all measurements are taken at the same moment in time. More precisely,

$$\text{AVDR} = \frac{\int_0^s \rho_2(\eta, t_o) \, V_2(\eta, t_o) \, \cos \beta_2(\eta, t_o) \, d\eta}{\int_0^s \rho_1(\eta, t_o) \, V_1(\eta, t_o) \, \cos \beta_1(\eta, t_o) \, d\eta} \qquad \text{D-(3)}$$

Since no means exists to take all measurements at once, the time dependence of these terms must be removed in some other manner.

In Equation D-(3), each integrand has the dimensions (velocity, density). Giving the integrands the symbol m_i, we have:

$$AVDR = \frac{\int_0^s m_2(\eta, t_o) \, d\eta}{\int_0^s m_1(\eta, t_o) \, d\eta} \qquad \text{D-(4)}$$

Now, assume a function, m_{ref}, can be found, with dimensions (velocity, density), such that:

$$f_i(\eta, t) = \frac{m_i(\eta, t)}{m_{ref}(t)} = k_i(\eta) \qquad \text{D-(5)}$$

where k_i is not a function of time (that is, it is not dependent on tunnel air supply conditions). Furthermore,

$$AVDR = AVDR\left(\frac{m_{ref}(t_o)}{m_{ref}(t_o)}\right) = \frac{[\dfrac{\int_0^s m_2(\eta, t_o) \, d\eta}{m_{ref}(t_o)}]}{\dfrac{[\dfrac{\int_0^s m_1(\eta, t_o) \, d\eta}{m_{ref}(t_o)}]}{m_{ref}(t_o)}} \qquad \text{D-(6)}$$

Since m_{ref} is not a function of η, it may be taken inside the integral, so that

$$AVDR = \frac{\int_0^s \frac{m_2(\eta, t_o)}{m_{ref}(t_o)} \, d\eta}{\int_0^s \frac{m_1(\eta, t_o)}{m_{ref}(t_o)} \, d\eta} \qquad \text{D-(7)}$$

Now consider the integrand in the numerator. By equation D-(5), the <u>integrand</u> is not a function of time as long as m_2

201

and m_{ref} are measured at the same time, t_o. In practice, where discrete measurements are taken and a numerical integration is performed, it is required only that m_2 and m_{ref} be measured at the same time for the same data point. In this way, m_2 and m_{ref} may vary with time, but their ratio (k_2) remains a function of η only.

Applying the same argument to the integrand in the denominator in equation D-(7), it can be seen that this integrand is $k_1(\eta)$. Furthermore, there is no requirement that both numerator and denominator integrands be measured at the same time, since each is, independently, a function of η only. Therefore:

$$AVDR = \frac{\int_0^s k_2(\eta)\ d\eta}{\int_0^s k_1(\eta)\ d\eta} \qquad\qquad D\text{-}(8)$$

In this manner, the time dependence of the measured "velocity-densities" can be eliminated.

One way to generate such a "reference velocity-density" is to establish a reference velocity which, when multiplied together, form a quantity which satisfies equation D-(5). We now also assume β_1 and β_2 are not time dependent. This is justified by the assumption that small changes in inlet dynamic pressure will have little effect on the air angles. Then,

$$\text{AVDR} = \frac{\int_0^s (\frac{\rho_2(\eta,t_o)}{\rho_{ref}(t_o)}) \cdot (\frac{V_2(\eta,t_o)}{V_{ref}(t_o)}) \cos \beta_2(\eta) \, d\eta}{\int_0^s (\frac{\rho_1(\eta,t_1)}{\rho_{ref}(t_1)}) \cdot (\frac{V_1(\eta,t_1)}{V_{ref}(t_1)}) \cos \beta_1(\eta) \, d\eta} \qquad \text{D-(9)}$$

where subscripts on t indicate which measurements must be taken simultaneously.

Subject to the assumptions that

1. The air acts as a perfect gas,

2. The specific heats are constant, and

3. The total temperature is a function of time only

   (not of position in the wind tunnel),

the following gas dynamic relationships can be used to express the integrands:

$$\rho = \rho_t [1 - X^2]^{1/\gamma - 1} \qquad \text{D-(10)}$$

$$\rho_t = \frac{p_t}{RT_t} \qquad \text{D-(11)}$$

$$V = X V_t = X\sqrt{2 c_p T_t} \qquad \text{D-(12)}$$

where subscript t refers to "total" quantities, and $V_t = \sqrt{2c_p T_t}$ is the "limiting" velocity. Then,

$$V = (\frac{p_t}{RT_t}) [1 - X^2]^{1/\gamma - 1} (X\sqrt{2 c_p T_t}) \qquad \text{D-(13)}$$

$$= \frac{p_t X}{\sqrt{T_t}} [1 - X^2]^{1/\gamma - 1} \frac{\sqrt{2 c_p}}{R} \qquad \text{D-(14)}$$

so that, at each data point, the integrand can be written as

$$\frac{m_i(\eta,t)}{m_{ref}(t)} = \frac{\dfrac{p_{t_i}(\eta,t)}{\sqrt{T_t(t)}} X_i(\eta,t)[1-X_i^2(\eta,t)]^{1/(\gamma-1)} \dfrac{\sqrt{2c_p}}{R}\cos\beta_i(\eta)}{\dfrac{p_{t_{ref}}(t)}{\sqrt{T_t(t)}} X_{ref}(t)[1-X_{ref}^2(t)]^{1/(\gamma-1)} \dfrac{\sqrt{2c_p}}{R}}$$

D-(15)

or,

$$\frac{m_i(\eta,t_j)}{m_{ref}(t_j)} = \left(\frac{p_{t_i}(\eta,t_j)}{p_{t_{ref}}(t_j)}\right)\left(\frac{X_i(\eta,t_j)}{X_{ref}(t_j)}\right)\left[\frac{1-X_i^2(\eta,t_j)}{1-X_{ref}^2(t_j)}\right]^{1/(\gamma-1)}\cos\beta_i(\eta)$$

D-(16)

so that, finally,

$$AVDR = \frac{\displaystyle\int_0^s \left(\frac{p_{t_2}(\eta,t_o)}{p_{t_{ref}}(t_o)}\right)\left(\frac{X_2(\eta,t_o)}{X_{ref}(t_o)}\right)\left[\frac{1-X_2^2(\eta,t_o)}{1-X_{ref}^2(t_o)}\right]^{1/(\gamma-1)}\cos\beta_2(\eta)\,d\eta}{\displaystyle\int_0^s \left(\frac{p_{t_1}(\eta,t_o)}{p_{t_{ref}}(t_1)}\right)\left(\frac{X_1(\eta,t_1)}{X_{ref}(t_1)}\right)\left[\frac{1-X_1^2(\eta,t_1)}{1-X_{ref}^2(t_1)}\right]^{1/(\gamma-1)}\cos\beta_1(\eta)\,d\eta}$$

D-(17)

The final assumption is that the plenum pressure satisfies the conditions imposed on $P_{t_{ref}}$, and that the conditions imposed on X_{ref} can be satisfied by the quantity

$$X_{ref} = \sqrt{1 - \left(\frac{p_{ref}}{p_{tref}}\right)^{(\gamma-1)/\gamma}}$$

D-(18)

where p_{ref} is the lower wall static pressure.

204

No testing was done to examine these last two assumptions. Consequently, it is possible that, in analyzing the data in this way, the time dependence of the measurements was only approximately, and not entirely, eliminated. Elimination of the time dependence would require the measurement of reference quantities which satisfy equation D-(5) exactly.

The X_i were calculated by application of the survey probe calibration. The p_{t_i} and β_i were measured directly by the probe. The AVDR was calculated by numerical integration of equation D-(17).

LIST OF REFERENCES

1. NASA Report SP-36, *Aerodynamic Design of Axial-Flow Compressors*, edited by Irving A. Johnsen and Robert A. Bullock, 1965.

2. Moebius, R.C. *Analysis and Testing to Improve the Flow from the Plenum of a Subsonic Cascade Wind Tunnel*, M.S. Thesis, Naval Postgraduate School, Monterey, CA., 1980.

3. Rose, Charles C., and Guttormson, Darold L., *Installation and Test of a Rectilinear Cascade*, M.S. Thesis, Naval Postgraduate School, Monterey, Ca., 1964.

4. Duval, David A., *Evaluation of a Subsonic Cascade Wind Tunnel For Compressor Blade Testing*, M.S. Thesis, Naval Postgraduate School, Monterey, Ca., 1980.

5. NASA/University Workshop, Internal Computational Mechanics Program for Turbomachinery, NASA Lewis Research Center, September 25-26, 1978.

6. NASA Technical Paper 1493, *Performance of Two-Stage Fan Having Low-Aspect-Ratio First-Stage Rotor Blading*, by Donald C. Urasek, William T. Gorrell and Walter S. Cunnan, 1979.

7. *3052A System Library (9845A)*, Hewlett-Packard Comapny, 1978.

8. Turbopropulsion Laboratory, Naval Postgraduate School, Technical Note 80-03, *Data Acquisition Programs for the Subsonic Cascade Wind Tunnel*, by D.A. Duval, 1980.

9. Turbopropulsion Laboratory, Naval Postgraduate School, Technical Note 81-01, *Data Acquisition Programs for the Subsonic Cascade Wind Tunnel* (revised), by D.A. Duval and F.S. Cina, 1981.

10. NACA Report 1016, *Effect of Tunnel Configuration and Testing Technique on Cascade Performance*, by John R. Erwin and James C. Emery, 1951.

11. Turbopropulsion Laboratory, Naval Postgraduate School, Technical Note 80-05, *Subsonic Cascade Wind Tunnel-- Preparatory Test Results*, by Alan G. McGuire, 1980.

12. Vavra, M.H., *Aero-Thermodynamics and Flow in Turbomachines*, Wiley, 1960.

13. NASA Technical Memorandum 75278, _The Execution of Systematic Measurements on Plane Cascades_, by Norbert Scholz, 1978.

INITIAL DISTRIBUTION LIST

		No. Copies

1. Defense Technical Information Center   2
   Cameron Station
   Alexandria, Virginia 22314

2. Library, Code 0142   2
   Naval Postgraduate School
   Monterey, CA 93940

3. Department Chairman, Code 67   1
   Department of Aeronautics
   Naval Postgraduate School
   Monterey, CA 93940

4. Director, Turbopropulsion Laboratory, Code 67Sf   1
   Naval Postgraduate School
   Monterey, CA 93940

5. LCDR D.A. DuVal, USN   1
   VC-1, NAS Barber Point
   FPO San Francisco, CA 96601

6. Turbopropulsion Laboratory   15
   Code 67
   Naval Postgraduate School
   Monterey, CA 93940

7. Dr. Gerhard Heiche   1
   Naval Air Systems Command
   Code AIR-310
   Department of the Navy
   Washington, D.C. 20360

8. Dr. A.D. Wood   1
   Office of Naval Research
   Eastern/Central Regional Office
   666 Summer Street
   Boston, Massachusetts 02210

9. Chief, Fan and Compressor Branch   1
   (Attn: Nelson Sanger)
   NASA Lewis Research Center
   Mail Stop 5-9
   21000 Brookpark Road
   Cleveland, Ohio 44135

10.   LT F.S. Cina, USN
      FAWPRA (Box 58)
      COMFAIRWESTPAC Det Cubi Point
      FPO San Francisco, CA 96654   1